UNIVERSITY OF CALIFORNIA
RIVERSIDE

Development of Butenolide Arylation Methodologies in the Total Synthesis of Fraxinellone and Progress Towards the Total Synthesis of Annotinolides A and B

A Dissertation submitted in partial satisfaction of
the requirements for the degree of

Doctor of Philosophy

in

Chemistry

By

Taylor Sean Alexander

March 2021

Dissertation Committee:
Dr. Kevin G. M. Kou, Chairperson
Dr. Catharine Larsen
Dr. Christopher Switzer

The Dissertation of Taylor Sean Alexander is approved:

_____

_____

_____

Committee Chairperson

University of California, Riverside

Acknowledgments

To Kevin: I would like to extend my deepest gratitude and appreciation for Prof. Kevin G. M. Kou for all that you have done for me during my time in your lab. First, thank you for warmly and enthusiastically welcoming me and providing me the opportunity to continue my PhD in your lab. Your commitment, dedication, and support of has not only strengthened my technical skills and knowledge of chemistry, but also as a presenter, writer, and scientist readily prepared to be successful after graduate school. Thank you for sharing with me your valuable insights, perspectives, and knowledge during my time in your lab, I cannot thank you enough. I have truly enjoyed every day in your lab, from the exciting projects I have been able to work on to the special personal relationships and friendships I have formed with you and the Kou lab members.

To Dave: Next, I would like to extend my deepest gratitude and appreciation to Prof. David B.C. Martin for all that you have done for me during the beginning of my graduate school career and your continued support and commitment to my success to this day. Thank you for accepting me into your lab and introducing me to the world of organic chemistry and all that it has to offer and for shaping my graduate career. Thank you for all the time you spent helping me prepare for my SYRE and candidacy exams, grants, manuscripts, and presentations. Thank you for sharing your knowledge with me, teaching me what it takes to be successful as an organic chemist, and supporting my broad interests in science and in the pharmaceutical industry. Almost as important, thank you for being an outstanding

snowboarding-buddy and for the special memories of our ski trips to Mammoth and Big Bear that I will always remember!

To my labmates: There are far too many lab mates to thank individually, but thank you all for your friendship, support, and companionship. I do have to extend a special thanks to my hood/desk buddies Viviene and Manny for putting up with me suddenly when I joined the Kou lab (and every day since). Thank you guys for letting me encroach on your personal space, especially when I had my own hood but just did it for fun. To Roni, thank you for making me laugh and aggressively offering me so many healthy foods that I really don't want to eat, no matter how many fake health benefits you tell me about. To Yujie, thank you for being my brave desk cubicle buddy and keeping me company. Thank you for our constant laughs and random conversations each day ranging from chemistry, stocks, and even foods. To Aaron, thank you for helping me relearn how to fix the LCMS and solvent system every time something went wrong because we forgot how we fixed it last time. To Andy, thank you for humorously commiserating with me as we each struggled through our routes at various times until we were ultimately successful. To Dana, thank you for your friendship inside and outside of the lab, keeping us both sane during stressful times, and road tripping with me to ski trips and conferences. To Bill, thank you for your friendship, jokes, advice, and pranks (mostly by me) throughout our time together. And thank you for playing videogames with me, even if I was really, really bad. To Corey, thank you for your unusual calm, laid-back personality, which was a refreshing change from the rest of us. Also, thank you to Ryan Stanton for his friendship, camaraderie, and

hilarious sense of humor as we navigated our way through the challenges of classes, exams, and research together.

Finally, I would like to thank my mum and Yana: To Yana, thank you for your love, support, and patience. First, thank you for very patiently waiting for me to graduate! Thank you for always being supportive, taking care of me, (like meal prepping excessive amounts of food every weekend) spending time traveling, bike riding, snowboarding, and exploring breweries with me. Last but certainly not least, a huge special thank you to my mommy: Thank you for all of your infinite love, support, and sacrifices that you have made for me. Without you, I would not be where I am today and I would not have all the opportunities that I do. Gracias por todo.

The text of this dissertation, in part, is a reprint of the material as they appear in the following publications:

Chapter 1: Alexander, T. S.; Clay, T. J.; Maldonado, B.; Nguyen, J. M.; Martin, D. B. C. Comparative Studies of Palladium and Copper-Catalysed γ-Arylation of Silyloxy Furans with Diaryliodonium Salts. *Tetrahedron* **2019**, *75* (14), 2229–2238.

The co-author David B. C. Martin listed in these publications directed and supervised the research which forms the basis for this dissertation. All other co-authors listed in these publications contributed technical expertise.

ABSTRACT OF DISSERTATION

Development of Butenolide Arylation Methodologies Related to the Total Synthesis of Fraxinellone and Progress Towards the Total Synthesis of Annotinolides A and B

by

Taylor Sean Alexander

Doctor of Philosophy, Graduate Program in Chemistry
University of California, Riverside, March 2021
Dr. Kevin G.M. Kou, Chairperson

The total synthesis of natural products allows organic chemists the opportunity to develop new methodologies and strategies to access targets that exert highly valuable and interesting biological activities with medicinal applications that could benefit the scientific and global community. Inspired and motivated by intriguing structural complexities and compelling biological activities, this dissertation work is centrally focused on the total synthesis of fraxinellone, a limonoid natural product, and annotinolides A and B, which are lycopodium alkaloid natural products. Both of these families of natural products potentially affect the central nervous system (CNS). Fraxinellone is a valuable natural product due to its interesting neuroprotective activity against glutamate toxicity, which is suggested to be involved in the pathogenesis of Alzheimer's disease and other CNS diseases. Similarly, annotinolides A and B are structurally and biologically intriguing because they have been found to inhibit beta-amyloid protein aggregation, which is also suggested to be involved in the pathogenesis Alzheimer's disease. Through both total

synthesis projects, there is an emphasis on developing novel synthetic methodologies and strategies to access the complex carbon frameworks.

Chapter 1 describes an overview of the most significant historical accomplishments and contributions to the subfield of limonoid total synthesis, including pioneering total synthesis strategies and methodologies for the highly complex limonoid natural products. Herein is described the development of a γ-butenolide arylation methodology designed for the total synthesis of fraxinellone and the synthetic route that ultimately led to the successful total synthesis and future directions of this work.

Chapter 2 describes an overview of the most significant pioneering strategies for the synthesis of lycopodium alkaloids as well as in-depth discussions of their biosynthesis pathway and immense medicinal interest. Herein is described the progress towards the total synthesis of annotinolides A and B through an exciting and efficient divergent route featuring a redox neutral Heck reaction, an intramolecular Mannich-type cyclization, a biomimetic radical cyclopropanation and a reversed-selective [2 + 2] photocycloaddition.

Chapter 3 describes the history of the of Morita–Baylis–Hillman (MBH) reaction and metal-catalyzed cross-couplings of enolates, which served as our foundation and inspiration to explore the α-functionalization of α,β-unsaturated ketones to effect a reversal in regioselectivity of the Heck reaction.

Table of Contents

List of Figures

List of Tables

List of Schemes

Chapter 1—The Development of a Novel Palladium and Copper Catalyzed Arylation of silyloxyfurans and the Total Synthesis of Fraxinellone

1.1 Introduction

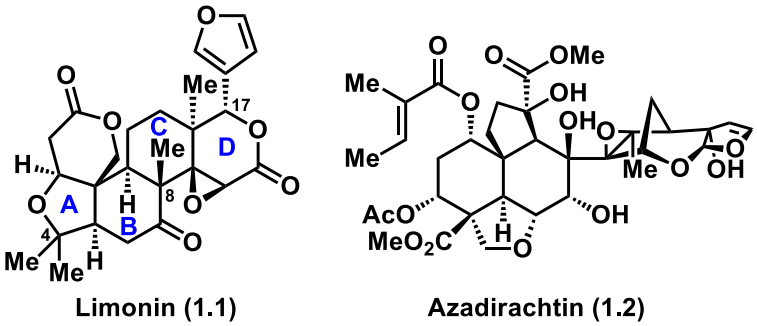

Figure 2.1 Structures of limonin and azadirachtin

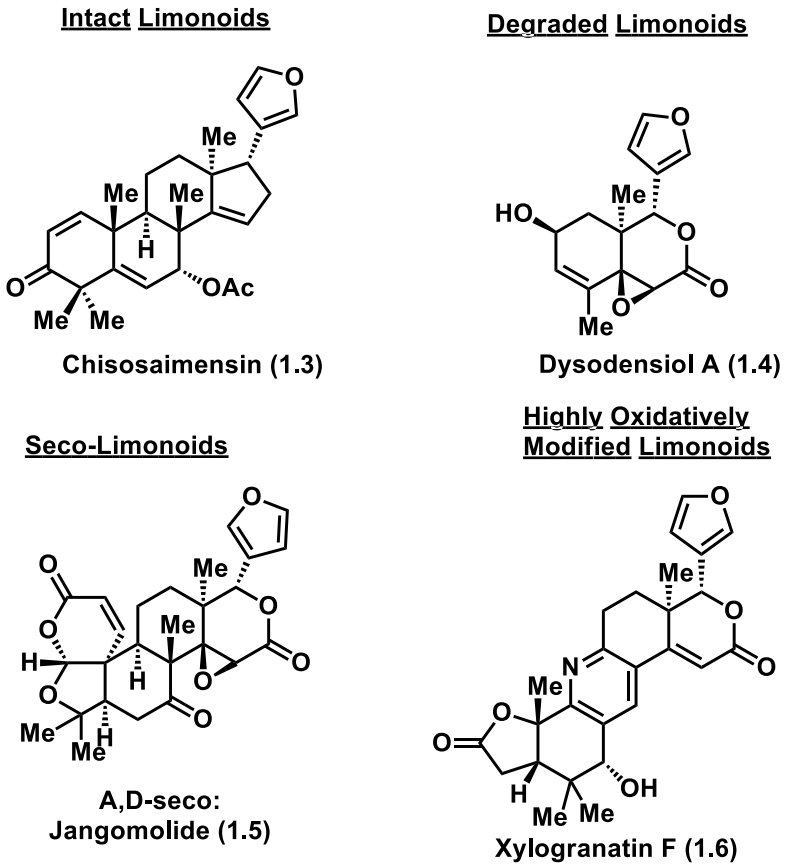

Figure 1.1 Representative members of each subclass of the limonoid family of natural products

Limonoid natural products belong to a family of triterpenoid compounds, typically containing at least four fused rings with subclasses that vary by the degree of oxygenation and unsaturation of the main carbon scaffold. The flagship limonoid, limonin (**1.1**), was isolated in 1960 by Watson[1] (Figure 1.1). Since the isolation of limonin (**1.1**), hundreds of limonoid natural products have been isolated and characterized. This natural product family is made up of modified triterpenes with a broad range of skeletal and oxidative diversity. Generally, the signature scaffold of limonoid natural products is the 4,4,8-trimethyl-17-furanylsteroid originating from limonin (**1.1**) shown in Figure 1.1.[2,3] All limonoids either exhibit or are hypothesized to be derived from this general scaffold. Within the large and complex family of limonoids, the sub-classes are classified as intact, degraded, seco-, and highly oxidative modified limonoids (Figure 1.2). The vast diversity of the chemical structures has rendered it historically difficult to propose a biosynthesis or natural origin for the limonoids, especially with some members of the family appearing to be structurally unrelated. This family of natural products has seen synthetic and medicinal focus due to their unique structures and biological activity. One of the most well-known members of the 'highly oxidative modified limonoids' is azadirachtin (**1.2**).[4] Azadirachtin was found to be a potent pesticide and was eventually commercialized as the active ingredient in AzaGuard. Despite immense interest in its biological activity, the complex polycyclic framework made synthesis efforts very difficult, and therefore limited the amount of material available for biological activity assays. Some researchers even regarded the more complex limonoids as synthetically inaccessible or highly impractical to access through synthesis. Considering the synthetic challenges posed by the more

complex members of the limonoid family, the oxidatively modified and degraded limonoids, which appear less synthetically daunting but still retain potent biological activities, have attracted the focus of synthetic and medicinal chemists. Limonoids exhibit a wide range of biological activities from antibiotic, antibotulinum, anti-inflammatory, anti-HIV, antioxidant, antiproliferative, antiviral, proapoptotic, insecticidal and insect antifeedant activity.[5–14]

1.1 Biosynthesis

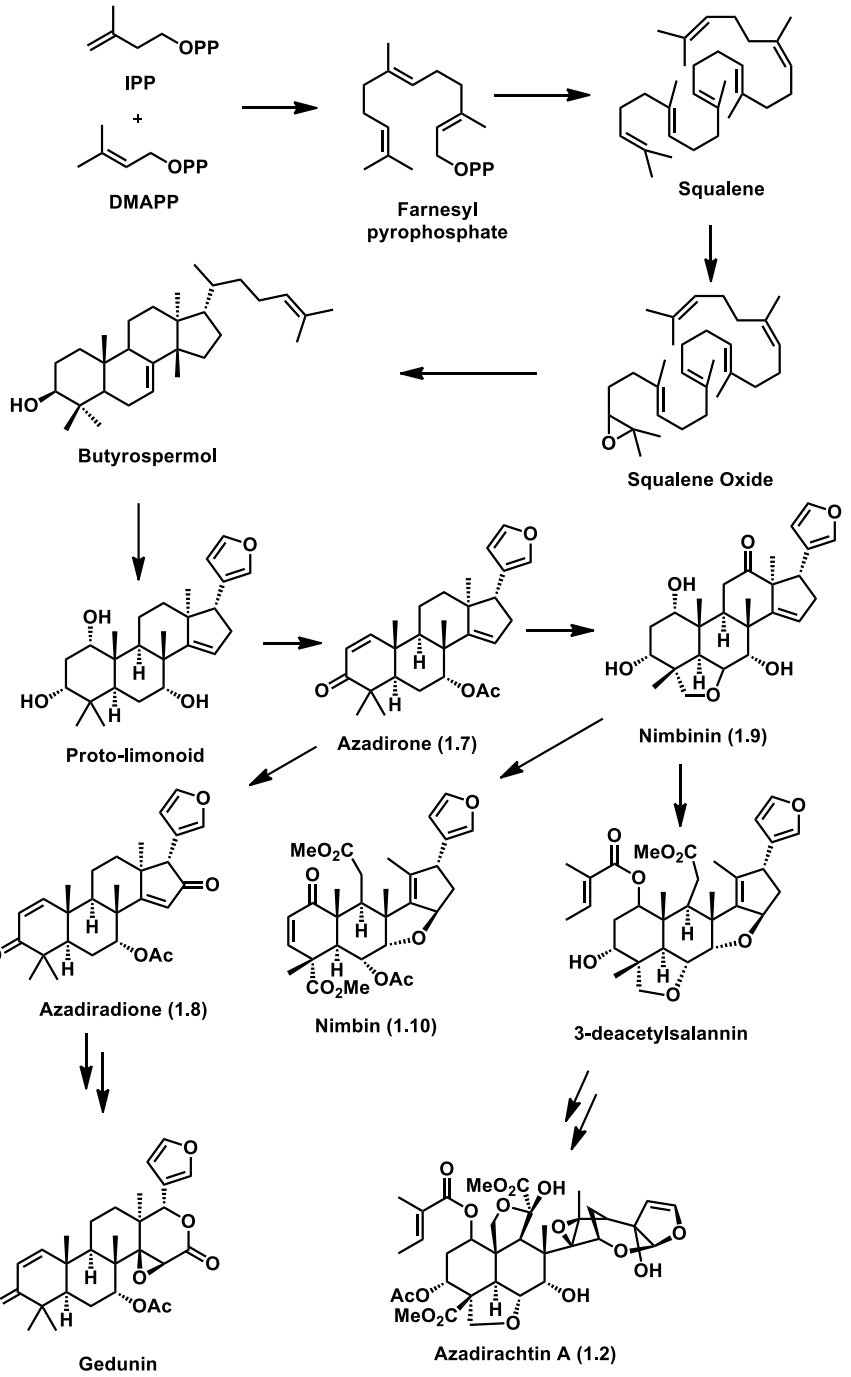

Scheme 1.1 Proposed biosynthesis of limonoid natural products

Given their biological and synthetic importance, thorough feeding experiments using stable isotope analogs have been performed to elucidate the biosynthetic pathway for the

limonoid family. The most detailed biosynthetic study was performed by Thulasiram and coworkers recently in 2018, however Hasegawa and coworkers have also proposed a similar biosynthetic pathway much earlier in 1986 although with less detail (scheme 1.1).[15,16,17]

The proposed biosynthetic pathway begins with traditional terpene biosynthesis in the combination of IPP and DMAPP forming farnesyl pyrophosphate as an intermediate to squalene, a triterpene. Squalene is then epoxidized and undergoes a cascade cyclization and skeletal rearrangement to form butyrospermol, which will then undergo cyclofuran ring formation and oxidation to afford the proto-limonoid scaffold. Next, a dehydration/oxidation of the 1,3-diol to the enone and acetylation are performed to generate azadirone (**1.7**). From azadirone (**1.7**) can then undergo C-H oxidation the ketone on the D-ring and acetylated to afford azadiradione (**1.8**). Alternatively, azadirone (**1.7**) can be reduced back from the enone to the 1.3-diol, C-H oxidized to the ketone on the C-ring and cyclized to form a tetrahydrofuran ring of nimbinin (**1.9**). Azadiradione (**1.8**) can then be expoxidized at the D-ring and oxidized from the cyclopentanone to the lactone to generate gedunin, an intact limonoid. Alternatively, Nimbinin (**1.9**) can be further functionalized through an oxidative cleavage of the C-ring followed by tigloylation, acetylation, and tetrahydrofuran ring formation to form Azadirachtin A (**1.2**), a c-seco limonoid. Nimbinin (**1.9**) can also be converted to Nimbin (**1.10**) via an oxidative cleavage of the C-ring. There are many other limonoids not shown in this summarized scheme. It is hypothesized that the more complex members of the limonoid family follow this type of biosynthesis beginning with a classical terpene biosynthesis route before being further

functionalized to form the more complex members of the limonoid family, and then degraded to form the less complex members, such as dysodensiol A (Figure 1.2).

1.2 Previous Synthesis of Limonoids

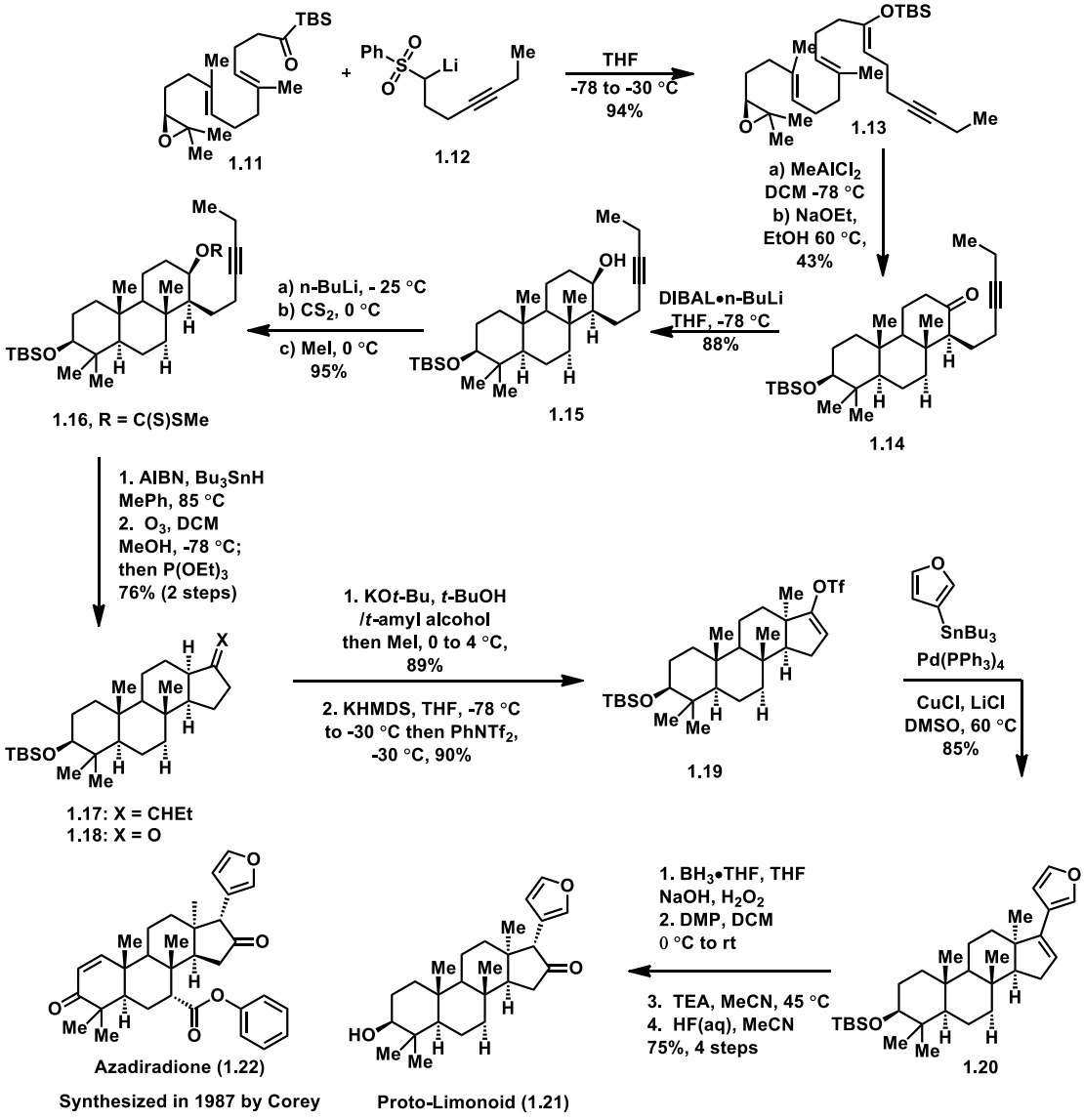

Scheme 1.2 Synthesis of limonoid scaffold by E. J. Corey in 2009

There have been several especially important and influential syntheses accomplished that have provided access to valuable limonoid natural products and led to the development of synthetic methodologies and approaches. The first example presented herein is the work developed by Corey and coworkers in 2009 of the intact proto-limonoid scaffold that is

generated rapidly by a novel cationic triple annulation and a free-radical-induced stereo-controlled ring closure (Scheme 1.2).[18] It should also be noted that many years previously in 1987, Corey and coworkers also accomplished the diastereoselective synthesis of azadiradione (**1.22**), a limonoid differing from the proto-limonoid by oxidation state at three positions.[19] Besides the oxidation state differences, the carbon skeleton of azadiradione (**1.22**) and the proto-limonoid are otherwise identical. A similar synthesis route was used for each target compound. The synthesis begins with a carbonyl addition and Brook rearrangement between acylsilane **1.11** and lithiosulfone **1.12** to access epoxy silyl enol ether **1.13**. From here, the key step is performed by treatment of silyl enol ether **1.13** with the Lewis acid, methylaluminum dichloride, at low temperature followed by treatment with NaOEt facilitated a cationic cyclization cascade and epimerization sequence. This step generated ketone **1.14** with three rings and five stereocenters in 43% yield. The rest of the synthesis builds the remaining D-ring and installs the furyl moiety. Following a diastereoselective reduction via DIBAL/nBuLi, the resulting alcohol (**1.15**) was converted to xanthate **1.16** by treatment with carbon disulfide and n-BuLi. The second key step involves a Barton–McCombie deoxygenation (AIBN and Bu_3SnH) utilizing xanthate **1.16**, leading to a carbon centered radical that reacts with the alkyne to cyclize in a 5-exo-dig cyclization to form tetracycle **1.17,** which is subsequently ozonolyzed at the alkene to yield ketone **1.18**. From ketone **1.18**, diastereoselective methylation followed by enolate trapping with phenyltriflimide yields vinyl triflate **1.19**. Finally, vinyl triflate **1.19** was subjected to a Stille reaction with tributylstannylfuran, generating vinyl furan **1.20** using non-standard Stille conditions developed as part of this work in 1999 when

conventional conditions were unsuccessful.[20,21] Typically, Stille reactions are hindered by sterically congested substrates. However, by using cuprous chloride as a cocatalyst, the slow reaction rates and steric limitations are overcome. Following TBS deprotection and C–H oxidation to the ketone, proto-limonoid **1.21** is generated, featuring functional handles that allow for further derivatization to access other limonoid congeners. The key contributions from this work was the establishment of a rapid route to the complex scaffold of intact limonoids through a cationic cyclization cascade to form the ABC-tricycle with five stereogenic centers, a Barton–McCombie deoxygenation-5-exo-dig cyclization to form the D-ring of the tetracycle, and furylation via a novel copper-catalyzed Stille reaction.[21,22]

Perhaps the most impressive achievement was by Ley and coworkers in 2007 in their synthesis campaign of the insect antifeedant azadirachtin (**1.2**), which took 22 years to complete (Scheme 1.3).[22] The synthetic challenges presented by this compound include sixteen contiguous stereocenters, seven of which are quaternary carbons. Additionally, azadirachtin is highly oxygenated and exhibits a unique conformation due to intramolecular hydrogen bonding interactions.[23] In pursuit of azadirachtin the Ley group was able to develop new methodologies and investigate the biological properties to this complex limonoid.[24,25]

The Ley group commenced the synthesis with diol **1.23**, which is prepared in three steps from β-D-galactose pentaacetate. From diol **1.23**, selective MOM protection, oxidation, and Grignardaddition/benzylation generated allyl tetrahydropyran **1.24** as a single diastereomer. The tetrahydrofuran ring was formed via deglycosidation followed

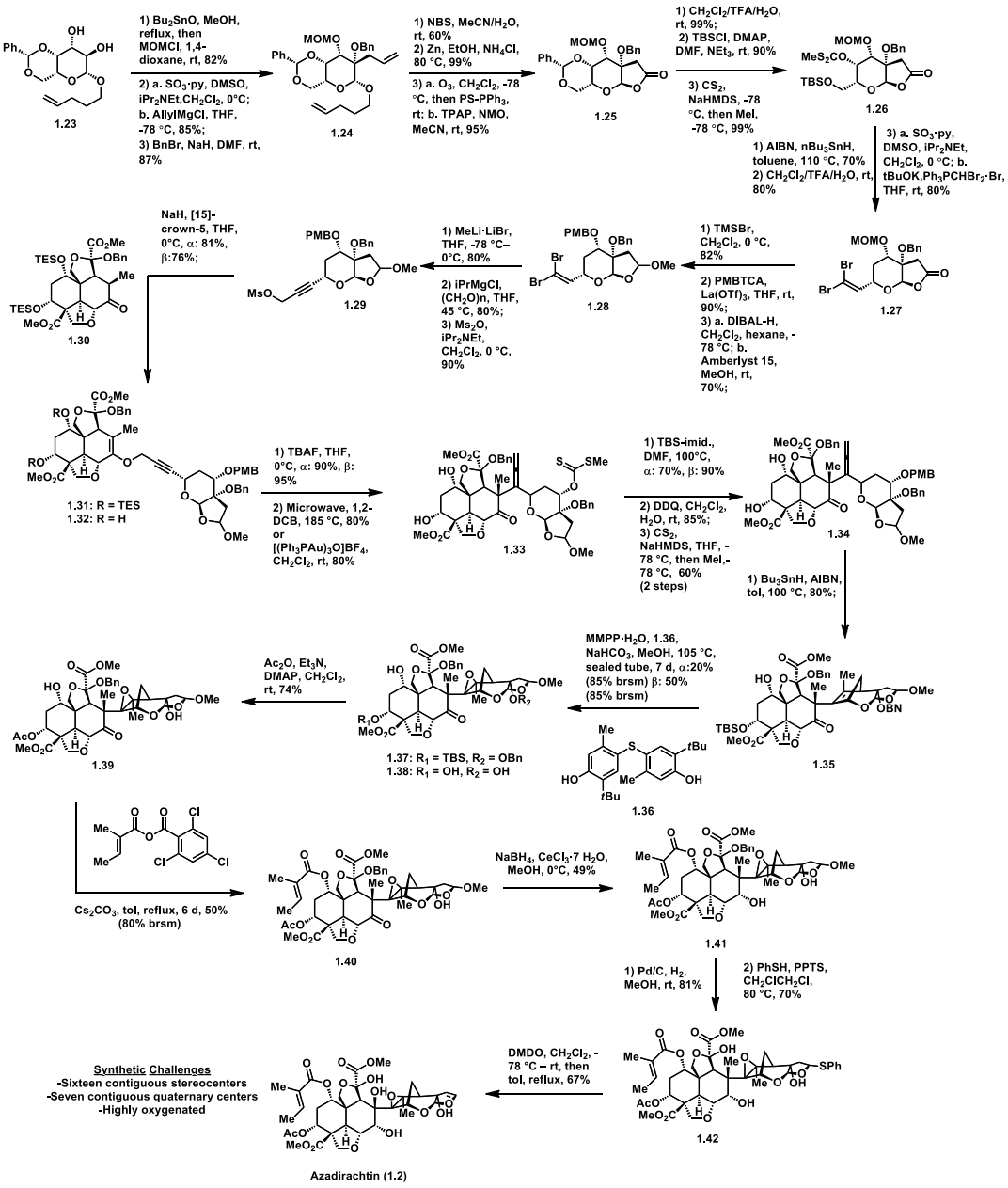

Scheme 1.3 Synthesis of azadirachtin by the Ley group in 2007. PS-PPh_3 = polymer bound PPh_3, TPAP = tetrapropylammonium perruthenate, MMPP = magnesium monoperoxyphthalate.

ozonolysis of allyl tetrahydropyran **1.24** generating a lactol that would be oxidized to the lactone **1.25**. Treatment of lactone **1.25** with trifluoroacetic acid facilitates ring opening of the benzylidene acetal, at which point the primary alcohol is silylated and the secondary

alcohol transformed to xanthane with CS_2 (**1.26**). Xanthate **1.26** then undergoes a Barton–McCombie deoxygenation followed by an oxidation and Wittig reaction to yield dibromo olefin **1.27**. Due to preliminary studies that suggested difficulties in cleaving the MOM protecting group at a subsequent stage in the synthesis, it was cleaved and replaced by a PMB ether, and then a reduction and acetalization sequence was carried out to give a 1:1 diastereomeric mixture of acetals **1.28**. It was found that both diastereomers served as viable precursors when evaluated separately for the next steps in the synthesis. α/β-**1.28** were alkynylated using Corey–Fuchs conditions and then underwent homologation using *para*-formaldehyde. The propargylic alcohol produced was reacted with methanesulfonic anhydride to generate propargylic mesylate **1.29**. The Ley group then coupled mesylate **1.29** with functionalized decalin derivative **1.30** which they had previously synthesized, forging propargylic ether **1.31**. Ether **1.31** was desilylated via treatment with TBAF and then a microwave-assisted or gold-catalyzed Claisen rearrangement installed the critical allene **1.33**. After protecting group manipulations to access radical precursor **1.34**, treatment with AIBN initiated a 5-*exo* cyclization to access alkene **1.35**. Subsequently, epoxidation of alkene **1.35** generated epoxide **1.37**, which was very similar to a known azadirachtin metabolite that they Ley group had previously used to synthesize azadirachtin (**1.2**). So, following their previously developed route, epoxide **1.37** was acetylated to generate epoxy-ketone **1.39**, which was then further functionalized to install the unique α,β-unsaturated ester **1.40**. Following a Luche reduction by $NaBH_4$ to give diol **1.41**, benzyl cleavage is performed by Pd/C hydrogenation. Subsquently, the methoxy furan is displaced under acidic conditions by thiophenol to form the thioglycosidic bond in

phenylsulfide **1.42**. Finally, oxidation of phenylsulfide **1.42** via DMDO followed by pyrolysis regenerated the dihydrofuran moiety and completed the synthesis of azadirachtin (**1.2)**. This synthesis is highlighted by a strategically designed convergent pathway utilizing two fragments furnished with all of the necessary functional handles for the conversions and transformations to key intermediates. Although the step count for this synthesis is quite high (32 steps), it represents a landmark synthesis of azadirachtin (**1.2**) with enormous prior efforts from the synthetic community. The synthetic challenges that led many previous efforts to failure was due to the structural complexity containing sixteen contiguous stereogenic centers, of which seven are quaternary centers, as well as fifteen oxygens present in the molecule. As previously mentioned, this synthetic achievement took the Ley group 22 years to complete, owing to the complex structural architecture.

1.3 Degraded Limonoids

Degraded limonoids are comparatively less structurally complex than the more elaborate members of the limonoid family. They often share structural similarities to more complex limonoids, and so they can be effectively used pharmacophore probes for structure-activity relationship (SAR) studies.[26] Degraded limonoids can also be used as

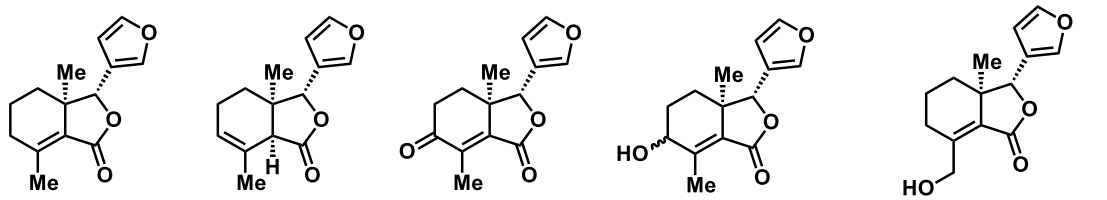

Figure 1.3 Structure of fraxinellone and derivatives

intermediates en route to more complex limonoids. Due to its biological activity, the most well known member of the degraded limonoid family is fraxinellone. Fraxinellones (Figure

1.3) contain a characteristic γ-butyrolactone core that is substituted at the C3 position with an α-furyl group and fused to a 6-membered ring that may be oxidized at the C6 position. The structure of fraxinellone was first isolated and characterized in 1965 and confirmed by X-ray crystallography.[27]

In 2008, Kim and coworkers isolated four limonoid natural products from *Dictamnus dasycarpus* rootbark that exhibited potent neuroprotective activity against glutamate toxicity in cultured rat cortical cells at a concentration of 0.1 μM. The four limonoids isolated were limonin (**1.1)**, obacunone (**1.8**), calodendrolide (**1.48**), and fraxinellone (**1.43**) (Figure 1.4). These compounds exhibit neuroprotective activity by inhibiting calcium influx and protecting antioxidant enzymes, which in turn, inhibits the

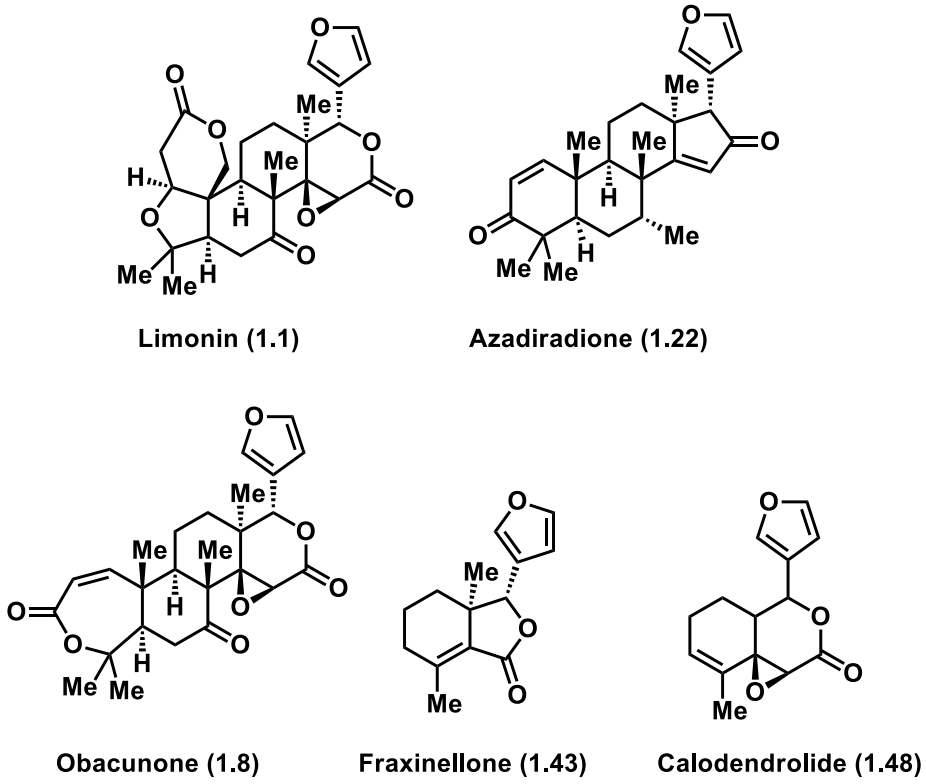

Figure 1.4 Limonoids natural products isolated from *Dictamus Dasycarpus* root bark

production of destructive reactive oxygen species (ROS) and reactive nitrogen species (RNS).[28] Fraxinellone is of particular interest because of its potent neuroprotective activity, but modest structural complexity compared to other members of the limonoid family.

It is estimated that within the United States alone, 5 million people suffer from Alzheimer's disease, 1 million from Parkinson's disease, 400,000 from multiple sclerosis, and 30,000 from both amyotrophic lateral sclerosis and Huntington's disease.[29] These neurodegenerative diseases can be described as the progressive deterioration of the structural integrity of the central nervous system (CNS) resulting in the death of neurons in the brain and spinal cord. As neurons deteriorate, cognitive ability rapidly declines, with symptoms often manifesting as loss in memory and coordination. Advanced stages of neurodegeneration ultimately result in the inability to function independently, both physically and cognitively. Left untreated, CNS diseases can be fatal and despite extensive research efforts limited therapeutics available. Furthermore, current therapeutics that do exist only treat the symptoms, and do not constitute a cure for the diseases.[30]

CNS diseases are strongly suggested to be related to excess L-glutamate (L-Glu), a major neurotransmitter in the brain, leading to the overactivation of ionotropic glutamate receptors.[31] These receptors are ligand-gated ion channels that control calcium ion influx across the plasma membrane of neurons. Due to beta-amyloid plaques destabilizing calcium ion homeostasis and the overexcitation of these receptors by L-Glu, calcium ions flood the cytosolic space, leading to the generation of reactive oxygen species (ROS) and reactive nitrogen species (RNS) through calcium dependent enzymatic processes. It is suggested that this oxidative stress leads to the destruction of post-synaptic structures such

as dendrites and cell bodies, eventually resulting in apoptosis. Additionally, it has been shown that glutamate excitotoxicity has been linked to the down-regulation of antioxidant enzymes such as superoxide dismutase, further exacerbating oxidative stress.[28,32] Given the proposed pathogenesis of these CNS diseases, developing fraxinellone derivatives to inhibit calcium influx and protect antioxidant enzymes could potentially lead to new effective therapeutics.

Based upon this compelling biological activity, the central hypothesis proposed is that the development of a strategic enantioselective route to access fraxinellone (**1.43**), utilizing a novel enantioselective metal-catalyzed coupling reaction, will provide access to a natural product with valuable therapeutic properties. Furthermore, it is hypothesized that the successful synthesis of fraxinellone through a strategically designed route will allow for meaningful late-stage functionalization opportunities to produce interesting analogs to conduct structure-activity-relationship studies to probe the neuroprotective activity and investigate the pathogenesis of CNS diseases related to glutamate toxicity.

1.4 Previous Synthesis of Fraxinellone (1.43)

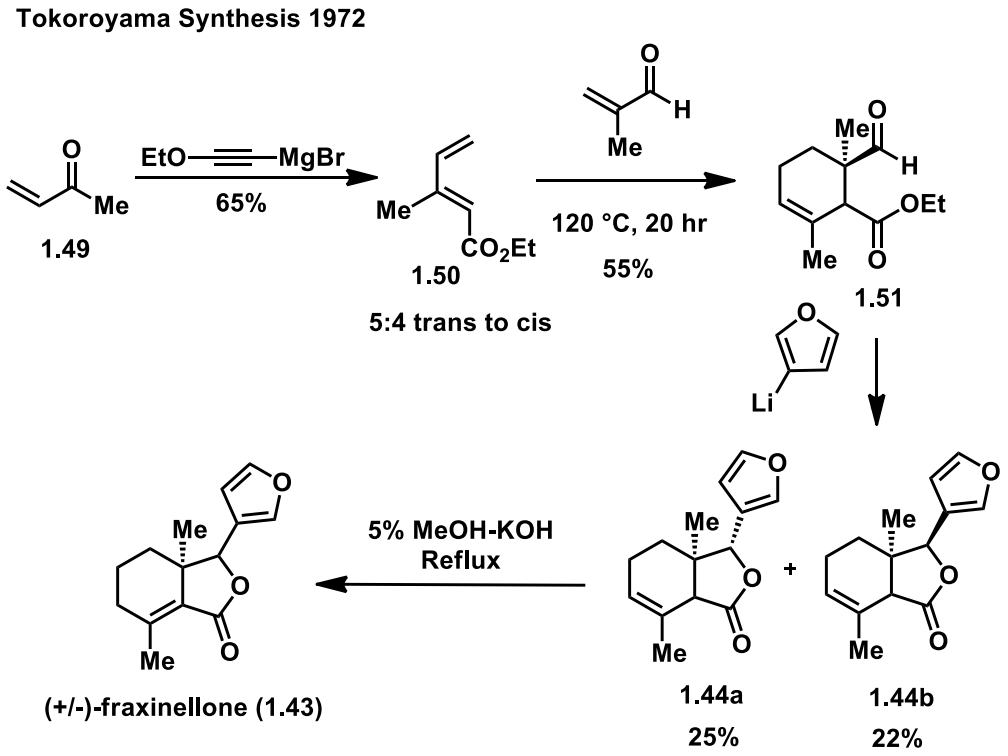

Scheme 1.4 Synthesis of fraxinellone by Tokoroyama in 1972

Despite significant efforts and interest, fraxinellone (**1.43**) and analogs thereof, have never been successfully synthesized in an enantioselective fashion. However, three racemic syntheses have been completed. The first racemic synthesis of fraxinellone (**1.43**) was completed in 1972 by Tokoroyama (Scheme 1.4) and coworkers.[33] Tokoroyama's synthesis is extremely efficient, accessing fraxinellone in only three steps, but it lacks stereocontrol in the installation of the furan moiety through a 3-lithiofuran species. The synthesis begins with methyl vinyl ketone (**1.49**) undergoing condensation with an alkynyl Grignard reagent to generate diene **1.50** in 65% yield. Then, diene **1.50** undergoes a Diels-Alder reaction with methacrolein to access cycloadduct **1.51** in 55% yield. At this point

the furyl moiety and the γ-butyrolactone ring is installed in one step by treatment of aldehyde **1.51** with a 3-lithiofuran species forms an alkoxide intermediate that lactonizes onto the ethyl ester, generating furylated isofraxinellone diastereomers **1.44A/B** in 25% and 22% yield, respectively. Finally, the furylated mixture of isofraxinellone diastereomers **1.44A/B** is isomerized vby refluxing in methanolic KOH to accomplish a racemic synthesis of fraxinellone (**1.43**). The strength of this synthesis lies in the efficiency in accessing fraxinellone, but the shortcomings are the low yield and lack of stereocontrol ontained from the lithiofuran addition.

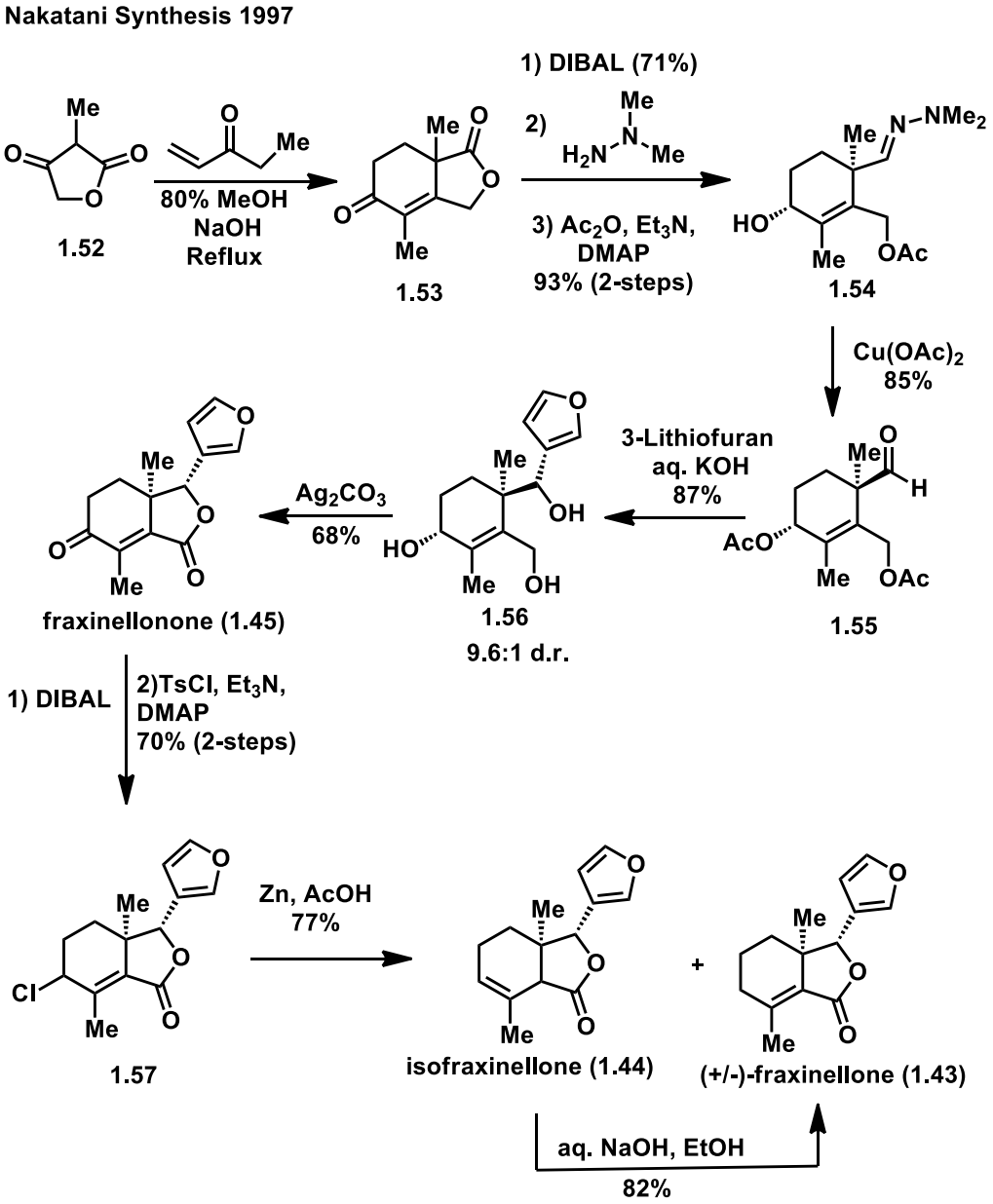

Scheme 1.5 Synthesis of fraxinellone by Nakatani in 1997

The next synthesis of fraxinellone (**1.43**) was completed over twenty years later in 1997 by Nakatani and coworkers (Scheme 1.5).[26] Nakatani's synthesis commences with a Robinson annulation between lactone **1.52** and ethyl vinyl ketone to form the bicyclic scaffold (**1.53**) of fraxinellone. Next, DIBAL-H reduction of oxo-butanolide **1.53**

generated the lactol intermediate as a single stereoisomer (not shown), which was then converted to the hydrazone, ring-opened, and acetylated to give hydrazone **1.54** in 93% yield over 3 steps. Hydrazone **1.54** was then subjected to Corey's Copper (II)-mediated hydrolysis protocol to generate aldehyde **1.55** in 85% yield, which would then react with 3-lithiofuran to install the furan moiety of furyl alcohol **1.56** in 87% yield, similar to Tokoroyama's approach to furan installation. In contrast to the low diastereoselectivity that resulted in Tokoroyama's synthesis, this furylation exhibited good Felkin-selectivity, favoring the desired α-furyl isomer **1.56** in9.6:1 dr. Additionally, the acetyl group was cleaved by hydrolysis in this step. Next, triol **1.56** was lactonized under Fetizon-oxidation conditions with Ag_2CO_3 to provide racemic fraxinellonone (**1.45**) in 68% yield. Subsequently, (+/-)-fraxinellonone (**1.45**) was treated with DIBAL-H followed by tosyl chloride and triethylamine to provide chlorinated intermediate **1.57**. A final reductive dehalogenation is performed using zinc to generate racemic (+/-)-fraxinellone (**1.43**) and isofraxinellone (**1.44**), in which the latter can be isomerized to (+/-)-fraxinellone under basic conditions in 82% yield. Nakatani's synthesis accesses the bicyclic framework of fraxinellone rapidly through the Robinson annulation, but installing the furyl moiety required opening the lactone which requires several additional steps to generate an aldehyde, thus decreasing step economy. However, this sets the stage for the lithiofuran addition, from which point several more steps are required to reform desired lactone, to ultimately arrive at racemic fraxinellone (**1.43**).

The most recent synthesis of fraxinellone was completed in 2005 by Morken and coworkers. This synthesis is unique because the γ-butyrolactone with the furyl substituent and quarternary carbon center was installed early in the synthesis, which is then followed

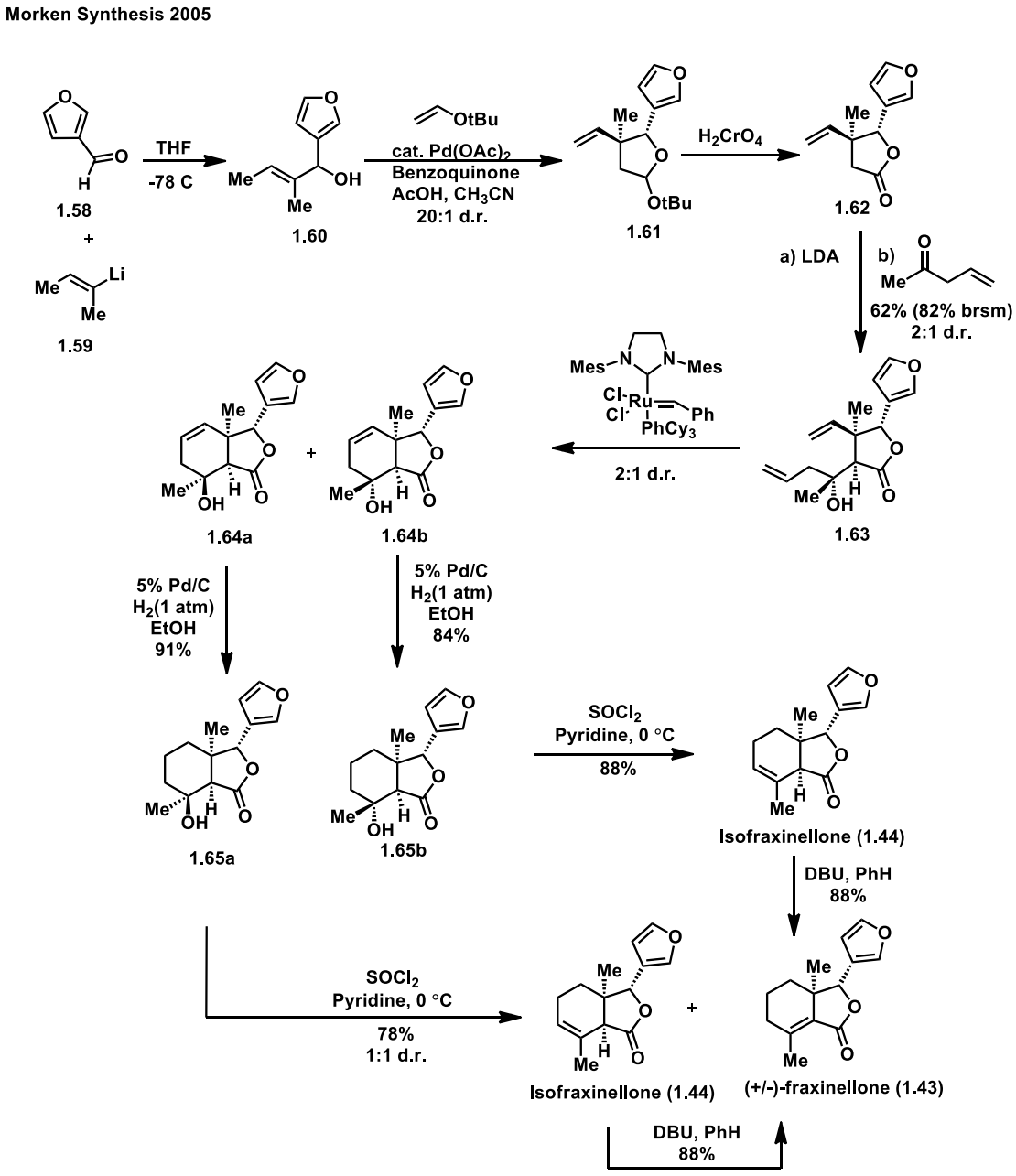

Scheme 1.6 Synthesis of fraxinellone by Morken in 2005.

by the construction of the six-membered ring. The synthesis begins with alkenylithium **1.59** adding to 3-furaldehyde (**1.58**) to produce furyl alcohol **1.60**. Furyl alcohol **1.60** then undergoes an Oshima-Utimoto reaction via treatment with 10 mol% palladium(II) acetate, three equivalents of benzoquinone, and 1.1 equivalents of acetic acid to effect cyclocondensation with tert-butyl vinyl ether to generate cyclic *tert*-butylacetal **1.61**. Following oxidation of **1.61** with Jones reagent to γ-butyrolactone **1.62**, an aldol reaction was performed to access tertiary alcohol **1.63** with modest stereocontrol. Tertiary alcohol **1.63** was then subjected to a ring-closing metathesis (RCM) using Grubb's second-generation catalyst to afford a separable mixture of cyclohexenol diastereomers **1.64a/b**. Each diastereomer was subjected to palladium-catalyzed hydrogenation in 91% and 84% yields to generate saturated cyclohexanol intermediates **1.65a/b**. Subsequently, cyclohexanol intermediates **1.65a/b** were dehydrated with thionyl chloride and pyridine to generate isofraxinellone and (±)-fraxinellone in 78% and 88% yields, respectively. Isofraxinellone is readily converted to (±)-fraxinellone by treatment with DBU in 88% yield. This synthesis highlights the early installation of the furyl moiety, an Oshima-Utimoto reaction to access the γ-butyrolactone scaffold and the efficient ring-closing metathesis using Grubb's catalyst to form the second ring. However, the synthesis lacks stereocontrol in the furylation step which ultimately leads to a racemic fraxinellone (**1.43**).

1.2 Results and Discussion

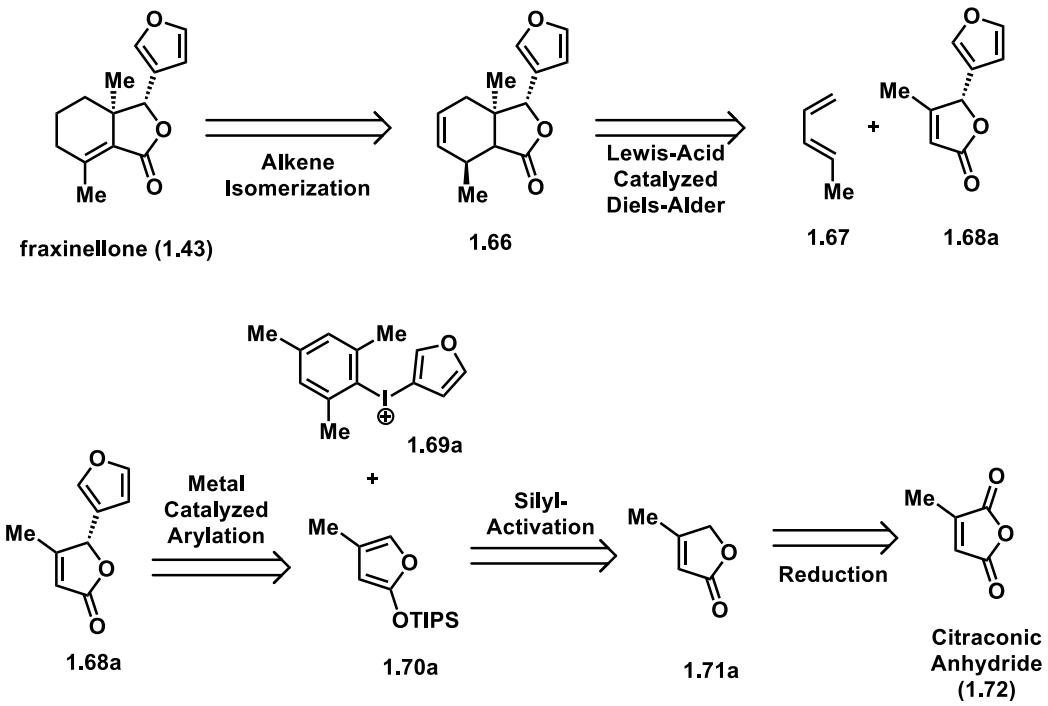

Scheme 1.7 Proposed retrosynthesis of fraxinellone starting from citraconic

The primary goal of this project was to develop an enantioselective chemical synthesis of fraxinellone (**1.43**) through a strategically designed route that would allow opportunities for late-stage derivatization to generate meaningful analogs. The development of an enantioselective synthesis of fraxinellone would not only be a significant synthetic advancement upon previously completed routes, but would also propel us towards our ultimate goal of probing the therapeutic properties and SAR to investigate the mechanism(s) of action to how these molecules achieve neuroprotective activity against glutamate toxicity. Additionally, the findings from SAR studies could influence the synthesis of more potent derivatives through rational and systematic structure design, leading to compounds with enhanced physical and biological properties.

Through a retrosynthetic analysis (Scheme 1.7), we proposed that fraxinellone could be accessed by alkene isomerization from intermediate **1.66**, which in turn could arise through a Diels–Alder reaction between 1,3-pentadiene (**1.67**) and γ-furylated lactone **1.68a**. This Diels–Alder cycloaddition could be catalyzed by heat and/or a Lewis-acid additive. We hypothesize that γ-furylated lactone **1.68a** could be the product of a transition metal catalyzed enantioselective furylation reaction, by coupling silyl-activated butenolide **1.70a** with hypervalent diaryl iodonium **1.69**, an unprecedented reaction. Although there is precedent for coupling reactions with hypervalent iodonium, there are no examples of iodonium couplings with silyloxy furans. More broadly, there is only one low yielding example of a furan coupling reaction, however, it is coupled with an indazole which is a very different electronic system. This arylation reaction between a silyl-activated butenolide and a hypervalent diaryl iodonium constitutes the key step in our proposal which would require the development of novel catalysis methodology. The silyl-activated butenolide (**1.70a)** could be generated from the silylation of β-methyl lactone **1.71a**, which could be prepared from the selective reduction of citraconic anhydride (**1.72**).

The synthetic route proposed here aims to access fraxinellone in an enantioselective manner and allow for facile derivatization opportunities. Specifically, it is our intention to

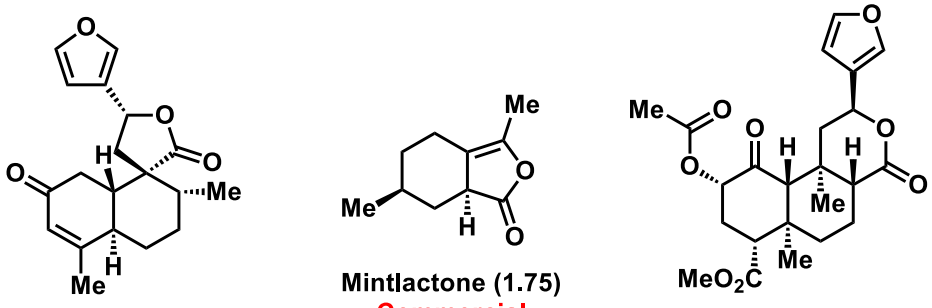

Figure 1.5 Biologically active lactone natural products

access derivatives by varying the silyl-activated butenolide and the diaryl hypervalent iodonium species, so that when coupled together, a library of γ-arylated butenolide products would result. In this work, we synthesized four silyl-activated butenolides and ten diaryl hypervalent iodonium coupling partners. The development of this novel coupling reaction would introduce a new tool with broad utility for synthetic organic chemists to incorporate furyl and other aromatic components, as well as provide the critical stereocontrol required to access fraxinellone. Given the possible permutations of coupling partners, this synthesis route could give rise to a compound library of enantioenriched fraxinellone analogs SAR studies.

We imagined the possibility of this type of reaction to be useful in accessing other biologically active compounds that are of interest to the medicinal and synthetic communities. Butenolides and other lactones are a common class of structural motifs widely distributed in biologically active natural products (Figure 1.5), including the terpene lactones mintlactone (**1.75**) and *trans*-crotonin (nor-clerodane) (**1.73**).[28,34–36] These moieties are also found in other terpenoids such as salvinorin A (neo-clerodane), which exhibits psychotropic activity.[37] Due to the pervasive occurrence of γ-lactones in valuable naturally occurring and pharmaceutically relevant compounds, there is a significant interest in the facile derivatization of butenolides. As a result, many methods for generating substituted butenolides have been reported, including condensations and cross-coupling methods.[38–43] Seminal studies performed by Kang and coworkers in 1997 presented one example of a γ-phenylation using a silylated butenolide and hypervalent iodonium compound, under palladium catalysis, and Buchwald has reported examples of arylation

with aryl halides under more forcing conditions (Scheme 1.8).[44,45] More recently, MacMillan and Gaunt have developed copper catalysed asymmetric α-arylation reactions between aryl iodonium salts and a variety of silylated nucleophiles.[46,47]

Interestingly, Kang and coworkers report a single example of a phenylation similar to our desired reaction that proceeds in good yield at 89%, catalysed by palladium acetate but in the absence of a ligand. It is still presumed that the active catalyst is a palladium (0) species, however it is not explicitly hypothesized as to how the palladium (0) is generated. Additionally, the phenylated butenolide intermediate formed in Kang's chemistry undergoes an isomerization where the α,β-unsaturated phenylbutenolide is converted to the β,γ-unsaturated phenylbutenolide, possibly because the double bond in resonance with the phenyl group is more thermodynamically favourable than with the lactone. Kang and coworkers do not isolate the α,β-unsaturated phenyl butenolide, but only the isomerized product.

In 2011, MacMillan and Gaunt reported very similar α-arylations of N-acyloxazolidinones that utilized a chiral copper catalyst. MacMillan reported an enantioselective arylation reaction between a TBS-protected N-acyloxazolidinone with an unsymmetric mesityl-aryl iodonium-hexafluorophosphate salt catalysed by a copper(I) bisoxazoline complex. Similarly, Gaunt reported an enantioselective arylation reaction between a TMS-protected N-acyloxazolidinone with an unsymmetrical mesityl-aryl iodonium-triflate salt catalysed by a copper(II) bisoxazoline complex. Other than the difference in the iodonium counterion and the copper (I) vs copper(II) precatalysts, the work developed by Gaunt and MacMillan

are very similar, even using the same PhMe$_2$Bis oxazoline ligand. They both developed arylation reactions of N-acyloxazolidinones that proceed in good yields

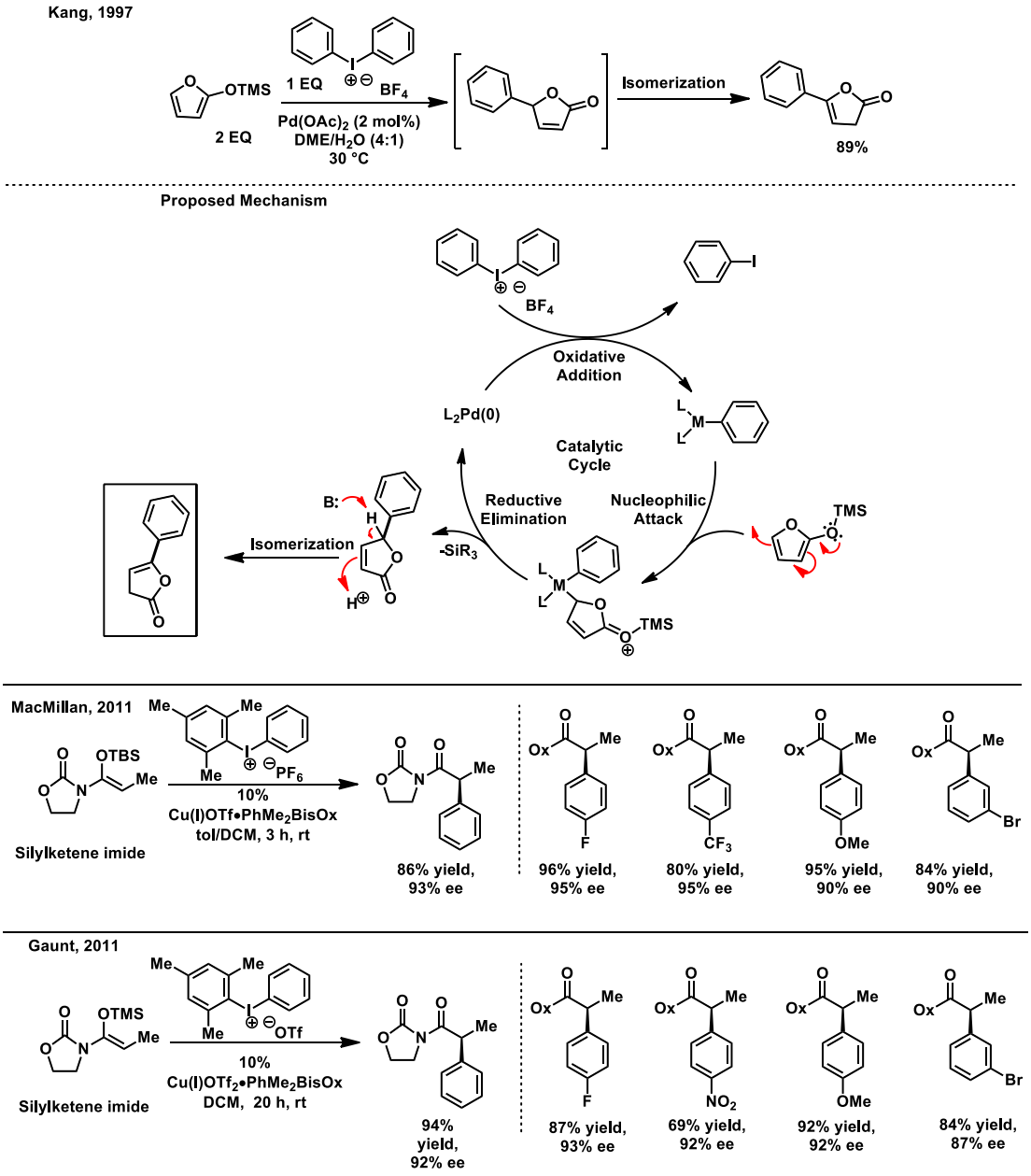

Scheme 1.8 Summary of previous arylation methodology by Kang, MacMillan, and Gaunt.

and ee and allow for a broad scope of electron-rich, electron deficient, bicyclic, and halogenated aryl groups. Additionally, both of these works proceeded with broad

tolerance of alkyl substitutions on the N-acyloxazolidinones. Despite these advances, a general method for the formation of arylated lactones under mild conditions has not been reported. It should also be noted that none of the previous literature precedent or the work to be described here can accommodate halogenated aryl substrates as coupling partners. Instead, a hypervalent iodonium is important to facilitate the oxidative addition of the metal catalyst. The previous literature precedent and the work to be described here build upon the extensive literature

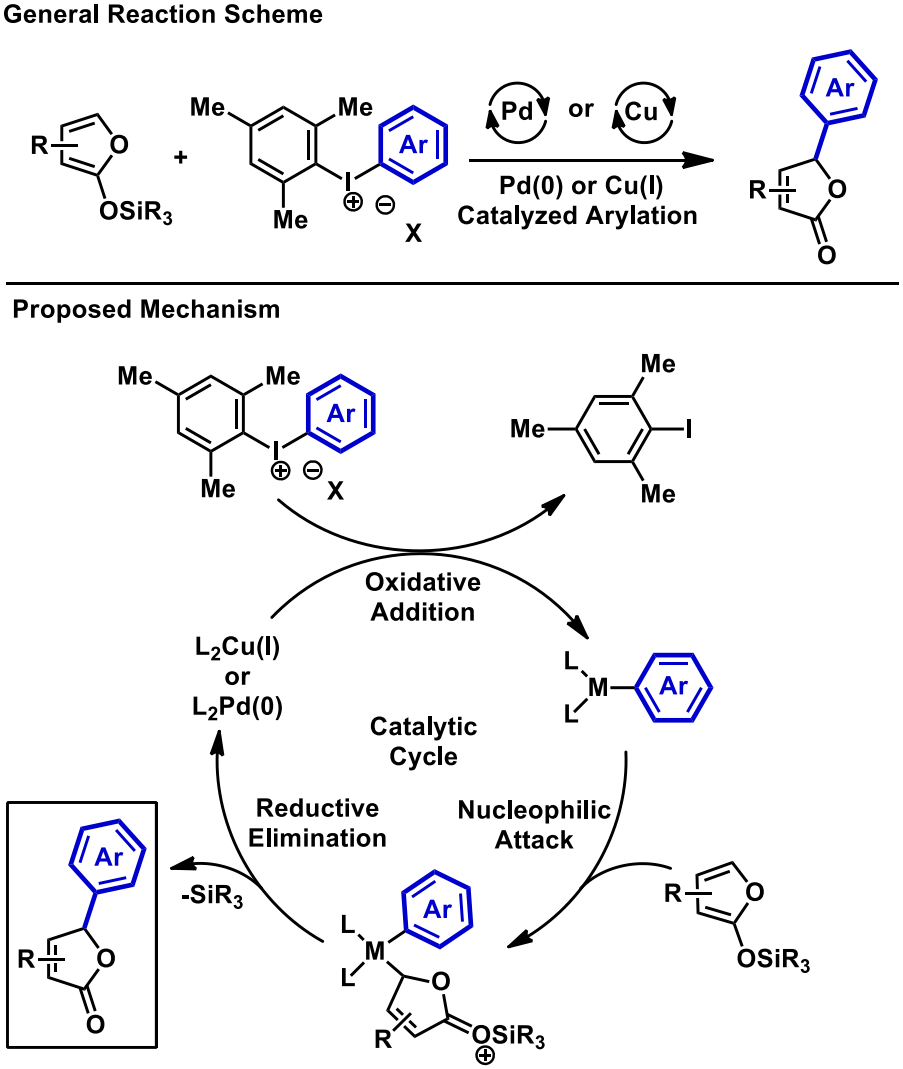

Scheme 1.9 General reaction scheme and proposed mechanism for the silyloxy furan arylation

precedent for the use of hypervalent iodoniums in coupling reactions including work by the research groups of Sarah Reisman and Melanie Sanford.[48–52] Hypervalent iodonium salts are good substitutes for organohalide and organotriflate coupling partners because, although they are not as abundant of a feedstock as halide starting materials, they can be synthesized readily and undergoes oxidative addition to metal complexes much more easily compared to halogen–carbon bonds.

Given our interest in the synthesis of terpene natural products including bioactive lactones, we recognized the potential of a general catalytic arylation reaction to synthesizethe furanolactones present in many members of the limonoid family and other interesting natural products.[3,28,34–36] We therefore sought to develop a transition metal-catalysed reaction to access a variety of aryl butenolides by coupling silyloxy furans and diaryl iodoniums, allowing for the γ-functionalization of the lactones (Scheme 1.9).[49] One anticipated challenge of this chemistry is the potential lability of the newly formed stereocenter that bears a mildly acidic hydrogen, similar to related enolate α-arylation reactions. The use of diaryl iodonium salts would allow for very mild conditions while the use of an activated silyloxy furan nucleophile would facilitate reactivity in the absence of strong base. With these design parameters in mind, we explored two distinct catalytic systems using palladium (0) and a copper (I) complexes for the arylation of silyloxy furans to give γ-aryl butenolides as described below.

Preliminary exploration efforts began with optimization studies using the TBS derivative of silyloxyfuran **1.70a**. We found desilylation of the TBS group to be

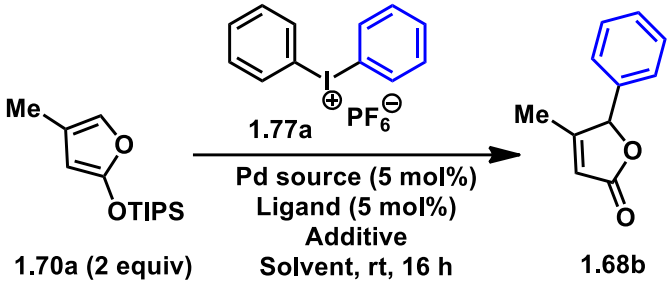

Entry	Pd Source	Ligand	Solvent	Additive	Yield[a]
1	$Pd(OAc)_2$	PCy_3 (10%)	DMA/H_2O	-	8%
2	Pd(COD)	-	DMA/H_2O	-	4%
3	$Pd_2(dba)_3$	PCy_3 (10%)	DMA/H_2O	-	6%
4	$Pd(OAc)_2$	DavePhos	DMA/H_2O	-	20%
5	$Pd(OAc)_2$	dppp	DMA/H_2O	-	9%
6	$Pd(OAc)_2$	dppe	DMA/H_2O	-	21%
7	$Pd(OAc)_2$	dppbz	DMA/H_2O	-	41%
8	$Pd(OAc)_2$	dppbz	THF	-	31%
9	$Pd(OAc)_2$	dppbz	DCE	-	38%
10	$Pd(OAc)_2$	dppbz	DCM	-	39%
11	$Pd(OAc)_2$	dppbz	DCM	NaOMe	19%
12	$Pd(OAc)_2$	dppbz	DCM	AgOAc	19%
13	$Pd(OAc)_2$	dppbz	DCM	LiOAc	21%
14	$Pd(OAc)_2$	dppbz	DCM	NaOAc (0.5 equiv)	55%
15	$Pd(OAc)_2$	dppbz	DCM	NaOAc (0.8 equiv)	80%

[a]Yields determined by ^1H NMR analysis with dibenzyl ether internal standard. Reaction Conditions: Silyloxy furan (2 equiv), diphenyliodonium (1 equiv), catalyst (5 mol%) and ligand (5 mol% for bidentate, 10 mol% for monodentate), and additives (0.8 equiv) in solvent (0.12M).

Table 1.1 Optimization of arylation reaction with diphenyliodonium

especially facile. The TBS-silyloxyfuran could not be purified by column chromatography due to undesireable protodesilylation back to the butenolide starting material, which resulted in a scenario in which the TBS-silyloxyfuran had to be synthesized and used immediately without purification. The extent of the degradation of the TBS-silyloxyfuran was extremely limiting to the optimization efforts and resulted in low or no product formation. Fortunately, after switching to the more resilient silyl-group in triisopropylsilane (TIPS), optimization efforts became more promising.

Early optimization efforts were carried out using silyloxy furan **1.70a** and symmetric diphenyliodonium salt **1.77a** as model substrates by examining various palladium sources, ligands, solvents, additives, iodonium counterions, and temperatures (Table 1.1). Initial conditions were adapted from Kang's singular example, using ligand-free $Pd(OAc)_2$ and a mixed solvent system of DME/H_2O.[44] Under these conditions, the desired product was produced in only 8% yield (Entry 1), but a significant increase in reactivity was achieved using PCy_3 as a ligand (39%, Entry 2). We evaluated different palladium sources such as $Pd_2(dba)_3$ (Entry 3, 6%) and $Pd(COD)(CH_2TMS)_2$ (6%, not shown). We evaluated known palladium (0) sources as well as palladium (II) sources. It was observed that some palladium catalyst crashed out of solution presumably as palladium (0) nanoparticles, indicating that the palladium catalyst suffered from variable stability depending upon the ligand and reaction solvent

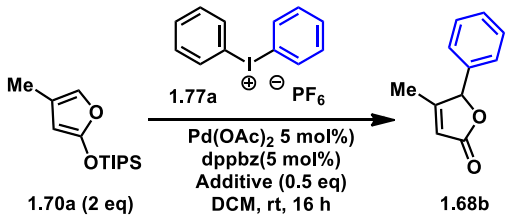

Organic Bases			Inorganic Bases			Metal/Halide Additives		
Entry	Additive	Yield[a]	Entry	Additive	Yield[a]	Entry	Additive	Yield[a]
1	iPr_2NEt	0%	18	$NaHCO_2$	26%	29	KF	11%
2	$N(CH_2CH_2OH)_3$	0%	19	$NaCH2O_3$	3%	30	CsF	11%
3	Pyrrolidine	0%	20	Na_2CHO_3	19%	31	ZnF_2	31%
4	NEt_3	10%	21	NaOHAc	55%	32	Bu_3SnF	1%
5	KOtBu	8%	22	Na_3PO_4	9%	33	Bu_3SnCl	11%
6	NaOMe	19%	23	K_2CHO_3	21%	34	TBACl	2%
7	NaOEt	0%	24	K_3PO_4	25%	35	TBABr	15%
8	NaOtBu	5%	25	K_2HPO_4	9%	36	TBAF	10%
9	DBU	9%	26	KOAc	18%	37	Cs_2CO_3	10%
10	TMEDA	0%	27	Li_2CO_3	12%	38	LiBr	11%
11	BiPy	2%	28	LiOAc	21%	39	LiCl	2%
12	Phenanthroline	5%				40	LiF	44%
13	DABCO	0%				41	$LiBF_4$	9%
14	KOH	3%				42	LiI	25%
15	2,6-lutidine	0%				43	TBAOAc	0%
16	pyridine	1%				44	NMe_4OAc	10%
17	PMP	7%				45	NMe_4NO_3	12%
						46	NMe_4I	0%
						47	CuI	20%
						48	AgOAc	19%
						49	$AgNO_3$	23%
						50	$AgBF_4$	11%

[a]Yields determined by ^1H NMR analysis with dibenzyl ether internal standard. Reaction Conditions: Silyloxy furan (2eq), diphenyliodonium (1eq), catalyst (5 mol%) and ligand (5 mol% for bidentate, 10 mol% for monodentate), and additives (0.5eq) in solvent (0.12M).

Table 1.2 Expanded summary of additives evaluated for the optimization of the arylation reaction with palladium acetate and diphenyliodonium

Unfortunately, neither source effectively catalysed the reaction. Additionally, Pd(II) sources such as Buchwald's 3rd generation precatalysts were

examined with different ligands but offered no advantage.[53] Next, phosphine ligands of various electronic and steric parameters were evaluated, including mono- and bi-dentate phosphines. The monophosphine ligands surveyed included commonly used Buchwald ligands such as DavePhos (20%, Entry 4), JohnPhos (17%) SPhos (20%), and XPhos (15%); however, the best monodentate phosphine

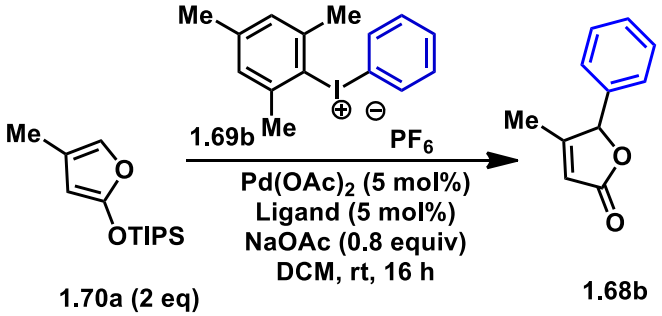

Entry	Ligand	Yield[a]	e.r.
1	P(furyl)$_3$	34%	-
2	P(*o*-tolyl)$_3$	2%	-
3	dppbz	43%	-
4	dppm	2%	-
5	dppe	51%	-
6	dppp	34%	-
7	dppb	8%	-
8	BINAP	61%	-
9	(S)-T-BINAP	50%	44:56 e.r.
10	(R)-SEGPhos	19%	49:51 e.r.
11	(R,R)-Quinox-P	20%	48:52 e.r.
12	(S)-Phox	15%	49:51 e.r.

[a]Yields determined by ^{1}H NMR analysis with dibenzyl ether internal standard. Reaction Conditions: Silyloxy furan (2eq), diphenyliodonium (1eq), Pd(OAc)$_2$ (5 mol%) and ligand (5 mol% for bidentate, 10 mol% for monodentate), and NaOAc (0.8eq) in solvent (0.12M).

Table 1.3 Ligand evaluation with mesityl phenyl iodonium

ligand was found to be PCy_3 (39%, Entry 2). Among bidentate phosphine ligands, dppp (9%, Entry 5) and dppe (21%, Entry 6) did not offer any improvement, but dppbz was found to perform slightly better (41%, Entry 7).

During our early optimization studies, we observed that although there was unreacted iodonium in the crude reaction mixture after 16 h, the silyloxyfuran was consumed, in large part by undesirable desilylation under the reaction conditions.

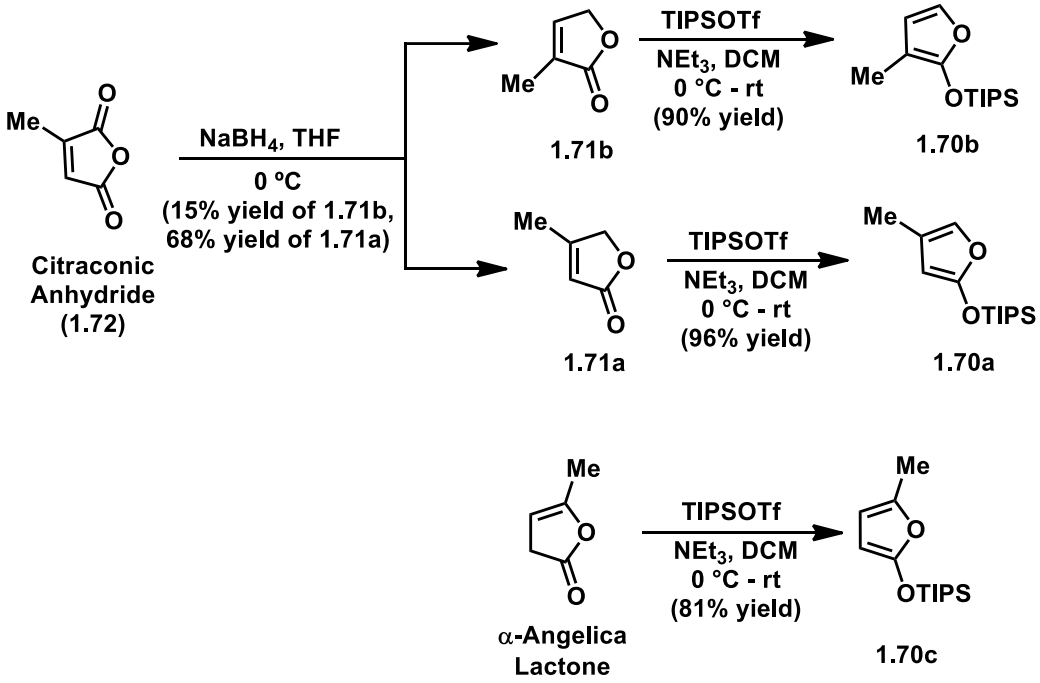

Scheme 1.10 Synthesis of silyloxyfuran coupling partners

Additionally, palladium nanoparticles were routinely observed to precipitate from the reaction mixture. An NMR time study performed by Travis Clay revealed that in the presence of water, full degradation of silyl enol ether occurred within 2 h. To address this, the solvent system was examined in an effort to exclude water as a co-solvent (Table 1.1, Entries 8–10). Upon switching to DCM, it was found that the silyloxyfuran no longer degraded, the reaction time was dramatically decreased, and

the precipitation of palladium was no longer observed. At this point, more than 60 additives were evaluated to improve the yield (Entries 11–15, Table 1.1). It was observed that acetate salts generally outperformed most other types of additives, including other organic and inorganic bases. These extensive optimization efforts led to an 80% yield of butenolide **1.68b** using NaOAc (0.8 equiv) and diphenyliodonium hexafluorophosphate as the limiting reagent. In total, 70 additives were screened in an effort to improve the yield. While still incomplete, a more detailed additive screening table is provided (Table 1.2). In summary, the best conditions developed for this coupling involves 2 equivalents of the silyloxyfuran, 1 equivalent of the iodonium salt, $Pd(OAc)_2$ (5 mol%), dppbz (5 mol%), NaOAc (0.8 equiv), stirring under nitrogen in DCM at room temperature for 16 h.

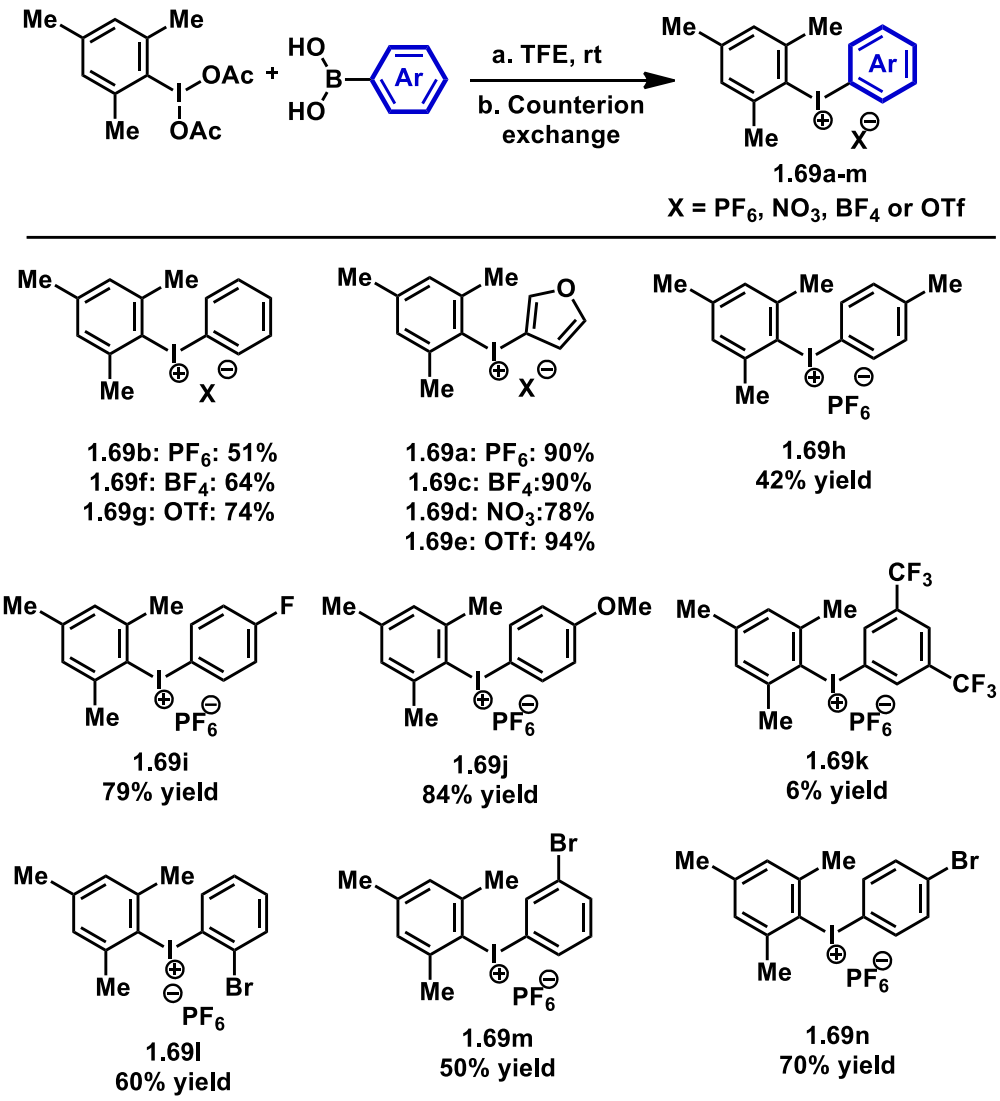

Scheme 1.11 Synthesis of mesityl aryl iodonium salt coupling partners

With optimized conditions in hand for the symmetric diphenyliodonium salt, we investigated the arylation using an unsymmetrical iodonium species to explore the generality of this transformation with other aryl groups.[50] Using (Ph-I-Mes)PF_6, the phenyl group was selectively transferred, generating phenyl butenolide **1.68b** in 43% yield (Table 1.3, Entry 3). Unfortunately, the yield was significantly lower than that in the optimized model system with diphenyliodonium tetrafluoroborate.

Therefore, reoptimization reaction conditions was warranted. We evaluated ligands that were structurally and electronically similar to dppbz, such as dppe and dppp, where the bite angle of the phosphines differ. Further optimization led to a yield of 61% with BINAP (Entry 8). Next, in pursuit of enantioselectivity, chiral bidentate phosphine ligands including (S)-T-BINAP, (R,R)-Quinox-P, and (S)-PHOX were evaluated, however, the observed enantioselectivity was very low (up to 12% ee). The ee is likely so low due to the lability of the γ-proton of the arylated butenolide product therefore resulting in the erosion of any ee generated from the initial carbon-carbon bond formation of this reaction. Indeed, the γ-proton of the arylated butenolide could be more labile than predicted due to the γ-proton being benzylic and thermodynamic driving forces such as deprotonating forming a tri-substituted alkene, forming an aromatic species, and forming a dienolate. All of these factors would render the γ-proton more labile, which could account for why there is such a low degree of ee.

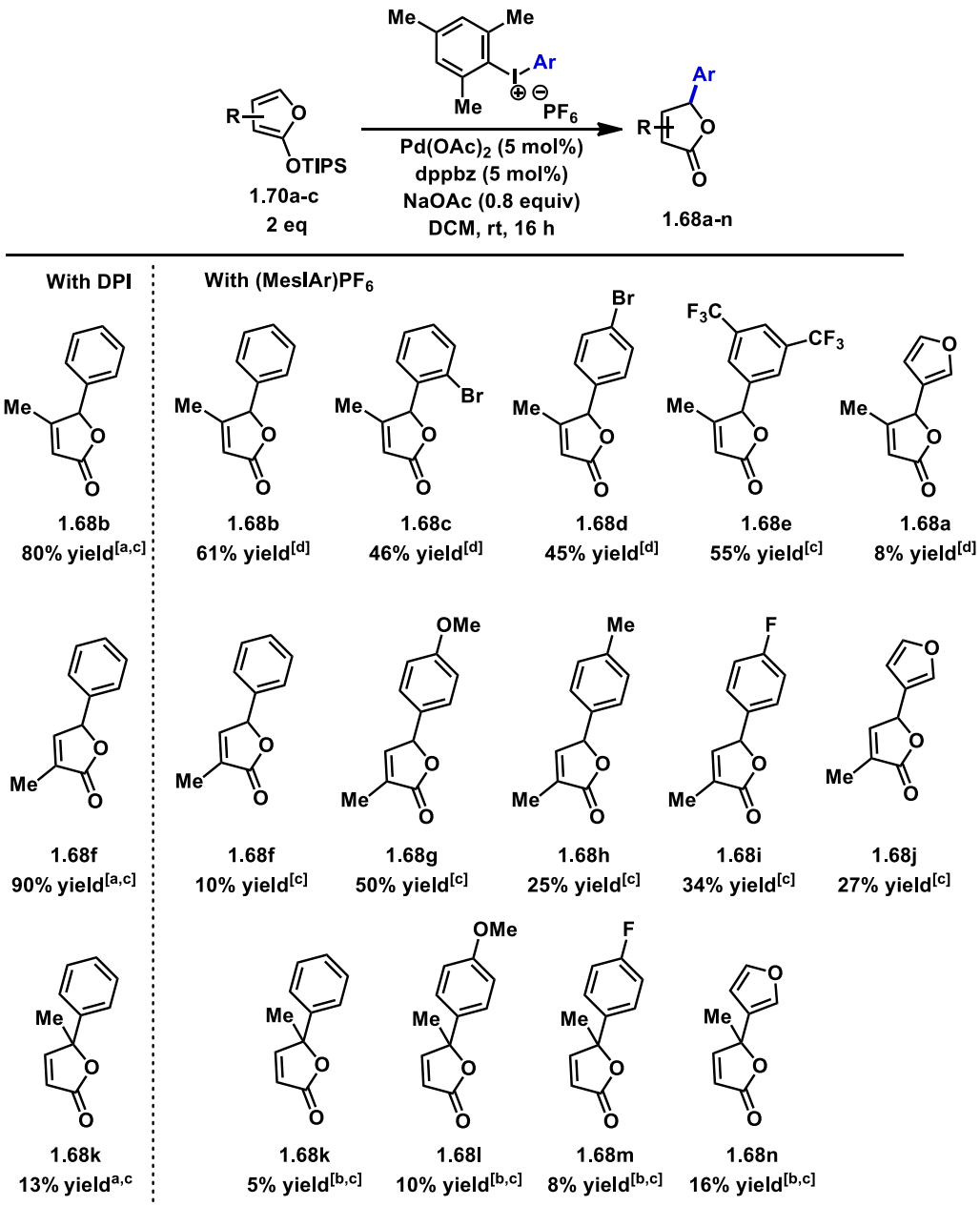

[a]Diphenyliodonium-hexaflourophosphate (DPI-PF_6) used.[b]Yield determined by internal standard.[c]Ligands is dppbz. [d]Ligand is BINAP.

Scheme 1.12 Scope of arylation reaction with palladium catalyst system

With our new optimized conditions in hand, we sought to investigate the scope and tolerance of this novel arylation reaction with various silyloxyfurans and unsymmetrical diaryl iodonium salts. Accessing the three isomeric methyl-

substituted silyloxy furans was accomplished over 1–2 steps (Scheme 1.10). Reduction of citraconic anhydride with $NaBH_4$ gave a 3:7 mixture of α-Me and β-Me butenolides **1.71a** and **1.71b**, which could be separated.[54] Subsequent silylation with TIPSOTf provided the desired silyloxy furans in excellent yield.[55] The γ-substituted silyloxy furan **1.70c** was accessed directly from commercially available α-angelica lactone in 81% yield. The unsymmetrical diaryliodonium salts were most

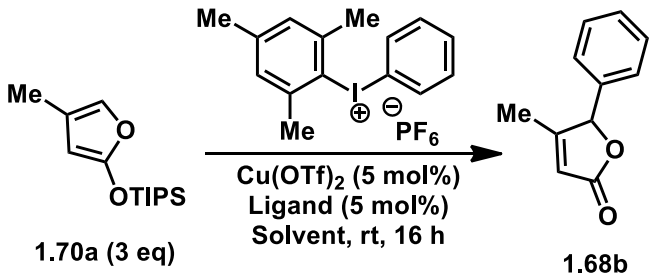

1.70a (3 eq) 1.68b

Entry	Ligand	Solvent	Yield	e.r.
1	None	DCM	0%	-
2	PhBox	DCM	80%	43:57
3	iPrBox	DCM	73%	42:58
4	tBuBox	DCM	0%	-
5	PhBox	EtOAc	22%	n.d.
6	PhBox	Dioxane	0%	-
7	PhBox	Hexanes	0%	-
8	PhBox	Toluene	25%	43:57

Isolated yields, e.r. determined by HPLC.

Table 1.4 Optimization of arylation reaction using copper catalyst system

efficiently synthesized by reacting iodomesitylene diacetate with the corresponding aryl boronic acid (Scheme 1.11), following the ligand exchange strategy reported by Widdowson.[56] The use of TFE as the solvent obviates the need for a strong Lewis

acid, as recently reported by MacMillan and coworkers, and a variety of aryl boronic acids could be employed, including acid- and oxidation-sensitive groups such as

furan (**1.68a–n**).[57] A wide range of aryl coupling partners with different

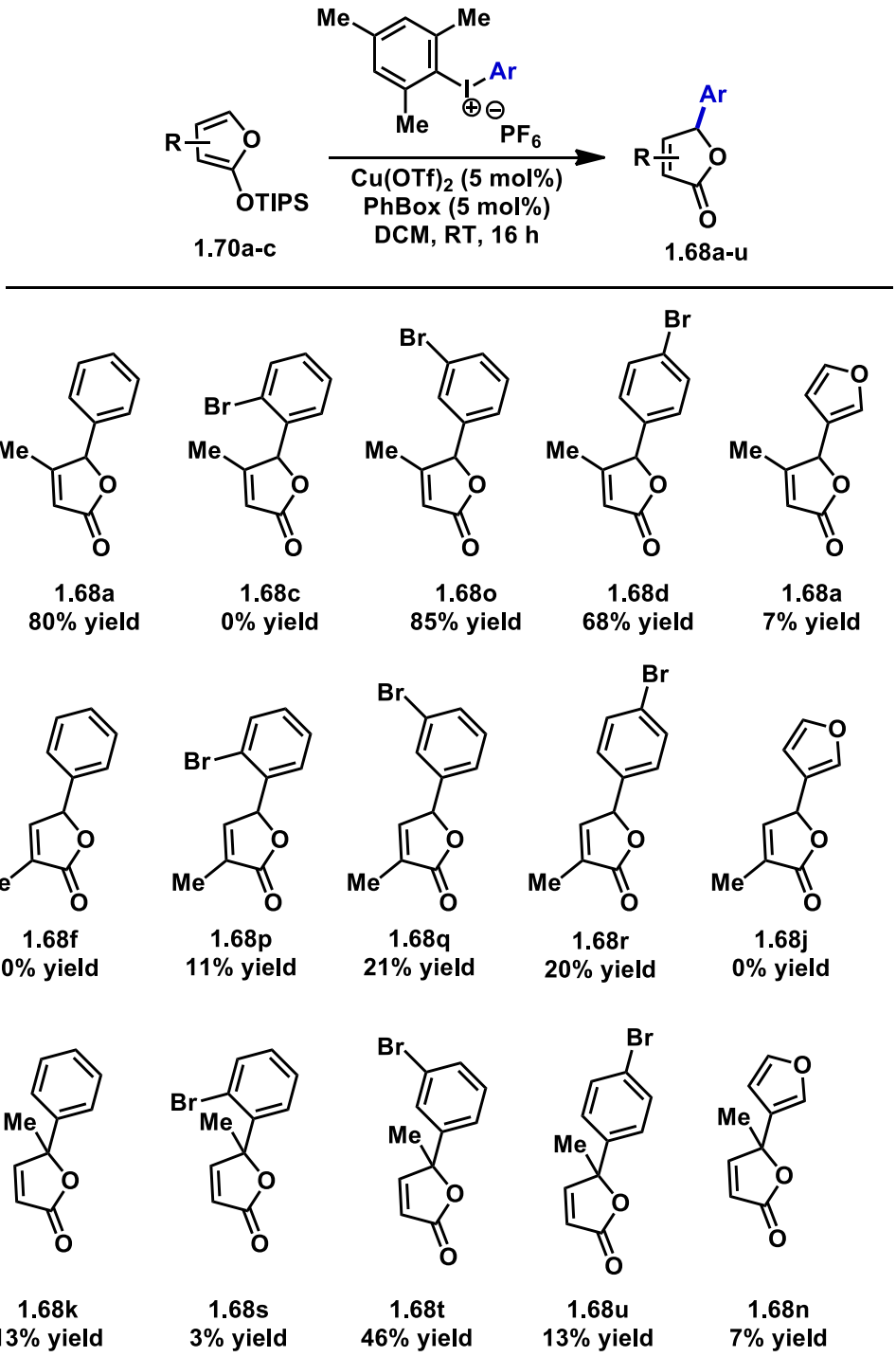

[a] *i*PrBox used as ligand.

Scheme 1.13 Scope of arylation reaction with copper catalyst system.

counteranions were prepared in moderate to high yields, with the exception of bis-CF_3 derivative **1.68e** due to the strong electron-withdrawing effect of the CF_3 groups. As shown in Scheme 1.12, the palladium-catalyzed arylation of β- and α-methyl silyloxyfurans **1.68b** and **1.68f** was efficient using the symmetrical diphenyliodonium salt and dppbz as ligand, at yields of 80% and 90%, respectively. In contrast, the arylation of γ-methyl **1.70c** to generate **1.68k** with a fully substituted quaternary carbon proceeded in only 13% yield. Using unsymmetrical diaryl iodonium salts, a lower 5% yield was obtained. The arylation of the β-methyl silyloxy furan **1.70a** proceeded in 45–61% yields for phenyl and bromophenyl derivatives, including the hindered *o*-bromophenyl **1.68c**. Protodebrominations were not observed under the mild reaction conditions with the remainder of the mass balance attributable to unreacted starting material or protodesilylation. 3-Furylation to produce **1.68a** occured in only 7% yield due to low conversion, undesired side reactions, and rapid degradation of the furylated product. The arylation of α-methyl silyloxy furan **1.70b** also suffered from reduced yields with electron-rich and electron-deficient aryl groups (25–50% yield). The 3-furyl group was transferred with modest efficiency in this case (27%) but isolation was not possible due to degradation of the product upon work up. The reproducibility of the furylation experiments was also inconsistent. Further optimization for mesityl furyl iodonium were pursued, including solvent, ligands and counterions, however, improved yields or reproducibility were not obtained. Furans are well known to be sensitive to oxidation and may be incompatible with oxidizing iodonium salts under these

reaction conditions. The arylation of the γ-methyl silyloxy furan **1.70c** (scheme 1.10) proved difficult as well, providing only low yields of the corresponding butenolide products (1.68k,s,t,u, and n), likely due to steric congestion. Notably, α-arylated products were not observed in any reactions. Overall, it was found that greater reactivity was observed with the less sterically hindered α- and β-methyl silyloxy furans using the palladium catalyst system. The poor yields with more challenging substrates, especially in targeting the synthesis of 3-furyl product **1.68a**, caused us to re-examine our strategy and look for a more efficient catalyst system.

In recent years, several innovative arylation methods have been reported using Cu(I) and Cu(II) precatalysts with various ligand systems.[47,46,58,48,59] Inspired by the precedent of Gaunt and MacMillan, we were pleased to find that $Cu(OTf)_2$ complexed with bisoxazoline ligands could also catalyse the desired arylation reaction (Table 1.4).[46,47] Using the β-methyl silyloxyfuran (**1.70a**) and (Ph-I-Mes)PF_6 **1.69b** as model substrates, the copper catalyst system was optimized with respect to solvent, ligand and other parameters. We observed that $Cu(OTf)_2$ and PhBox (5 mol%) in DCM at room temperature provided optimal reaction conditions, providing an 80% yield, albeit with low enantioselectivity (Entry 2, Table 1.4). Other solvents and ligands did not provide any improvement upon these results (Entries 3–8). Although the chiral catalyst does not effect enantioselectivity, we wondered whether the copper catalyst could influence reactivity compared to the

palladium-catalyzed system. Therefore, the scope of the arylation was investigated using Cu-PhBOX system.

Interestingly, it was found that with the copper catalyst system, the reactivity generally improved for the β-methyl silyloxyfurans **1.70b**, as noted by good yields of the arylation process using the phenyl iodonium (80%, Table 1.13) as well as the *m*-bromophenyl and *p*-bromophenyl derivatives (85% and 68% for **1.68o** and **1.68d**, respectively). This stands in contrast to the palladium catalyst system which showed

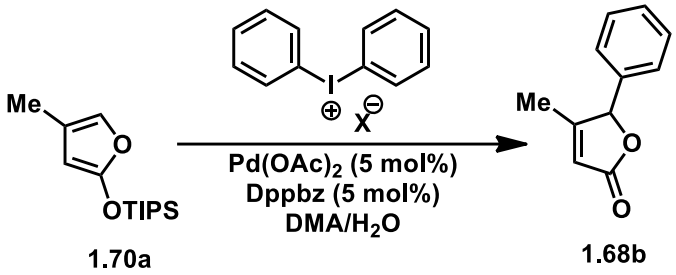

Entry	Ion	Yield (%)
1	PF_6	36%
2	NO_3	34%
3	OTf	32%
4	BF_4	18%

Table 1.5 Evaluation of anion effect on reaction yield using diphenyliodonium with palladium catalyzed system

better reactivity of the α-methyl silyloxyfuran **1.70b**. Again, protodebrominations were not observed with the copper catalyst system. Additionally, although the reactivity of the γ-methyl silyloxyfuran remained quite poor, it was found that there was moderate success using a *m*-bromophenyl iodonium, which provided product **1.68t** in 46% yield. Overall, copper appears to be generally more effective with the

sterically hindered β-methyl-silyloxyfuran partner, and less reactive with the α-methyl-silyloxyfuran. Unfortunately, the variable efficiency of these transformations did not reveal any notable trends and the low yields obtained with furyl iodonium derivatives (7% yield for **1.68n**) hampered further development of this arylation reaction toward the synthesis of furanolactone natural products.

For thoroughness, additional optimization efforts for the general transformation included experimenting with different counterions to the hypervalent iodonium salt for the palladium catalysed arylation with diphenyliodonium. These experiments were

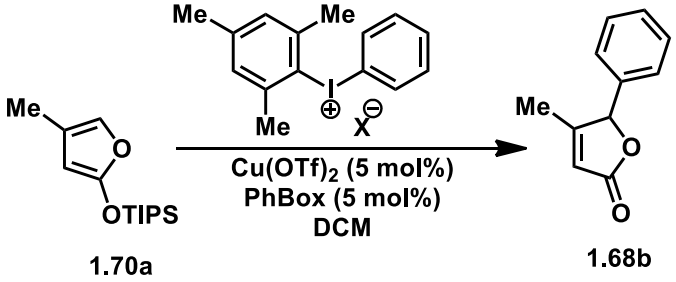

1.70a 1.68b

Entry	Ion	Yield (%)
1	PF_6	80%
2	BF_4	53%
3	OTf	51%

Table 1.6 Evaluation of anion effect on reaction yield using diphenyliodonium with copper catalyst system

performed early in the optimization efforts (Table 1.5), as it was speculated that the choice of counterion could have a profound effect on reactivity, as seen in the related work by Gaunt and MacMillan.[46,47,59] Hexafluorophosphate worked as the counterion giving a 36% yield at this point in the optimization process, while nitrate and triflate

anions provided similar yields at 34% and 32% respectively. The use of tetrafluoroborate as a counterion resulted in significantly lower 18% yield. Similar counterion evaluations were performed for the copper catalysed arylation with the mesityl-iodophenyl coupling partner (Table 1.6). Again, employing hexafluorophosphate as a counterion to the hypervalent iodonium resulted in the best yield at 80%. However, with the copper catalysed system, the counterion of tetrafluoroborate or triflate both resulted in significantly diminished yields of 53% and 51% respectively. Finally, we evaluated various ligands for the copper catalysed arylation with diphenyliodonium. It was found that the PhBox ligand gave the best yield at 63%. *i*PrBox and *t*BuBox did not improve upon the yield, resulting 55% and 53% yields, respectively. It is interesting to note that the conditions for the copper catalysed reaction in Table 1.7 generate a 53% yield at best with diphenyliodonium, but in the optimized conditions the mixed mesitylphenyl iodonium is employed and achieves an 80% yield to generate the same product. It

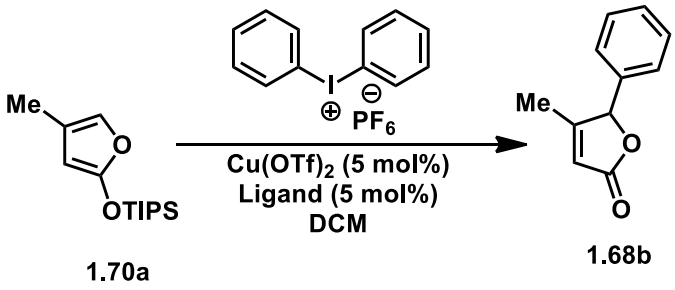

1.70a 1.68b

Entry	Ligand	Yield (%)
1	PhBox	63%
2	IPrBox	55%
3	tBuBox	53%

Table 1.7 Evaluation of bisoxazoline ligands in copper catalyst system.

remains unclear as to why the reaction proceeds better for the phenylation with the mesitylphenyl iodonium reagent than the diphenyl iodonium reagent.

1.2 Furylation Optimization

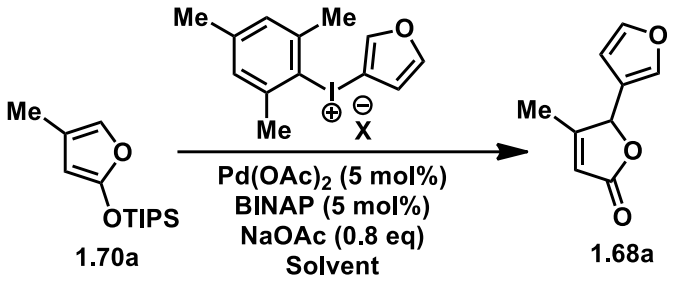

Entry	Counterion	Solvent	Result
1	PF_6	DCM	5%
2	PF_6	DCE	3%
3	PF_6	MeCN	3%
4	PF_6	EtOAc	3%
5	OTF	DCM	0%
6	BF_4	DCM	4%
7	NO_3	DCM	0%

Table 1.8 Evaluation of solvent and counterion for furylation reaction with palladium catalyst

Although the yields of the arylation reactions were not as high yielding as we expected, the most critical problem for the synthesis of fraxinellone was the inability to furylate the β-methyl butenolide. Even in the best scenarios, only trace amounts of the γ-furylation product (**1.68a**) formed, which were not enough to proceed with the synthesis plan. Discouragingly, the trace amounts of furylated product could never be isolated and the yields remained low despite extensive optimization efforts. At this point, we could no

longer improve the overall reactivity of the arylation reactions, so we focused solely on optimizing the furylation reaction, as the furylation was necessary to pursue a synthesis of fraxinellone.

In our efforts to improve the furylation, we revisited all of the previously optimized reaction conditions developed around the phenylations. We began by re-examining the reaction solvent (Table 1.9), screening DCM, DCE, MeCN, and EtOAc. We were cognizant in avoiding alcoholic solvents due to their capacity to desilylate the γ-silyloxyfuran. Unfortunately, each solvent screen resulted in similarly low yields with DCM providing the best yield at only 5% and DCE, MeCN, and EtOAc all generating 3% yields. Additionally, the trace amounts of product could not be isolated due to rapid degradation upon work up and on the silica. Next, we revaluated the counterion to the mesitylfuryliodonium. The mesitylfuryliodonium was resynthesized with various anions including triflate, tetrafluoroborate, and nitrate and then evaluated under the same reaction conditions. Unfortunately, hexafluorophosphate still led to the highest yield of only 5%, while triflate, tetrafluoroborate, and nitrate produced < 5% yields. Tetrafluoroborate's 4% yield was essentially as productive as hexafluorophosphate, but both were still underwhelming results.

Next, we revaluated the ligand for the palladium catalyst system by screening a significant number phosphine ligands with varying degrees of electronic and structural characteristics, including varying bite angles for bidentate ligands (Table 1.9). We

evaluated monodentate ligands, including some that had shown some success with similar optimization work previously carried out such as tricyclohexylphosphine, but none produced encouraging results. Other monodentate phosphines were evaluated, including

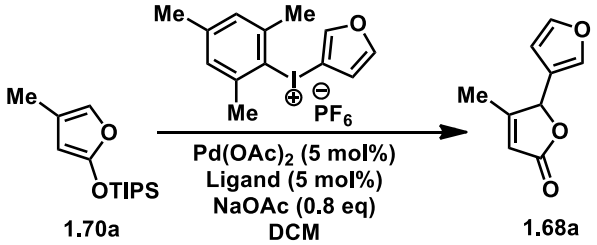

1.70a 1.68a

Entry	Ligand	Result
1	P(furyl)$_3$	6%
2	P(O-tolyl)$_3$	0%
3	dppm	5%
4	dppb	4%
5	dppe	0%
6	dppp	8%
7	DavePhos	3%
8	*t*BuDavePhos	0%
9	PCyPh$_2$	3%
10	PCy$_3$	0%
11	JohnPhos	3%
12	XPhos	4%
13	Dppbz	4%
14	BINAP	3%
15	Quinox-P	4%
16	R-SEGPhos	4%
17	RuPhos	3%
18	DuPhos	3%
19	BozPhos	3%
20	(S)-MeOBIPHEP	4%
21	(S)-2-furyl-MeOBIHEP	3%

Table 1.9 Evaluation of ligands for furylation reaction with palladium

tri(2-furyl)phosphine, tri(o-tolyl)phosphine, DavePhos, *t*BuDavePhos, cyclohexyldiphenylphosphine, JohnPhos, XPhos, RuPhos, BozPhos, and several others, none of which were fruitful. Given the previous success with bidentate dppbz and BINAP in promoting the arylation of the β-methyl silyloxfurans, we evaluated bidentate ligands with various bite angles and electronic characteristics. Unfortunately, altering the bite angle (*e.g.*, dppm, dppe, dppp, and dppb) did not significantly affect the yield. Some chiral

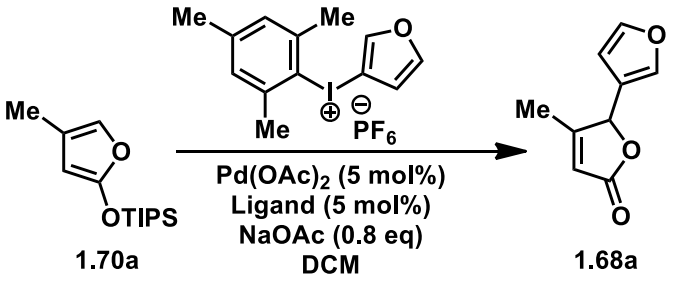

1.70a 1.68a

Entry	Additive	Result
1	NaOAc	4%
2	LiF	0%
3	K_3PO_4	0%
4	$NaCO_2H$	0%
5	AgOAc	0%
6	$AgNO_3$	0%
7	LiOAc	0%
8	K_2CO_3	0%
9	Na_2CO_3	0%
10	LiI	0%
11	TBABr	0%
12	NaOTFA	0%

Table 1.10 Evaluation of additives for furylation reaction with mesityl furyl iodonium with palladium catalyst system

bidentate phosphine ligands evaluated include Quinox-P, ®-SEGPhos, DuPhos, (S)-MeOBIPHEP, and (S)-2-furyl-MeOBIPHEP. The results of this ligand screen were discouraging, as the yield could not be improved and no reactivity trends or patterns could be deciphered to guide ligand selection. A significant effort was devoted to studying ligand effects, but we surmise that only a relatively small subset of ligands were investigated compared to the abundance of ligands that are commercially available. Due to practical considerations and limitations, and the lack of an obvious reactivity trend, we did not elect to pursue further ligand screening. Therefore, given these results, we proceeded to revaluate additives that could help improve the yield.

We were optimistic that re-evaluating additives could lead to improvement in yield because, as discussed previously in the optimization of the phenylation reaction, we found that the use of 0.8 equivalents of sodium acetate improved the yield drastically to 80% (from 17% in its absence). When we revaluated additives (Table 1.1 and 1.2), we focused on those that were promising in the phenylation optimization studies. However, when these additives were investigated in the furylation, no product formation was detected by NMR analysis. Of the fourteen additives presented in Table 1.10., only sodium acetate led to trace amounts of product formation, while the others were ineffective in promoting the desired reactivity. The discrepancy for why similar conditions that were successful for the arylation of the silyloxyfurans essentially were ineffective for the furylation is perplexing. We were unable to force the furylation to proceed in appreciable yields. Although not presented here, we also performed degradation studies, where the mesitylphenyl iodonium

was subjected to each component of the reaction mixture, separately and in every permutation, and then examined for possible degradation. The degradation studies revealed that in fact very minimal degradation, if any, was occurring. Before concluding that the furylation reaction could not be forced under any conditions we could employ, we finally switched to a copper catalyst system as our last resort (Table 1.11). Upon switching to a copper catalyst system, we revaluated conditions developed by Gaunt and MacMillan for use in the furylation reaction.[46,47] We screened copper (I) triflate and copper (II) triflate respectively with bisoxazoline ligands *i*PrBox, *t*BuBox, and PhBox. The best yields came from using copper(I)OTf-PhBox at 8% and copper(II)OTf-PhBox at 10%. The furylated product could not be isolated, presumably due to oxidative sensitivity. Realizing that furylation is a limitation in this newly developed methodology, we could not rely on this

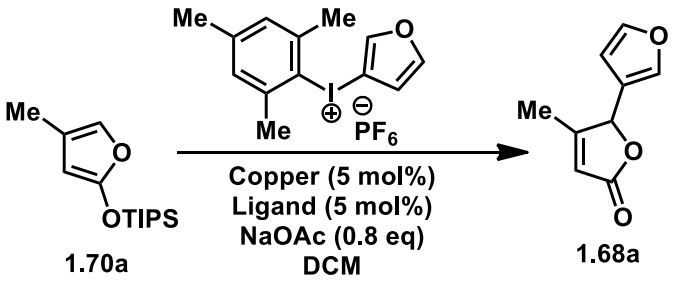

Entry	Catalyst	Yield by NMR
1	Cu(I)OTf-iPrBox	0%
2	Cu(I)OTf-tBuBox	0%
3	Cu(I)OTf-PhBox	8%
4	Cu(II)OTf-iPrBox	0%
5	Cu(II)OTf-tBuBox	0%
6	Cu(II)OTf-PhBox	10%

Table 1.11 Evaluation of copper catalyst systems for furylation reaction

coupling reaction to pursue the synthesis of fraxinellone, therefore, a new synthesis route was envisioned.

In summary, we have developed two transition metal-catalysed arylation methodologies to access aryl butenolides using a palladium or copper catalytic system, both of which provide selective arylation at the γ-position. The main degradation pathway for the silyloxy furan nucleophile, namely protodesilylation, was overcome by the proper selection of reaction solvent and basic additive. In both cases, these reactions occur under mild conditions at ambient temperature and with low catalyst loading. The yields under palladium catalysis are variable with more sterically hindered substrates generally leading to lower yields, in part due to degradation pathways by hydrolysis of the products and silyloxyfuran starting materials. The palladium and copper catalyssts offer complimentary reactivity profiles. Better yields were observed for the α-methyl silyloxyfuran when using a palladium catalyst, while better yields for the β-methyl silylloxyfuran were achieved with a copper catalyst. The arylation reaction outlined here allows for a wide range of electronically and sterically varied aromatic groups to be coupled successfully, although the yields remain low for many substrates including the 3-furyl coupling partner. The development of this reaction provides access to a variety of aryl butenolides that are synthetically interesting due to their incorporation as building blocks in natural products and other interesting biologically active molecules.

1.3 Diels–Alder Experiments

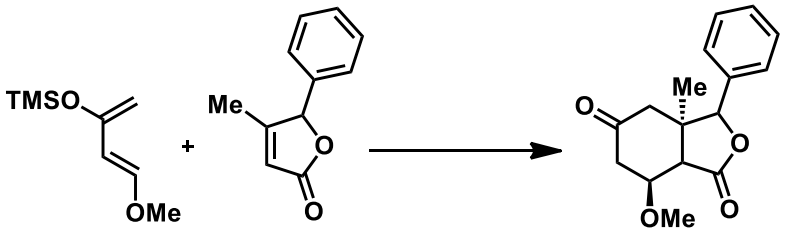

1.78 1.68b 1.79

1.2 equiv

Entry	Additive	Temp.	Solvent	Yield
1	5:1 $AlBr_3/AlMe_3$ 50 mol%	0 °C	DCM	0%
2	10:1 $AlBr_3/AlMe_3$ 50 mol%	0 °C	DCM	0%
3	5:1 $AlBr_3/AlMe_3$ 50 mol%	rt	Toluene	0%
4	5:1 $AlBr_3/AlMe_3$ 50 mol%	120 °C	Toluene	0%

Table 1.12 Lewis acid catalyzed Diels–Alder reaction with phenyl butenolide

As the development of the key novel coupling reaction was underway, we were simultaneously pursuing Diels–Alder experiments in constructing the fused bicyclic core structure of fraxinellone (Table 1.12). We were concerned that this Diels–Alder reaction could be problematic because of the electronics of the arylated β-methyl butenolide scaffold only containing one electron-deficient carbonyl instead of two and the steric hindrance of the methyl group, so we chose to study a more simple model system. To that end, we selected β-methyl phenyl-γ-butenolide **1.68b** that was synthesized using our coupling methodology. The diene we employed for these preliminary studies was

Danishefsky's diene (**1.78**), as it is well precedented as a strongly activated diene for Diels–Alder reactions.[60] Additionally, we would be using Lewis-acid catalysed conditions inspired by work performed by Jung and coworkers, where Diels–Alder reactions were successful in constructing sterically hindered cycloadducts.[61–65] The first two entries in Table 1.12 show the implementation of Jung's conditions for sterically hindered Diels—Alder reactions. The first entry utilizes a 5:1 mixture of aluminium tribromide and trimethylaluminium at 50 mol% catalyst loading at 0 ˚C in DCM, while entry 2 of utilizes a 10:1 mixture of aluminium tribromide and trimethylaluminium at 50 mol% catalyst loading at 0 ˚C in DCM. These conditions mimicked exactly Jung's conditions used for seemingly more sterically hindered adducts, but admittedly more electronically favourable. Unfortunately, neither set of conditions resulted in any detectable product formation by NMR analysis. It was hypothesized that the lack of reactivity may be due to the unfavourable electronics of phenylated butenolide **1.68b** in that it was not activated enough to proceed, so we experimented with elevated temperatures after switching the reaction solvent from DCM to toluene, which has a much higher boiling point. However, at both room temperature and 120 ˚C, no product formation was observed.

Given the lack of reactivity with the β-methylphenyl butenolide (**1.68b**), we hypothesized that the steric hindrance imposed by the phenyl ring may be causing the issue.

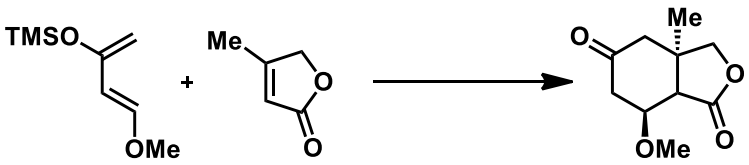

1.78 1.71a 1.80

1.2 equiv

Entry	Additive	Temp.	Solvent	Yield
1	5:1 $AlBr_3/AlMe_3$ 50 mol%	0 °C	DCM	0%
2	10:1 $AlBr_3/AlMe_3$ 50 mol%	0 °C	DCM	0%
3	-	rt	Toluene	0%

Table 1.13 Lewis acid catalyzed Diels–Alder reactions with methyl butenolide

So, in order to test this hypothesis, we attempted the Diels–Alder reaction with the β-methyl butenolide (**1.71a)** because it was structurally and electronically similar to our desired adduct without the furyl moiety installed (Table 1.13). We again evaluated the same reaction conditions (Table 1.13, entries 1 and 2) with the 5:1 mixture of aluminium tribromide and trimethylaluminium at 50 mol% catalyst loading at 0 ˚C in DCM and the 10:1 mixture of aluminium tribromide and trimethylaluminium at 50 mol% catalyst loading at 0 ˚C in DCM . We also revisited elevated temperatures at room temperature and 120 ˚C (Table 1.13, entries 3 and 4). Unfortunately, even with the reduced steric bulk of the phenyl ring, no product formation was observed and only starting material was recovered. Surprised by these preliminary results, we speculated that perhaps it was the methyl group that was hindering this reaction. We found this to be peculiar because there are many

successful examples of more complex and more sterically hindered Diels–Alder reactions, including work by Jung.

To follow up on this hypothesis, we attempted to synthesize the des-methyl phenyl butenolide **1.84** (Scheme 1.14) in order to attempt the Diels–Alder reaction with a butenolide substrate (**1.84b**) lacking the β-methyl but maintaining the phenyl moiety. We began this sequence by performing a Dakin oxidation on 2-furaldehyde (**1.81**), by treatment with hydrogen peroxide, formic acid, and dimethylaminoalcohol in DCM at room temperature for 15 h. Pleasingly, the Dakin oxidation provided butenolide **1.82** in 70%

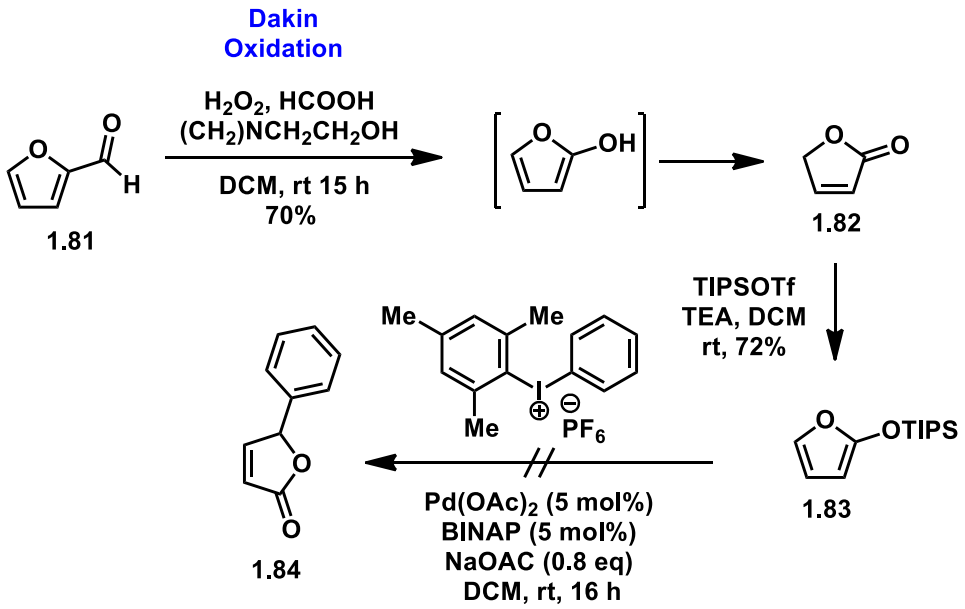

yield. We then silylated butenolide **1.82** by treatment with triisopropylsilyl trifluoromethanesulfonate, and TEA to give the des-methyl silyloxy furan (**1.83**). From here, we attempted to perform a phenylation reaction using our copper-catalyzed arylation reaction to generate nor-methyl phenyl butenolide **1.84**. We employed our best conditions

at the time, using mesitylphenyl iodonium hexafluorophosphate catalysed by $Pd(OAc)_2$ and BINAP and with NaOAc as an additive. Surprisingly, the phenylation of the unsubstituted silyloxy furan **1.83** could not be performed despite being less sterically hindered that other substrates we have successfully arylated, suggesting that the methyl group is necessary for this phenylation to proceed. Further attempts to induce reactivity were unsuccessful. We were finding that the underlying electronic characteristics of the butenolide scaffold may be more complex and critical for reactivity than we had previously surmised.

Unable to synthesize the des-methyl phenyl butenolide **1.84**, we decided to attempt the Diels–Alder with unsubstituted butenolide **1.82** because it was the most simple model

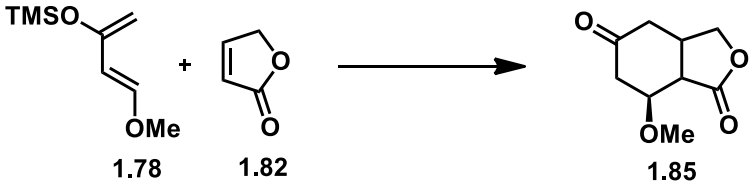

1.2 equiv

Entry	Additive	Temp.	Solvent	Yield
1	5:1 $AlBr_3/AlMe_3$ 50 mol%	0 °C	DCM	0%
2	10:1 $AlBr_3/AlMe_3$ 50 mol%	0 °C	DCM	0%
3	5:1 $AlBr_3/AlMe_3$ 50 mol%	rt	Toluene	0%
4	5:1 $AlBr_3/AlMe_3$ 50 mol%	120 °C	Toluene	0%

Table 1.14 Diels–Alder reactions with unsubstituted butenolide.

system we could conceivably use that would still be a structurally representative system of the desired furyl butenolide that we would need to include to pursue fraxinellone. Unfortunately, when we subjected the unsubstituted butenolide **1.82** to the same Lewis acid catalysed or heat promoted Diels–Alder conditions (Table 1.14), we again saw no product formation by NMR analysis. The lack of reactivity of our butenolide adducts was concerning for our initially proposed synthesis route to fraxinellone, however, as these were only preliminary results, we had planned to explore harsher conditions in forcing the Diels–Alder reaction to proceed, but the insurmountable issues with the furylation reaction ultimately forced us to redesign the synthesis route before the Diels–Alder reaction was explored any further.

1.5 Revised Synthesis Route to Fraxinellone

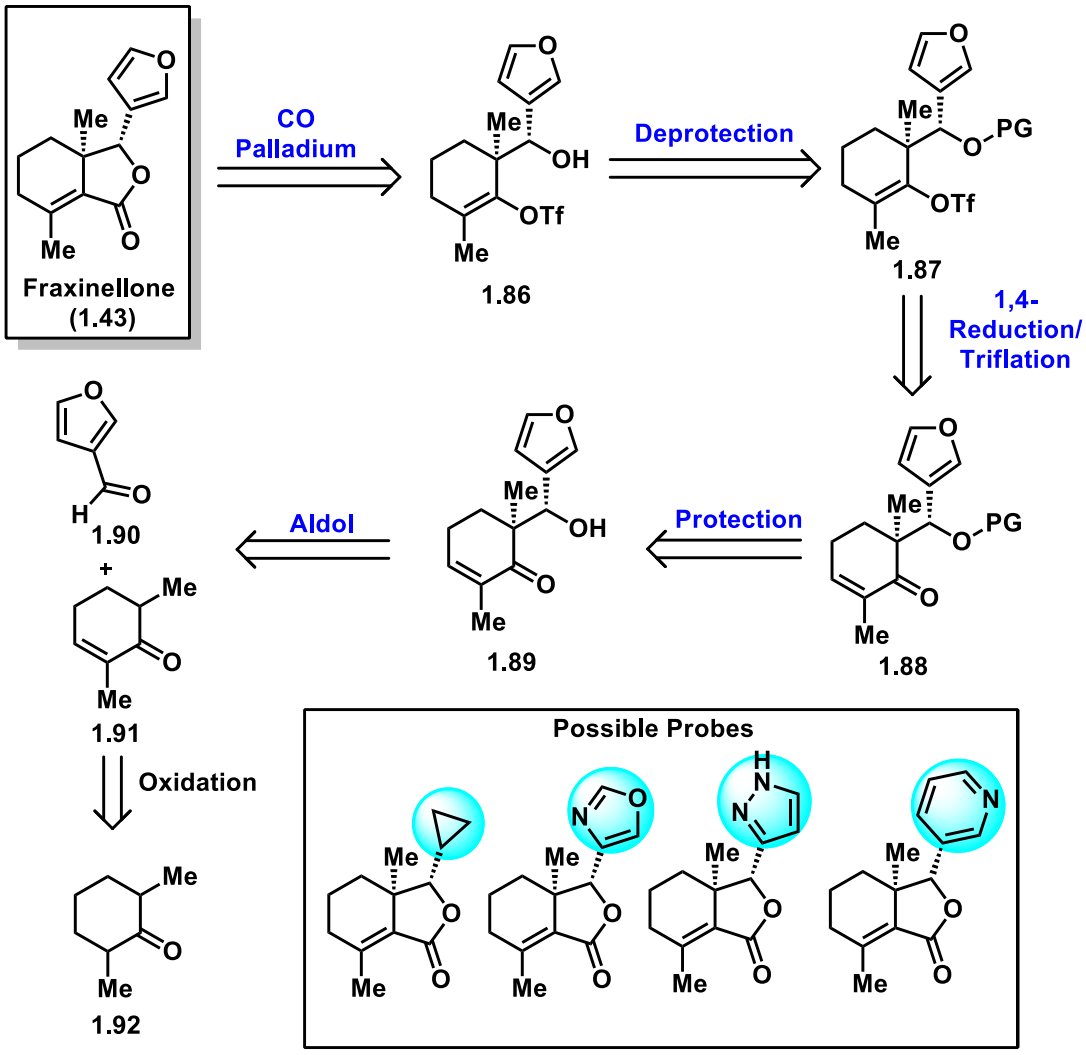

Scheme 1.15 Revised retrosynthetic route to fraxinellone and analogs

Given the realization that the previous synthesis route to fraxinellone was no longer viable because the furylation was unsuccessful, we proposed a new synthesis, presented in Scheme 1.15). Retrosynthetically, we propose to access fraxinellone by disconnecting the lactone ring through a palladium catalysed carbonylation-lactonization reaction from enol-

triflate **1.86**. The enol-triflate (**1.86)** intermediate could be generated from the deprotection of protected alcohol **1.87**, which could in turn be accessed from the reduction-triflation of α,β-unsaturated ketone **1.88**. We anticipated that protecting group manipulations would have to be used in order to mitigate the reactivity of the pseudo-benzylic alcohol. Thus α,β-unsaturated ketone **1.88** could be generated from the protection of alcohol Pseudo-benzylic alcohol **1.89**. Psuedo-benzylic alcohol **1.89** could be formed from a diastereoselective aldol reaction between 3-furaldehyde (**1.90**) and dimethylcyclohexenone (**1.91**). Finally, dimethylcyclohexenone **1.91** could be generated from the oxidation of dimethylcyclohexanone (**1.92**). As with the previous route, we still envisioned being able to access valuable analogues and molecular probes that would allow for the elucidation of the pathogenesis of neurodegenerative diseases through structure-activity relationship

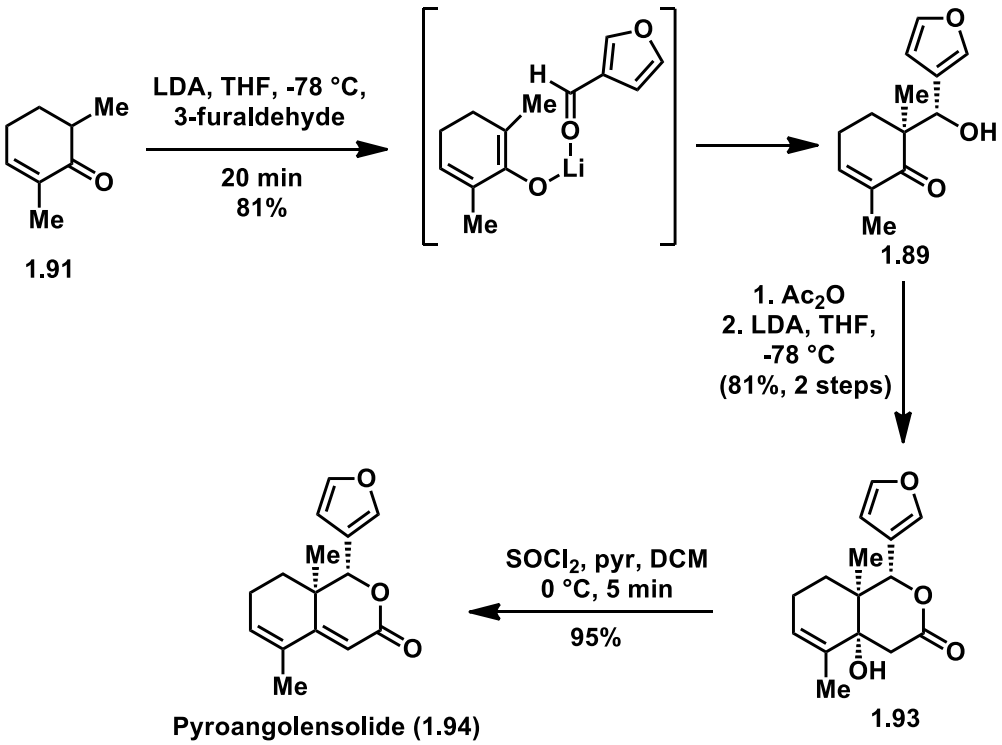

Scheme 1.16 Synthesis route of pyroangolensolide by Fernandez—Mateos.

studies. In this revised route, the most facile step to access analogues would be in the aldol addition step by incorporating the wide pool of aldehyde substrates that are commercially available or easily synthetically accessible.

This revised synthesis route was inspired by a previous synthesis of (+)-pyranglolensolide (**1.94**) by Fernandez–Mateos and coworkers in 1995 (Scheme 1.16).[66] The key step in the Fernandez–Mateos synthesis involves a highly diastereoselective aldol reaction providing a single diastereomer. The diastereoselectivity has been investigated thoroughly and it has been hypothesized that the stereoselectivity arises from a non-bonding repulsion between the cyclohexenic double bond π-orbital and the ring system of the aldehyde, when examined in a Zimmerman-Traxler-type transition state.[67] We noticed structural similarities in the carbon skeletons of fraxinellone (**1.43**) and (+)-pyranglolensolide (**1.93**), where the most significant difference was the 5-membered lactone of fraxinllone's B-ring versus the 6-membered lactone of (+)-pyranglolensolide. Therefore, we proposed utilizing the diastereoselective aldol developed by Fernandez–

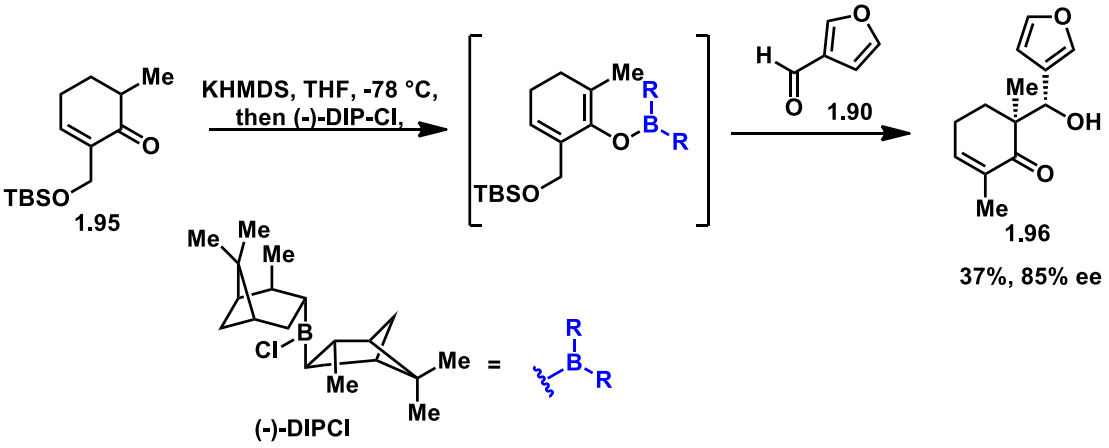

Scheme 1.17 Williams' enantioselective aldol addition using (–)-DIPCl as a chiral Lewis acid.

Mateos and coworkers as one of the key steps in our revised synthesis route to access fraxinellone.

Ultimately, we still maintained our original goal of carrying out an enantioselective synthesis of fraxinellone and generating meaningful analogues for structure-activity relationship studies. In order to make this synthesis enantioselective, we proposed here to use a chiral Lewis acid in the aldol addition step. We are confident that this would be possible based on an anlogous reaction developed by Williams' and coworkers in 2012 (Scheme 1.17).[68] In their reaction, also inspired by the seminal work of Fernandez–Mateos and co-workers, Williams employs a (–)-diisopinocampheyl chloroborane ((–)-DIP-Cl)) as a chiral Lewis-acid to trap the enolate that is formed after deprotonating the α-proton of enone **1.95** by KHDMS. The resulting chiral boron enolate reacts with furaldehyde through an aldol addition, which generate an enantioenriched pseudobenzylic alcohol **1.96** in 37% yield and 85% ee. It is interesting to note that the 37% yield reported by Williams' is much lower than the aldol addition reported by Fernandez–Mateos, which gave an 81% yield. It is unclear if the diminished yield attained by Williams is due to the additional steric bulk of the tertbutyldimethylsilylether at the α'-position of Williams' aldol adduct, enone **1.95** compared to the less sterically demanding methyl group at the α'-position of Fernandez–Mateos' aldol adduct in enone **1.91**, or if the chiral borane Lewis-acid is actually hindering the reaction in terms of yield even though it is imposing an enantioselective bias. Regardless, the literature precedented by both Fernandez–Mateos and Williams provided

the foundation of work that would influence and inspire this revised synthesis route to access fraxinellone enantioselectively.

1.6 Progress of Revised Synthesis Route to Fraxinellone

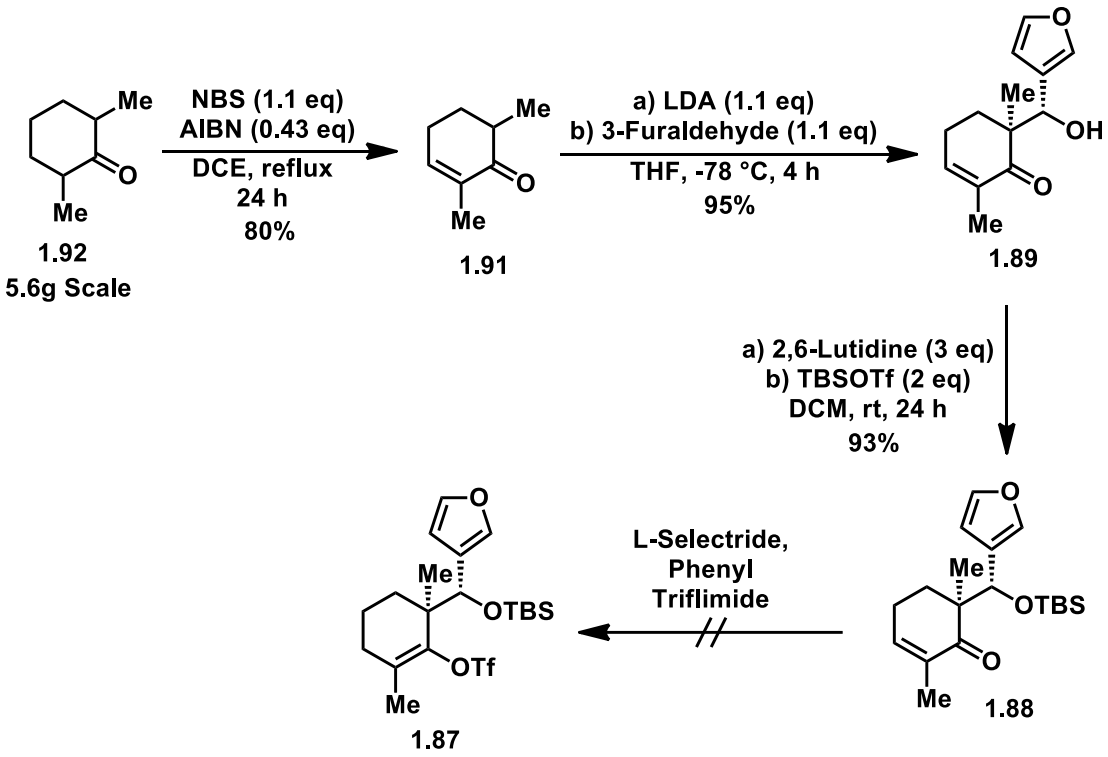

Scheme 1.18 Forward synthesis to fraxinellone through the revised route

The revised synthesis route commences with the oxidation of 2,6-dimethylcyclohexanone (**1.92**) to generate α,β-unsaturated ketone **1.91** (Scheme 1.18). The oxidation proceeds through a radical bromination and then elimination by treatment with NBS and AIBN to provide the α,β-unsaturated ketone (**1.91**) in a satisfying 80% yield. This reaction can be performed on a relatively large scale (6g);, however, there are some practical limitations to this reaction. Firstly, the reaction must be set up carefully in regards

to the number of equivalents of NBS used because of the susceptibility of the α,β-unsaturated ketone (**1.91**) to overoxidation. The overoxidation of α,β-unsaturated ketone **1.91** is problematic it represents a thermodynamically favourable pathway that will ultimately lead to form 2,6-dimethylphenol. NMR analysis of the crude reaction mixture suggests that even at a loading of only 1.1 equivalents of NBS, there is still some overoxidation to the phenolic side-product, which accounts for some of the remainder of the mass balance. Therefore, this reaction could most likely be optimized further by lowering the NBS loading to 1 equivalent or 1.05 equivalents to minimize overoxidation. Fortunately, the phenolic side-product can be easily removed during the work-up procedure by washing the organic layer with 3M NaOH to deprotonate the phenol. The basic wash procedure removes the phenol and allows for relatively straight forward purification by silica gel column chromatography. A second practical limitation to this reaction is that the α,β-unsaturated ketone **1.91** will slowly degrade over time even when stored under nitrogen in below 0 °C. This is particularly problematic because the next step in the synthesis, the aldol addition, is extremely sensitive to impurities. We find that the α,β-unsaturated ketone **1.91** needs to be purified within 24–72 h of being used in the subsequent aldol reaction. The degradation pathway of the α,β-unsaturated ketone **1.91** is likely through polymerization.

The next step in the synthesis is the aldol reaction. Although we eventually intend to perform this reaction enantioselectively by incorporating a chiral borane Lewis acid as previously discussed, we decided to initially perform the diastereoselective aldol addition

in the absence of a chiral Lewis acid to alleviate the optimization efforts of developing an enantioselective reaction. At this point, our primary goal was to rapidly determine if this was a viable route to fraxinellone. If we found that this route did in fact allow us to access fraxinellone, we planned on revisiting the enantioselective aldol conditions. Following this logic, α,β-unsaturated ketone **1.91** is subjected to a highly diastereoselective aldol addition by treatment with lithium diisopropylamide (LDA) and 3-furaldehyde to give pseudobenzylic furyl alcohol **1.89** in 95% yield. It was found that the aldol reaction was extremely sensitive to the degree of purities of the α,β-unsaturated ketone **1.91** and 3-furaldehyde. When the reaction was first attempted, the α,β-unsaturated ketone **1.91** was still reasonably pure, void of significant degradation, and the 3-furaldehyde was newly purchased and also appeared pure by proton NMR analysis;, however, the yield was extremely low as it only gave 13% yield of the pseudobenzylic furyl alcohol product (**1.89**). For comparison, the same reaction performed by Fernandez–Mateos in 1995 (Scheme 1.18) gave an 81% yield.[66] This was a troubling result but fortunately the problem was determined to be most attributed to the purity of 3-furaldehyde. The purity of the α,β-unsaturated ketone **1.91** played a significant role in the success of the reaction, but 3-furaldehyde was much more sensitive to degradation and would much more severely diminish the reaction efficiency, as is evident by the initial 13% yield. The aldol addition reaction was dramatically improved to 95% yield by purifying a fresh bottle of 3-furaldehyde by Kugelrohr distillation and then using it in the next reaction immediately. Unsurprisingly, the key to attaining consistently high yields from the aldol addition was to purify both α,β-unsaturated ketone **1.91** and 3-furaldehyde immediately before using them.

Additionally, the LDA was also prepared in-situ which likely improved the yield over the use of commercially available LDA, although a head-to-head comparison was not performed to evaluate LDA sources. It was also pleasing to be able to attain good reactivity from the aldol addition reaction because this is the step that we intended to perform enantioselectively if it is found that this synthesis route is a viable way to access fraxinellone.

The silylation of pseudobenzylic furyl alcohol **1.89** in the next step by treatment with 2,6-lutidine and TBSOTf proceeded smoothly, providing a high yield of 93% of siloxy-enone **1.88**. The use of a protecting group was necessary to mask the reactivity of the free alcohol during the triflation step that would follow. However, the choice of protecting group was scrutinized when we finally ran into reactivity issues in the following attempts to install the vinyl triflate for the key carbonylation reaction. We had hoped to install the vinyl triflate by first treating siloxy enone **1.88** with L-Selectride to achieve a 1,4-reduction of the α,β-unsaturated ketone by hydride attack at the β-position, which forms an enolate *in situ* that would then be trapped as the vinyl triflate by treatment with phenyltriflamide. However, over the course of optimizing this reaction, we encountered highly unusual and unexpected reactivity that required extensive investigation.

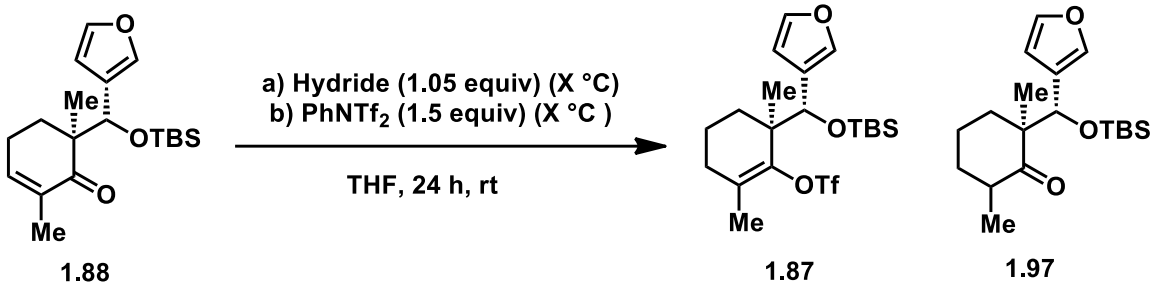

Entry	Temp.	Hydride Source	Triflate:Ketone
1	-78 °C	L-Selectride	0:0
2	-40 °C	L-Selectride	0:100
3	0 °C	L-Selectride	0:100
4	23 °C	L-Selectride	0:100
5	50 °C	L-Selectride	0:100
6	0 °C	K-Selectride	0:100

Table 1.15 Evaluation of temperatures and hydride sources for the 1,4-reduction/triflation sequence

Initial efforts to perform the 1,4-reduction/triflation of siloxy enone **1.87** (Table 1.15) began with evaluating temperature and hydride sources. We had originally thought that this reaction would proceed more efficiently at low temperatures due to literature precedent relating to 1,4-reductions so we began our experimentations at –78 ˚C for the reduction as well as the triflation (Table 1.15, entry 1—3). Unfortunately, we only observed the siloxy ketone **1.97**, suggesting that the 1,4-reduction was proceeding as desired to form the enolate, but the triflation was not occurring and the enolate simply protonated to form the corresponding ketone. Given the lack of reactivity in the triflation step, we experimented with increasing temperatures at -40 ˚C, 0 ˚C, 23 ˚C, and 50 ˚C. Unfortunately, each temperature condition tested resulted in formation of the siloxy ketone **1.97** exclusively. We also tried to use K-Selectride instead of L-Selectride in case the

counterion was important to the reactivity, but still only the silylketone **1.97** was synthesized. We never observed even trace formation of the desired vinyl triflate. Since the 1,4-reduction was proceeding well, indicated by the predominant recovery of the siloxy ketone **1.97**, we decided to continue optimization of this reaction starting from the siloxyketone. We had hoped that once we were able to find optimal conditions for the triflation step, we could revisit the one-pot 1,4-reduction/triflation to eliminate a step in the synthesis. The 1,4-reduction of the siloxyenone (**1.88**) by treatment with L-Selectride generated the corresponding siloxyketone **1.97** in 85% yield, allowing for the generation of plenty of material to develop the triflation conditions (Scheme 1.19).

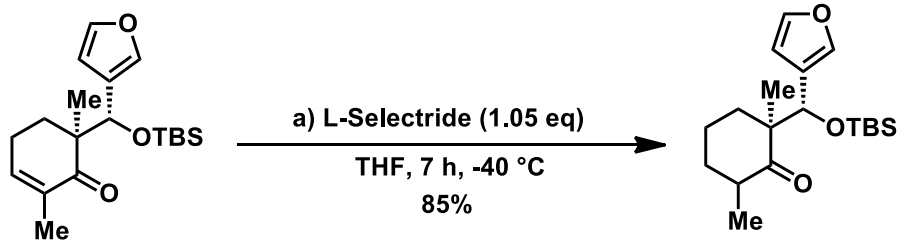

Scheme 1.19 1,4-reduction of TBS-Ketone **1.88** by L-Selectride

We reinitiated our triflating experiments with the siloxy ketone (**1.97**) by exploring different bases and triflating agents (Table 1.16). In these experiments, we hoped to form the enolate by deprotonation of the α-proton and then treatment with a triflating agent to trap the enolate as a triflate. We began by employing the most commonly used triflating agents: phenyltriflimide, Comin's reagents and triflic anhydride. Unfortunately, none of these triflating agents resulted in product formation. Triflic anhydride was evaluated because it was a smaller, highly reactive triflating agent that has been commonly used to

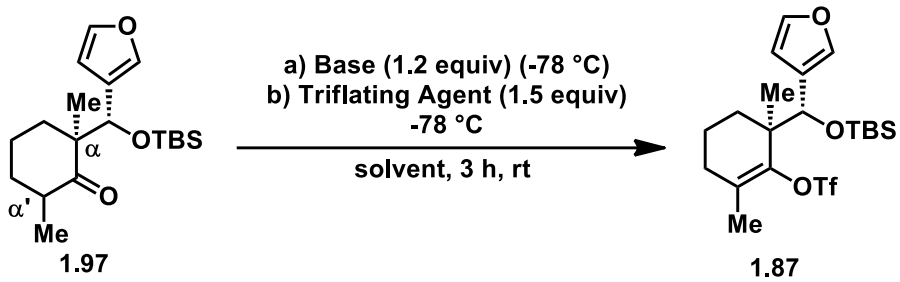

Entry	Base	Triflating Agent	Solvent	Result
1	KHMDS	$PhNTf_2$	DCM	0%
2	KHMDS	Comin's Reag.	DCM	0%
3	KHMDS	Tf_2O	DCM	0%
4	LiHMDS	$PhNTf_2$	DCM	0%
5	NaH	$PhNTf_2$	DCM	0%
6	KHMDS	$PhNTf_2$	THF	0%
7	KHMDS	$PhNTf_2$	MeCN	0%
8	KHMDS	$PhNTf_2$	Dioxane	0%
9	KHMDS	$PhNTf_2$	Et_2O	0%
10	KHMDS	$PhNTf_2$	Toluene	0%

Table 1.16 Evaluation of triflating agents, bases, and solvents for the 1,4-reduction/triflation sequence

synthesize vinyl triflates from ketones, including recent work by Nelson and coworkers.[69a] We also evaluated LiHMDS and NaH as bases to form the enolate, but neither were successful. Next, we experimented with the solvent (Table 1.16), while still using phenyltriflimide as the triflating agent. We evaluated THF, MeCN, dioxane, diethyl ether, and toluene, all obtained dry from a solvent dispensary system. Unfortunately, none of the solvents evaluated led to product formation.

Throughout our unsuccessful efforts to install the vinyl triflate, we hypothesized that the lack of reactivity was due to the large steric bulk of the TBS protecting group.

Additionally, we hypothesized additional steric hindrance from the quaternary carbon at the α-position and the methyl group at the α'-position (Table 1.16). Furthermore, there would presumably also be a potassium cation from the KHMDS also coordinated to the enolate. Each of these steric hinderances effectively make for an extremely crowded enolate oxygen, such that the triflating agent cannot approach in a reactive fashion. To this effect, we explored the possibility that perhaps we were not able to even deprotonate the

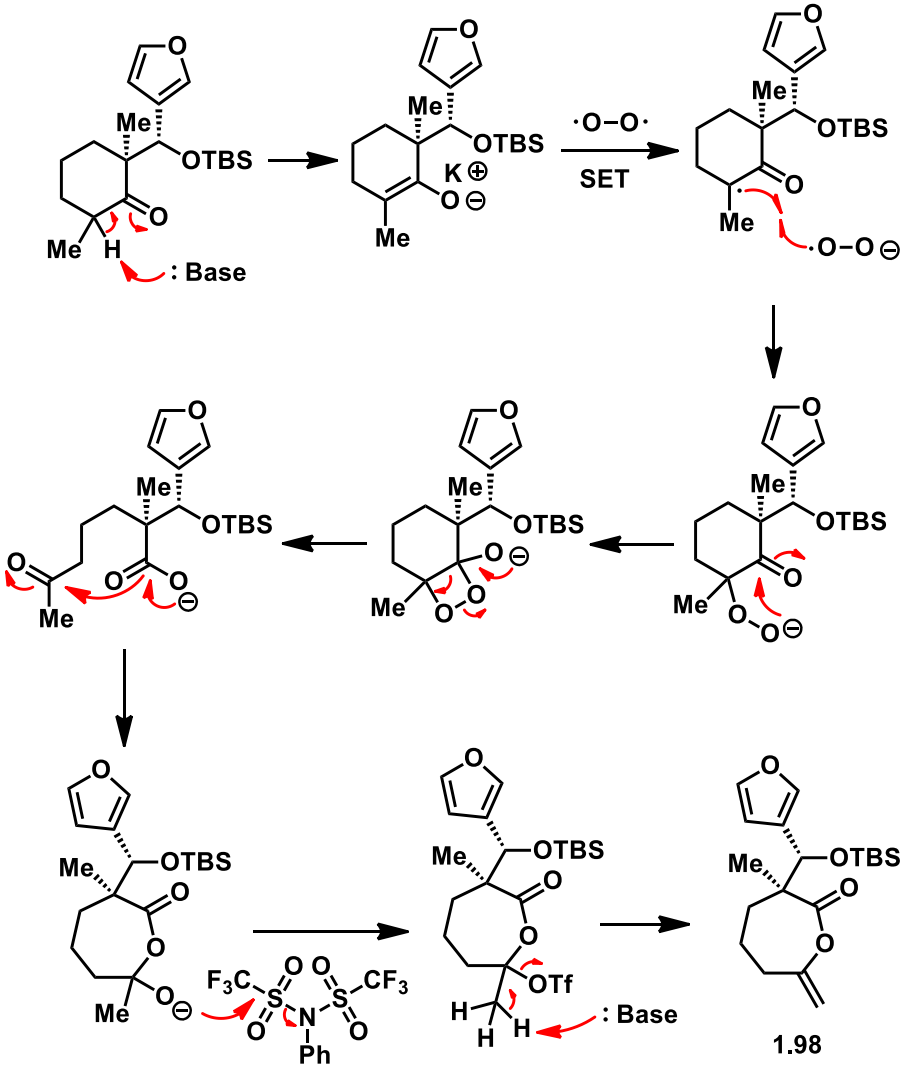

Figure 1.6 Proposed mechanism for the formation of side product from the triflation reactions based on HRMS and NMR analysis

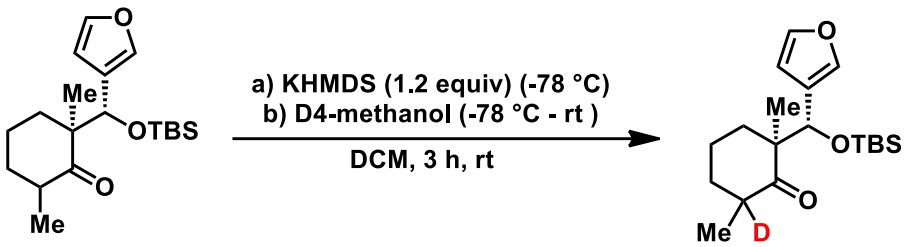

Scheme 1.20 Deuterium quenching experiments to explore deprotonation of ketone

α-proton due to this steric bulk, and therefore not forming the reactive enolate necessary for the triflation. To experimentally assess whether enolate formation was occurring, we performed a deuterium quenching experiment to confirm that we were in fact deprotonating the α-position despite the formidable steric bulk of the substrate (Scheme 1.20). To perform the deuterium quenching experiment, we simply treated the siloxyketone **1.97** with KHMDS and then quenched the reaction mixture with deuterated methanol. We observed by proton NMR analysis the disappearance of the proton at the α-position, indicating that the α-proton in the reaction mixture was deuterated during the quenching process.

An interesting observation that was made during the triflation attempts was that reactions with KHMDS and phenyltriflimide in DCM, THF, Et_2O, or toluene would lead to the production of an unknown side-product in varying degrees (Figure 1.6). Under some conditions, this mysterious side-product was predominantly formed. After fully characterizing the side-product by 1D and 2D NMR and HRMS analyses, we tentatively assigned the side-product to be macrocyclic lactone **1.98**. This structure is most consistent with the spectral data that we have acquired. This side-product could result from the enolate formed *in situ* reacting with triplet oxygen to form a dioxetane intermediate that decomposes to generate a carboxylate and methyl ketone that then lactonize to form a

tertiary alkoxide. The tertiary alkoxide could then be triflated and then eliminated most like through an E1 mechanism (carbocation intermediate not shown) to afford the observed macrocyclic side-product **1.98**.[69b]

Given the consistent generation of this undesired macrocyclic lactone **1.98**, we continued to pursue the triflation while also trying to minimize the production of this side-product. Our next idea was to try to render the enolate more reactive so that it may be able to overcome the steric bulk all around it and proceed through a productive pathway rather than the evidently more favorable lactone **1.98** formation. To this end, we decided to use 18-crown-6 as an additive to sequester the potassium cation away from the enolate to expose a naked enolate that would in theory be less sterically hindered and therefore more

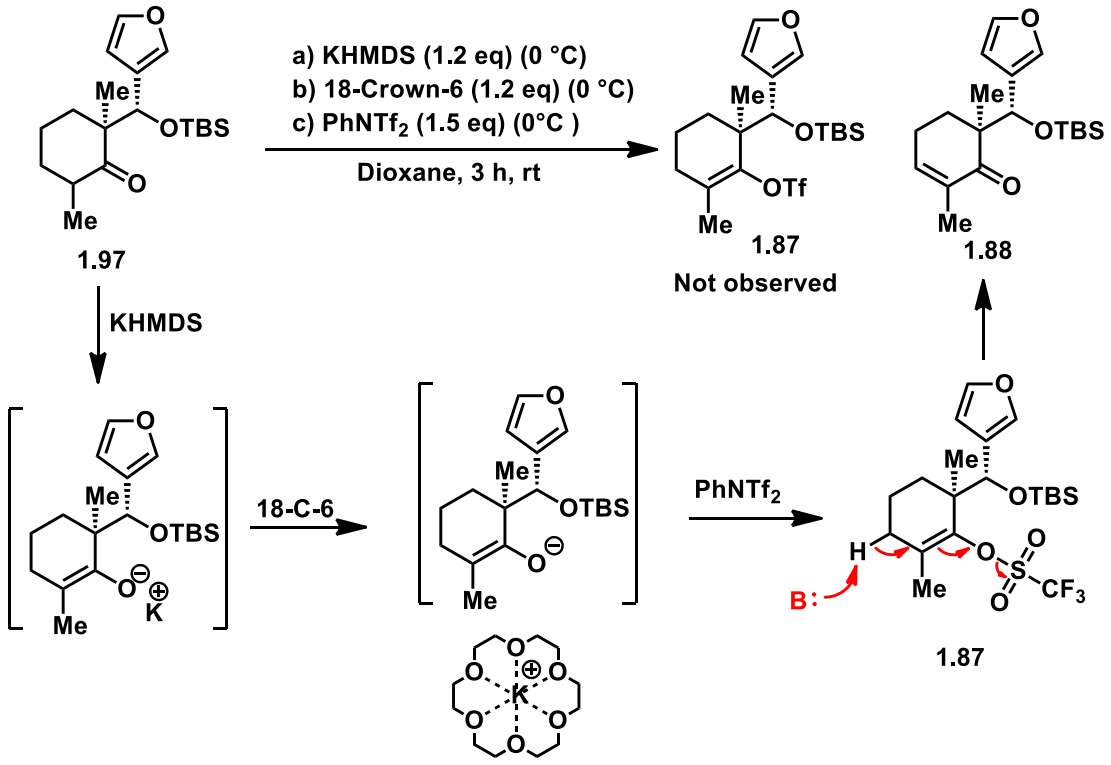

Scheme 1.21 Results and proposed mechanism of triflation reaction with 18-crown-6 as an additive

reactive. This series of experiments generated very interesting and unexpected results that are illustrated in Scheme 1.21. The reactions were set up by treating siloxy ketone **1.97** with KHMDS at 0 ˚C to form the potassiated enolate, and then adding 18-crown-6, still at 0 ˚C, to sequester the potassium cation. Once we had presumably generated the naked enolate, we added phenyltrilimide was added. We were very surprised to see that we had cleanly generated α, β-unsaturated ketone **1.88**, the very same enone from that we initially performed the 1,4-reduction on to generate siloxy ketone **1.97**. This was a perplexing result, but it did however give us some hope for this transformation because the plausible mechanistic pathway traversed through our desired product. We proposed that after formation of the naked enolate, the addition of phenyltriflimide leads to the formation of our desired vinyl triflate **1.87**. Unfortunately, we propose that the viny triflate **1.87** is possibly a transient species that is rapidly deprotonated at the β-position to reform the α,β-unsaturation and reform the ketone and simultaneously ejecting a triflinate anion. We followed up on these unexpected results by experimenting with various temperature profiles to try to prevent the elimination of the triflinate anion but all attempts were unsuccessful.

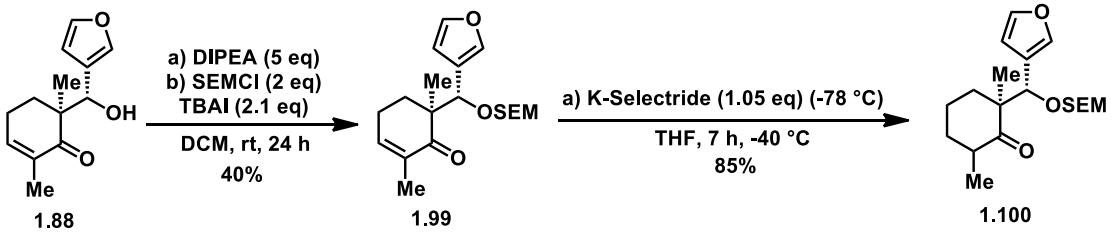

Scheme 1.22 Synthesis of SEM protected ketone starting from furyl alcohol **1.88**

Given the intriguing, although undesirable results from triflation attempts with 18-crown-6 additive, we decided to switch protecting groups from tertbutyldimethylsilyl to a [2-(trimethylsilyl)ethoxy]methyl acetal (SEM). We made this change to a SEM protecting group to reduce the steric bulk of the enolate which we hoped would result in better reactivity. Unfortunately, the SEM protection of furyl-alcohol **1.88** did not proceed efficiently when treated with DIPEA, SEMCl, and TBAI to generate 40% yield,

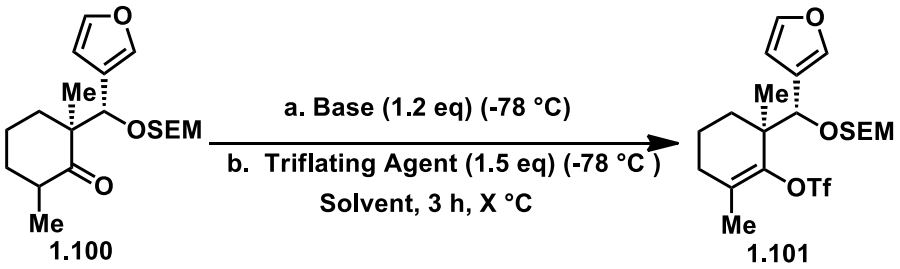

Entry	Base.	Triflating Agent	Solvent	Result
1	KHMDS	$PhNTf_2$	THF (rt)	0%
2	KHMDS	Comin's Reag.	THF (rt)	0%
3	KHMDS	Tf_2O	THF (rt)	0%
4	LiHMDS	$PhNTf_2$	DCM (rt)	0%
5	NaH	$PhNTf_2$	DCM (rt)	0%
6	KHMDS	$PhNTf_2$	THF (rt)	0%
7	KHMDS	$PhNTf_2$	DCM (rt)	0%
8	KHMDS	$PhNTf_2$	MeCN (rt)	0%
9	KHMDS	$PhNTf_2$	DCE (rt)	0%
10	KHMDS	$PhNTf_2$	MePh (rt)	0%
11	KHMDS	$PhNTf_2$	DCM (0 °C)	0%
12	KHMDS	$PhNTf_2$	DCM (-20 °C)	0%
13	KHMDS	$PhNTf_2$	DCM (-40 °C)	0%
14	KHMDS	$PhNTf_2$	DCM (-72 °C)	0%

Table 1.17 Triflation optimization reactions with SEM-ketone **1.100**

unoptimized (Scheme 1.22). None the less, we proceeded to perform the 1,4-reduction of SEM-enone **1.99** with K-Selectride, generating the SEM-ketone in 85% yield. With the SEM-ketone in hand, we proceeded to once again try to effect triflation. We evaluated the triflating agents phenyltriflimide, Comin's reagent, and triflic anhydride but none resulted in product formation. We also evaluated KHMDS, LiHMDS, and NaH but none resulted in product formation, even though we were confident that deprotonation was occurring due to our previous deuterium quenching. We also performed a solvent screen, evaluating THF, DCM, MeCN, DCE, and toluene but still no product was observed. Next, we evaluated a wide range of temperatures, including – 72 ˚C, – 40 ˚C, – 20 ˚C, and 0˚C. Unfortunately, varying temperature profiles were ineffective in promoting the desired reaction. We also tried reactions with 18-crown-6 as an additive to sequester the potassium cation to expose the naked enolate but still no product formation occurred. It was generally found that the SEM-ketone appeared to be more reactive, and less stable, than its -siloxy ketone counterpart because less of the SEM-ketone was recovered at the end of the reaction. Despite the increased reactivity of the SEM-ketone, we were surprised that no product was formed. Interestingly, neither the intriguing macrocyclic lactone **1.98** side-product or the triflinate anion elimination were observed from any reactions with the SEM-ketone. The macrocyclic lactone **1.98** and the triflinate anion elimination were only fomred from the siloxy ketone **1.97**. This suggests that the protecting group strongly influences the reactivity of the ketone substrate, although we do not fully understand how apart from the steric considerations.

1.7 Completion of the Total Synthesis of Fraxinellone

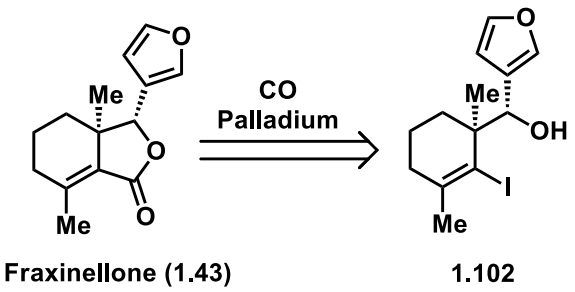

Fraxinellone (1.43) 1.102

Scheme 1.23 Retrosynthesis of carbonylation from vinyl iodide

Given the discouraging results of our extensive efforts to install the vinyl triflate needed for the carbonylation reaction in the final step of the synthesis, we revaluated our synthesis route again. However, this time we considered changing the coupling partners of the carbonylation to a vinyl iodide and the alcohol (Scheme 1.23). The installation of vinyl iodides from ketones was developed in 1962 by Barton.[70,71] Barton's work (Scheme 1.24), referred to as the "Barton vinyl iodide procedure", transforms a ketone to the vinyl iodide in high yield with relatively mild reagents. Through Barton's vinyl iodide sequence, a ketone is treated with hydrazine to form a hydrazone intermediate, from which treatment with iodine results in the synthesis of a new carbon-iodine bond. The resulting diazonium

spontaneously ejects to form a carbocation stabilized by the iodine. Finally, base-promoted elimination neutralizes the carbocation to afford the desired vinylic iodide.

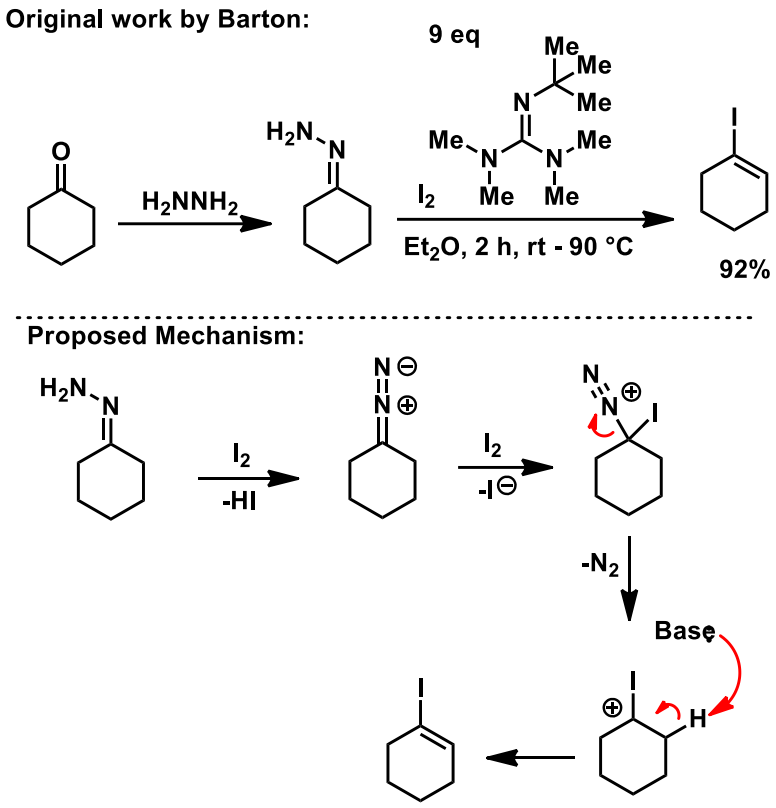

We envisioned Barton's vinyl iodide procedure could be used to circumvent the challenges we have experienced thus far in installing the vinyl triflate. These final steps of the synthesis were completed by Dr. Raeisi, also a member of the Martin lab. We began the sequence by condensing silyloxy ketone **1.97** with hydrazine to give the corresponding hydrazone (**1.103)**. Hydrazone **1.103** was then treated with triethylamine and iodine to furnish siloxy vinylic iodide **1.104** in 48% yield (unoptimized). The TBS group was then removed by treatment with TBAF, providing the vinylic iodide with the free alcohol **1.102**

in near quantitative yield at 98%. Finally, this set the stage for the last step. Treatment of vinylic iodide **1.102** with 5 mol % palladium dichloride and 10 mol % triphenylphosphine in the presence of carbon monoxide and potassium carbonate at 100 ˚C in DMF successfully promoted the carbonylative lactonization thereby generating fraxinellone in 72% yield and completing the total synthesis.

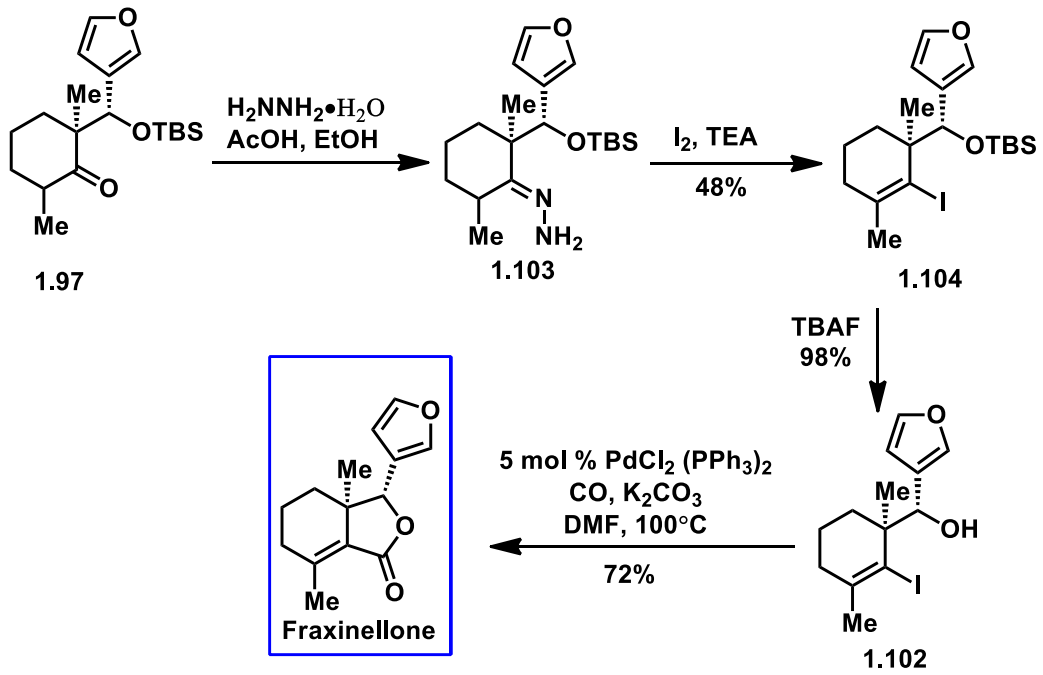

Scheme 1.25 Implementation of Barton's vinyl iodide synthesis and carbonylation to access fraxinellone (completed by Dr. Raeisi)

1.3 Conclusions and Future Directions

Although we are pleased to have been able to complete the total synthesis of fraxinellone, future work will be focused upon revisiting the aldol addition step to achieve enantioselectivity so that we can complete an enantioselective synthesis of fraxinellone. Additionally, we are interested in synthesizing valuable analogues and probes by varying the aldehyde substrate used in the aldol reaction. The synthesis of a library of analogues

and probes will allow us to perform SAR studies to further elucidate and investigate the pathogenesis of neurodegenerative diseases as well as give us the opportunity to characterize the mechanism of action of fraxinellone's neuroprotective activity.

1.4 Experimental Section

General Considerations

i) Solvents and reagents

Unless noted below, commercial reagents were purchased from MilliporeSigma, Acros Organics, Chem-Impex, Combi-blocks, TCI, and/or Alfa Aesar, and used without additional purification. Solvents were purchased from Fisher Scientific, Acros Organics, Alfa Aesar, and Sigma Aldrich. Tetrahydrofuran (THF), diethyl ether (Et_2O), acetonitrile (CH_3CN), benzene, methanol (MeOH), and triethylamine (Et_3N) were sparged with argon and dried by passing through alumina columns using argon in a Glass Contour solvent purification system. Dichloromethane (CH_2Cl_2) was freshly distilled over calcium hydride under a N_2 atmosphere prior to each use. DMSO and toluene (PhMe) were distilled over calcium hydride under a N_2 atmosphere, degassed via freeze-pump-thaw (3 cycles), and stored over 4 Å molecular sieves in a Schlenk flask under N_2. Dimethoxyethane (DME), *p*-xylene, dimethylformamide (DMF), MeLi solution, *n*-BuLi solution, LiHMDS solution, Red-Al® solution, and pyridine were purchased in Sure/Seal, AcroSeal, or ChemSeal bottling, and used directly. 1,4-Dioxane was purchased in AcroSeal bottling (99.5%, anhydrous, stabilized, over 4 Å molecular sieves) and additionally sparged with N_2 prior to use.

ii) Reaction setup, progress monitoring, and product purification

Unless otherwise noted in the experimental procedures, reactions were carried out in flame or oven dried glassware under a positive pressure of N_2 in anhydrous solvents using

standard Schlenk techniques. Reaction progresses were monitored using thin-layer chromatography (TLC) on EMD Silica Gel 60 F254 or Macherey–Nagel SIL HD (60 Å mean pore size, 0.75 mL/g specific pore volume, 5–17 μm particle size, with fluorescent indicator) silica gel plates. Visualization of the developed plates was performed under UV light (254 nm). Purification and isolation of products were performed via silica gel chromatography (both column and preparative thin-layer chromatography). Commercial reagents were purchased from Sigma Aldrich, Acros Organics, Chem-Impex, TCI, Oakwood, and Alfa Aesar, and used without additional purification. Solvents were purchased from Fisher Scientific, Acros Organics, Alfa Aesar, and MilliporeSigma. Tetrahydrofuran (THF), diethyl ether (Et_2O), acetonitrile (MeCN), dichloromethane (CH_2Cl_2), benzene, 1,4-dioxane, and triethylamine (Et_3N) were sparged with argon and dried by passing through alumina columns using argon in a Glass Contour (Pure Process Technology) solvent purification system. Dimethylformamide (DMF), dimethyl sulfoxide (DMSO), and dichloroethane (DCE) were purchased in Sure/Seal or AcroSeal bottling and additionally sparged with N_2 prior to use.

iii) Analytical instrumentation

NMR spectral data were obtained using deuterated solvents obtained from Cambridge Isotope Laboratories, Inc. or MilliporeSigma. ^1H NMR and ^{13}C NMR data were recorded on Bruker Avance NEO400 or Bruker Avance 600 MHz spectrometers using $CDCl_3$, typically at 20–23 °C.. Chemical shifts (δ) are reported in ppm relative to the residual solvent signal (δ 7.26 for ^1H NMR, δ 77.16 for ^{13}C NMR in $CDCl_3$). Data for ^1H NMR

spectroscopy are reported as follows; chemical shift (δ ppm), multiplicity (s = singlet, d = doublet, t = triplet, q = quartet, m = multiplet, br = broad, dd = doublet of doublets, dt = doublet of triplets), coupling constant (Hz), integration. Data for ^{13}C and ^{19}F NMR spectroscopy are reported in terms of chemical shift (δ ppm). IR spectroscopic data were recorded on a NICOLET 6700 FT-IR spectrophotometer using a diamond attenuated total reflectance (ATR) accessory. Samples are loaded onto the diamond surface either neat or as a solution in organic solvent and the data acquired after the solvent had evaporated. High resolution accurate mass spectral data were obtained from the Analytical Chemistry Instrumentation Facility at the University of California, Riverside, on an Agilent 6545 Q-TOF LC/MS instrument (supported by NSF grant CHE-0541848)

1.5 Experimental Procedures and Characterization Data

Synthesis of Butenolides

Preparation of 4-Methyl-2(5*H*)-furanone (1.71a) and 3-Methyl-2(5*H*)-furanone (1.71b).

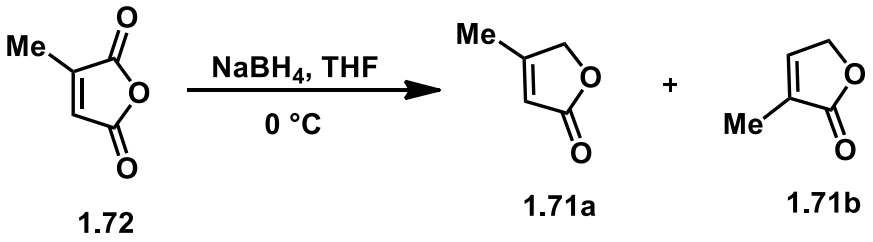

1.72 1.71a 1.71b

To a flame-dried vial was added citraconic anhydride (10 mL, 110 mmol), THF (250 mL), and $NaBH_4$ (5.24 g, 126.4 mmol). The reaction was stirred at 0 ˚C for 6 h. The reaction mixture was quenched with H_2O (30 mL), and then acidified with aqueous 6 M HCl. The reaction mixture was then extracted with Et_2O (three times), then the combined organic layers were dried over anhydrous Na_2SO_4, filtered, and concentrated under reduced pressure. The resulting crude yellow oil was purified by flash chromatography (SiO_2) using 4:1 Et_2O/hexanes to afford the desired product as a yellow/green oil (1.62 g, 15%). ^{1}H NMR ($CDCl_3$, 400 MHz) δ 7.14 (m, 1H), 4.77 (t, J = 2.0 Hz, 2H), 1.94 (m, 3H); ^{13}C NMR ($CDCl_3$, 100 MHz) δ 10.6, 70.2, 129.8, 144.6, 174.8. Spectral data matched literature sources.[72]

To a flame-dried vial was added citraconic anhydride (10 mL, 110.0 mmol), THF (250 mL), and $NaBH_4$ (5.24 g, 126.4 mmol). The reaction was stirred at 0 °C for 6 h. The reaction mixture was quenched with H_2O (30 mL), and then acidified with aqueous 6M HCl. The reaction mixture was then extracted with Et_2O (three times), then the combined organic layers were dried over anhydrous Na_2SO_4, filtered, and concentrated under reduced pressure. The resulting crude yellow oil was purified by flash chromatography (SiO_2) using 4:1 Et_2O/hexanes to afford the desired product as a yellow/green oil (7.35 g, 68%). ^1H NMR ($CDCl_3$, 400 MHz) δ 5.86 (s, 1H), 4.72 (s, 2H), 2.14 (s, 3H); ^{13}C NMR (100 MHz, $CDCl_3$) δ 174.2, 166.4, 115.9, 73.8, 13.9. Spectral data matched literature sources.[54]

Synthesis of Silyl Enol Ethers

Preparation of 2-(triisopropylsiloxy)-3-methyl-furan (1.70b).

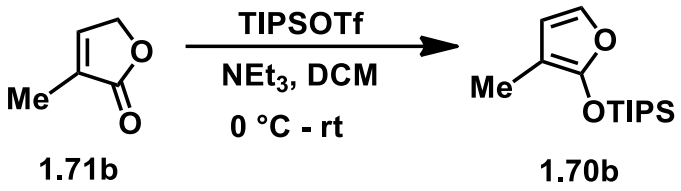

1.71b 1.70b

To a flame-dried round bottom flask was added the α-methyl butenolide (1.5 g, 15.3 mmol) and DCM (15 mL). The reaction flask was then cooled to 0℃. Next, Et_3N (6.3 mL, 45 mmol) and TIPSOTf (4.88 mL, 18 mmol) were added to the reaction flask. The reaction flask was then allowed to warm to room temperature and stirred for 6 h. The reaction mixture was quenched with a saturated aqueous solution of $NaHCO_3$ and extracted with EtOAc. The combined organic layers were washed with brine and then dried over

anhydrous Na_2SO_4. The organic layers were then filtered and concentrated under reduced pressure. The crude yellow oil was purified by flash chromatography (SiO_2) using 1% Et_3N in 50:1 Et_2O/EtOAc to afford the desired product as a yellow oil. This material was further purified by vacuum distillation to yield the desired product as a colorless oil (3.5 g, 90%). ^1H NMR ($CDCl_3$, 400 MHz) δ 6.74 (d, J = 2.03 Hz, 1H), 6.09 (d, J = 2.03 Hz, 1H), 1.84 (s, 3H), 1.26 (septet, J = 7.12 Hz, 3H), 1.08 (d, J = 7.12 Hz, 18H); ^{13}C NMR ($CDCl_3$, 100 MHz) δ 153.0, 130.6, 113.7, 91.4, 17., 12.4, 8.3. Spectral data matched literature sources.[73]

Preparation of 2-(triisopropylsiloxy)-4-methyl-furan (1.70a).

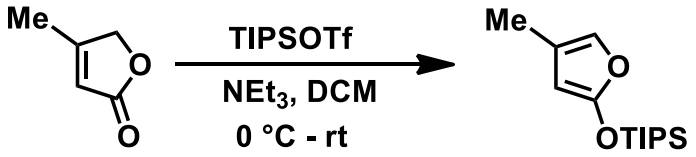

1.71a 1.70a

To a flame-dried round bottom flask was added the β-methyl butenolide (1.5 g, 15.3 mmol) and DCM (15 mL). The reaction flask was then cooled to 0℃. Next, Et_3N (6.3 mL, 45 mmol) and TIPSOTf (4.9 mL, 18 mmol) were added to the reaction flask. The reaction flask was then allowed to warm to rt and stirred for 6 h. The reaction was quenched with saturated $NaHCO_3$ solution and extracted with EtOAc. The combined organic layers were washed with brine, dried over anhydrous Na_2SO_4, filtered, and concentrated *in vacuo*. The crude yellow oil was purified by flash chromatography (SiO_2) using 1% Et_3N in 50:1 Et_2O/EtOAc to afford the desired product as a yellow oil. This

material was further purified by distillation to yield the desired product as a colorless oil (3.73 g, 96%). IR (ATR): 2939, 2867, 1785, 1750, 1630, 1571, 1468, 1394, 1369, 1294, 1206, 1169 cm^{-1}. ^{1}H NMR ($CDCl_3$, 400 MHz) δ 6.60 (s, 1H), 5.04 (s, 1H), δ 1.96 (s, 3H), 1.26 (septet, J = 7.1 Hz, 3H), 1.08 (d, J = 7.12 Hz, 18H); ^{13}C NMR (100 MHz, $CDCl_3$) δ 156.8, 128.2, 121.6, 86.3, 17.8, 12.4, 10.6. HRMS (ESI): calculated for $C_{14}H_{27}O_2Si$, $[M+H]^+$ 255.1775, found 255.1769. Spectral data matched literature sources.[73]

Preparation of 2-(triisopropylsiloxy)-5-methyl-furan (1.70c).

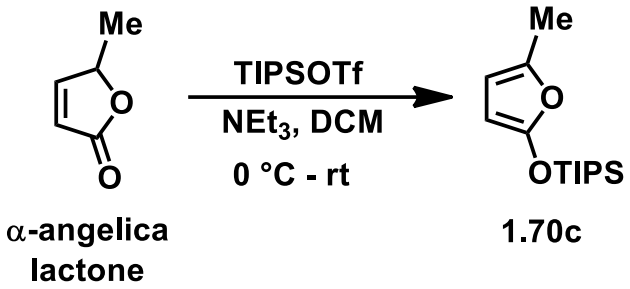

To a flame-dried round bottom flask was added angelica lactone (1.5 g, 15.29 mmol) and DCM (15 mL). The reaction flask was then cooled to 0 ℃. Next, Et_3N (6.3 mL, 45 mmol) and TIPSOTf (4.9 mL, 18 mmol) were added to the reaction flask. The reaction flask was then allowed to warm to rt and stirred for 6 h. The reaction was quenched with saturated $NaHCO_3$ solution and extracted with EtOAc. The combined organic layers were washed with brine, dried over anhydrous Na_2SO_4, filtered, and concentrated under reduced pressure. The crude yellow oil was purified by flash chromatography (SiO_2) using 1% Et_3N in 50:1 Et_2O/EtOAc to afford the desired product as a yellow oil. This material was further purified by distillation to yield the desired product as a colorless oil (3.15 g, 81%).

^{1}H NMR ($CDCl_3$, 400 MHz) δ 5.74 (s, 1H), 4.96 (d, J = 2.7 Hz, 1H), 2.16 (s, 3H) 1.26 (m, 3H), 1.08 (d, J = 7.1 Hz, 18H); ^{13}C NMR ($CDCl_3$, 100 MHz) δ 155.4, 140.9, 106.1, 83.6, 17.6, 13.6, 12.3. Spectral data matched literature sources.[55]

Synthesis of Iodonium Salts

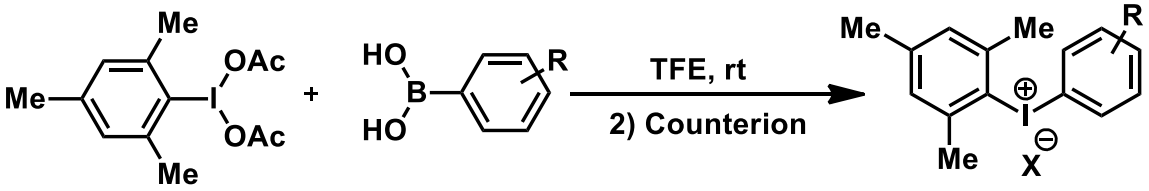

1.69a-m

General Procedure A: Synthesis of Iodonium Salts

To a flame-dried round bottom flask was charged was added the aryl boronic acid (1 equiv) and trifluoroethanol (0.22 M). The reaction flask was cooled to 0 ˚C, then iodomesityl was added (1.05 equiv) and then the reaction was allowed to warm to room temperature and stirred for 4 h. The corresponding salts (NH_4PF_6, NH_4BF_4, AgOTf, or $AgNO_3$) were added as saturated solutions and stirred vigorously for an additional 1 h. After 1 h, the reaction mixture was extracted three times with DCM. The combined organic layers were dried over anhydrous Na_2SO_4, filtered, and concentrated under reduced pressure. If further purification was necessary, trituration in Et_2O was performed. Procedure adapted from Widdowson et al.[74]

Preparation of mesityl(phenyl)iodonium hexafluorophosphate (1.69b).

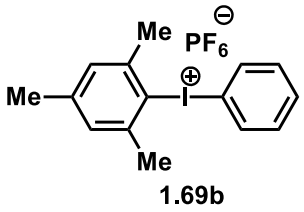

1.69b

Prepared according to General Procedure A. Reaction run on 4.10 mmol (500 mg) scale of the aryl boronic acid, yielding a white solid (985.3mg, 51%). ^{1}H NMR ($CDCl_3$, 400 MHz) δ 7.69 (m, *J* = 7.6 Hz, 2H), 7.57 (m, *J* = 7.4 Hz, 1H), 7.44 (m, *J* = 7.6 Hz, 2H), 7.13 (s, 2H), 2.62 (s, 6H), 2.36 (s, 3H); ^{13}C NMR ($CDCl_3$, 100 MHz) δ 145.1, 142.9, 133.1, 132.7, 132.3, 130.7, 118.9, 110.5, 27.2, 21.17. Spectral data matched literature sources.[47]

Preparation of mesityl(phenyl)iodonium tetrafluoroborate (1.69f).

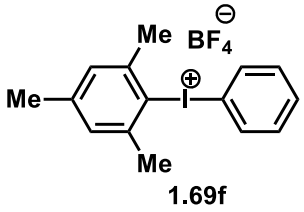

1.69f

Prepared according to General Procedure A. Reaction run on 2.05 mmol (250 mg) scale of the aryl boronic acid, yielding a white solid (538 mg, 64%). ^{1}H NMR ($CDCl_3$, 400 MHz) δ 7.69 (m, *J* = 7.6 Hz, 2H), 7.57 (m, *J* = 7.4 Hz, 1H), 7.44 (m, *J* = 7.6 Hz, 2H), 7.13 (s, 2H), 2.62 (s, 6H), 2.36 (s, 3H); ^{13}C NMR ($CDCl_3$, 100 MHz) δ 145.1, 142.9, 133.1, 132.7, 132.3, 130.7, 118.9, 110.5, 27.2, 21.2. Spectral data matched literature sources.[47]

Preparation of mesityl(phenyl)iodonium triflate (1.69g).

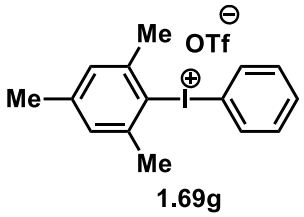

1.69g

Prepared according to General Procedure A. Reaction run on 2.05 mmol (250 mg) scale of the aryl boronic acid, yielding a white solid (716 mg, 74%). ^{1}H NMR ($CDCl_3$, 400 MHz) δ 7.69 (m, *J* = 7.6 Hz, 2H), 7.57 (m, *J* = 7.4 Hz, 1H), 7.44 (m, *J* = 7.6 Hz, 2H), 7.13 (s, 2H), 2.62 (s, 6H), 2.36 (s, 3H); ^{13}C NMR ($CDCl_3$, 100 MHz) δ 145.1,

142.9, 133.1, 132.7, 132.3, 130.7, 118.9, 110.5, 27.9, 21.2. Spectral data matched literature sources.[47]

Preparation of mesityl(furyl)iodonium hexafluorophosphate (1.69a).

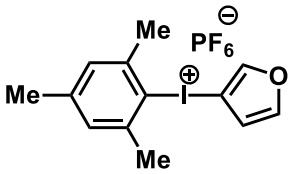

1.69a

Prepared according to General Procedure A. Reaction run on 2.2 mmol (250mg) scale of the aryl boronic acid, yielding an orange solid (845.21mg, 90%). ^{1}H NMR ($CDCl_3$, 400 MHz) δ 7.84 (s, 1H), 7.49 (s, 1H), 7.06 (s, 2H), 6.53 (s, 1H), 2.67 (s, 6H), 2.32 (s, 3H); ^{13}C NMR ($CDCl_3$, 100 MHz) δ 148.23, 145.64, 143.93, 141.56, 130.15, 129.22, 127.94, 112.74, 27.07, 21.03.[74]

Preparation of mesityl(furyl)iodonium tetrafluoroborate (1.69c).

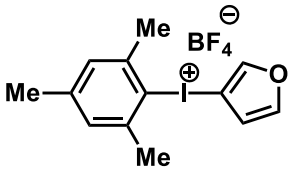

1.69c

Prepared according to General Procedure A. Reaction run on 2.2 mmol (250 mg) scale of the aryl boronic acid, yielding an orange solid (845 mg, 1.8 mmol, 90%). ^{1}H NMR ($CDCl_3$, 400 MHz) δ 7.84 (s, 1H), 7.49 (s, 1H), 7.06 (s, 2H), 6.53 (s, 1H), 2.67 (s, 6H), 2.32 (s, 3H); ^{13}C NMR ($CDCl_3$, 100 MHz) δ 148.2, 145.6, 143.9, 141.6, 130.2, 129.2, 127.9, 112.7, 27.1, 21.03.[74]

Preparation of mesityl(furyl)iodonium triflate (1.69e).

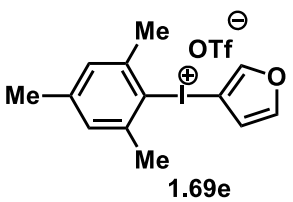

1.69e

Prepared according to General Procedure A. Reaction run on 2.2 mmol (250 mg) scale of the aryl boronic acid, yielding an orange solid (957 mg, 94%). ^{1}H NMR ($CDCl_3$, 400 MHz) δ 7.84 (s, 1H), 7.49 (s, 1H), 7.06 (s, 2H), 6.53 (s, 1H), 2.67 (s, 6H), 2.32 (s, 3H); ^{13}C NMR ($CDCl_3$, 100 MHz) δ 148.2, 145.6, 143.9, 141.6, 130.2, 129.2, 127.9, 112.7, 27.1, 21.0.[74]

Preparation of mesityl(furyl)iodonium nitrate (1.69d).

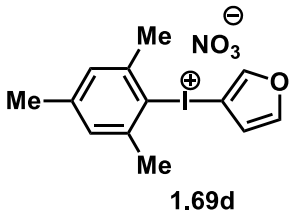

1.69d

Prepared according to General Procedure A. Reaction run on 2.2 mmol (250 mg) scale of the aryl boronic acid, yielding an orange solid (644 mg, 78%). ^{1}H NMR ($CDCl_3$, 400 MHz), δ 7.84 (s, 1H), 7.49 (s, 1H), 7.06 (s, 2H), 6.53 (s, 1H), 2.67 (s, 6H), 2.32 (s, 3H); ^{13}C NMR ($CDCl_3$, 100 MHz), δ 148.2, 145.6, 143.9, 141.6, 130.2, 129.2, 127.9, 112.7, 27.1, 21.0.[74]

Preparation of mesityl(p-tolyl)iodonium hexafluorophosphate (1.69h).

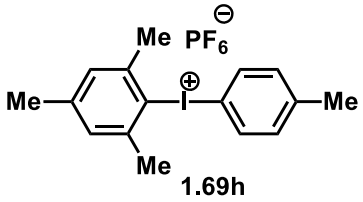

1.69h

Prepared according to General Procedure A. Reaction run on 1.0 mmol (136 mg) scale of the aryl boronic acid, yielding a white solid (203 mg, 42%). ^{1}H NMR ($CDCl_3$, 400 MHz) δ 7.62 (m, *J* = 8.5 Hz, 2H), 7.27 (m, *J* = 8.5 Hz, 2H), 7.13 (s, 2H), 2.64 (s, 6H), 2.39 (s, 3H), 2.36 (s, 3H). ^{13}C NMR ($CDCl_3$, 100 MHz) δ 145.2, 143.8, 142.8, 133.7, 133.6, 130.87, 119.04, 106.47, 27.24, 21.37, 21.18. Spectral data matched literature sources.[75]

Preparation of mesityl(4-fluorophenyl)iodonium hexafluorophosphate (1.69i)

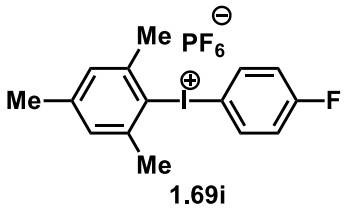

1.69i

Prepared according to General Procedure A. Reaction run on 1.0 mmol (140 mg) scale of the aryl boronic acid, yielding a tan solid (367 mg, 79%). ^{1}H NMR ($CDCl_3$, 400 MHz) δ 7.75 (m, 2H), 7.25 (m, 2H), 7.15 (s, 2H), 2.64 (s, 6H), 2.34 (s, 3H). ^{13}C NMR (100 MHz, $CDCl_3$)

δ 164.77 (d, $J_{C\text{-}F}$ = 256.4 Hz), 145.1, 142.7, 136.1, 130.8, 120.31, 120.08, 104.35, 27.18, 21.18. Spectral data matched literature sources.[75]

Preparation of mesityl(4-methoxyphenyl)iodonium hexafluorophosphate (1.69j).

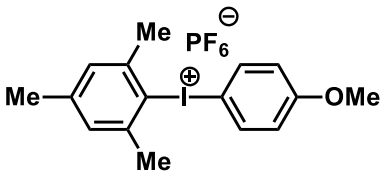

1.69j

Prepared according to General Procedure A. Reaction run on 1.0 mmol (152 mg) scale of the aryl boronic acid, yielding a tan solid (416 mg, 84%). ^{1}H NMR (400 MHz, $CDCl_3$) δ 7.69 (m, *J* = 9.2 Hz, 2H), 7.09 (s, 2H) 6.96 (m, *J* = 9.2 Hz, 2H), 3.80 (s, 3H), 2.63 (s, 6H), 2.32 (s, 3H). ^{13}C NMR (100 MHz, $CDCl_3$) δ 162.9, 144.9, 142.5, 136.1, 130.7, 127.9, 120.1, 118.5, 55.8, 27.05, 21.05. Spectral data matched literature sources.[47]

Preparation of mesityl(3,5-bis(trifluoromethyl)phenyliodonium hexafluorophosphate (1.69k).

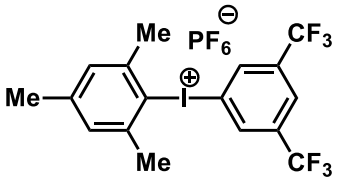

1.69k

Prepared according to General Procedure A. Reaction run on 3.94 mmol (1.0 g) scale of the aryl boronic acid, yielding a white solid (131 mg, 6%). ^{1}H NMR (400 MHz, $CDCl_3$) δ 8.19 (s, 2H), 7.94 (s, 1H) 7.10 (s, 2H), 2.60 (s, 6H), 2.34 (s, 3H); ^{13}C NMR (100 MHz, $CDCl_3$) δ 144.92, 142.97, 134.47 (q, $J_{C\text{-}F}$ = 34.7 Hz), 133.2, 130.4, 125.2, 124.6 (d, $J_{C\text{-}F}$ = 273.7 Hz), 120.0, 112.1, 26.9, 21.1. Spectral data matched literature sources.[76]

Preparation of mesityl(2-bromophenyl)iodonium hexafluorophosphate (1.69l).

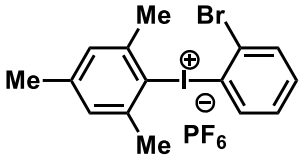

1.69l

Prepared according to General Procedure A. Reaction run on 1.25 mmol (250 mg) scale of the aryl boronic acid, yielding a white solid (404 mg, 60%). ^{1}H NMR (400 MHz, $CDCl_3$) δ 7.77

(m, *J* = 8.0 Hz, 1H), 7.52 (m, *J* = 7.3 Hz, 1H), 7.40 (m, *J* = 7.3 Hz, 1H), 7.24 (s, 2H) 6.93 (m, *J* = 8.0 Hz, 1H), 2.60 (s, 6H), 2.42 (s, 3H); ^{13}C NMR (100 MHz, $CDCl_3$) δ 146.2, 143.3, 134.8, 133.7, 131.6, 131.3, 124.4, 119.8, 114.9, 27.1, 21.3. Spectral data matched literature sources.[77]

Preparation of mesityl(3-bromophenyl)iodonium hexafluorophosphate **(1.69m).**

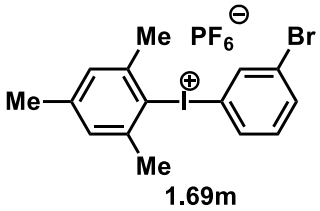

1.69m

Prepared according to General Procedure A. Reaction run on 1.25 mmol (250 mg) scale of the aryl boronic acid, yielding a white solid (340 mg, 50%). ^{1}H NMR (400 MHz, $CDCl_3$) δ 7.73 (m, *J* = 7.8 Hz, 2H), 7.62 (m, *J* = 8.4 Hz, 1H), 7.30 (m, *J* = 8.1 Hz, 1H), 7.11 (s, 2H), 2.60 (s, 6H), 2.35 (s, 3H). ^{13}C NMR (100 MHz, $CDCl_3$) δ 145.0, 142.9, 135.2, 134.8, 133.4, 131.9, 130.6, 125.1, 119.4, 111.0, 27.2, 21.2. Spectral data matched literature sources.[47]

Preparation of mesityl(4-bromophenyl)iodonium hexafluorophosphate (1.69n).

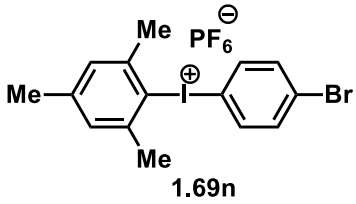

1.69n

Prepared according to General Procedure A. Reaction run on 2.05 mmol (250 mg) scale of the aryl boronic acid, yielding a white solid (474 mg, 70%). ^{1}H NMR (400 MHz, DMSO-d_6) δ 7.86 (m, *J* = 8.7 Hz, 2H), 7.71 (m, *J* = 8.7 Hz, 2H), 7.22 (m, 2H), 2.68 (s, 6H), 2.30 (s, 3H). ^{13}C NMR (100 MHz, DMSO-d_6) δ 143.2, 141.6, 136.3, 134.7, 129.8, 125.8, 122.8, 113.2, 26.3, 20.5. Spectral data matched literature sources.[77]

Synthesis of Aryl-Butenolides and Spectral Data

General Procedure B: Synthesis of Aryl-butenolides Using Palladium

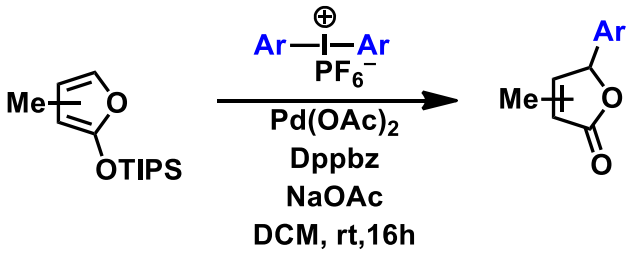

To a flame dried vial was added palladium acetate (5 mol %) and 1,2-bis(diphenylphosphino)benzene (5 mol %), followed by the iodonium salt (1 equiv) and sodium acetate (0.8 equiv). The reaction vial was then evacuated and backfilled with nitrogen three times. Once under a nitrogen atmosphere, DCM (0.052 M) was added, followed by the silyloxyfuran (2 equiv). The reaction was stirred for 16 h at room temperature under nitrogen atmosphere. After 16 h, the reaction mixture was extracted three times with diethyl ether. The combined organic layers were dried over anhydrous Na_2SO_4, filtered, and concentrated under reduced pressure. The crude product was purified by flash chromatography (SiO_2) using a 50:50 diethyl ether/hexanes to afford the desired product as a colorless or yellow oil.

General Procedure C: Synthesis of Aryl-butenolides Using Copper

To a flame dried vial in a glovebox was added copper(II) triflate (5 mol %) and (S,S)-2,2'-isopropylidenebis(4-phenyl-2-oxazoline) (5 mol %). The vial was then placed under a nitrogen atmosphere followed by the addition of DCM (0.05M). Next, the

iodonium (1 equiv) was added to a separate vial and then evacuated and backfilled three times with nitrogen before the addition of DCM (1 mL). The solution containing catalyst was then allowed to stir under nitrogen atmosphere for 10 min before being transferred to the iodonium solution. After the catalyst and iodonium solution were combined, the silyl enol ether (3 equiv) was added to the reaction vial. The reaction was allowed to stir at rt for 24 h under a nitrogen atmosphere. The reaction mixture was quenched with saturated sodium bicarbonate solution and extracted three times with DCM. The combined organic layers were dried over anhydrous Na_2SO_4, filtered, and concentrated *in vacuo*. The crude product was purified by flash chromatography (SiO_2) using a 50:50 diethyl ether/hexanes to afford the desired product as a colorless or yellow oil.

4-Methyl-5-phenylfuran-2(5H)-one (1.68b). Prepared according to General Procedure B using diphenyliodonium hexafluorophosphate with 5 mol % $Pd(OAc)_2$ and 5 mol % dppbz for 16 h. Reaction was run on 0.165 mmol (70.3 mg) scale of the iodonium salt. The crude material was purified using silica gel with a solvent system of 50:50 hexanes/Et_2O to afford **1.68b** as a clear oil. (23 mg, 80% yield)

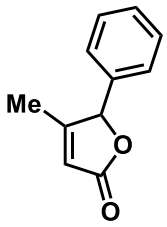

1.68b

1.68b: Prepared according to General Procedure B using (Mesityl-I-Phenyl)PF_6 with 5 mol % $Pd(OAc)_2$ and 5 mol % BINAP for 16 h. Reaction was run on 0.165 mmol (77.2 mg) scale of the iodonium salt. The crude material was purified using silica gel with a solvent system of 50:50 hexanes/Et_2O to afford **1.68b** as a clear oil. (18 mg, 61% yield)

1.68b: Prepared according to General Procedure C using (Mesityl-I-Phenyl)PF_6 with 5 mol % $Cu(OTf)_2$ and 5 mol % PhBox for 16 h. Reaction was run on 0.165 mmol (77.2 mg) scale of the iodonium salt. The crude material was purified using silica gel with a solvent system of 50:50 hexanes/Et_2O to afford **1.68b** as a clear oil. (223 mg, 80% yield)

^{1}H NMR (400 MHz, $CDCl_3$) δ 7.39 (m, 3H), 7.24 (m, 2H), 5.93 (s, 1H), 5.71 (s, 1H), 1.92 (s, 3H) ^{13}C NMR (100 MHz, $CDCl_3$) δ 173.5, 168.6, 134.3, 129.5, 129.1, 126.8, 116.4, 86.6, 14.1. Spectral data matched literature sources.[78]

5-(2-Bromophenyl)-4-methylfuran-2(5H)-one (1.68c). Prepared according to General Procedure B using with 5 mol % $Pd(OAc)_2$ and 5 mol % BINAP for 16 s. Reaction was run on 0.165 mmol (70 mg) scale of the iodonium salt. The crude material was purified using silica gel with a solvent system of 50:50 hexanes/Et_2O to afford **1.68c** as a clear oil. (19 mg, 46% yield). IR (ATR): 2355, 1763, 1644, 1460, 1288, 1151, 1025, 968 cm^{-1}. ^{1}H NMR (400 MHz, $CDCl_3$) δ 7.62 (s, *J* = 8.0 Hz, 1H), 7.35 (s, *J* = 7.6 Hz, 1H), 7.25 (m, *J* = 7.6 Hz, 1H), 7.11 (m, *J* = 8.0 Hz, 1H), 6.36 (s, 1H), 5.95 (s, 1H), 2.00 (s, 3H) ^{13}C NMR (100 MHz, $CDCl_3$) δ 173.3, 168.9, 133.9, 133.3, 130.8, 128.3, 127.6, 123.5, 116.6, 84.6, 14.3. HRMS (ESI) calculated for $C_{11}H_{10}BrO_2$ $[M+H]^+$ 252.9859, found 252.9852.

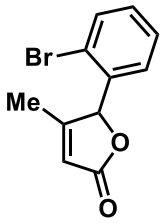

1.68c

5-(4-Bromophenyl)-4-methylfuran-2(5H)-one (1.68d). Prepared according to General Procedure B using with 5 mol % $Pd(OAc)_2$ and 5 mol % BINAP for 16 h. Reaction was run on 0.165 mmol (70 mg) scale of the iodonium salt. The crude material was purified using silica gel with a solvent system of 50:50 Hexanes/Diethyl Ether to afford **1.68d** as a clear oil. (19 mg, 45 % yield)

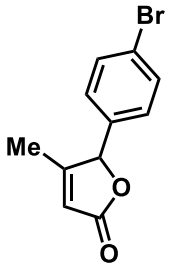

1.68d

1.68d: Prepared according to General Procedure C with 5 mol % $Cu(OTf)_2$ and 5 mol % PhBox for 16 h. Reaction was run on 0.165 mmol (77 mg) scale. The crude material was purified using silica gel with a solvent system of 50:50 Hexanes/Diethyl Ether to afford **1.68d** as a clear oil. (28.4 mg, 68 % yield) IR (ATR): 2353, 1746, 1627, 1498, 1278, 1007, 963 cm^{-1}. ^1H NMR (400 MHz, $CDCl_3$) δ 7.53 (m, J = 8.4 Hz, 2H), 7.13 (m, J = 8.4 Hz, 2H), 5.94 (s, 1H), 5.67 (s, 1H) 1.92 (s, 3H) ^{13}C NMR (100 MHz, $CDCl_3$) δ 173.0, 168.0, 133.5, 132.4, 128.5, 123.7, 116.7, 85.7, 14.1. HRMS (ESI) calculated for $C_{12}H_{12}O_2$ [M + H]$^+$ 252.9859, found 252.9856.

3-Methyl-5-phenyl-2(5H)-furanone (1.68f). Prepared according to General Procedure B using diphenyliodonium-hexafluorophosphate with 5 mol % $Pd(OAc)_2$ and 5 mol % dppbz for 16 h. Reaction was run on 0.165 mmol (70.3 mg) scale of the iodonium salt. The crude material was purified using silica gel with a solvent system of 50:50 hexanes/Et_2O to afford **1.68f** as a clear oil. (26 mg, 90% yield)

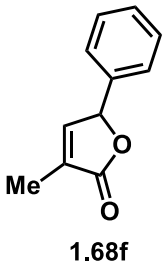

1.68f

1.68f: Prepared according to General Procedure B using (Mesityl-I-Phenyl)PF_6 with 5 mol % $Pd(OAc)_2$ and 5 mol % dppbz for 16 h. Reaction was run on 0.165 mmol (77.2 mg) scale. The crude material was purified using silica gel with a solvent system of 50:50 hexanes/Et_2O to afford **1.68f** as a clear oil. (3 mg, 10% yield). ^1H NMR (400 MHz, $CDCl_3$) δ 7.38 (m, 5H), 7.13 (s, 1H), 5.88 (s, 1H), 2.01 (s, 3H) ^{13}C NMR (100 MHz, $CDCl_3$) δ 148.4, 129.1, 128.9, 126.5, 82.1, 17.9, 11.9, 10.7. Spectral data matched literature sources.[79]

5-(4-Methylphenyl)-3-methylfuran-2(5H)-one (1.68h). Prepared according to General Procedure B with 5 mol % $Pd(OAc)_2$ and 5 mol % dppbz for 16 h. Reaction was run on 0.165 mmol (77 mg) scale of the iodonium salt. The crude material was purified using silica gel with a solvent system of 50:50 hexanes/Et_2O to afford 21b as a clear oil. (16 mg, 0.08 mmol, 50% yield). ^1H NMR (400 MHz, $CDCl_3$) δ 7.16 (m, 4H), 7.11 (m, 1H), 5.85 (m, 1H), 2.36 (s, 3H), 2.00 (s, 3H) ^{13}C NMR (100 MHz, $CDCl_3$) δ 148.4, 139.1, 137.2, 132.1, 130.6, 129.6, 126.5, 82.1, 18.2, 13.4. Spectral data matched literature sources.[80]

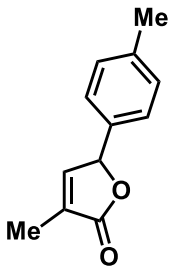

1.68h

5-(4-Methoxyphenyl)-3-methylfuran-2(5H)-one (1.68g). Prepared according to General Procedure B with 5 mol % $Pd(OAc)_2$ and 5 mol % dppbz for 16 h. Reaction was run on 0.165 mmol (77.2 mg) scale of the iodonium salt. The crude material was purified using silica gel with a solvent system of 50:50 hexanes/Et_2O to afford **1.68g** as a clear oil. (8 mg, 25% yield).

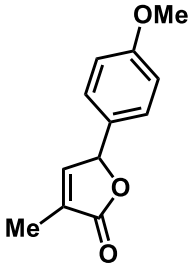

1.68g

^{1}H NMR (400 MHz, $CDCl_3$) δ 7.18 (m, *J* = 8.7 Hz, 2H), 7.10 (s, 1H), 6.92 (m, *J* = 8.7 Hz, 2H), 5.83 (s, 1H), 3.82 (s, 3H), 2.01 (s, 3H) ^{13}C NMR (100 MHz, $CDCl_3$) δ 160.3, 148.3, 129.7, 128.2, 126.9, 114.3, 82.0, 55.4, 29.7, 10.7. Spectral data matched literature sources.[81]

5-(4-Fluorophenyl)-3-methylfuran-2(5H)-one (1.68i). Prepared according to General Procedure B with 5 mol % $Pd(OAc)_2$ and 5 mol % dppbz for 16 h. Reaction was run on 0.165 mmol (77 mg) scale of the iodonium salt. The crude material was purified using silica gel with a solvent system of 50:50 hexanes/Et_2O to afford **1.68i** as a clear oil. (10.7 mg, 34% yield)

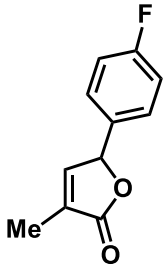

1.68i

^{1}H NMR (400 MHz, $CDCl_3$) δ 7.24 (s, 1H), 7.11 (m, 4H), 5.86 (s, 1H), 2.01 (s, 3H) ^{13}C NMR (100 MHz, $CDCl_3$) δ 148.1, 130.0, 128.5, 116.2, 115.9, 81.5, 29.8, 20.3, 10.7. Spectral data matched literature sources.[79]

5-Methyl-5-phenylfuran-2(5H)-one (1.68k). Prepared according to General Procedure B using diphenyliodonium hexafluorophosphate with 5 mol % $Pd(OAc)_2$ and 5 mol % dppbz for 16 h. Reaction was run on 0.165 mmol (70.3 mg) scale of the iodonium salt. The crude material was purified using silica gel with a solvent system of 50:50 hexanes/Et_2O to afford **1.68k** as a clear oil. (4 mg, 13% yield)

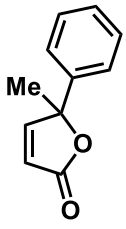

1.68k

1.68k: Prepared according to General Procedure B using (Mesityl-I-Phenyl)PF_6 with 5 mol % $Pd(OAc)_2$ and 5 mol % dppbz for 16 h. Reaction was run on 0.165 mmol (77.2 mg)

scale. The crude material was purified using silica gel with a solvent system of 50:50 hexanes/Et_2O to afford **1.68k** as a clear oil. (1.4 mg, 5% yield)

1.68k: Prepared according to General Procedure C using (Mesityl-I-Phenyl)PF_6 with 5 mol % $Cu(OTf)_2$ and 5 mol % PhBox for 16 h. Reaction was run on 0.165 mmol (77.2 mg) scale of the iodonium salt. The crude material was purified using silica gel with a solvent system of 50:50 Hexanes/Diethyl Ether to afford **1.68k** as a clear oil. (4 mg, 13% yield)

^{1}H NMR (400 MHz, $CDCl_3$) δ 7.65 (d, J = 5.6 Hz, 1H), 7.63 (m, 2H), 7.50 (m, 1H), 7.40 (m, 2H), 6.08 (d, J = 5.6 Hz, 1H), 1.84 (s, 3H) ^{13}C NMR (100 MHz, $CDCl_3$) δ 172.4, 160.4, 139.2, 128.9, 128.4, 124.8, 119.4, 88.9, 26.4. Spectral data matched literature sources.[76]

5-(4-Methylphenyl)-4-methylfuran-2(5H)-one (**1.68p).** Prepared according to General Procedure C with 5 mol % $Cu(OTf)_2$ and 5 mol % iPrBox for 16 h. Reaction was run on 0.165 mmol (77.2 mg) scale of the iodonium salt. The crude material was purified using silica gel with a solvent system of 50:50 Hexanes/Diethyl Ether to afford **1.68p** as a clear oil. (16 mg, 51 % yield).

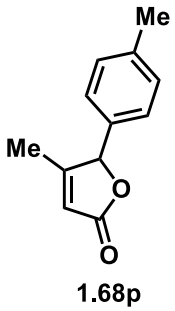

1.68p

IR (ATR): 2365, 1758, 1641, 1460, 1289, 1021, 965 cm^{-1}. ^{1}H NMR (400 MHz, $CDCl_3$) δ 7.20 (m, *J* = 8.0 Hz, 2H), 7.13 (m, *J* = 8.4 Hz, 2H), 5.93 (s, 1H), 5.68 (s, 1H), 3.12 (s, 3H), 1.91 (s, 3H) ^{13}C NMR (100 MHz, $CDCl_3$) δ 173.4, 168.5, 139.5, 131.3, 129.7, 126.8, 116.3, 86.5, 21.3, 14.1. HRMS (ESI) calculated for $C_{12}H_{12}O_2$ $[M + H]^+$ 189.0910, found 189.0899.

5-(3-Bromophenyl)-4-methylfuran-2(5H)-one (1.68o). Prepared according to General Procedure B using with 5 mol % $Pd(OAc)_2$ and 5 mol % dppbz for 16 h. Reaction was run on 0.165 mmol (700 mg) scale of the iodonium salt. The crude material was purified using silica gel with a solvent system of 50:50 hexanes/Et_2O to afford **1.68o** as a clear oil. (15 mg, 35% yield)

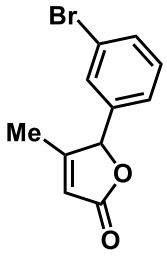

1.68o

1.68o: Prepared according to General Procedure C with 5 mol % $Cu(OTf)_2$ and 5 mol % PhBox for 16 h. Reaction was run on 0.165 mmol (77 mg) scale. The crude material was purified using silica gel with a solvent system of 50:50 hexanes/Et_2O to afford **1.68o** as a clear oil. (35 mg, 85% yield)

IR (ATR): 2349, 1745, 1629, 1498, 1277, 1007, 961 cm^{-1}. ^1H NMR (400 MHz, $CDCl_3$) δ 7.56 (s, *J* = 8.0 Hz, 2H), 7.43 (s, *J* = 7.8 Hz, 1H), 7.34 (m, *J* = 8.0 Hz, 1H), 7.24 (m, 1H), 6.00 (s, 1H), 5.71 (s, 1H), 1.98 (s, 3H) ^{13}C NMR (100 MHz, $CDCl_3$) δ 172.9, 167.9, 136.7, 132.7, 130.7, 129.8, 125.5, 123.2, 116.7, 85.5, 14.1. HRMS (ESI) calculated for $C_{11}H_{10}BrO_2$ $[M + H]^+$ 252.9859, found 252.9858.

5-(3-Bromophenyl)-3-methylfuran-2(5H)-one (1.68q) Prepared according to General Procedure C with 5 mol % $Cu(OTf)_2$ and 5 mol % PhBox for 16 h. Reaction was run on 0.165 mmol (77.2 mg) scale of the iodonium salt. The crude material was purified using silica gel with a solvent system of 50:50 Hexanes/Diethyl Ether to afford **1.68q** as a clear oil. (9 mg, 21% yield). ^1H NMR (400 MHz, $CDCl_3$) δ 7.49 (m, *J* = 7.9 Hz, 1H), 7.42 (s, 1H), 7.23 (m, *J* = 7.9 Hz, 2H), 7.11 (s, 1H), 5.84 (s, 1H), 2.01 (s, 3H) ^{13}C NMR (100 MHz, $CDCl_3$)

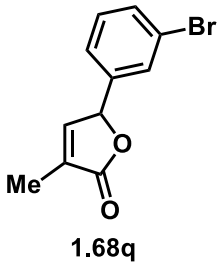

1.68q

δ 173.8, 147.7, 137.5, 132.2, 130.5, 130.0, 129.4, 125.0, 81.1, 29.7, 10.7. Spectral data matched literature sources.[83]

5-(4-Bromophenyl)-3-methylfuran-2(5H)-one (1.68r). Prepared according to General Procedure C with 5 mol % $Cu(OTf)_2$ and 5 mol % PhBox for 16 h. Reaction was run on 0.165 mmol (77 mg) scale of the iodonium salt. The crude material was purified using silica gel with a solvent system of 50:50 Hexanes/Diethyl Ether to afford **1.68r** as a clear oil. (8 mg, 0.03 mmol, 20% yield). ^{1}H NMR (400 MHz, $CDCl_3$) δ 7.52 (m, *J* = 8.4 Hz, 2H), 7.16 (m, *J* = 8.4 Hz, 2H), 7.10 (s, 1H), 5.83 (s, 1H), 2.01 (s, 3H) ^{13}C NMR (100 MHz, $CDCl_3$) δ 147.8, 132.2, 128.1, 81.3, 29.7, 10.7. Spectral data matched literature sources.[81]

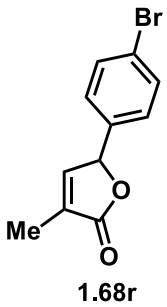

1.68r

5-Methyl-5-(3-bromophenylfuran-2(5H)-one (1.68t). Prepared according to General Procedure C with 5 mol % $Cu(OTf)_2$ and 5 mol % PhBox for 16 h. Reaction was run on 0.165 mmol (77.2 mg) scale of the iodonium salt. The crude material was purified using silica gel with a solvent system of 50:50 hexanes/Et_2O to afford **1.68t** as a clear oil. (19 mg, 46% yield). IR (ATR): 3090-3069, 2989, 2406, 1743, 1608, 1505, 1461, 1120, 969, 451 cm^{-1}. ^{1}H NMR (400 MHz, $CDCl_3$) δ 7.62 (d, J = 5.6 Hz, 1H), 7.35 (m, 1H), 7.25 (m, 1H), 7.11 (m, 1H), 6.08 (d, J = 5.6 Hz, 1H), 1.82 (s, 3H) ^{13}C NMR (100 MHz, $CDCl_3$) δ 173.3, 168.9, 133.9, 133.3, 130.8, 128.3, 127.6, 123.5, 116.6, 84.6, 14.3. HRMS (ESI) calculated for $C_{11}H_{10}BrO_2$ $[M + H]^+$ 252.9859, found 252.9852.

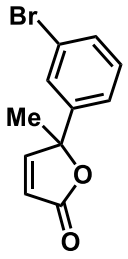

1.68t

Synthesis of 2,6-dimethylcyclohex-2enone (1.91)

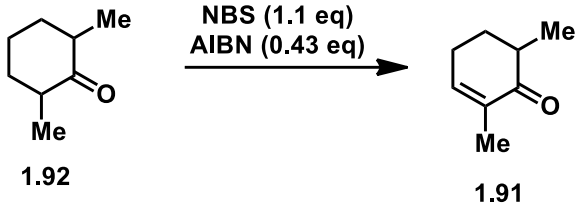

2,6-dimethylcyclohex-2-enone (1.91). To a round-bottomed flask was added 2,6-dimethylcyclohexanone (5.0 g, 40 mmol, 1 equiv) and DCE (32.5 mL). The reaction mixture was heated to reflux at 84˚C, then NBS (7.76 g, 43.9 mmol, 1.1 equiv) and AIBN (2.80 g, 0.43 equiv) were added. The reaction was stirred at reflux for 24 h. After 24 h, the reaction was allowed to cool to rt and then diluted with Et_2O (15 mL). The organic layer was washed with a saturated solution of metabisulfite, a saturated solution of sodium bicarbonate, and a saturated solution of brine. The combined organic layer was dried over sodium sulfate and filtered and then concentrated in *vacuo*. The crude mixture was purified by silica gel flash chromatography eluting with a gradient of 98:2 hexanes/EtOAc to 9:1 hexanes/EtOAc to provide 2,6-dimethylcyclohex-2-enone **1.91** (3.93 g, 80%) as a viscous colorless oil.

^{1}H NMR ($CDCl_3$) δ: 6.58 (m, 1 H), 2.34-2.20 (m, 3 H), 1.99 (dddd, *J* = 9.1, 5.7, 4.8, 1.1 Hz, 1H), 1.73-1.70 (m, 3H), 1.70-1.63 (m, 1 H), 1.09 (d, J = 6.8 Hz, 3H); ^{13}C NMR (100 MHz, $CDCl_3$) δ: 202.2, 144.4, 134.7, 41.4, 31.1, 25.1, 15.9, 15.0. Spectral data matched literature sources.[84]

Preparation of (S)-6-((S)-furan-3-yl(hydroxy)methyl)-2,6-dimethylcyclohex-2-enone (1.89)

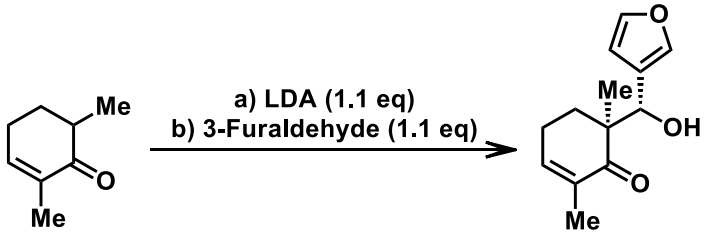

1.91 1.89

(S)-6-((S)-furan-3-yl(hydroxy)methyl)-2,6-dimethylcyclohex-2-enone (1.89). To a round-bottomed flask was added diisopropylamine (122 μL, 0.88 mmol, 1.1 equiv) and THF (3.0 mL). The reaction mixture was cooled to 0 ˚C, then *n*BuLi (0.55 mL, 0.80 mmol, 1.0 equiv) was added dropwise. The reaction mixture was then stirred for 15 min at 0 ˚C. After 15 min, the reaction mixture was cooled to – 78 ˚C, then 2,6-dimethylcyclohex-2-enone **1.91** (100 mg, 0.80 mmol, 1 equiv) was added dropwise as a solution in THF (3.0 mL). The reaction mixture was then stirred at – 78 ˚C for 25 min. After 25 min, 3-furaldehyde (83 μL, 0.88 mmol, 1.1 equiv) was added rapidly. The reaction was allowed to stir at – 78 ˚C for 20 min and then allowed to slowly warm to rt over 60 min. After warming to rt, the reaction mixture was extracted with Et_2O (3 x 5mL) and the combined organic layers were washed with a saturated solution of brine. The combined organic layers were dried over sodium sulfate, filtered, and then concentrated under reduced pressure. The crude mixture was purified by silica gel flash chromatography eluting with 9:1 hexanes/Et_2O to provide (S)-6-((*S*)-furan-3-yl(hydroxy)methyl)-2,6-dimethylcyclohex-2-enone **1.89** (166 mg, 95%) as a viscous colorless oil.

^{1}H NMR ($CDCl_3$) δ: 7.33 (s, 1H), 7.35 (t, *J* = 1.6 Hz, 1H), 6.70 (s, 1H), 6.36 (s, 1H), 4.89 (s, 1H), 4.55 (d, *J* = 1.7 Hz, 1H), 2.40–2.32 (m, 1H), 2.28–2.25 (m, 1H), 1.78 (s, 3H), 1.73 (tdd, *J* = 10.7, 5.4, 2.2 Hz, 1H), 1.52–1.48 (m, 1H), 1.17 (s, 3H); ^{13}C NMR ($CDCl_3$) δ 207.3, 145.7, 142.5, 140.7, 134.0, 124.1, 110.3, 71.7, 47.5, 31.5, 22.7, 16.3, 14.7. Spectral data matched literature sources.[66,85]

Preparation of (S)-6-((S)-((tert-butyldimethylsilyl)oxy)(furan-3-yl)methyl)-2,6-dimethylcyclohex-1-en-1-yl trifluoromethanesulfonate (1.88)

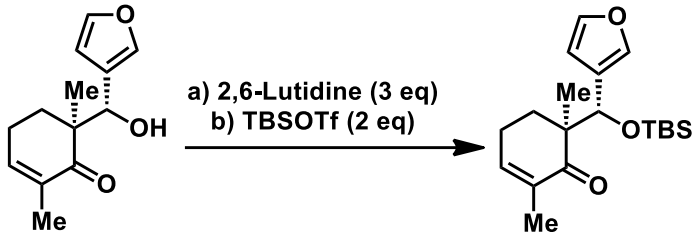

1.89 **1.88**

(S)-6-((S)-((tert-butyldimethylsilyl)oxy)(furan-3-yl)methyl)-2,6-dimethylcyclohex-1-en-1-yl trifluoromethanesulfonate (1.88). To a round-bottomed flask was added (*S*)-6-((S)-furan-3-yl(hydroxy)methyl)-2,6-dimethylcyclohex-2-enone **1.89** (580 mg, 2.56 mmol, 1 equiv) and DCM (61 mL). The reaction mixture was then cooled to 0 ˚C, then 2,6-lutidine (1.11 mL, 7.64 mmol, 3 equiv) was added and allowed to stir for 15 min. After 15 min, TBSOTF (1.6 mL, 5.2 mmol, 2 equiv) was added to the reaction mixture dropwise and then allowed to warm to rt and stir for 16 h. After 16 h, the reaction mixture was quenched with an aqueous solution of $NaHCO_3$ and then extracted with Et_2O (3 x 10 mL). The combined organic layers were washed with brine, dried over sodium sulfate, filtered and then concentrated in under reduced pressure. The crude mixture was purified by silica

gel flash chromatography eluting with 9:1 hexanes/EtOAc to provide (*S*)-6-((*S*)-((*tert*-butyldimethylsilyl)oxy)(furan-3-yl)methyl)-2,6-dimethylcyclohex-1-en-1-yl trifluoromethanesulfonate **1.88** (792.3 mg, 93%) as a viscous colorless oil. IR (ATR): 3492, 2962, 2927, 1641, 1360, 1271, 1199, 1027, 608 cm^{-1}. ^{1}H NMR ($CDCI_3$) δ: 7.35 (1H, s), 7.27 (1H, s), 6.59 (1H, br s), 6.28 (1H, s), 5.22 (1H, s), 2.27 (2H, br m), 1.82 (2H, m), 1.71 (3H, s), 0.91 (9H, s), 0.04 (3H, s), -0.19(3H, s). ^{13}C NMR (100 MHz, $CDCl_3$) δ: 202.90, 143.91, 141.73, 140.32, 134.5, 126.7, 110.8, 71.2, 50.7, 27.5, 3.9, 22.5, 20.0, 18.2, 16.3, -4.6, -5.2. HRMS (ESI) calculated for $C_{19}H_{31}O_3Si$ $[M + H]^+$ 335.1964, found 335.1965.

Preparation of (2S)-2-((S)-furan-3-yl((2-(trimethylsilyl)ethoxy)methoxy)methyl)-2,6-dimethylcyclohexanone (1.99)

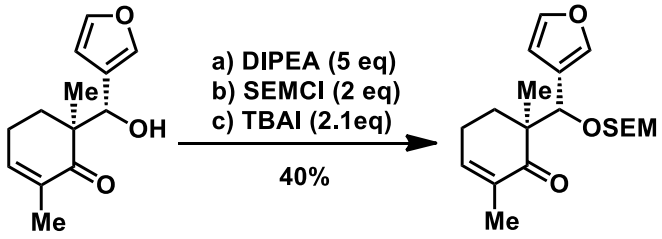

1.88 **1.99**

(2S)-2-((S)-furan-3-yl((2-(trimethylsilyl)ethoxy)methoxy)methyl)-2,6-dimethylcyclohexanone (1.99). To a round-bottomed flask was added (*S*)-6-((*S*)-furan-3-yl(hydroxy)methyl)-2,6-dimethylcyclohex-2-enone **1.88** (300 mg, 1.36 mmol, 1 equiv) and DCM (40.0 mL). The reaction mixture was then cooled to 0 ˚C, then diispropylamine (1.6 mL, 9.1 mmol, 5 equiv) was added and allowed to stir for 15 min. After 15 min, SEMCl

(651 μL, 3.62 mmol, 2 equiv) and TBAI (740 mg, 2.0 mmol, 1.1 equiv) were added to the reaction mixture then allowed to warm to rt and stir for 16 h. After 16 h, the reaction was diluted with Et_2O (10 mL) and then the organic layer was washed with brine. The combined organic layers were dried over sodium sulfate, filtered and then concentrated in under reduced pressure. The crude mixture was purified by silica gel flash chromatography eluting with 9:1 hexanes/EtOAc to provide (2S)-2-((S)-furan-3-yl((2-(trimethylsilyl)ethoxy)methoxy)methyl)-2,6-dimethylcyclohexanone **1.99** (190 mg, 40%) as a viscous colorless oil. ^{1}H NMR ($CDCI_3$) δ: 7.33 (1H, s), 7.30 (1H, s), 6.60 (1H, br s), 6.31 (1H, s), 5.15 (1H, s), 4.58 (2H, s), 3.65 (2H, m), 2.30 (2H, s), 1.84 (2H, m), 1.74 (3H, s), 1.22 (3H, s), 0.96 (2H, m), 0.00 (12H, s). HRMS (ESI) calculated for $C_{19}H_{31}O_4Si$ [M + H]$^+$ 351.1913, found 351.1912.

Preparation of (2S)-2-((S)-((tert-butyldimethylsilyl)oxy)(furan-3-yl)methyl)-2,6-dimethylcyclohexanone (1.97)

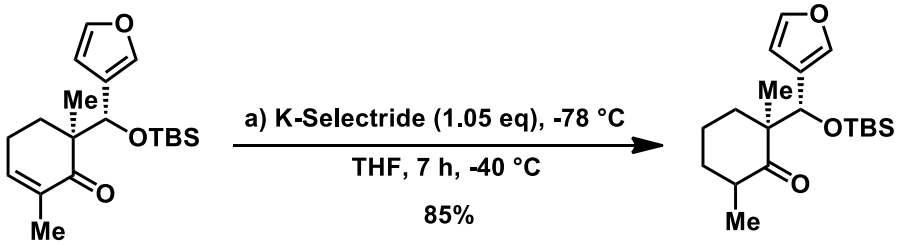

1.88 **1.97**

(2S)-2-((S)-((tert-butyldimethylsilyl)oxy)(furan-3-yl)methyl)-2,6-dimethylcyclohexanone (**1.97**).

To a round-bottomed flask was added enone **1.88**, (100 mg, 0.3 mmol, 1 equiv) and Et_2O (15 mL). The reaction mixture was then cooled to –78 ˚C before adding K-Selectride (320.6 μL, 0.32 mmol, 1.05 equiv). The reaction mixture was allowed to warm to – 40 ˚C and allowed to stir for 7 h. After 7 h, the reaction mixture was allowed to warm to room temperature. The reaction was quenched with MeOH (250.0 μL). The aqueous layer was extracted with Et_2O (3 x 5 mL) and the combined organic layers were washed with brine and dried over sodium sulfate, filtered and then concentrated under reduced pressure. The crude mixture was purified by silica gel flash chromatography eluting with 9:1 hexanes/Et_2O to provide (2*S*)-2-((*S*)-((*tert*-butyldimethylsilyl)oxy)(furan-3-yl)methyl)-2,6-dimethylcyclohexanone **1.88**, (101 mg, 85%) as a viscous colorless oil.

IR (ATR): 2959, 2923, 1641, 1361, 1268, 1203, 1028, 603 cm^{-1}. NMR ^1H ($CDCI_3$) δ: 7.27 (1H, s), 7.23 (1H, s), 6.31 (1H, s), 5.16 (1H, s), 2.53 (1H, m), 1.90(1H, m), 1.68 (5H, m), 1.29 (3H, s), 0.96 (3H, d J = 6.5 Hz), 0.89 (9H, s), 0.06 (3H, s), -0.14 (3H, s). ^{13}C NMR (100 MHz, $CDCl_3$) δ: 216.2, 141.7, 140.9, 127.3, 111.3, 71.3, 54.3, 41.6, 35.2, 32.4, 26.0, 22.2, 21.0, 18.3, 15.1, -4.5, -5.0. HRMS (ESI) calculated for $C_{19}H_{33}O_3Si$ $[M + H]^+$ 337.2121, found 337.2124.

Preparation of (2S)-2-((S)-furan-3-yl((2-(trimethylsilyl)ethoxy)methoxy)methyl)-2,6-dimethylcyclohexanone (1.100)

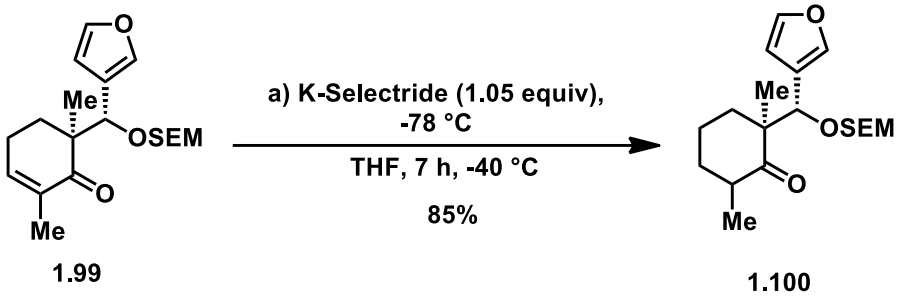

(2S)-2-((S)-furan-3-yl((2-(trimethylsilyl)ethoxy)methoxy)methyl)-2,6-dimethylcyclohexanone (1.100).

To a round-bottomed flask was added enone **1.99** (315 mg, 0.898 mmol, 1 equiv) and Et_2O (30 mL). The reaction mixture was then cooled to –78 ˚C before adding K-Selectride (0.943 mmol, 1.05 equiv). The reaction mixture was allowed to warm to –40 ˚C and allowed to stir for 7 h. After 7 h, the reaction mixture was allowed to warm to room temperature. The reaction was quenched with MeOH (250.0 μL). The aqueous layer was extracted with Et_2O (3 x 5 mL) and the combined organic layers were washed with brine and dried over sodium sulfate, filtered and then concentrated under reduced pressure. The crude mixture was purified by silica gel flash chromatography eluting with 9:1 hexanes/Et_2O to provide (2*S*)-2-((*S*)-furan-3-yl((2-(trimethylsilyl)ethoxy)methoxy)methyl)-2,6-dimethylcyclohexanone **1.100**, (260 mg, 83%) as a viscous colorless oil. ^{1}H NMR ($CDCl_3$) δ: 7.41 (2H, s), 6.35 (1H, s), 5.34 (1H, s), 4.49 (2H, q), 3.62 (2H, m), 2.90 (1H, m), 2.25 (2H, m), 1.7-1.3 (4H, m), 1.05 (3H, d, *J* = 6.5 Hz), 1.00 (3H, s), 0.95 (2H, m).

1.6 NMR Spectra

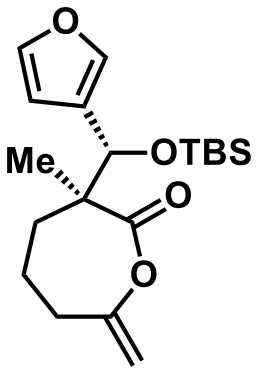

Proposed structure of side-product from triflation reactions based on HRMS and NMR analysis.

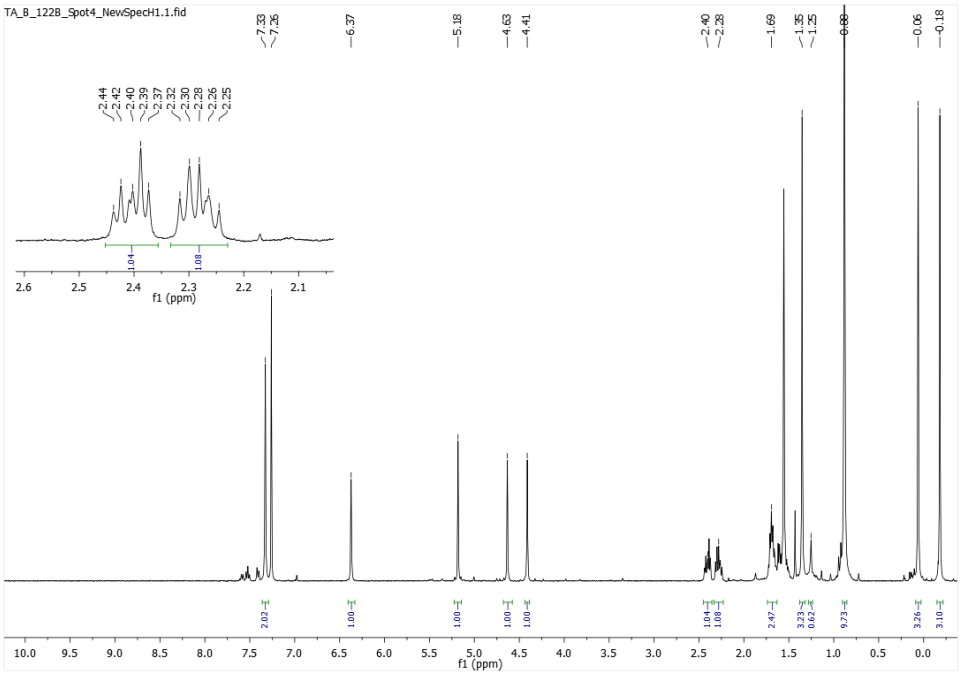

Proton NMR

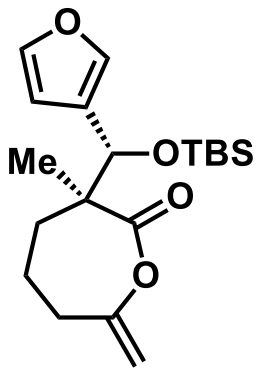

Proposed structure of side-product from triflation reactions based on HRMS and NMR analysis.

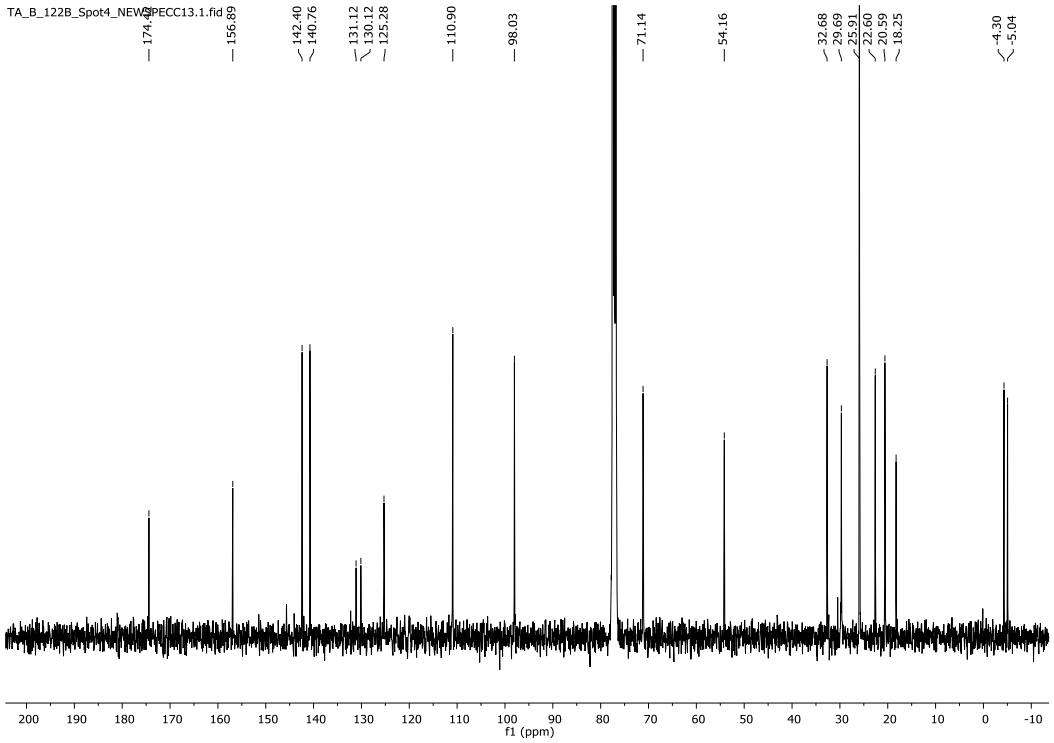

Carbon NMR

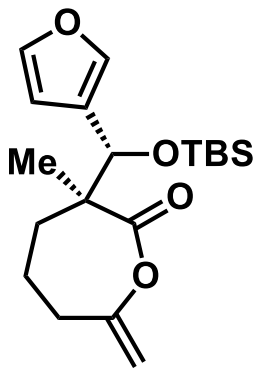

Proposed structure of side-product from triflation reactions based on HRMS and NMR analysis.

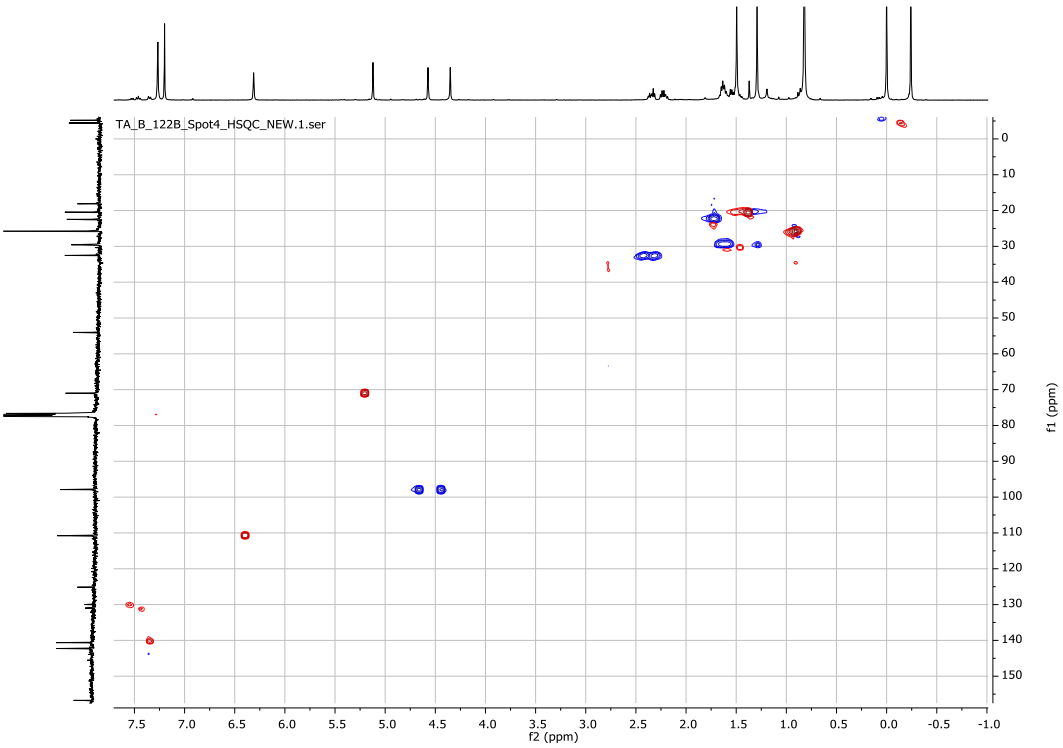

HSQC

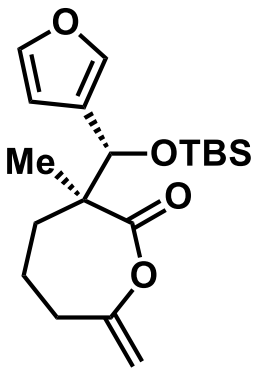

Proposed structure of side-product from triflation reactions based on HRMS and NMR analysis.

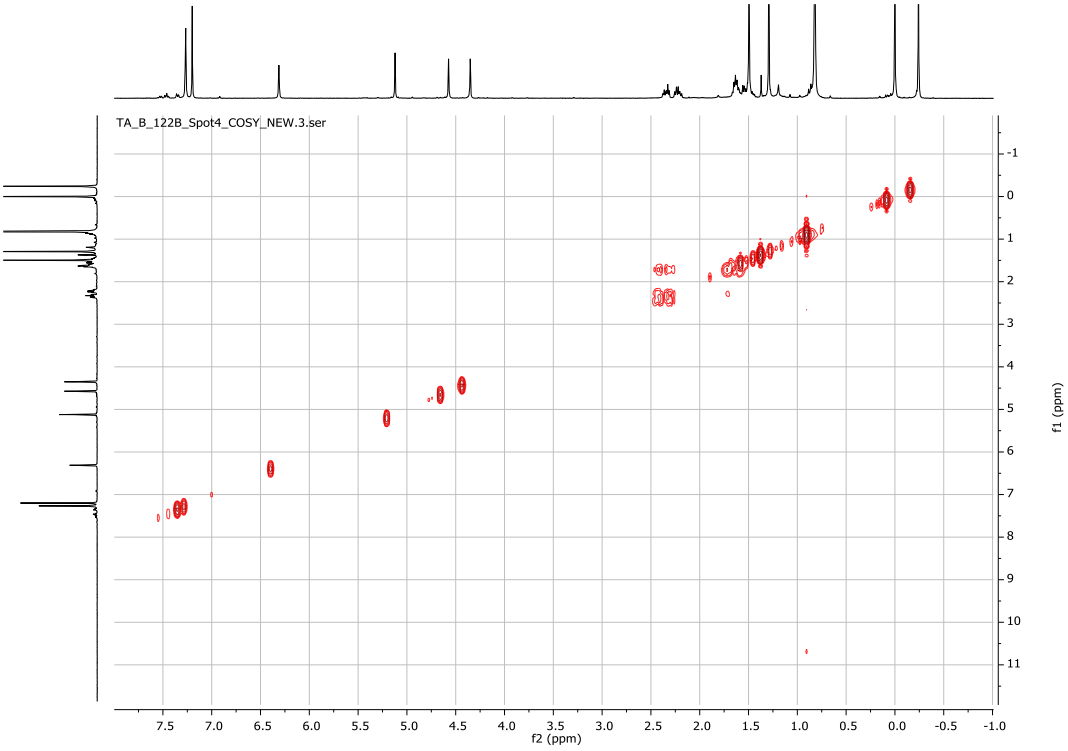

COSY

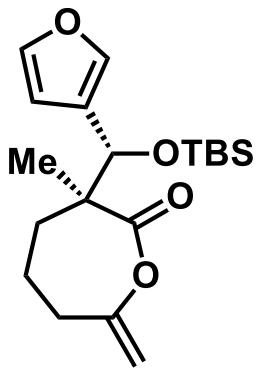

Proposed structure of side-product from triflation reactions based on HRMS and NMR analysis.

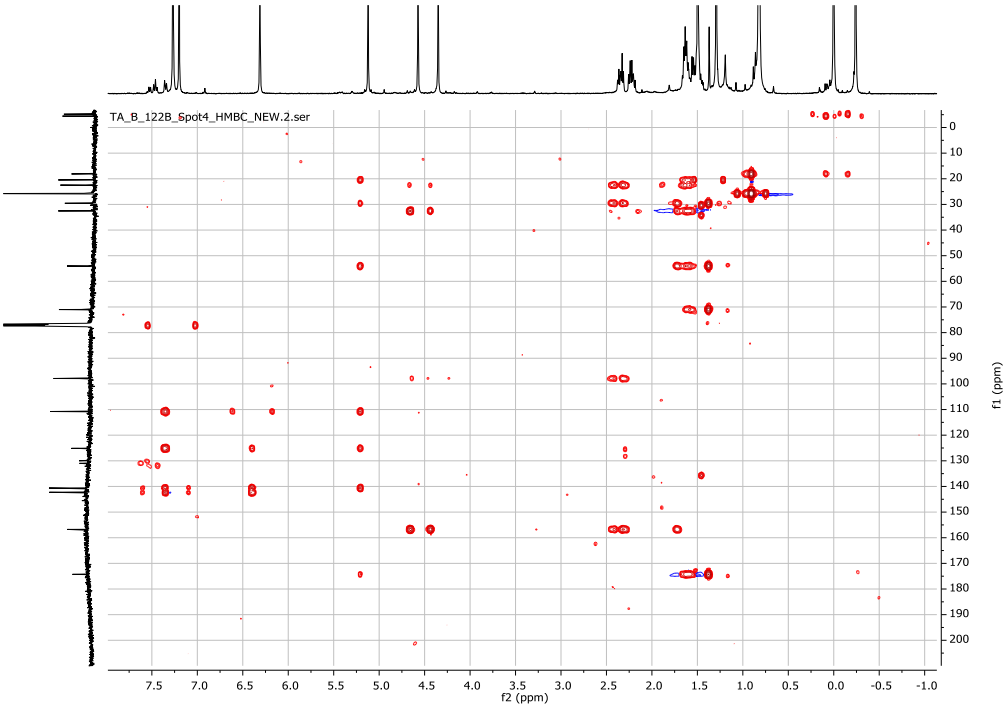

HMBC

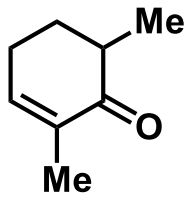
Me
O
Me

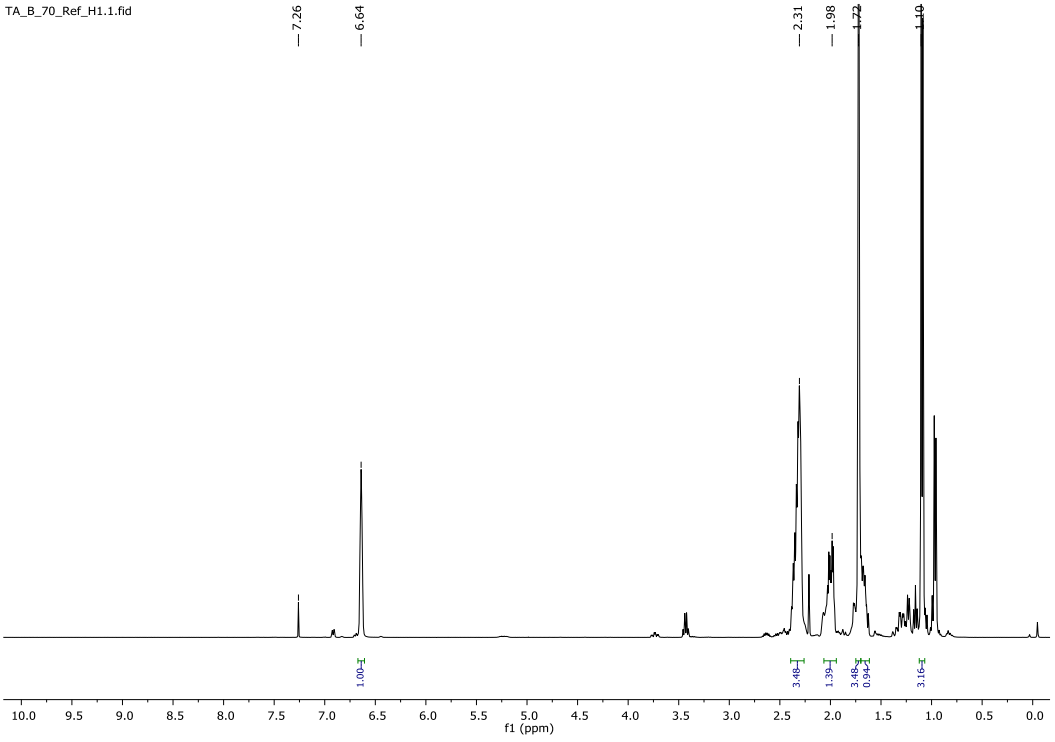
TA_B_70_Ref_H1.1.fid
7.26
6.64
2.31
1.98
1.72
1.10
1.00
3.48
1.39
3.48
0.94
3.16
10.0 9.5 9.0 8.5 8.0 7.5 7.0 6.5 6.0 5.5 5.0 4.5 4.0 3.5 3.0 2.5 2.0 1.5 1.0 0.5 0.0
f1 (ppm)

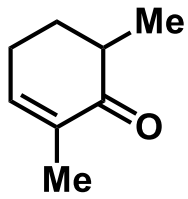
Me
O
Me

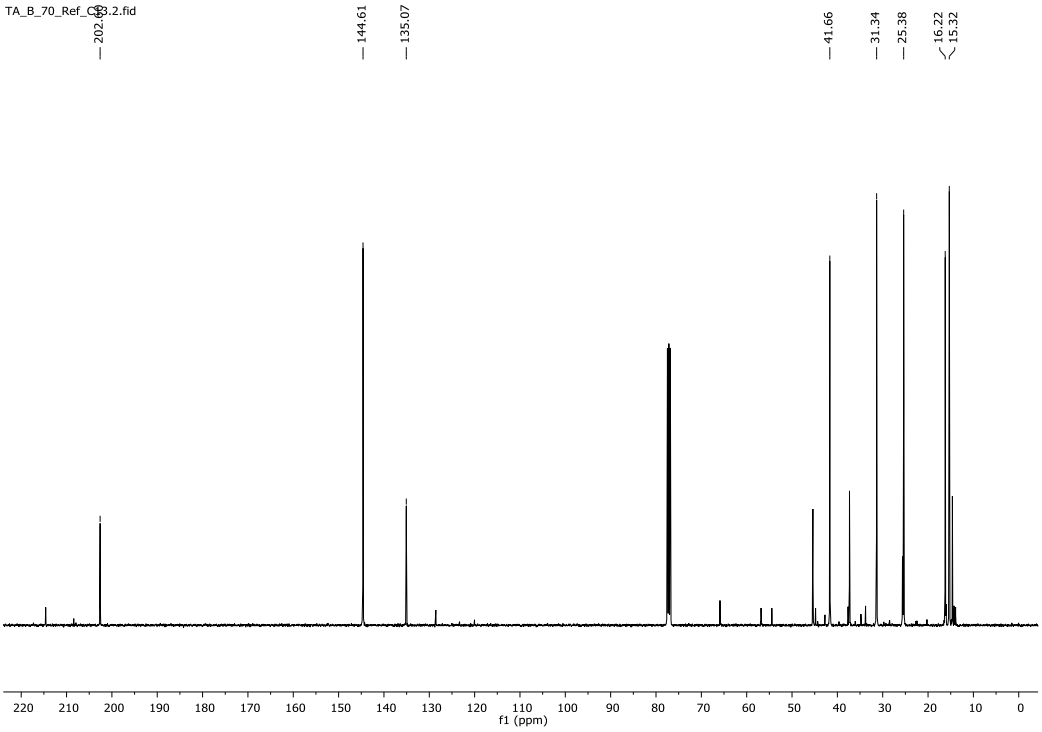
TA_B_70_Ref_CD3.2.fid
202.66
144.61
135.07
41.66
31.34
25.38
16.22
15.32
220 210 200 190 180 170 160 150 140 130 120 110 100 90 80 70 60 50 40 30 20 10 0
f1 (ppm)

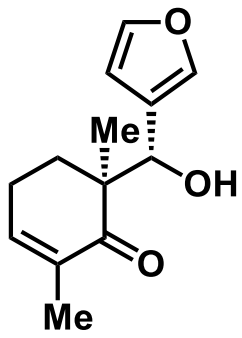
O
Me
OH
O
Me

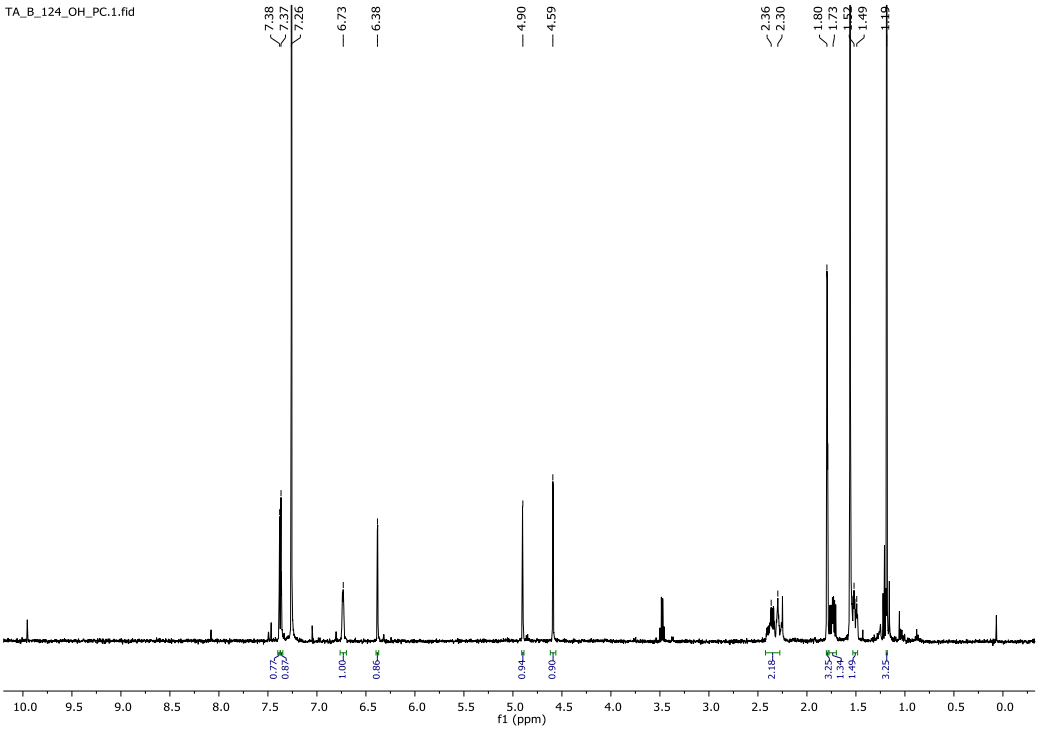
TA_B_124_OH_PC.1.fid
7.38
7.37
7.26
6.73
6.38
4.90
4.59
2.36
2.30
1.80
1.73
1.52
1.49
1.10
0.77
0.87
1.00
0.86
0.94
0.90
2.18
3.25
1.34
1.46
3.25
10.0
9.5
9.0
8.5
8.0
7.5
7.0
6.5
6.0
5.5
5.0
4.5
4.0
3.5
3.0
2.5
2.0
1.5
1.0
0.5
0.0
f1 (ppm)

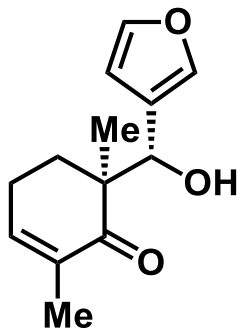
O
Me
OH
O
Me

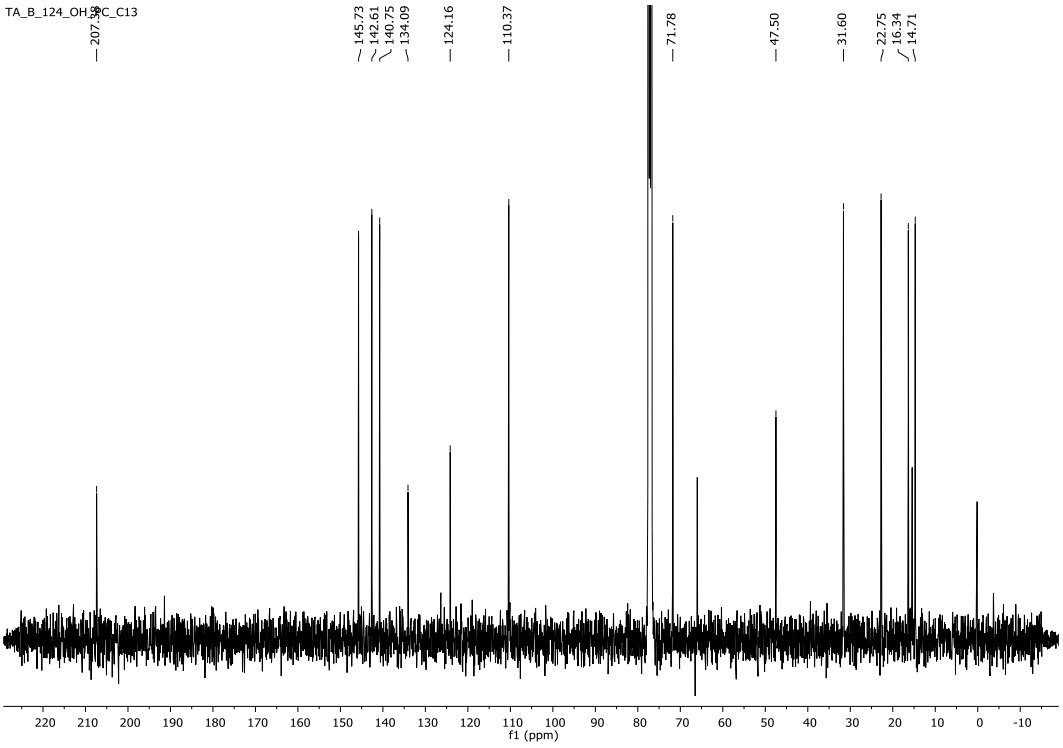
TA_B_124_OH_13C_C13
207.36
145.73
142.61
140.75
134.09
124.16
110.37
71.78
47.50
31.60
22.75
16.34
14.71
220 210 200 190 180 170 160 150 140 130 120 110 100 90 80 70 60 50 40 30 20 10 0 -10
f1 (ppm)

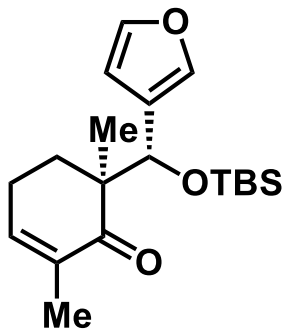
O
Me
OTBS
O
Me

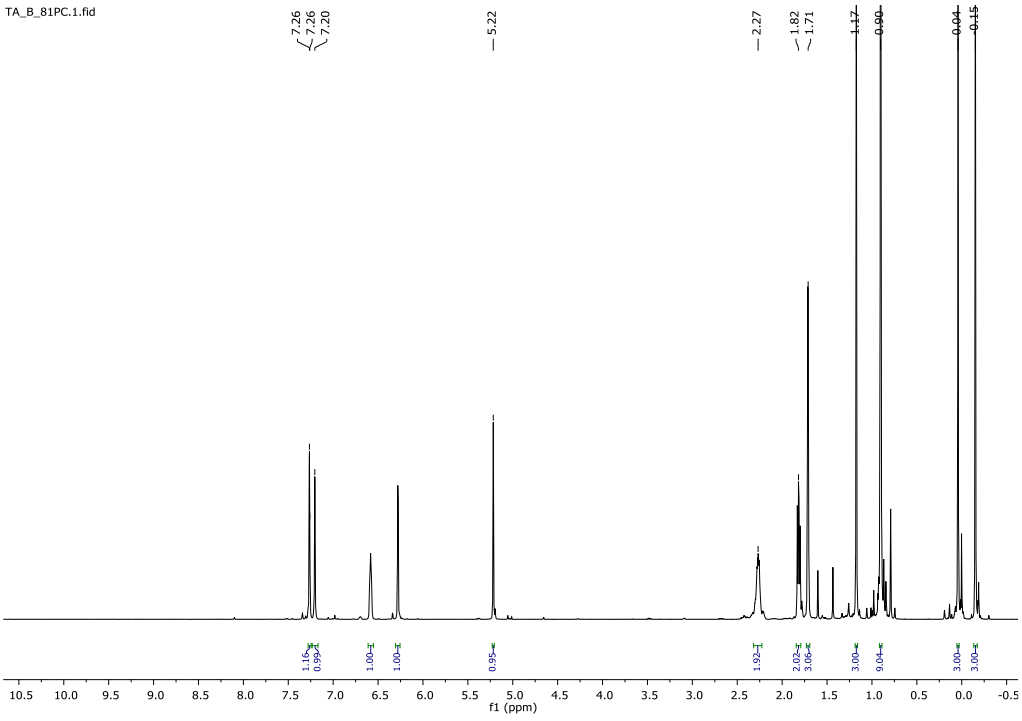
TA_B_81PC.1.fid
7.26
7.26
7.20
5.22
2.27
1.82
1.71
1.17
0.90
0.04
0.15
1.16
0.99
1.00
1.00
0.95
1.92
2.02
3.06
3.00
9.04
3.00
3.00
10.5
10.0
9.5
9.0
8.5
8.0
7.5
7.0
6.5
6.0
5.5
5.0
4.5
4.0
3.5
3.0
2.5
2.0
1.5
1.0
0.5
0.0
-0.5
f1 (ppm)

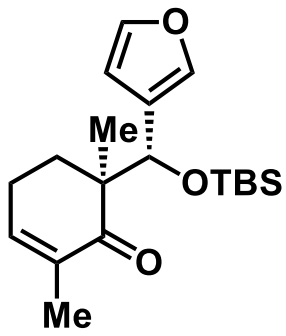
O
Me
OTBS
O
Me

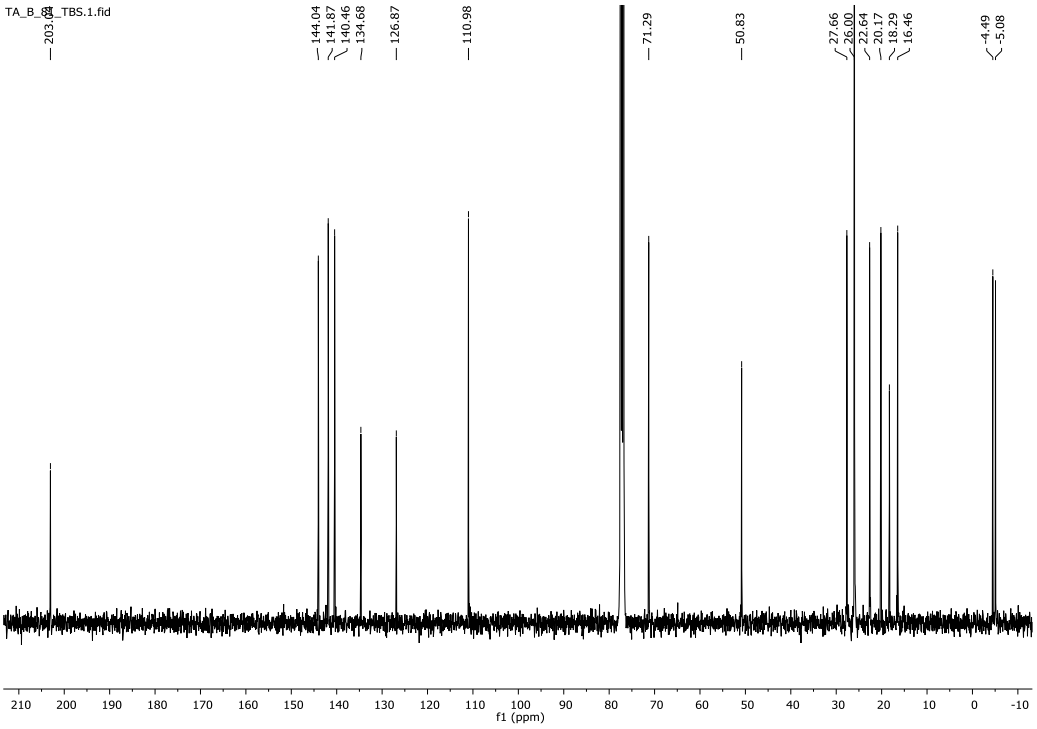
TA_B_88_TBS.1.fid
203.04
144.04
141.87
140.46
134.68
126.87
110.98
71.29
50.83
27.66
26.00
22.64
20.17
18.29
16.46
-4.49
-5.08
210 200 190 180 170 160 150 140 130 120 110 100 90 80 70 60 50 40 30 20 10 0 -10
f1 (ppm)

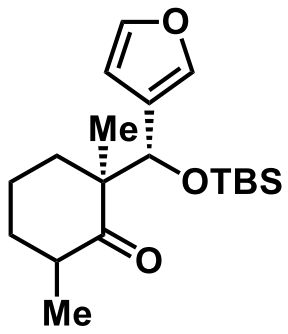
O
Me
OTBS
O
Me

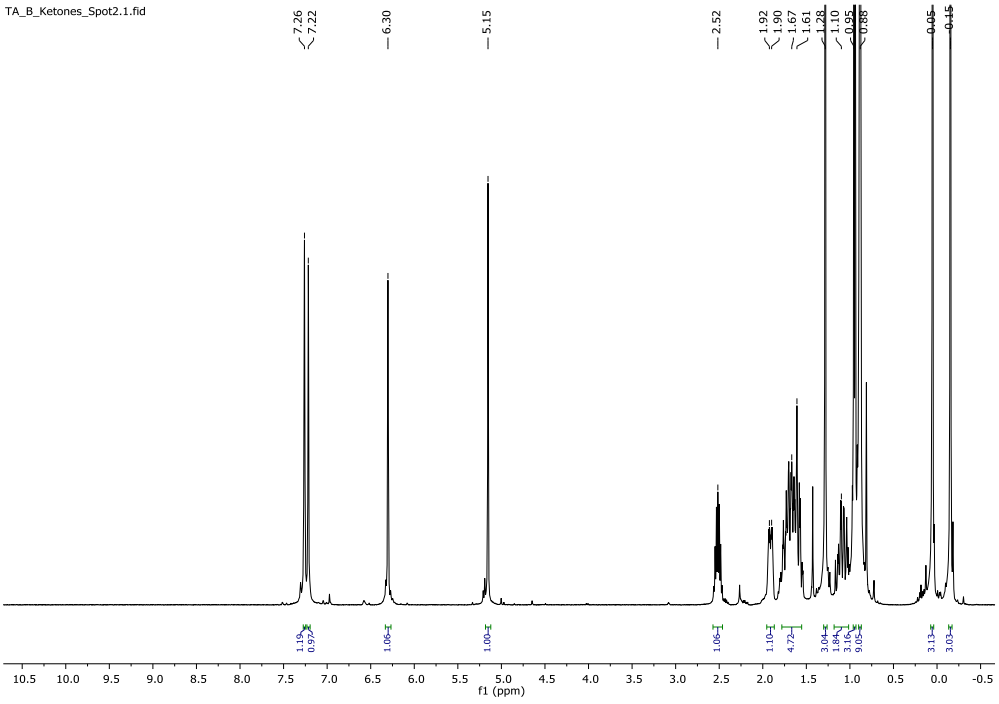
TA_B_Ketones_Spot2.1.fid
7.26
7.22
6.30
5.15
2.52
1.92
1.90
1.67
1.61
1.28
1.10
0.95
0.88
0.05
0.15
1.19
0.97
1.06
1.00
1.06
1.10
4.72
3.04
3.84
3.15
9.00
3.13
3.00
10.5 10.0 9.5 9.0 8.5 8.0 7.5 7.0 6.5 6.0 5.5 5.0 4.5 4.0 3.5 3.0 2.5 2.0 1.5 1.0 0.5 0.0 -0.5
f1 (ppm)

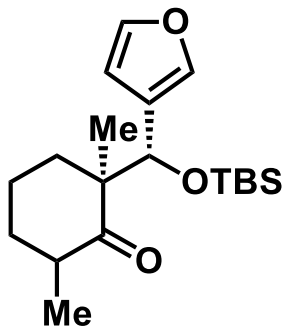
O
Me
OTBS
O
Me

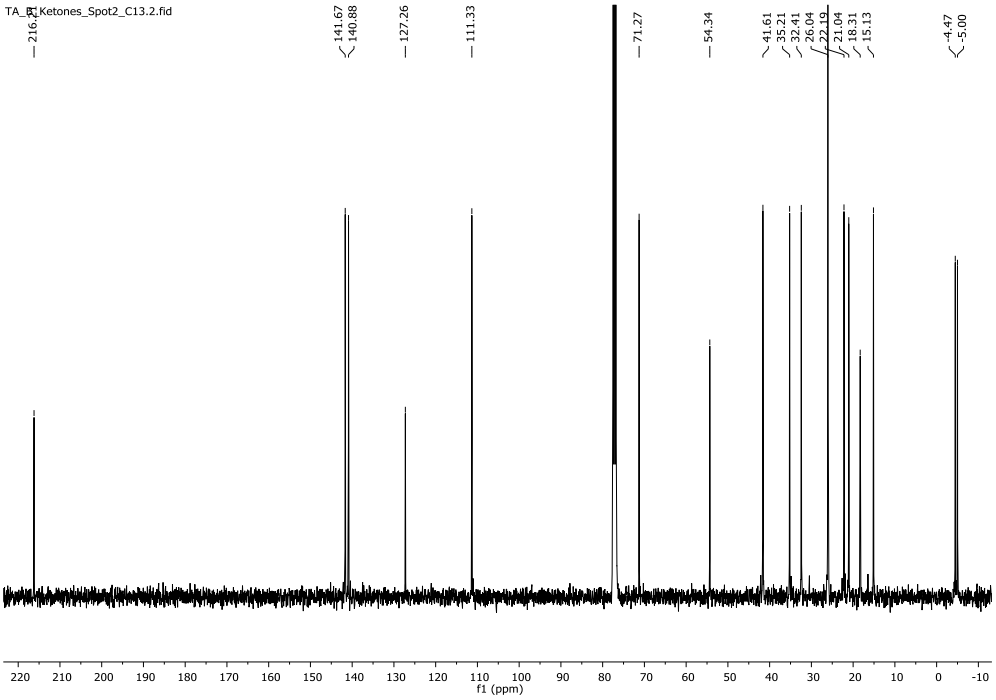
TA_Pd Ketones_Spot2_C13.2.fid
216.47
141.67
140.88
127.26
111.33
71.27
54.34
41.61
35.21
32.41
26.04
22.19
21.04
18.31
15.13
-4.47
-5.00
220 210 200 190 180 170 160 150 140 130 120 110 100 90 80 70 60 50 40 30 20 10 0 -10
f1 (ppm)

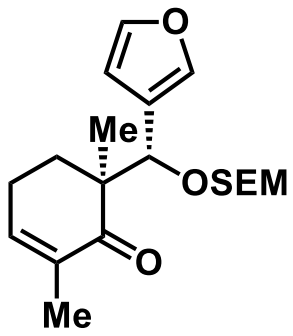
O
Me
OSEM
O
Me

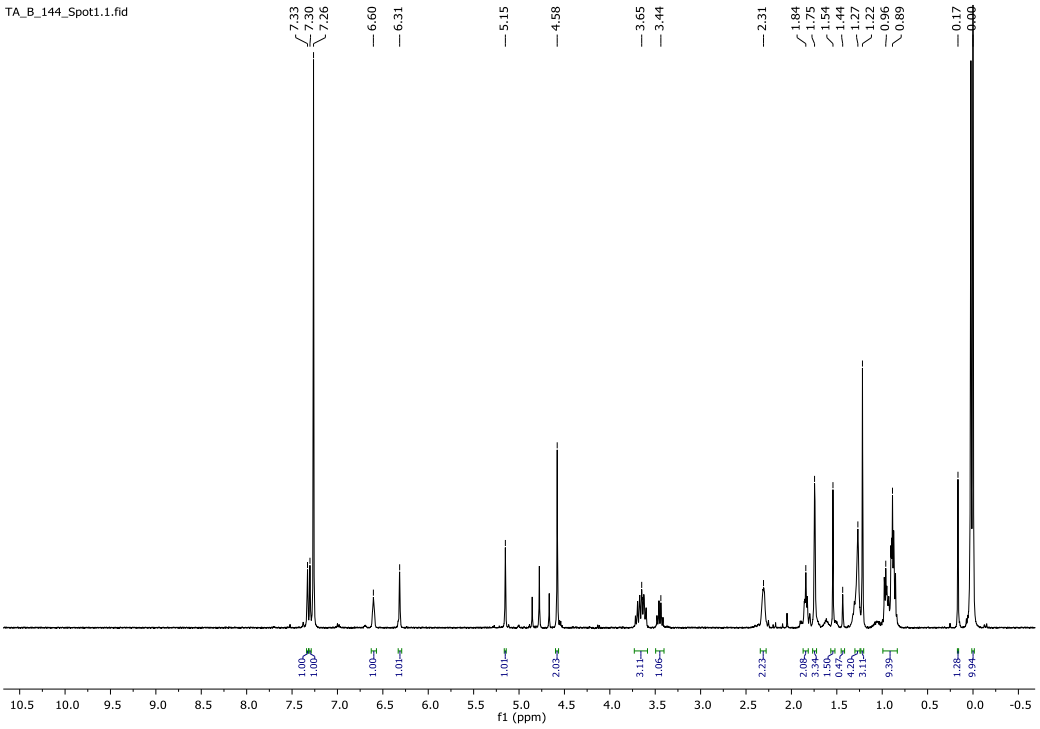
TA_B_144_Spot1.1.fid
7.33
7.30
7.26
6.60
6.31
5.15
4.58
3.65
3.44
2.31
1.84
1.75
1.54
1.44
1.27
1.22
0.96
0.89
0.17
0.00
f1 (ppm)

1.7 References

(1) Arnott, S.; Davie, A. W.; Robertson, J. M.; Sim, G. A.; Watson, D. G. The Structure of Limonin. *Experientia* **1960**, *16* (2), 49–51.

(2) Champagne, D. E.; Koul, O.; Isman, M. B.; Scudder, G. G. E.; Neil Towers, G. H. Biological Activity of Limonoids from the Rutales. *Phytochemistry* **1992**, *31* (2), 377–394. https://doi.org/10.1016/0031-9422(92)90003-9.

(3) Heasley, B. Synthesis of Limonoid Natural Products. *Eur. J. Org. Chem.* **2011**, *2011* (1), 19–46. https://doi.org/10.1002/ejoc.201001218.

(4) Morgan, E. D. Azadirachtin, a Scientific Gold Mine. *Bioorganic & Medicinal Chemistry* **2009**, *17* (12), 4096–4105. https://doi.org/10.1016/j.bmc.2008.11.081.

(5) Fischer, A.; Nakai, Y.; Eubanks, L. M.; Clancy, C. M.; Tepp, W. H.; Pellett, S.; Dickerson, T. J.; Johnson, E. A.; Janda, K. D.; Montal, M. Bimodal Modulation of the Botulinum Neurotoxin Protein-Conducting Channel. *PNAS* **2009**, *106* (5), 1330–1335. https://doi.org/10.1073/pnas.0812839106.

(6) Kuo, R.-Y.; Qian, K.; L. Morris-Natschke, S.; Lee, K.-H. Plant-Derived Triterpenoids and Analogues as Antitumor and Anti-HIV Agents. *Natural Product Reports* **2009**, *26* (10), 1321–1344. https://doi.org/10.1039/B810774M.

(7) Uddin, S. J.; Nahar, L.; Shilpi, J. A.; Shoeb, M.; Borkowski, T.; Gibbons, S.; Middleton, M.; Byres, M.; Sarker, S. D. Gedunin, a limonoid from Xylocarpus granatum, inhibits the growth of CaCo-2 colon cancer cell line In Vitro. *Phytotherapy Research* **2007**, *21* (8), 757–761. https://doi.org/10.1002/ptr.2159.

(8) Tanaka, T.; Maeda, M.; Kohno, H.; Murakami, M.; Kagami, S.; Miyake, M.; Wada, K. Inhibition of Azoxymethane-Induced Colon Carcinogenesis in Male F344 Rats by the Citrus Limonoids Obacunone and Limonin. *Carcinogenesis* **2001**, *22* (1), 193–198. https://doi.org/10.1093/carcin/22.1.193.

(9) Brandt, G. E. L.; Schmidt, M. D.; Prisinzano, T. E.; Blagg, B. S. J. Gedunin, a Novel Hsp90 Inhibitor: Semisynthesis of Derivatives and Preliminary Structure−Activity

Relationships. *J. Med. Chem.* **2008**, *51* (20), 6495–6502. https://doi.org/10.1021/jm8007486.

(10) Caboni, P.; Ntalli, N. G.; Bueno, C. E.; Alchè, L. E. Isolation and Chemical Characterization of Components with Biological Activity Extracted from Azadirachta Indica and Melia Azedarach. In *Emerging Trends in Dietary Components for Preventing and Combating Disease*; ACS Symposium Series; American Chemical Society, 2012; Vol. 1093, pp 51–77. https://doi.org/10.1021/bk-2012-1093.ch004.

(11) Li, X. Recent Studies on Insecticidal Activities of Limonoids from Meliaceous Plants. *Insect Science* **1999**, *6* (3), 283–288. https://doi.org/10.1111/j.1744-7917.1999.tb00124.x.

(12) Sarria, A. L. F.; Soares, M. S.; Matos, A. P.; Fernandes, J. B.; Vieira, P. C.; Silva, M. F. das G. F. da. Effect of Triterpenoids and Limonoids Isolated from Cabralea Canjerana and Carapa Guianensis (Meliaceae) against Spodoptera Frugiperda (J. E. Smith). *Zeitschrift für Naturforschung C* **2011**, *66* (5–6), 245–250. https://doi.org/10.1515/znc-2011-5-607.

(13) Chen, W.; Isman, M. B.; Chiu, S.-F. Antifeedant and Growth Inhibitory Effects of the Limonoid Toosendanin and Melia Toosendan Extracts on the Variegated Cutworm, Peridromasaucia (Lep., Noctuidae). *Journal of Applied Entomology* **1995**, *119* (1–5), 367–370. https://doi.org/10.1111/j.1439-0418.1995.tb01302.x.

(14) Manners, G. D. Citrus Limonoids: Analysis, Bioactivity, and Biomedical Prospects. *J. Agric. Food Chem.* **2007**, *55* (21), 8285–8294. https://doi.org/10.1021/jf071797h.

(15) Aarthy, T.; Mulani, F. A.; Pandreka, A.; Kumar, A.; Nandikol, S. S.; Haldar, S.; Thulasiram, H. V. Tracing the Biosynthetic Origin of Limonoids and Their Functional Groups through Stable Isotope Labeling and Inhibition in Neem Tree (Azadirachta Indica) Cell Suspension. *BMC Plant Biology* **2018**, *18* (1), 230.

.

(16) Hasegawa, S. Biochemistry of Limonoids in Citrus. In *Citrus Limonoids*; ACS Symposium Series; American Chemical Society, 2000; Vol. 758, pp 9–30. https://doi.org/10.1021/bk-2000-0758.ch002.

(17) Hasegawa, S.; Herman, Z. Biosynthesis of Limonoids: Conversion of Deacetylnomilinate to Nomilin in Citrus Limon. *Phytochemistry* **1986**, *25* (11), 2523–2524. https://doi.org/10.1016/S0031-9422(00)84500-8.

(18) Behenna, D. C.; Corey, E. J. Simple Enantioselective Approach to Synthetic Limonoids. *J. Am. Chem. Soc.* **2008**, *130* (21), 6720–6721. https://doi.org/10.1021/ja802376g.

(19) Corey, E. J.; Reid, J. G.; Myers, A. G.; Hahl, R. W. Simple Synthetic Route to the Limonoid System. *J. Am. Chem. Soc.* **1987**, *109* (3), 918–919. https://doi.org/10.1021/ja00237a058.

(20) Stoltz, B. M.; Kano, T.; Corey, E. J. Enantioselective Total Synthesis of Nicandrenones. *J. Am. Chem. Soc.* **2000**, *122* (37), 9044–9045. https://doi.org/10.1021/ja0024892.

(21) Han, X.; Stoltz, B. M.; Corey, E. J. Cuprous Chloride Accelerated Stille Reactions. A General and Effective Coupling System for Sterically Congested Substrates and for Enantioselective Synthesis. *J. Am. Chem. Soc.* **1999**, *121* (33), 7600–7605. https://doi.org/10.1021/ja991500z.

(22) Veitch, G. E.; Beckmann, E.; Burke, B. J.; Boyer, A.; Maslen, S. L.; Ley, S. V. Synthesis of Azadirachtin: A Long but Successful Journey. *Angewandte Chemie International Edition* **2007**, *46* (40), 7629–7632. https://doi.org/10.1002/anie.200703027.

(23) Broughton, H. B.; Ley, S. V.; Slawin, A. M. Z.; Williams, D. J.; Morgan, E. D. X-Ray Crystallographic Structure Determination of Detigloyldihydroazadirachtin and Reassignment of the Structure of the Limonoid Insect Antifeedant Azadirachtin. *J. Chem. Soc., Chem. Commun.* **1986**, No. 1, 46–47. https://doi.org/10.1039/C39860000046.

(24) Denholm, A. A.; Jennens, L.; Ley, S. V.; Wood, A. Chemistry of Insect Antifeedants from Azadirachta Indica (Part 19): 1A Potential Relay Route for the Synthesis of Azadirachtin. *Tetrahedron* **1995**, *51* (23), 6591–6604. https://doi.org/10.1016/0040-4020(95)00297-L.

(25) Veitch, G. E.; Beckmann, E.; Burke, B. J.; Boyer, A.; Ayats, C.; Ley, S. V. A Relay Route for the Synthesis of Azadirachtin. *Angewandte Chemie International Edition* **2007**, *46* (40), 7633–7635. https://doi.org/10.1002/anie.200703028.

(26) Okamura, H.; Yamauchi, K.; Miyawaki, K.; Iwagawa, T.; Nakatani, M. Synthesis and Biological Activities of Degraded Limonoids, (±)-Fraxinellonone and Its Related Compounds. *Tetrahedron Letters* **1997**, *38* (2), 263–266. https://doi.org/10.1016/S0040-4039(96)02277-0.

(27) Pailer, M.; Schaden, G.; Spiteller, G.; Fenzl, W. Die Konstitution des Fraxinellons. *Monatshefte für Chemie* **1965**, *96* (4), 1324–1346. https://doi.org/10.1007/BF00904284.

(28) Yoon, J. S.; Yang, H.; Kim, S. H.; Sung, S. H.; Kim, Y. C. Limonoids from Dictamnus Dasycarpus Protect Against Glutamate-Induced Toxicity in Primary Cultured Rat Cortical Cells. *J Mol Neurosci* **2010**, *42* (1), 9–16. https://doi.org/10.1007/s12031-010-9333-1.

(29) The Challenge of Neurodegenerative Diseases https://neurodiscovery.harvard.edu/challenge (accessed Aug 17, 2017).

(30) Why Choose Neurodegenrative Diseases http://www.neurodegenerationresearch.eu/about/why/ (accessed Aug 17, 2017).

(31) Lewerenz, J.; Maher, P. Chronic Glutamate Toxicity in Neurodegenerative Diseases—What Is the Evidence? *Front Neurosci* **2015**, *9*. https://doi.org/10.3389/fnins.2015.00469.

(32) Atlante, A.; Calissano, P.; Bobba, A.; Giannattasio, S.; Marra, E.; Passarella, S. Glutamate Neurotoxicity, Oxidative Stress and Mitochondria. *FEBS Lett.* **2001**, *497* (1), 1–5.

(33) Fukuyama, Y.; Tokoroyama, T.; Kubota, T. Total Synthesis of Fraxinellone. *Tetrahedron Letters* **1972**, *13* (33), 3401–3404. https://doi.org/10.1016/S0040-4039(01)94055-9.

(34) Santos, K. P. dos; Motta, L. B.; Santos, D. Y. A. C.; Salatino, M. L. F.; Salatino, A.; Ferreira, M. J. P.; Lago, J. H. G.; Ruiz, A. L. T. G.; Carvalho, J. E. de; Furlan, C. M. Antiproliferative Activity of Flavonoids from Croton sphaerogynus Baill. (Euphorbiaceae) https://www.hindawi.com/journals/bmri/2015/212809/ (accessed Aug 16, 2018). https://doi.org/10.1155/2015/212809.

(35) Youn, U. J.; Miklossy, G.; Chai, X.; Wongwiwatthananukit, S.; Toyama, O.; Songsak, T.; Turkson, J.; Chang, L. C. Bioactive Sesquiterpene Lactones and Other Compounds Isolated from Vernonia Cinerea. *Fitoterapia* **2014**, *93*, 194–200. https://doi.org/10.1016/j.fitote.2013.12.013.

(36) Yoon, J. S.; Sung, S. H.; Kim, Y. C. Neuroprotective Limonoids of Root Bark of Dictamnus Dasycarpus. *J. Nat. Prod.* **2008**, *71* (2), 208–211. https://doi.org/10.1021/np070588o.

(37) Roth, B. L.; Baner, K.; Westkaemper, R.; Siebert, D.; Rice, K. C.; Steinberg, S.; Ernsberger, P.; Rothman, R. B. Salvinorin A: A Potent Naturally Occurring Nonnitrogenous κ Opioid Selective Agonist. *PNAS* **2002**, *99* (18), 11934–11939. https://doi.org/10.1073/pnas.182234399.

(38) Knight, D. W. Synthetic Approaches to Butenolides. *Contemporary Organic Synthesis* **1994**, *1* (4), 287. https://doi.org/10.1039/co9940100287.

(39) Shi, Y.; Roth, K. E.; Ramgren, S. D.; Blum, S. A. Catalyzed Catalysis Using Carbophilic Lewis Acidic Gold and Lewis Basic Palladium: Synthesis of Substituted Butenolides and Isocoumarins. *J. Am. Chem. Soc.* **2009**, *131* (50), 18022–18023. https://doi.org/10.1021/ja9068497.

(40) Zhang, W.; Tan, D.; Lee, R.; Tong, G.; Chen, W.; Qi, B.; Huang, K.-W.; Tan, C.-H.; Jiang, Z. Highly Enantio- and Diastereoselective Reactions of γ-Substituted Butenolides Through Direct Vinylogous Conjugate Additions. *Angewandte Chemie* **2012**, *124* (40), 10216–10220. https://doi.org/10.1002/ange.201205872.

(41) Demnitz, F. W. J. The Mukaiyama Reaction of Ketene Bis(Trimethylsilyl) Acetals with α-Halo Acetals: A Convenient Butenolide Synthesis. *Tetrahedron Letters* **1989**, *30* (45), 6109–6112. https://doi.org/10.1016/S0040-4039(01)93317-9.

(42) Beck, B.; Magnin-Lachaux, M.; Herdtweck, E.; Dömling, A. A Novel Three-Component Butenolide Synthesis. *Org. Lett.* **2001**, *3* (18), 2875–2878. https://doi.org/10.1021/ol016328u.

(43) Marcaccini, S.; Pepino, R.; Marcos, C. F.; Polo, C.; Torroba, T. Studies on Isocyanides and Related Compounds. Synthesis of Furan Derivatives and Their Transformation into Indole Derivatives. *Journal of Heterocyclic Chemistry* **2000**, *37* (6), 1501–1503. https://doi.org/10.1002/jhet.5570370615.

(44) Kang, S.-K.; Yamaguchi, T.; Ho, P.-S.; Kim, W.-Y.; Yoon, S.-K. Palladium-Catalyzed Coupling and Carbonylative Coupling of Silyloxy Compounds with Hypervalent Iodonium Salts. *Tetrahedron Letters* **1997**, *38* (11), 1947–1950. https://doi.org/10.1016/S0040-4039(97)00230-X.

(45) Hyde, A. M.; Buchwald, S. L. Synthesis of 5,5-Disubstituted Butenolides Based on a Pd-Catalyzed γ-Arylation Strategy. *Org. Lett.* **2009**, *11* (12), 2663–2666. https://doi.org/10.1021/ol9007102.

(46) Harvey, J. S.; Simonovich, S. P.; Jamison, C. R.; MacMillan, D. W. C. Enantioselective α-Arylation of Carbonyls via Cu(I)-Bisoxazoline Catalysis. *J. Am. Chem. Soc.* **2011**, *133* (35), 13782–13785. https://doi.org/10.1021/ja206050b.

(47) Bigot, A.; Williamson, A. E.; Gaunt, M. J. Enantioselective α-Arylation of N-Acyloxazolidinones with Copper(II)-Bisoxazoline Catalysts and Diaryliodonium Salts. *J. Am. Chem. Soc.* **2011**, *133* (35), 13778–13781. https://doi.org/10.1021/ja206047h.

(48) Kieffer, M. E.; Chuang, K. V.; Reisman, S. E. A Copper-Catalyzed Arylation of Tryptamines for the Direct Synthesis of Aryl Pyrroloindolines. *Chem Sci* **2012**, *3* (11), 3170–3174. https://doi.org/10.1039/C2SC20914D.

(49) Deprez, N. R.; Sanford, M. S. Reactions of Hypervalent Iodine Reagents with Palladium: Mechanisms and Applications in Organic Synthesis. *Inorganic Chemistry* **2007**, *46* (6), 1924–1935. https://doi.org/10.1021/ic0620337.

(50) Kalyani, D.; Deprez, N. R.; Desai, L. V.; Sanford, M. S. Oxidative C−H Activation/C−C Bond Forming Reactions: Synthetic Scope and Mechanistic Insights. *Journal of the American Chemical Society* **2005**, *127* (20), 7330–7331. https://doi.org/10.1021/ja051402f.

(51) Kitamura, T.; Fujiwara, Y. Recent Progress in the Use of Hypervalent Iodine Reagents in Organic Synthesis. a Review. *Organic Preparations and Procedures International* **1997**, *29* (4), 409–458. https://doi.org/10.1080/00304949709355217.

(52) Hyatt, I. F. D.; Dave, L.; David, N.; Kaur, K.; Medard, M.; Mowdawalla, C. Hypervalent Iodine Reactions Utilized in Carbon–Carbon Bond Formations. *Org. Biomol. Chem.* **2019**, *17* (34), 7822–7848. https://doi.org/10.1039/C9OB01267B.

(53) Bruno, N. C.; Tudge, M. T.; Buchwald, S. L. Design and Preparation of New Palladium Precatalysts for C–C and C–N Cross-Coupling Reactions. *Chem. Sci.* **2013**, *4* (3), 916–920. https://doi.org/10.1039/C2SC20903A.

(54) Gogoi, S.; Argade, N. P. A Facile Chemoenzymatic Approach to Natural Cytotoxic Ellipsoidone A and Natural Ellipsoidone B. *Tetrahedron* **2006**, *62* (11), 2715–2720. https://doi.org/10.1016/j.tet.2005.12.020.

(55) Manabe, A.; Matsumoto, R.; Shinada, T. Cyclopropanation of (E)-Dehydroaspartic Acid Esters with Furan Derivatives: The Synthesis of Highly Functionalized α-2,3-Methanoamino Acid Esters. *Synlett* **2015**, *26* (12), 1710–1714. https://doi.org/10.1055/s-0034-1380812.

(56) Wang, W.; Li, H.; Wang, J. Enantioselective Organocatalytic Mukaiyama−Michael Addition of Silyl Enol Ethers to α,β-Unsaturated Aldehydes. *Org. Lett.* **2005**, *7* (8), 1637–1639. https://doi.org/10.1021/ol0503337.

(57) Denmark, S. E.; Heemstra, J. R. Lewis Base Activation of Lewis Acids. Catalytic Enantioselective Addition of Silyl Enol Ethers of Achiral Methyl Ketones to Aldehydes. *Org. Lett.* **2003**, *5* (13), 2303–2306. https://doi.org/10.1021/ol034641l.

(58) Zhu, S.; MacMillan, D. W. C. Enantioselective Copper-Catalyzed Construction of Aryl Pyrroloindolines via an Arylation–Cyclization Cascade. *Journal of the American Chemical Society* **2012**, *134* (26), 10815–10818. https://doi.org/10.1021/ja305100g.

(59) Cahard, E.; Male, H. P. J.; Tissot, M.; Gaunt, M. J. Enantioselective and Regiodivergent Copper-Catalyzed Electrophilic Arylation of Allylic Amides with Diaryliodonium Salts. *Journal of the American Chemical Society* **2015**, *137* (25), 7986–7989. https://doi.org/10.1021/jacs.5b03937.

(60) Danishefsky, S.; Kitahara, T.; Yan, C. F.; Morris, J. Diels-Alder Reactions of Trans-1-Methoxy-3-Trimethylsilyloxy-1,3-Butadiene. *J. Am. Chem. Soc.* **1979**, *101* (23), 6996–7000. https://doi.org/10.1021/ja00517a036.

(61) Jung, J. Human Tumor Xenograft Models for Preclinical Assessment of Anticancer Drug Development. *Toxicol Res* **2014**, *30* (1), 1–5. https://doi.org/10.5487/TR.2014.30.1.001.

(62) Jung, M. E.; Davidov, P. Efficient Synthesis of a Tricyclic BCD Analogue of Ouabain: Lewis Acid Catalyzed Diels–Alder Reactions of Sterically Hindered Systems. *Angew. Chem. Int. Ed.* **2002**, *41* (21), 4125–4128. https://doi.org/10.1002/1521-3773(20021104)41:21<4125::AID-ANIE4125>3.0.CO;2-E.

(63) Jung, M. E.; Guzaev, M. Trimethylaluminum–Triflimide Complexes for the Catalysis of Highly Hindered Diels–Alder Reactions. *Org. Lett.* **2012**, *14* (20), 5169–5171. https://doi.org/10.1021/ol302172y.

(64) Jung, M. E.; Ho, D. G. Stepwise Acid-Promoted Double-Michael Process: An Alternative to Diels−Alder Cycloadditions for Hindered Silyloxydiene−Dienophile Pairs. *Org. Lett.* **2007**, *9* (2), 375–378. https://doi.org/10.1021/ol062980j.

(65) Jung, M. E.; Ho, D.; Chu, H. V. Synthesis of Highly Substituted Cyclohexenes via Mixed Lewis Acid-Catalyzed Diels−Alder Reactions of Highly Substituted Dienes and Dienophiles. *Org. Lett.* **2005**, *7* (8), 1649–1651. https://doi.org/10.1021/ol050361p.

(66) Fernández-Mateos, A.; Grande Benito, M.; Pascual Coca, G.; Rubio González, R.; Tapia Hernández, C. Synthesis of Dl-Pyroangolensolide. *Tetrahedron* **1995**, *51* (27), 7521–7526. https://doi.org/10.1016/0040-4020(95)00375-I.

(67) Mateos, A. F.; Coca, G. P.; Pérez Alonso, JoséJ.; González, R. R.; Hernández, C. T. Diastereoselective Aldol Reactions of 2,6-Dimethylcyclohexenone Lithium Enolate. *Tetrahedron Letters* **1995**, *36* (6), 961–964. https://doi.org/10.1016/0040-4039(94)02401-V.

(68) Faber, J. M.; Eger, W. A.; Williams, C. M. Enantioselective Total Synthesis of the Mexicanolides: Khayasin, Proceranolide, and Mexicanolide. *J. Org. Chem.* **2012**, *77* (20), 8913–8921. https://doi.org/10.1021/jo301182f.

(69a) Popov, S.; Shao, B.; Bagdasarian, A. L.; Benton, T. R.; Zou, L.; Yang, Z.; Houk, K. N.; Nelson, H. M. Teaching an Old Carbocation New Tricks: Intermolecular C–H Insertion Reactions of Vinyl Cations. *Science* **2018**, *361* (6400), 381–387. https://doi.org/10.1126/science.aat5440.

(69b) Von E. Doering, W.; Haines, R. M. Alkoxide-Catalyzed Autoxidative Cleavage of Ketones and Esters1. *J. Am. Chem. Soc.* **1954**, *76* (2), 482–486. https://doi.org/10.1021/ja01631a044.

(70) Barton, D. H. R.; O'Brien, R. E.; Sternhell, S. 88. A New Reaction of Hydrazones. *J. Chem. Soc.* **1962**, No. 0, 470–476. https://doi.org/10.1039/JR9620000470.

(71) Barton, D. H. R.; Bashiardes, G.; Fourrey, J.-L. An Improved Preparation of Vinyl Iodides. *Tetrahedron Letters* **1983**, *24* (15), 1605–1608. https://doi.org/10.1016/S0040-4039(00)81721-9.

(72) Boukouvalas, J.; Loach, R. P. General, Regiodefined Access to α-Substituted Butenolides through Metal−Halogen Exchange of 3-Bromo-2-Silyloxyfurans. Efficient Synthesis of an Anti-Inflammatory Gorgonian Lipid. *J. Org. Chem.* **2008**, *73* (20), 8109–8112. https://doi.org/10.1021/jo8015924.

(73) Funakoshi, Y.; Miura, T.; Murakami, M. Synthesis of Penta-2,4-Dien-1-Imines and 1,2-Dihydropyridines by Rhodium-Catalyzed Reaction of N-Sulfonyl-1,2,3-Triazoles with 2-(Siloxy)Furans. *Org. Lett.* **2016**, *18* (24), 6284–6287. https://doi.org/10.1021/acs.orglett.6b03143.

(74) Carroll, M. A.; Pike, V. W.; Widdowson, D. A. New Synthesis of Diaryliodonium Sulfonates from Arylboronic Acids. *Tetrahedron Letters* **2000**, *41* (28), 5393–5396. https://doi.org/10.1016/S0040-4039(00)00861-3.

(75) Kieffer, M. E.; Chuang, K. V.; Reisman, S. E. A Copper-Catalyzed Arylation of Tryptamines for the Direct Synthesis of Aryl Pyrroloindolines. *Chem Sci* **2012**, *3* (11), 3170–3174. https://doi.org/10.1039/C2SC20914D.

(76) Engl, P. S.; Fedorov, A.; Copéret, C.; Togni, A. N-Trifluoromethyl NHC Ligands Provide Selective Ruthenium Metathesis Catalysts. *Organometallics* **2016**, *35* (6), 887–893. https://doi.org/10.1021/acs.organomet.6b00028.

(77) Laudadio, G.; Gemoets, H. P. L.; Hessel, V.; Noël, T. Flow Synthesis of Diaryliodonium Triflates. *J. Org. Chem.* **2017**, *82* (22), 11735–11741. https://doi.org/10.1021/acs.joc.7b01346.

(78) Rainka, M. P.; Milne, J. E.; Buchwald, S. L. Dynamic Kinetic Resolution of α,β-Unsaturated Lactones through Asymmetric Copper-Catalyzed Conjugate Reduction: Application to the Total Synthesis of Eupomatilone-3. *Angewandte Chemie International Edition* **2005**, *44* (38), 6177–6180. https://doi.org/10.1002/anie.200501890.

(79) Joannesse, C.; Morrill, L. C.; Campbell, C. D.; Slawin, A. M. Z.; Smith, A. D. Isothiourea-Catalyzed Asymmetric O- to C-Carboxyl Transfer of Furanyl Carbonates. *Synthesis* **2011**, *2011* (12), 1865–1879. https://doi.org/10.1055/s-0030-1260602.

(80) He, R. J.; Zhu, B. C.; Wang, Y. G. Lewis Base-Catalyzed Electrophilic Lactonization of Selenyl Bromide Resin and Facile Solid-Phase Synthesis of Furan-2(5H)-One Derivatives. *Applied Organometallic Chemistry* **2014**, *28* (7), 523–528. https://doi.org/10.1002/aoc.3157.

(81) Yoneda, E.; Zhang, S.-W.; Zhou, D.-Y.; Onitsuka, K.; Takahashi, S. Ruthenium-Catalyzed Cyclocarbonylation of Allenyl Alcohols and Amines: Selective Synthesis of Lactones and Lactams. *J. Org. Chem.* **2003**, *68* (22), 8571–8576. https://doi.org/10.1021/jo0350615.

(82) Browne, D. M.; Niyomura, O.; Wirth, T. Catalytic Addition-Elimination Reactions Towards Butenolides. *Phosphorus, Sulfur, and Silicon and the Related Elements* **2008**, *183* (4), 1026–1035. https://doi.org/10.1080/10426500801901053.

(83) Ban, Y.; Ashida, Y.; Nakatsuji, H.; Tanabe, Y.; Ban, Y.; Ashida, Y.; Nakatsuji, H.; Tanabe, Y. Straightforward Synthesis of 2(5H)-Furanones as Promising Cross-Coupling Partners: Direct Furanone Annulation Utilizing Ti-Mediated Aldol Addition. *Molbank* **2016**, *2016* (4), M908. https://doi.org/10.3390/M908.

(84) Burns, A. S.; Rychnovsky, S. D. Total Synthesis and Structure Revision of (−)-Illisimonin A, a Neuroprotective Sesquiterpenoid from the Fruits of Illicium Simonsii. *J. Am. Chem. Soc.* **2019**, *141* (34), 13295–13300. https://doi.org/10.1021/jacs.9b05065.

(85) Schuppe, A. W.; Zhao, Y.; Liu, Y.; Newhouse, T. R. Total Synthesis of (+)-Granatumine A and Related Bislactone Limonoid Alkaloids via a Pyran to Pyridine Interconversion. *J. Am. Chem. Soc.* **2019**, *141* (23), 9191–9196. https://doi.org/10.1021/jacs.9b04508.

Chapter 2—Total Synthesis of Annotinolides A and B

2.1 Introduction

Background and Biological Activity

Lycopodium alkaloids are a class of structurally-diverse natural products consisting of over 200 compounds isolated from 54 plant species.[1,2] *Lycopodium* alkaloids can generally be described as quinolizine-type alkaloids. The first *Lycopodium* alkaloid isolated was lycopodine (Figure 2.1), isolated from *Lycopodium complanatum* in 1881 by Bodecker.[3] However, it was not until later in 1938 that Achmatowicz reisolated and determined its molecular formula. Since then, a greater understanding of the *Lycopodium* family's organization and biological activity has been advanced.[1] The *Lycopodium* alkaloids can be organized into four structural subclasses: the lycopodines, lycodines, fawcettimines, and a miscellaneous group. The miscellaneous group commonly features a tricyclic backbone and lacks a carboncarbon bond that establishes the B-ring of the more complex subclasses. Examples of each subclass are lycopodine, lycodine, fawcettimine, and phlegmarine, respectively (Figure 2.1). These *Lycopodium* alkaloids have attracted great interest from medicinal and synthetic chemists due to their potentially therapeutic biological activity, as well as their unique, complex structures.[1]

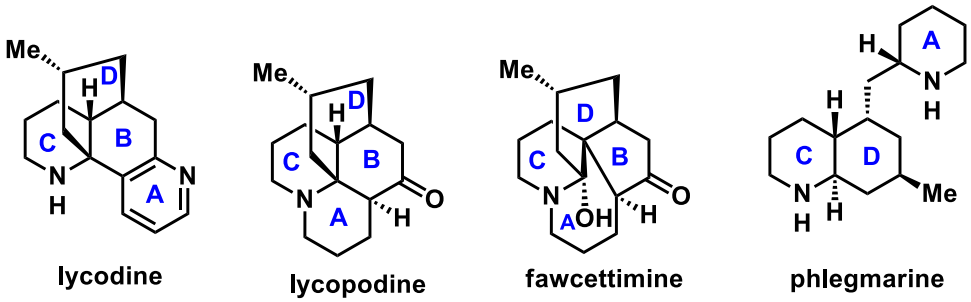

Figure 2.1 Representative members of each subclass of the lycopodium alkaloid family

During the mid-1980's, interest in *Lycopodium* alkaloids intensified as it was found that some members of this natural product family possess potent acetylcholinesterase (AChE)

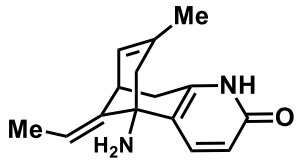

Huperzine A

Figure 2.2 Structure of huperzine

inhibition activity. This is significant because acetylcholinesterase is suggested to play a key role in the pathogenesis of Alzheimer's disease (AD), a devastating neurodegenerative disease that affects over 44 million people worldwide.[4,5] One of the most common markers of AD in the brain is characterized by a deficiency in AChE, as well as the aggregation of β-amyloid plaques and tau protein tangles. An observed deficiency of AChE has been linked to a decline in cognitive function, although the exact etiology is still unknown, as the broader pathogensis of AD eludes scientist to this day.[6] Cholinesterases are a ubiquitous class of serine hydrolases that function to hydrolyze choline esters. AChE rapidly hydrolyzes acetylcholine in the cholinergic synapses.[7] Of all the *Lycopodium* alkaloids evaluated, it was discovered that huperzine A (HupA) was the most potent.[8–10] HupA was first isolated from the Chinese herb *Qian Ceng Ta* by Liu and co-workers (Figure 2.2).[11,12] One major challenge for treating neurological diseases in the central nervous system (CNS) arises from the difficulty in the therapeutics penetrating the blood-brain-barrier to access the brain, which is necessary for carrying out their medicinal effect. Interestingly, it has been demonstrated that HupA is able to penetrate the blood-brain-barrier more efficiently, with better bioavailability and longer inhibition of acetylcholinesterase than several FDA approved Alzheimer's disease therapeutics,

including galantamine, tacrine, rivastigmine, or donepezil (Figure 2.3).[8,9,13] Additionally, HupA was able to reverse or attenuate cognitive deficits in a wide range of animal models.[10] Due to HupA's potent anti-acetylcholinesterase activity and selectivity, HupA was used in studies to determine structure-activity-relationships (SAR).[11,12] Furthermore, many research groups used HupA as inspiration for derivatives and analogs with the ultimate goal of improving potency and selectivity.[14]

In 1991, Mckinney and coworkers published a pivotal study on the stereoselectivities of the inhibition of rat cortical AChE by the two enantiomers of HupA.[14] It was ultimately discovered that (–)-HupA was more potent than its enantiomer (+)-HupA. (–)-HupA exhibited a K_i of 8 nM while (+)-HupA exhibited a K_i of 300 nM, making (–)-HupA 38 times more potent as an inhibitor. Interestingly, racemic samples of huperzine

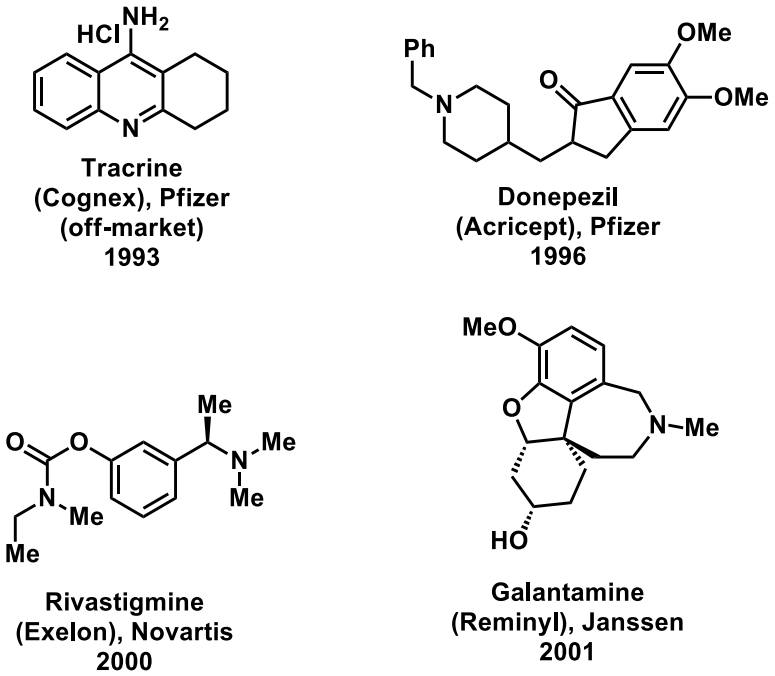

Figure 2.3 Currently approved Alzheimer's or dementia drugs

were only two times less potent than (–)-HupA. It was not until 1997 that Kozikowski and coworkers published their structural biology research using X-ray crystallography and computational modelling where they described the mechanism of action of HupA.[13–15] Kozikowski and coworkers found that HupA inhibits acetylcholinesterase by directly binding to the unoccupied active site of the enzyme and therefore preventing the natural substrate to access the active site. They went on to further hypothesize that the three-carbon, alkene-containing bridge is the pharmacophore, the structural part of the molecule

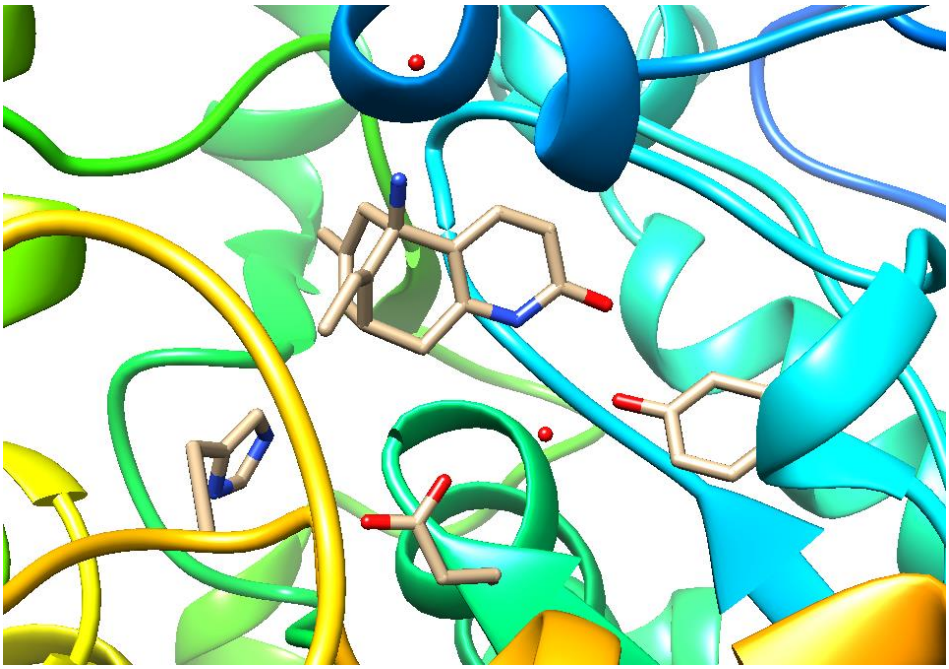

Figure 2.4 Huperzine A binding to acetylcholinesterase

responsible for the biological activity. When they examined the binding motif of (–)-Hup A to acetylcholinesterase through X-ray crystallography, they found that the three-carbon bridge of (–)-HupA was inserted into the hydrophobic area of the enzyme, where it was surrounded by aromatic amino acid residues.[15] It has also been shown that the amine also experiences multipoint hydrogen bonding interactions.[16] Further studies by Tang and

coworkers on the inhibitory effects of the enantiomers of HupA in vivo and in vitro in rat brain model systems found that synthetic racemate mixture was 3 times less potent than (–)-HupA.[8–10,13] Tang and coworkers went on to conclude that HupA was likely a potent inhibitor because it structurally resembles acetylcholine, the natural substrate of the enzyme. Clinical trials in China were performed using HupA to treat elderly subjects suffering from Alzheimer's disease and found that HupA was able to significantly relieve memory deficits.[10] In the United States, HupA is currently available as a dietary supplement. Given the evidence that the pathogenesis of Alzheimer's disease is related to the impairment or dysregulation of cholinergic neurotransmission in the central nervous system, one area of focus is the development of small molecule therapeutics that target acetylcholinesterase, similarly to the mechanism of action of *Lycopodium* alkaloids.

Although HupA and several other small molecule AChE inhibitors have been extensively studied and developed, Alzheimer's disease remains devastating, affecting 44 million people globally and is still uncurable.[5] Given the underwhelming results of AChE inhibitors, it is clear that new treatment options with new biological targets and novel mechanisms of action are desperately needed. Fortunately, the vast diversity of *Lycopodium* alkaloids can provide inspiration for new potential therapeutic approaches through novel mechanisms of action against Alzheimer's disease.[17]

Biological Synthesis

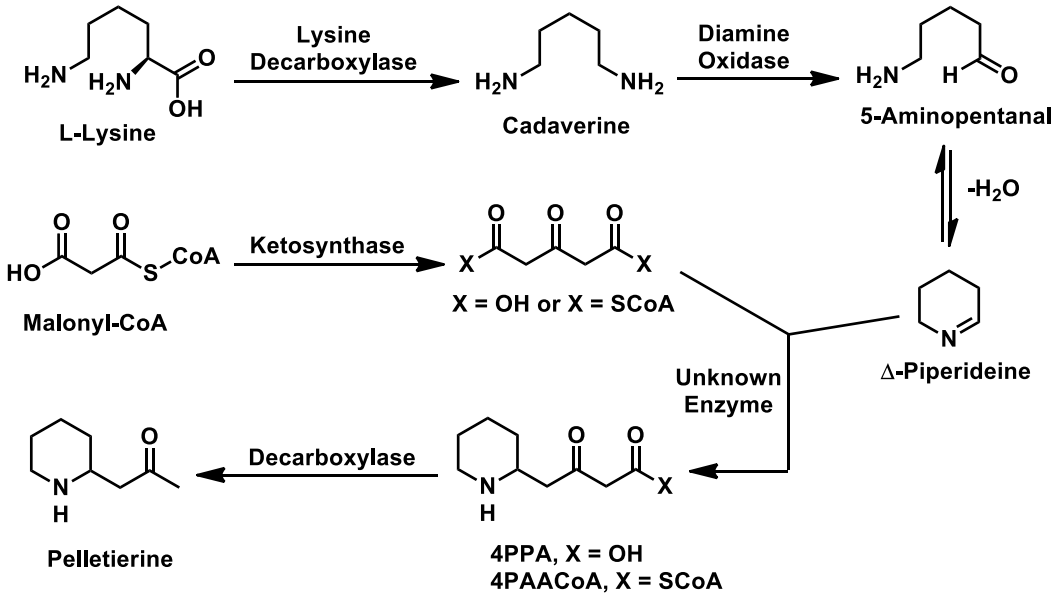

Scheme 2.1 Proposed biosynthesis pathway beginning from L-Lysine to pellertierine and 4PAA precursors of *Lycopodium* alkaloids

Despite a strong interest in the *Lycopodium* alkaloid family, the biosynthesis of this family of natural products has not been fully elucidated. However, several potential biosynthetic pathways have been proposed based on interesting experimental observations.[1] Over the years, several researchers have contributed to the proposed biosynthesis of *Lycopodium* alkaloids including Ayer, Blumenkopf, MacLean, Hemscheidt.[18–22] The first proposed biological pathways were based on the identification of new members of each of the sub-families of *Lycopodium* alkaloids, following the hypothesis that the smaller, less structurally complex, and less oxidized members were possibly intermediates en-route to the more complex members.[18] However, it was not until

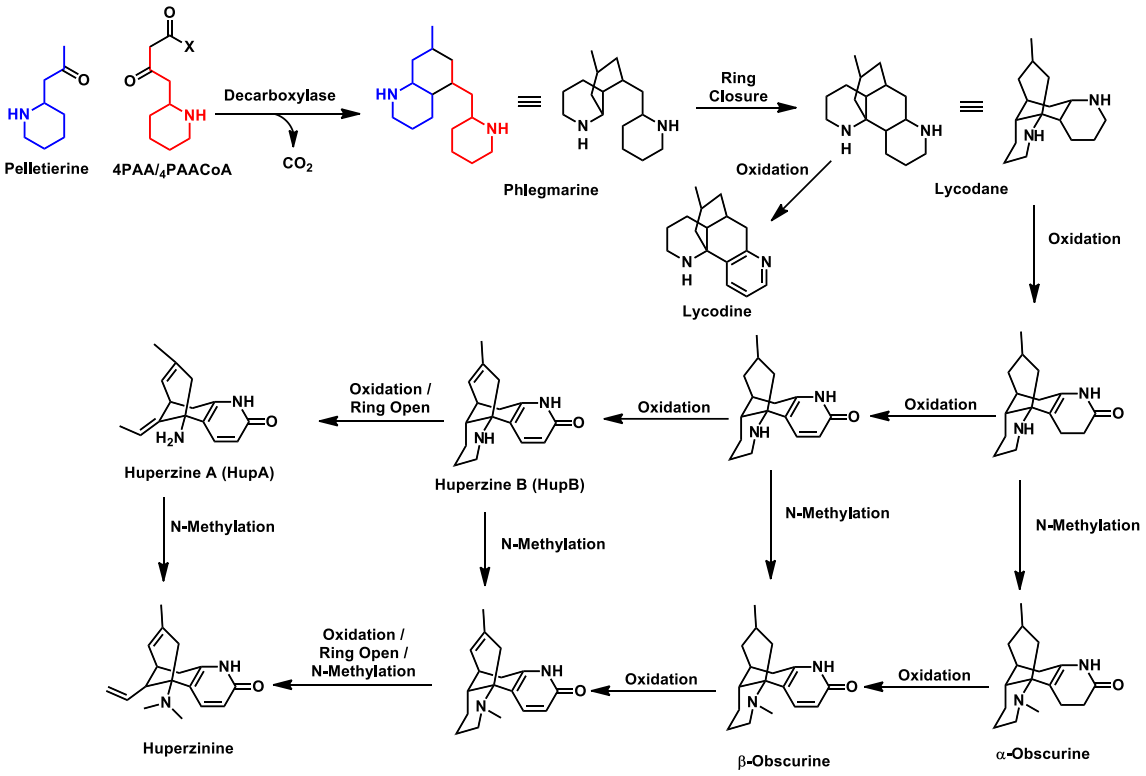

Scheme 2.2 Proposed biosynthetic pathway from pelletierine and 4PAA to huperzine A, huperzinine, and related intermediates

later that Spenser (with contributions by Hemscheidt) was able to provide some experimental support for their biosynthesis through the use of feeding experiments that were reported over the span of 30 years from 1970 to 1996.[20–26] These feeding experiments were critically necessary because at this time the *Lycopodium* plants could not be grown or cultivated outside of their natural habitat; therefore, the feeding experiments needed to be conducted where the plants naturally grew. This was convenient for Ian Spenser, a professor at McMaster University in Ontario, Canada, which was where some species of *Lycopodium* plants grew naturally. In these feeding experiments, the goal was to determine and identify intermediates in the biosynthetic pathway. The feeding experiments involved feeding ^{13}C- and ^{14}C radio- or stable isotope- labeled potential precursor materials to shoots

of *Lycopodium* species. After one to five days, the fed plants were harvested, and the tissues were analyzed for incorporation of the radio- or stable isotope-labeled potential precursors. Specifically, Spenser analyzed intermediates or the 'end product' of *Lycopodium* alkaloids. If it was found that the radio- or stable isotope-labeled potential precursor material was in fact incorporated into more complex, higher order, *Lycopodium* alkaloids, then it was interpreted that the precursor material fed to the plants was the correct starting material for the biosynthesis, or at least consumed and incorporated in the biosynthetic pathway at some point. Understandably and unsurprisingly, Spenser described these feeding experiments as being very difficult to perform, but they generated critical results that would allow insight into the biosynthesis pathways of *Lycopodium* alkaloids (Schemes 2.1 and 2.2).[1] Specifically, much of the scientific community, including Spenser, were interested in the biosynthesis of Huperzine A (HupA) due to its inhibitory effect on acetylcholinesterase previously discussed.

Through feeding experiments with L-lysine, it was determined that the biosynthesis begins with decarboxylation by lysine decarboxylase to generate cadaverine (Scheme 2.1).[1] Next, cadaverine is successively converted to 5-aminopentanal by diamine oxidase, and then to Δ-piperideine through an amine condensation. At this point, acetonedicarboxylic acid (bisCoA ester) is coupled with Δ-piperideine to form 4-(2-piperidyl) acetoacetate (4PAA) or 4-(2-piperidyl) acetoacetyl-CoA (4PAACoA) via an unknown enzyme. The acetonedicarboxylic acid unit is produced from two molecules of malonyl-CoA that are condensed by a ketosynthase enzyme. 4PPA and/or 4PAACoA are then decarboxylated by an unknown decarboxylase to form pelletierine, which is considered to be the

intermediate that diverges to all the *Lycopodium* alkaloids in the biosynthesis. Pelletierine is then coupled with 4PAA or 4PAACoA through a decarboxylation catalyzed by an unknown decarboxylase, producing phlegmarine (Scheme 2.2). Phlegmarine is the subsequent intermediate believed to be central to the *Lycopodium* alkaloids. It is also the representative member of a subclass of *Lycopodium* alkaloids. Lycopodine was previously speculated to be the central biosynthetic intermediate; however, further experimental work favors phlegmarine to be the central intermediate leading to the *Lycopodium* alkaloids. From phlegmarine, an oxidative ring closure to form lycodane could be catalyzed by an enzyme related to berberine bridge enzyme, and then a series of oxidases could lead to the formation of lycodine following oxidation of the piperidine moiety. Lycodine is another representative member of a subclass of *Lycopodium* alkaloids. The remaining oxidation steps are carried out presumably by cytochrome P450 enzymes or 2-oxoglutarate-dependent dioxygenases. Lycodane could undergo a series of oxidations to access huperzine B. Huperzine B could be converted to huperzine A through a final oxidation and ring opening. Huperzine A could then be bis-*N*-methylated and undergo alkene isomerization to generate huperzinine. An alternative proposed route leading to huperzinine involves oxidation of the piperidine A ring of lycodane to the cyclic enamide, followed by *N*-methylation of the C ring, generating α-obscurine. α-Obscurine could be oxidized to β-obscurine, and then further oxidized and ring-opened to again access huperzinine. It is possible that any of the intermediates first described to access huperzinine could be methylated and then follow the second described route to huperzinine.

Additionally, it is possible that huperzinine could be de-methylated and alkene-isomerized to form huperzine A (Scheme 2.2).

Previous Total Syntheses of *Lycopodium* Alkaloids

From the late 1990's until now, syntheses of *Lycopodium* alkaloids have been completed by Sarpong, Rychnovsky, Heathcock, Trauner, Takayama, Lei, and Liao.[27–36] Sarpong in particular has completed five syntheses of various *Lycopodium* alkaloids from 2008 to 2015 and has successfully developed novel C–H functionalization methodologies motivated by the pursuit of these natural products.[19,29–31,35–37] Sarpong's initial entry into the arena of *lycopodium* alkaloid synthesis began with a racemic synthesis of lyconadin A in 2009.[29] In this work, Sarpong went on to describe a tractable unified strategy to access lycopodium alkaloids of the 'miscellaneous' subclass. Sarpong's 18-step synthesis of lyconadin A (Scheme 2.3) begins with a Stork–Danheiser sequence between a lithiated methoxypicoline (**2.1**) and vinyligous ester **2.2** to produce enone **2.3** which then underwent a ring closing metathesis via Grubb's II catalyst, leading to α,β-unsaturated alkene **2.4**. Heck cyclization of enoate **2.4** afforded cycloheptadiene **2.5**, the 7-membered ring feature of lyconadin A (**2.10**). Over the next 14 steps, cycloheptadiene **2.5** is transformed through a β-methylation reaction and several oxidation state manipulations before closing the final ring via KO*t*Bu facilitated carbene or dianion formation followed by N–H insertion. Finally, methylether cleaveage of the methoxypyridine by NaSEt furnished lyconadin A (**2.10**). The highlights of this synthesis include rapid construction of the core scaffold via a Stork–Danheiser/olefin metathesis/Heck cyclization sequence and the penultimate carbene or dianion

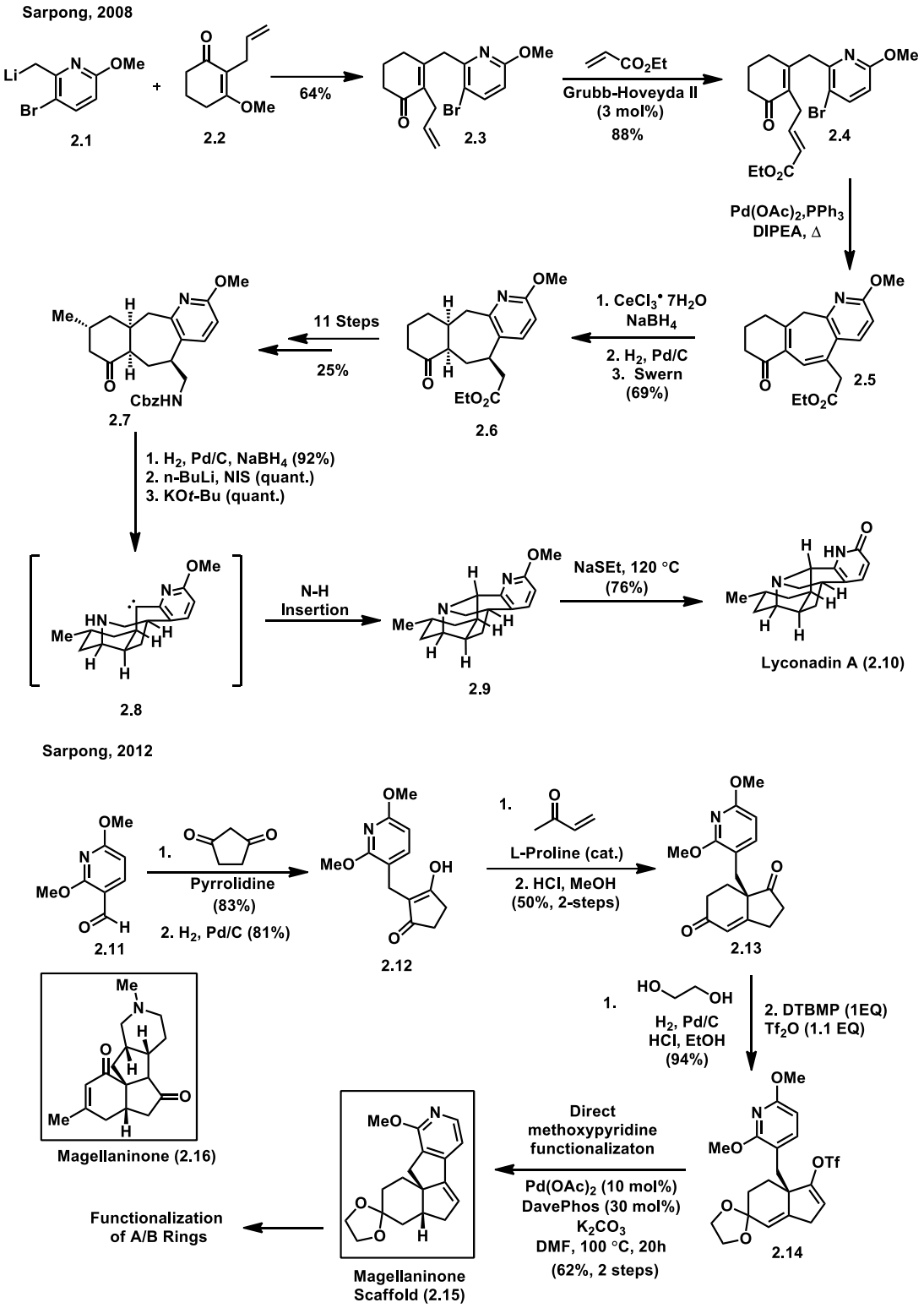

Scheme 2.3 Summary of Sarpong's lycopodium alkaloid synthesis work

formation, and N–H insertion to form the final ring. The Sarpong group utilized a similar strategy in the 13-step synthesis of (±)-lycoposerramine R, emphasizing the utility of methoxypyridine as a masked pyridine.[30] In 2012, Sarpong detailed a general strategy to access the tetracyclic core of the magellanine-type *Lycopodium* alkaloids utilizing an enantioselective Hajos–Parrish reaction between enol **2.12** and methyl vinyl ketone to install the chiral quaternary center in enone **2.13** and direct methoxypyridine functionalization to complete the carbon skeleton of magellaninone (**2.15**) (Scheme 2.3).[36] Sarpong and co-workers installed the chiral quaternary center early in the synthesis with the intention of using it to guide subsequent stereoselective manipulations of the core molecule. In each of these previous syntheses by Sarpong, the carbon scaffold is accessed very efficiently, but the drawback is the many oxidation state manipulations that increase the step count in accessing the target *Lycopodium* alkaloids.

With numerous syntheses of *Lycopodium* alkaloids, one of the best known strategies and syntheses was developed by Heathcock in the synthetic pursuit of fawcettimine (**2.19**) (Scheme 2.4).[31] Fawcettimine (**2.19**), the representative member of a subfamily of *Lycopodium* alkaloids was first synthesized diastereoselectively in 1979 by Inubushi and co-workers over 26 steps in an overall 0.1 % yield.[38] At the completion of Inubushi's synthesis, there was some controversy about the stereochemistry of the C4 position. About 10 years later in 1986 and 1989, fawcettimine (**2.19**) was synthesized again by Heathcock in 13 steps in 17% yield, producing enough material for X-ray crystallography to be employed to conclusively determine the stereochemistry at the C4 position.[19,37,38] The key intermediate of the 'Heathcock strategy' is a 6-5-9-tricycle (**2.18**).

This method has been used in several syntheses to access fawcettimine-type molecules, as it allows rapid access to the fawcettimine core with minimal oxidation state manipulations. Further development of this strategy has focused upon novel and creative ways to access the 'Heathcock tricycle' (**2.18**), as one challenge of employing this strategy lies in the synthesis of the tricycle's C4 quaternary

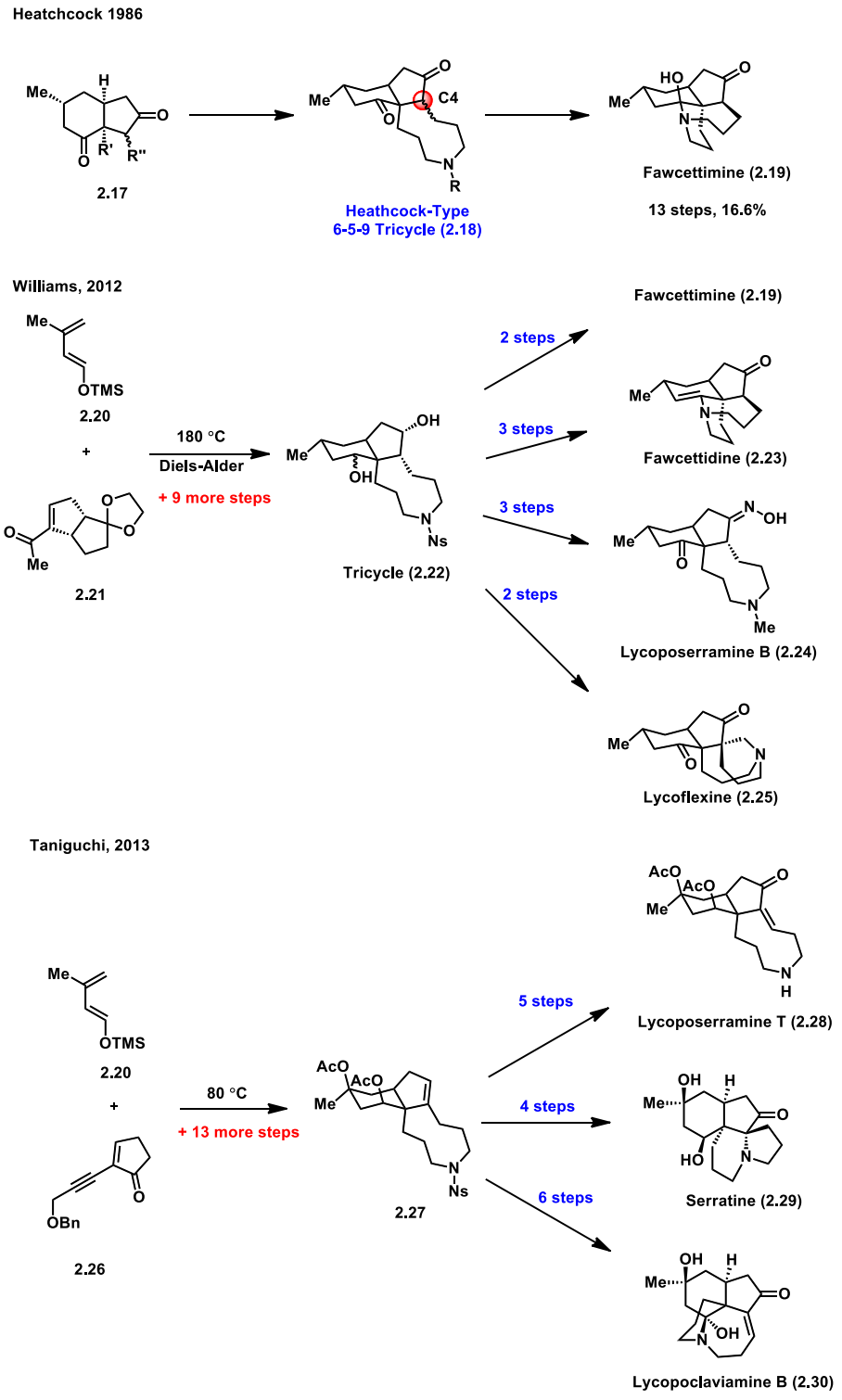

Scheme 2.4 Summary of Heathcock's tricyclic intermediate and adaptations

center located at the ring fusion. One of the most significant advances based upon the Heathcock strategy was developed by Williams and co-workers in 2013, where they were able to generate fawcettimine (**2.19**), fawcettidine (**2.23**), lycoposerramine B (**2.24**), and lycoflexine (**2.25**) all from the 6-5-9 tricycle (**2.22**). The Diels–Alder reaction performed by William's and co-workers was interesting because enone **2.21** is actually a poorly reactive dienophile due to steric hindrance and the presence of only one activating group. In 2013 Taniguchi and co-workers adapted William's Diels–Alder approach to access Heathcock's tricycle by substituting the dienophile for an alkyne.[39] By altering the Diels–Alder adducts, they arrived at a different tricyclic intermediate scaffold **2.27** that allowed them to access lycoposerramine T (**2.28**), serratine (**2.29**), and lycopoclavamine B (**2.30**). Each of the natural products generated by Taniguchi are racemic.

One of the few examples of a biomimetic synthetic approach to a *Lycopodium* alkaloid has been completed by Rychnovsky and co-workers recently in 2019 in their 17 step enantioselective total synthesis of (–)-himeradine A, a member of the lycodine sub-family.[27] The synthesis commences with a Sonogoshira coupling reaction between bromopicoline **2.31** and butynol **2.32** to give propargylpyridine **2.33** which is then undergoes a diastereoselective global hydrogenation to generate piperidine **2.34**, which was resolved using D-dithiothreitol. Following Boc-protection and TBS-protection, the piperidine was lithiated with sBuLi in the presence of TMEDA and then converted to the alkyl component by treatment with CuCN•2LiCl and then coupled with allyl bromide to carry out the diastereoselective allylation to produce alkene **2.37**. Alkene **2.37** undergoes cross-metathesis with crotonaldehyde and 1,2-reduction by treatment with $NaBH_4$ to give

allylic alcohol **2.38**. Allylic alcohol **2.38** is then subjected to a diastereoselective Overman rearrangement by treating the trichloroacetimidate with (–)-COP-Cl as the chiral palladium catalyst to generate the trichloroacetamide, which is then

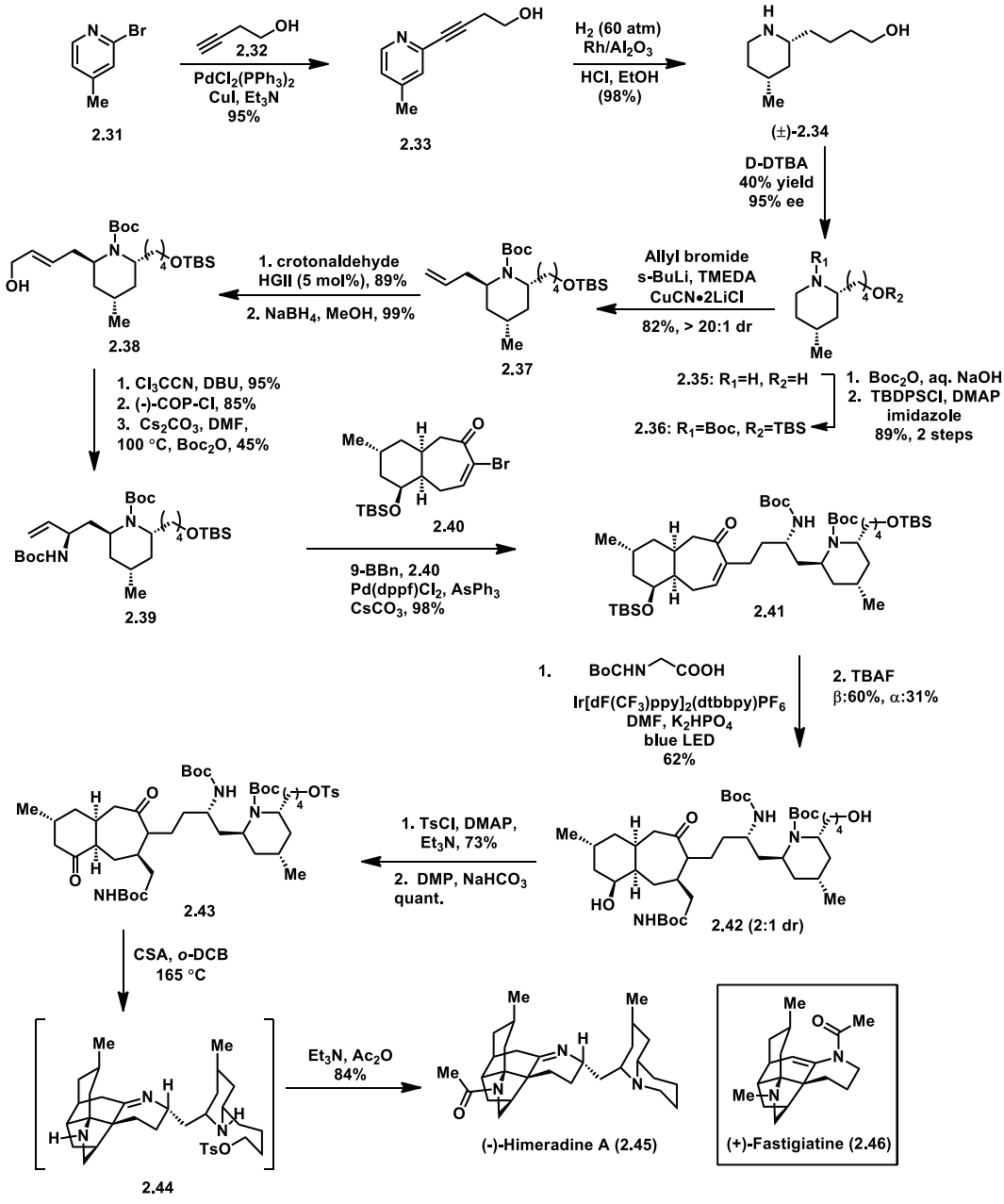

Scheme 2.5 Summary of Rychnovsky's synthesis of (–)-himeradine A

converted to the Boc-protected amine **2.39**. Subsequent hydroboration of **2.**39 allowed for a Suzuki–Miyaura cross coupling with vinylic bromide **2.40** to give enone **2.41**. Next, an aminomethylene fragment was installed by photochemically decarboxylating *N*-Boc glycine using an iridium photocatalyst to generate a stabilized α-amino radical that then performed a stereoselective 1,4-addition to enone **2.41** and then subsequently desilylated by treatment with TBAF to give ketone **2.42** in 2:1 dr favoring the β-stereoisomer. Following tosylation of the primary alcohol of ketone **2.42**, the secondary alcohol is oxidized by to the ketone by treatment with NMP and $NaHCO_3$ to give diketone **2.43**. Cleavage of the boc-groups in diketone **2.43**allowed for intramolecular imine formation, then set the stage for the key transannular Mannich reaction Final treatment with triethylamine and acetic anhydride furnished (–)-himeradine A (**2.45**) as the bis-TFA salt. The key steps in this synthesis include a diastereoselective piperidine hydrogenation, a diastereoselective Overman rearrangement, and an impressive biomimetic transannular Mannich cascade reaction that efficiently forms 5 bonds and 4 rings all in one step and in 84% yield (Scheme 2.5). Rychnovsky previously applied this same biomimetic transannular Mannich cascade to two syntheses of (+)-fastigiatine (**2.46**) in 2018.[40] The transannular Mannich cascade was inspired by the proposed biosynthesis of the lycodine sub-family from acetonedicarboxylic acid by Spenser in 1996.[25] The same proposed biosynthesis is more thoroughly summarized and discussed in the biosynthesis section of this dissertation (Scheme 2.1 and 2.2).

An approach that contrasts biomimetic strategies was developed in 2004 by Lei and co-workers.[34] This strategy focused on diversity-oriented synthesis (DOS) utilizing a build-couple-pair (B/C/P) algorithm (Scheme 2.6 and 2.7, and 2.8). Diversity-

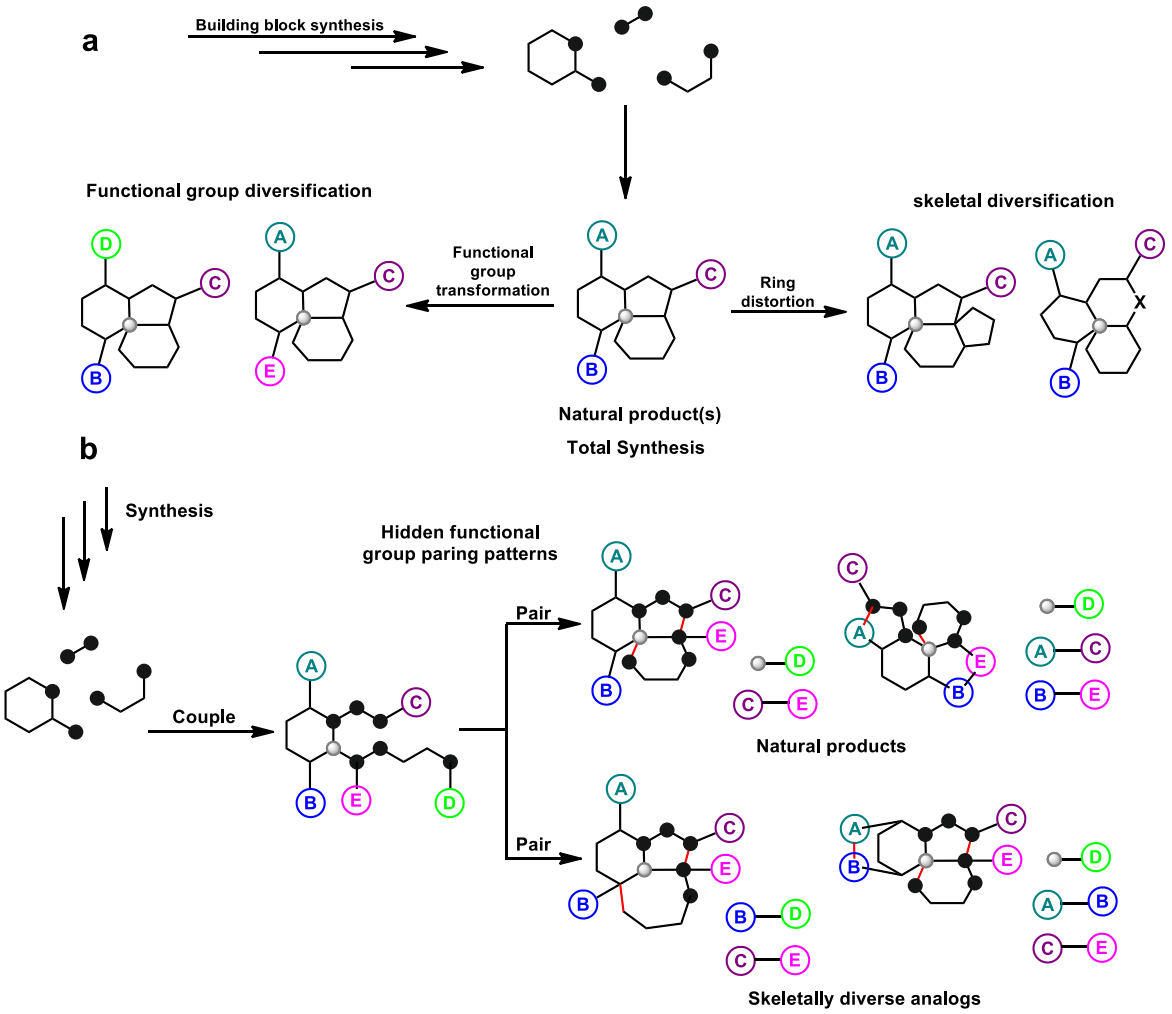

a) Classical total synthesis strategies, such as biomimetic pathways, and functional group and skeletal diversifications of natural products. b) Hidden functional group pairing patterns within a class of natural products are identified and then a build/couple/pair route is designed to synthesize skeletally diverse derivatives an analogs of natural products utilizing different functional group parings. The circled letter A-E represent different functional groups and the grey circle indicates the active carbon center. New bond formations are represented by red bonds.

Scheme 2.6 Lei's comparison of the classical total synthesis strategies with the functional group pairing patterns inspired build/couple/pair strategy

oriented synthesis focuses on efficiently synthesizing skeletally, oxidatively, and stereochemically diverse molecules that will be further evaluated in biological assays for

drug discovery and molecular biology. It is further argued that while classical syntheses have allowed efficient access of a target product, the approach is limited in its ability to produce unified access to multiple target products from a common intermediate, and therefore, lacking a facile way to access a significant degree of diversity. The logic of

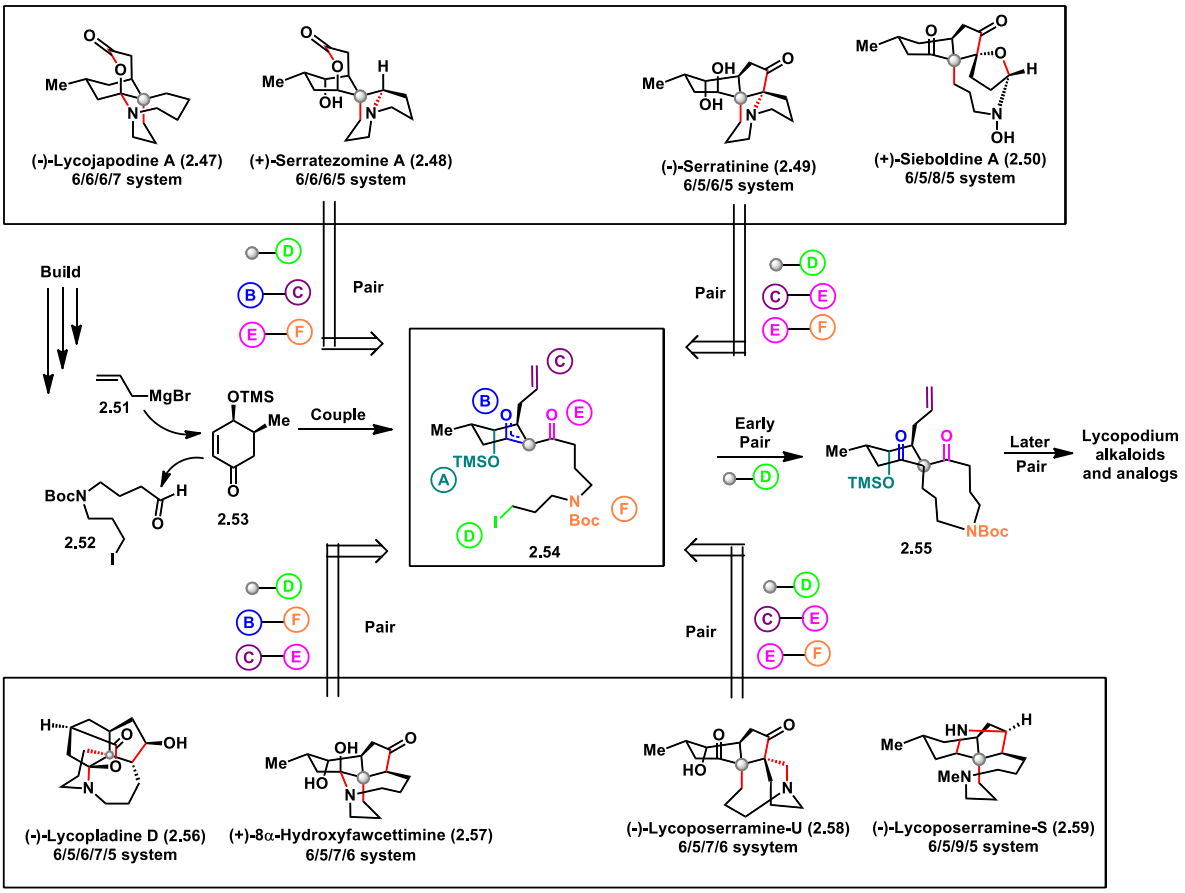

New bonds are highlighted in red. Disconnecting functional group pairing from eight lycopodium alkaloid targets led to a common multi-functionalized intermediate that could be easily assembled through a multicomponent reaction between **2.51-2.53**. From intermediate **2.54**, variations of functional group pairing reactions allowed access to each of the desired targets.

Scheme 2.7 Outline of Lei's diversity oriented synthesis retrosynthesis to Lycopodium alkaloids using build/couple/pair approach

diversity-oriented synthesis through build-couple-pair (BCP) aims to solve the short-coming of classical syntheses.[34] As summarized in scheme 2.6, part B, the DOS strategy begins with a 'building' (B) phase, where simple building blocks are synthesized and then

coupled (C) together to access a common intermediate with multiple reactive handles in the form of various functional groups. From that common intermediate, functional groups are 'paired' (P) by employing highly chemoselective reactions to ensure the desired 'pairing' of functional groups, therefore forming the desired new bonds to access the natural products as well as skeletally and oxidatively diverse analogs. In Scheme 2.7, Lei

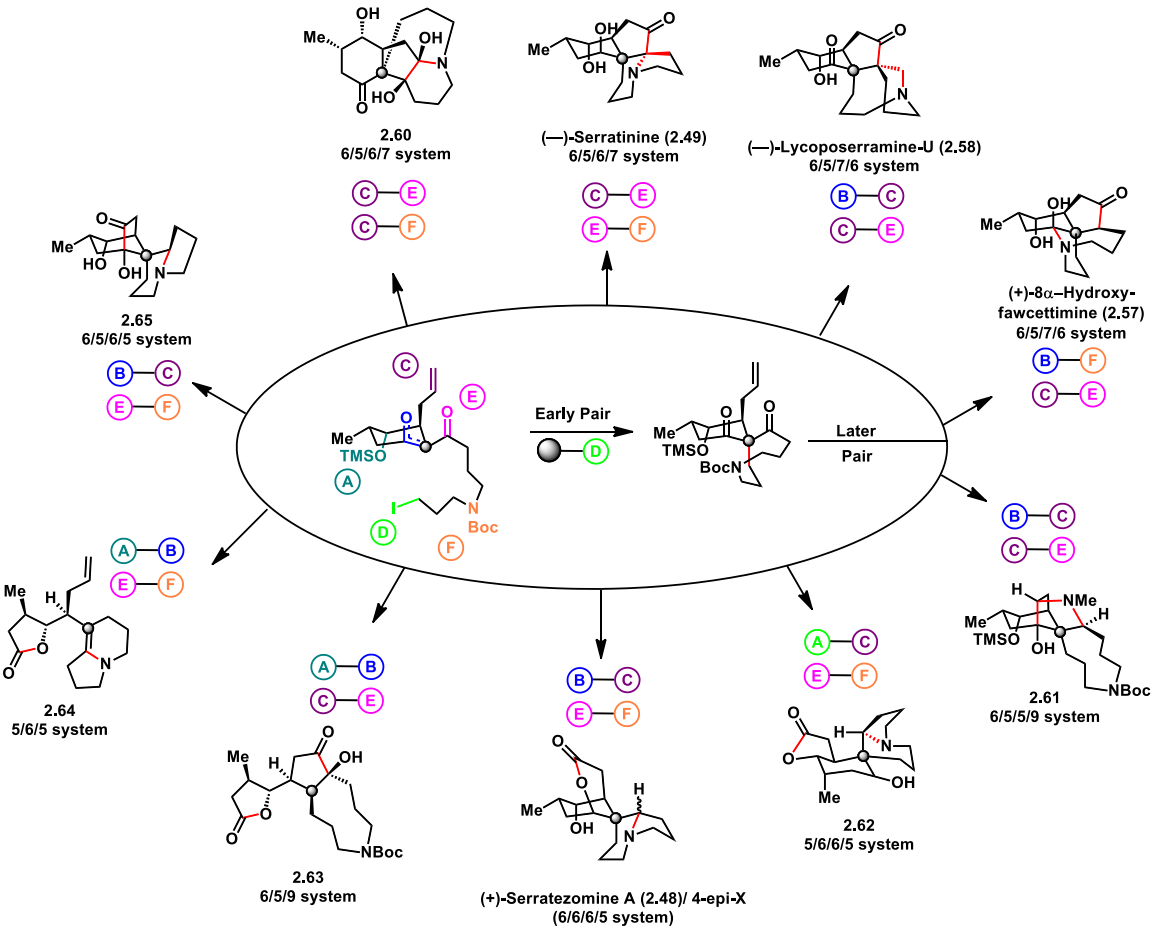

Scheme 2.8 Summary of lycopodium alkaloid natural products and analogs synthesized using diversity oriented synthesis via build-couple-pair strategy by Lei and coworkers

applies the DOS-BCP approach to *Lycopodium* alkaloids. With (–)-lycojapodine A (**2.47**), (+)-serratezomine A (**2.48**), (–)-serratinine (**2.49**), (+)-sieboldine A (**2.50**), (–)-lycopladine D (**2.56**), (+)-8α-hydroxyfawcettimine (**2.57**), (–)-lycoposerramine-U (**2.58**), and (–)-

lycoposerramine-S (**2.59**) as targets, Lei retrosynthetically disconnects bonds highlighted in red to identify a common intermediate **2.54** and the functional group pairs that need to react form the necessary bonds. Through this approach, Lei identifies common intermediate **2.54**, which is multi-functionalized with all the necessary functional groups to form the desired new bonds. Additionally, from common intermediate **2.54**, by reacting, or 'pairing' functional groups with different partners and in different orders, access to other *Lycopodium* alkaloids and analogs thereof are possible. Lei proposes accessing analogs from polycyclic intermediate **2.55** after the 'early pair' step. It is important to note that this intermediate is essentially the same 'Heathcock intermediate', containing the 6-9-fused ring system that would be forced to ring-contract to obtain new scaffolds and products. The final results of Lei's DOS-BCP approach is summarized in Scheme 2.8, showing the multi-functionalized common intermediate **2.54** and the 'Heathcock intermediate' (**2.55**) providing access to a total of 11 polycyclic molecules, some of them *Lycopodium* alkaloids targets and someanalogs thereof.

Annotinolides A-C

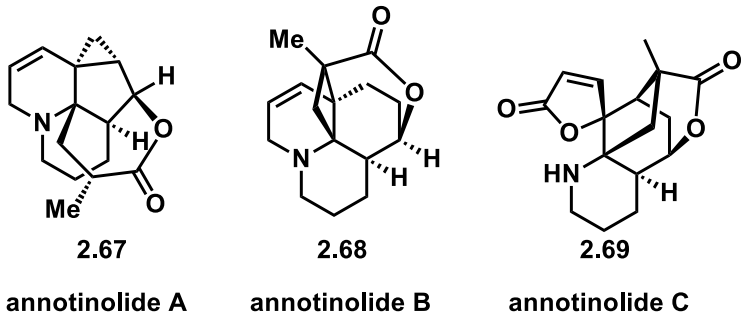

Figure 2.5 Structures of annotinolides A-C

Two members of the lycopodine subclass are of particular interest to us: annotinolide A and B (Figure 2.5) Although we are interested in other annotinlides, we have chosen to synthetically target the more complex members first. Annotinolides A–C were isolated from *Lycopodium annotinum*, a club moss found in the Taibai Mountains in Shaanxi, China.[17] These alkaloids have been found to exhibit intriguing biological activity against the aggregation of Aβ-peptide, which is unusual for *Lycopodium* alkaloids. Aβ aggregation is a key factor in the pathogenesis of Alzheimer's disease.[17] In a thioflavin T fluorescence assay performed with annotinolides A, B, and C, it was shown that all three compounds exhibited significant inhibition against aggregation of $A\beta_{42}$-peptide at a concentration of only 50 μM, as compared to a positive control in EGCG (epigallocatechin gallate, inhibitory ratio of 86.6% at 10 μM). It was found that the inhibitory ratios of annotinolide A, B, and C was 42.4%, 38.1%, and 36.1%, respectively.[17] The biological activity of annotinolides A–C is especially interesting because although the mechanism of action is unknown, it is reported that annotinolides A–C do not exhibit any AChE activity. This means that annotinolides A–C exhibit a novel mechanism of action for a potential

treatment of Alzheimer's disease. However, in order to better understand the potential therapeutic properties of the annotinolides, significant synthetic challenges must be overcome.

Annotinolides A (**2.67**) and B (**2.68**) are both 7,8-*seco*-lycopodane-derived 8,5-lactones. Each of these compounds contain a fused A-B-C ring system (akin to the lycopodine-type molecules) with a bridging lactone connected through a quaternary carbon. Annotinolide A (**2.67**) is further complicated by the presence of a cyclopropane motif on the B-ring, opposite the lactone on the same ring system. Annotinolide B (**2.68**) is further complicated by the presence of a cyclobutane on the B-ring, bound through two quaternary centers and connecting to the bridging lactone. Annotinolides A (**2.67**) and B (**2.68**) were ultimately chosen as target compounds because they are structurally complex, and we ambitiously envisioned a divergent synthesis approach that would allow access to both molecules from a common intermediate. Owing to the formidable challenges of this synthesis, annotinolides A, B, and C (**2.67**–**2.68**) were isolated in 2016 but have yet to be synthesized, despite their unique biological activity.

Retrosynthetic Analysis

We sought a common intermediate that would allow access to both annotinolides A and B, so we began by retrosynthetically simplifying each target to identify a more simple common intermediate that may be readily accessible (Scheme 2.9). From annotinolide A (**2.67**), we envision breaking/forming the bridging D-ring through a reduction/lactonization sequence from ester **2.70**. Ester **2.70** could be accessed through a radical alkylation via a Michael addition from tertiary radical **2.71**. We propose radical **2.71** can be generated in situ from a biomimetic cyclopropanation of tricyclic quinolone **2.72**, the key intermediate containing the A-B-C fused ring framework in this divergent synthesis.[41] From annotinolide B (**2.68**), we envisioned first disconnecting the D- and cyclobutane rings via an intramolecular [2 + 2] cycloaddition, leading to α,β-unsaturated

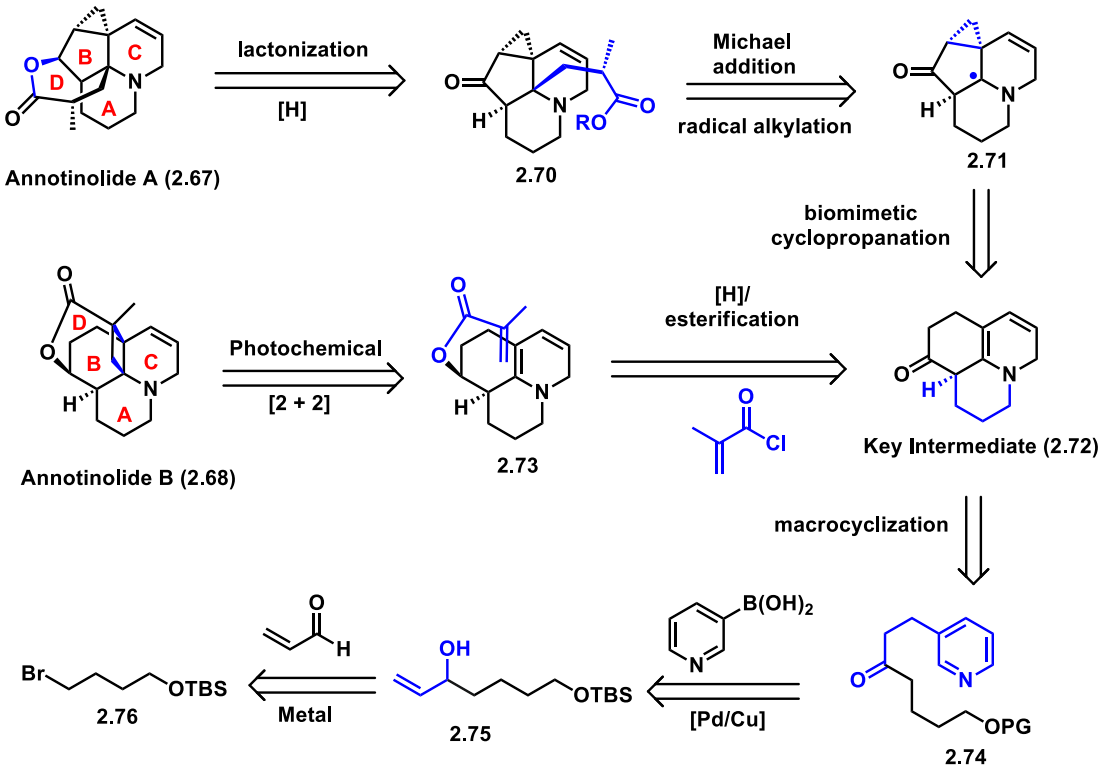

ester **2.73**.[42] Ester **2.73** could be generated from the reduction and esterification of tricyclic quinolone **2.72**, the key intermediate that we anticipate would allow the divergent synthesis of both annotinolides A (**2.67**) and B (**2.68**). We propose that quinolone **2.72** could be the product of a macrocyclization/dearomatization sequence from pyridine **2.74**. We envision forming pyridine **2.74** through the oxidative coupling of a allylic alcohol **2.75** to 3-pyridyl boronic acid.[43] In our initial route, allyl alcohol **2.75** is synthesized from the Grignard addition of halide **2.76** to acrolein. Finally, halide **2.75** can be formed over two steps from inexpensive, commercially-available starting materials.[44]

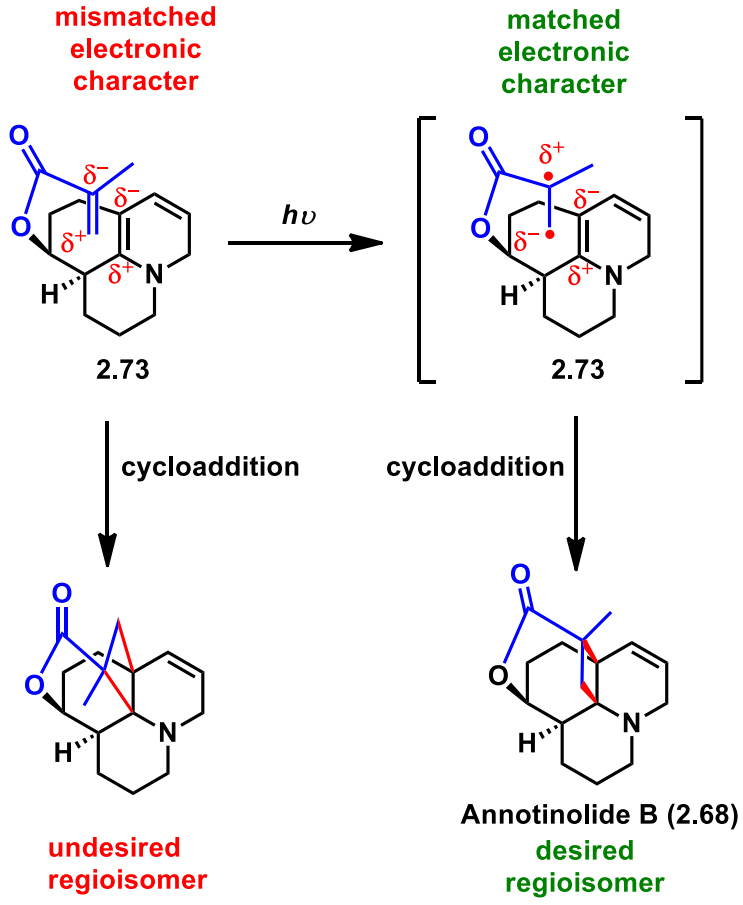

Scheme 2.10 Electronic character of enone compared to the diradical intermediate and the influence on regioselectivity of the cycloaddition

There are several key features and challenges posed by this proposed total synthesis route of annotinolides A (**2.67**) and B (**2.68**). The initial challenges stem from the inherent structural complexity of the polycyclic scaffolds of annotinolides A and B. The strained rings of the cyclopropane of annotinolide A and the cyclobutene of annotinolide B could be synthetically challenging to install. Additionally, the labile bridging lactone rings pose synthetic challenges due to decomposition concerns. Finally, the 6,6,5- and 6,6,6-tricyclic scaffolds are highly susceptible to overoxidation, specifically of the nitrogen-containing C-ring. The cyclopropanation process to access annotinolide A is challenging yet intriguing because we propose a biomimetic radical pathway that relies on the electronic characteristics of the substrate to influence multiple C–C bond formations, including a strained ring.[41] Employing a [2 + 2] cycloaddition is a common approach in forming cyclobutanes; however, this cycloaddition would have to be intramolecular and regioselective in regards to the conformation of the alkene to access our desired cyclobutene. Upon closer analysis of the α,β-unsaturated ester **2.73** (Scheme 2.10), the electronics of the enone and vinylic amine are mismatched for our desired bond formations. That is to say, the electronics of the enone are such that the α-position is partially negatively charged while the β-position is partially positively charged. When compared to the electronics of the vinylic amine, the vinylic carbon is partially positively charged while the adjacent carbon is partially negatively charged. Given these electronic configurations, it would suggest that the electronically favored cycloaddition would result in the undesired regioisomer. However, if we perform a photochemical [2+2] cycloaddition, the enone is converted to a diradical species *in situ* with now reversed electronic character. The α-keto

radical is now electrophilic and partially positively charged, while the β-keto radical is nucleophilic and partially negatively charged. As the diradical species, the electronic characters match for a cycloaddition with the desired regioselectivity, therefore achieving an inverse regioselectivity cycloaddition to generate our desired product, annotinolide B (**2.68**).

Given the formidable challenges posed by the total synthesis of annotinolides A (**2.67**) and B (**2.68**), the strategically designed divergent synthesis would allow for the synthesis of both annotinolides A and B from a common intermediate. Thus, the immediate goal was to access key intermediate **2.72**. Although structurally less complex than annotinolides A and B, the macrocyclization and subsequent ring contraction of pyridine **2.74** to access the key intermediate (**2.72**) would also pose significant synthetic challenges due to the formation cationic macrocyclic intermediate that must be intercepted with base or acid to carry out tricyclization to the neutral product **2.72**.

2.2 Results and Discussion

It is worth noting that significant efforts were focused on pursuing many different synthetic routes to access intermediate quinolone **2.77** (Scheme 2.11) en route to

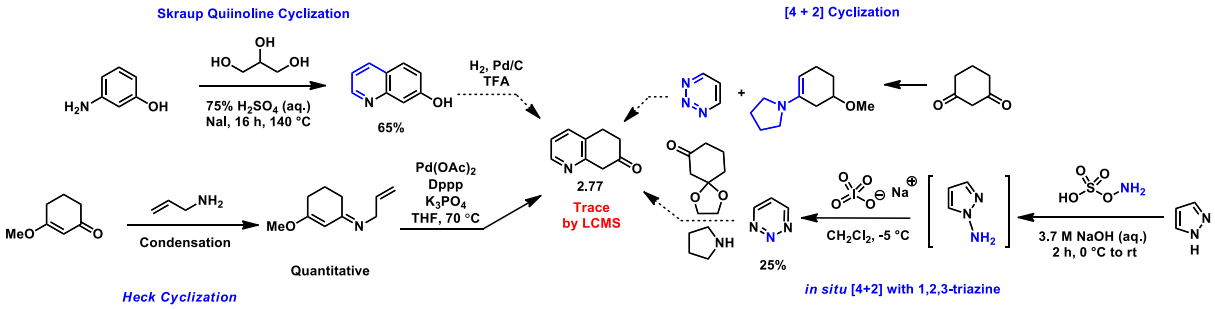

Scheme 2.11 Summary of some attempted routes to access quinilone **2.77**

annotinolides A and B, but a facile synthesis of **2.77** has proven difficult, thus we re-evaluated our synthesis plan and began pursuing the route summarized in Scheme 2.12. Bromobutoxysilane **2.76** was synthesized through two different routes (Scheme 2.12). First, starting from 1,4-butanediol (**2.77**), a monosilylation is accomplished in 97% yield by treatment with TBSCl and NaH.[45] Next, chlorination of silanol **2.78** was attempted using thionyl chloride, but the reaction conditions were found to be too harsh, resulting in desilylation and further decomposition of the starting material. Appel conditions were attempted to transform the alcohol to the alkyl bromide. This reaction proceeded well, providing a 88% yield, however, the brominated product (**2.78**) was found to be unstable under the handling conditions: the extensive purification and handling required to remove triphenylphosphine oxide resulted in decomposition. The decomposition pathway appears

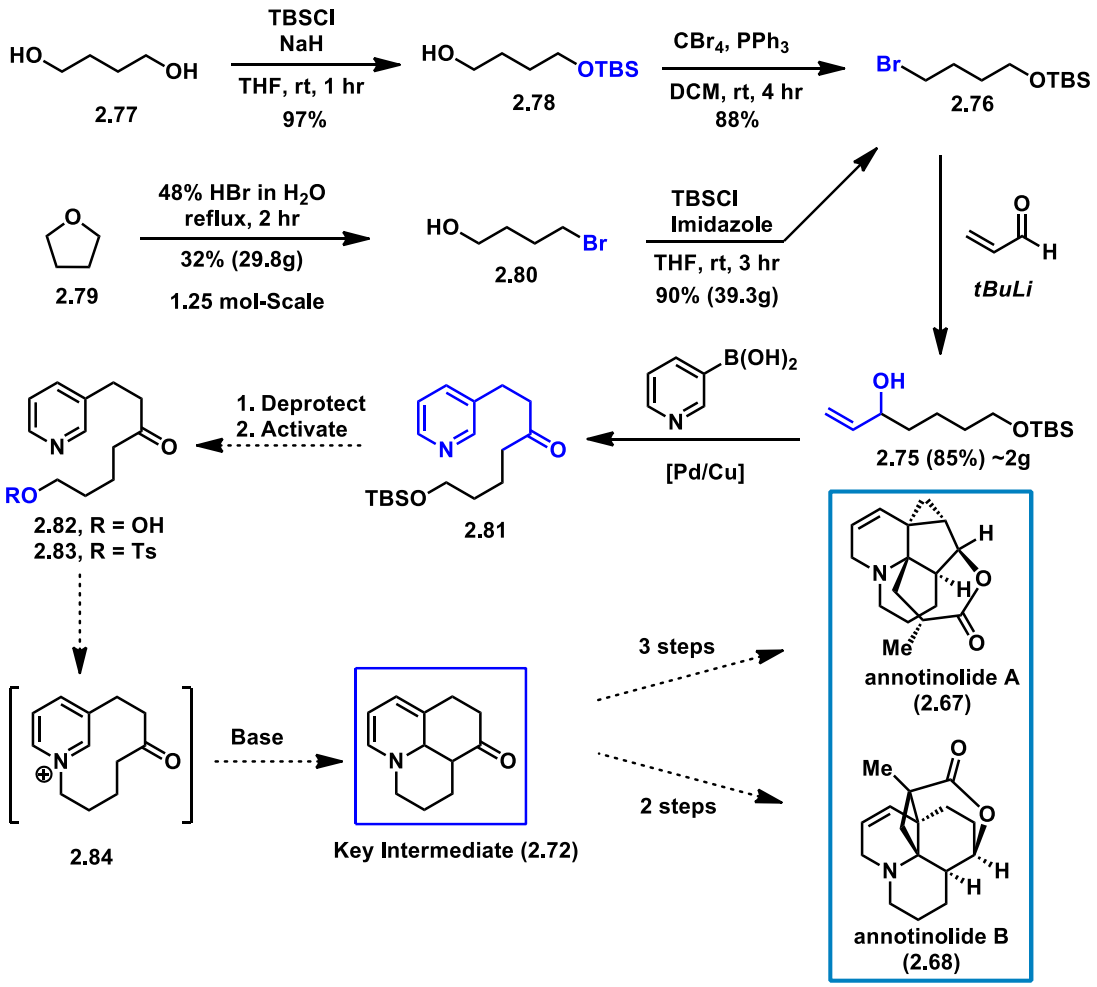

to be desilylation followed by intramolecular displacement of the bromide to produce tetrahydrofuran that could not be easily removed, presumably as a consequence of strong coordination to the silyl group of **2.76**. The next route to access bromobutoxysilane **2.76** begins from the acid-catalyzed ring opening of THF to produce bromobutanol **2.80** in 32% yield. Although low yielding, the starting materials are inexpensive, readily available, and the reaction proceeds on large scale to yield about 30 g of product. Bromobutanol **2.80** is

then silylated with TBSCl and imidazole to generate bromobutoxysilane **2.76** in 90% yield, providing access to 39 g of product.

Significant efforts were devoted to studying the Grignard reaction between bromobutoxysilane **2.76** and acrolein to afford allylic alcohol **2.75**. This reaction has been difficult to reproduce, and thus would require optimization of the reaction conditions. The best yield achieved is 41% using $CeCl_3$ as the Lewis acid. The reaction is unsuccessful when performed at room temperature in the absence of $CeCl_3$ with only the unreacted alkyl halide recovered. This suggests that formation of the Grignard reagent may be difficult.

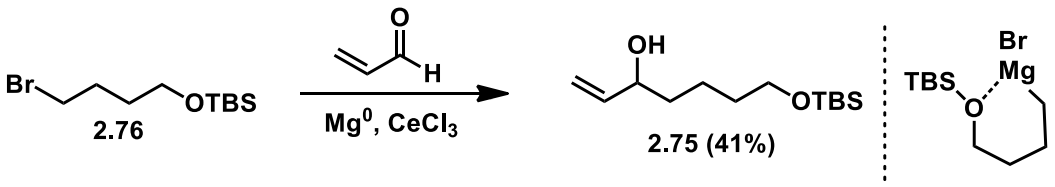

However, when the reaction is performed by pre-mixing $CeCl_3$ with acrolein prior to the addition of the Grignard reagent, which is prepared using pristine halide **10**, a 41% yield is obtained. The remainder of the mass balance is unreacted bromobutoxysilane **2.76**. When the reaction is performed by generating the Grignard reagent by refluxing magnesium turnings with the alkyl halide, complete consumption of the starting bromobutoxysilane **2.76** is observed, but the yield is not improved. Despite significant efforts to optimize the reaction set-up, the Grignard reaction has proven to be unreliable and inconsistent. It is speculated that the Grignard reagent formed in-situ can achieve a 6-membered cyclic conformation through a dative bonding interaction between the oxygen of the OTBS group and the magnesium atom, rendering it less reactive or less capable of approaching acrolein

(Scheme 2.13). Given that the Grignard reaction was not proceeding well, we attempted a lithium-halogen exchange using nBuLi instead. Pleasingly, the lithium-halogen exchange and subsequent nucleophile addition occurred well on the first attempt, providing 79% yield of allylic alcohol **2.75** on a 200 mg scale. The reaction proceeded fairly cleanly, with complete consumption of the starting bromobutoxysilane **2.76**. The reaction could most

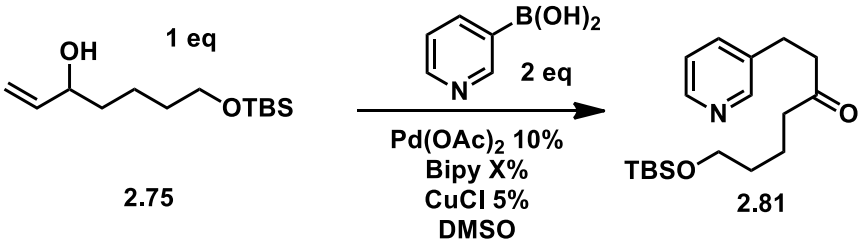

Entry	Ligand Loading	Temp.	Reaction Time	Result
1	50%	80 °C	12h	30% Conv.
2	30%	80 °C	12h	34% Conv.
3	20%	80 °C	12h	37% Conv.*
4	10%	80 °C	12h	31% Conv.
5	30%	50 °C	12h	No Rxn
6	30%	70 °C	12h	No Rxn
7	30%	100 °C	12h	38% Conv.
8	30%	120 °C	12h	26% Conv./ Decomp
9	30%	140 °C	12h	Decomp.
10	30%	80 °C	12h	1:1 OH / $B(OH)_2$ (34%)
11	30%	80 °C	12h	2:1 OH / $B(OH)_2$ (34%)
12	30%	80 °C	72h	1:2 OH / $B(OH)_2$ (100%)
13	30%	80 °C	72h	1:1 OH / $B(OH)_2$ (79%)

likely be used without purification but very slight amounts of desilylation were observed. The lithium-halogen exchange reaction was scaled up to a 2.0 g scale giving an 85% yield (95% crude yield) of allylic alcohol **2.75**.

With sufficient amounts of allylic alcohol **2.75** in hand, we have been optimizing the redox-neutral Heck reaction to generate pyridine **2.85**. Encouragingly, the reaction proceeds to form product, although in very low yields. The pyridine product has been confirmed by ^{1}H NMR spectroscopy and by mass spectrometry. Current issues are that the yield is quite low at <10%, and the purification is difficult, requiring a preparative TLC. Therefore, optimization of reaction conditions and purification methods are currently being explored. Additionally, I have synthesized allyl alcohol **2.91**, (the desilylated analog of allylic alcohol **2.75**), from the Grignard addition of vinyl magnesium bromide to a mixture of aldehyde **2.90** and the cyclic hemiacetal from the intramolecular cyclization**.** The reaction to generate unprotected allylic alcohol **2.91** proceeded in 40% using a shorter reaction time and different setup than literature precedent, so the reaction can be easily optimized. When allylic alcohol **2.91** is subjected to the Heck reaction conditions, the corresponding pyridine **2.82** is produced in very low yields and was also susceptible to a 'chain-walking' pathway leading to the oxidation of the alcohol to the aldehyde. The pyridyl alcohol product **2.82** has been confirmed by ^{1}H NMR spectroscopy as well as by mass spectrometry, but also suffers from purification difficulties. Given these considerations at the time, we focused on optimizing around the silylated allylic alcohol **2.75** (Table 2.1) because it is likely that this reaction will proceed more efficiently, and with less side reactivity, with only one alcohol exposed. We believe that the presence of

the exposed primary alcohol would lead to undesirable coordination to the palladium, which could hinder the reaction, as well as lead to oxidation side reactions to generate an aldehyde side-product through a Heck-relay type reaction mechanism.[46] Optimization (Table 2.1) of the Heck reaction to generate pyridine **2.81** began with experimenting with difficult catalyst loading of the BiPy ligand (entries 1–4). The results were determined by ^{1}H NMR spectroscopy analysis of the crude reaction mixtures. Catalyst loadings of 50% to 10% were evaluated: revealing that 30% $Pd(OAc)_2$, resulted in 34% conversion, while 50% and 10% loadings performed similarly, at 30% and 31% conversions, respectively. Next, I evaluated reaction temperatures ranging from 50 ℃ to 140 ℃ (entries 5–9). Both 50 ℃ and 70 ℃ resulted in no reactivity. Experimentations at 80 ℃ and 100 ℃ gave very similar results at 34% and 38% conversion respectively. At 120 ℃ about 26% conversion occurred, but signs of decomposition were also observed. At 140 ℃, extensive amounts of degradation were observed with only trace amounts of product detectable. Given these results, it appears that the reaction should be ran at a lower temperature, possibly at around 80 ℃. At this point, I evaluated varying equivalents of allylic alcohol **2.75** with respect to the pyridyl boronic acid (entries 10 and 11). However, at 1:1 alcohol to boronic acid equivalents ratio, the conversion was similarly 34%. The same result was observed when a 2:1 ratio of alcohol to boronic acid was employed. Given these inconclusive results, I decided to follow up with reaction time experiments because in most experiments, there is large amount of starting materials recovered, so perhaps a longer reaction time at a moderate temperature (*e.g.*, 80 ℃) would lead to greater product formation (entries 12 and 13). This hypothesis seems to have been correct because when the reaction was performed

at 80 ℃ for 72 h, the conversion increased significantly. In parallel (Table 2.1), the time experiments were performed with 1:1 ratio of the allylic alcohol to the pyridyl boronic acid (entry 12) and 1:2 ratio with the pyridyl boronic acid in excess (entry 13). Pleasingly, the 1:2 ratio reaction resulted in complete consumption of the allylic alcohol, showing 100% conversion by crude ^{1}H NMR analysis, but still significant decomposition. The reaction using a 1:1 ratio of reactants yielded a 79% conversion, but also suffered from decomposition primarily via desilylation.

Interestingly, improvements were observed as we began to deviate more significantly from our initial conditions based on Dr. Yangjie Wu's work.[43] In an attempt to improve the reactivity

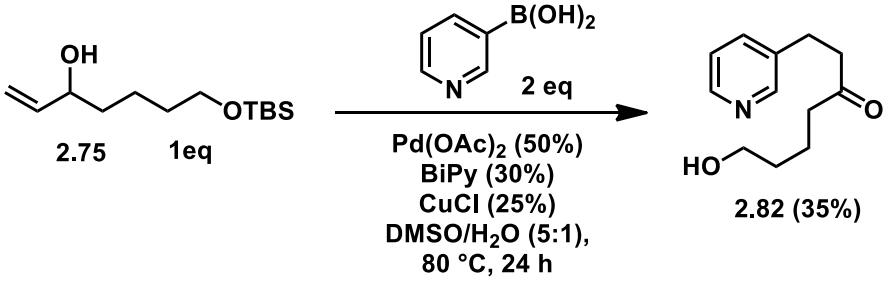

Scheme 2.14 Inclusion of water as a cosolvent for Heck reaction

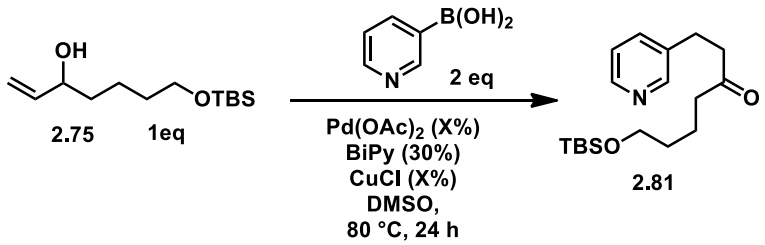

Entry	Palldium Loading	Copper Loading	Conversion
1	10%	5%	33%
2	20%	10%	46%
3	30%	15%	55%
4	40%	20%	82%
5	50%	25%	96%

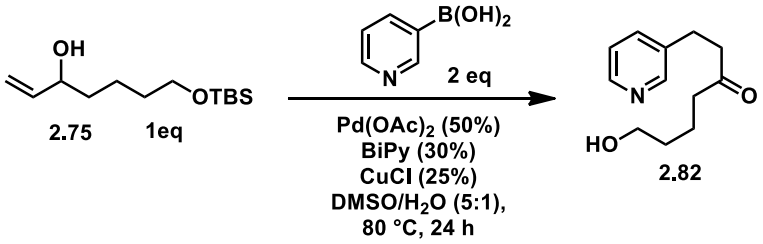

Entry	Palldium Loading	Copper Loading	Conversion
1	10%	5%	40%
2	20%	10%	51%
3	30%	15%	74%
4	40%	20%	100%
5	50%	25%	100%

Table 2.2 Comparison of catalyst loading with and without water as a cosolvent

and efficiency of this reaction to allow for lower catalyst loading and shorter reaction times, we added water as a cosolvent (5:1 DMSO/H_2O) to aid formation of the more reactive boron-ate complex from the 3-pyridyl boronic acid (Scheme 2.14). Pleasingly, we isolated

the desilylated alcohol **2.82** in 35% yield. The silylated product **2.81** was not observed or isolated from this reaction. We found that the Heck reaction, both with and without water as a cosolvent, benefited moderately in terms of conversion using a new batch of $Pd(OAc)_2$ that is stored in the glovebox and pre-stirring the $Pd(OAc)_2$, CuCl, and BiPy catalysts.

We observed improved reactivity by including water as a cosolvent when cross experimented with varying the catalyst loading. We also compared the same catalyst loading reactions to conditions without water and pre-stirring (Table 2.2). In both the wet and dry reaction setups, the conversions improved with the increase in catalyst loading. In dry conditions, full conversion (96%) to silyl pyridine product **2.81** was not achieved until 50% catalyst loading (Table 2, entry 5) after 24 h. However, when compared to the wet conditions, full conversion to the pyridyl alcohol product **2.82** was achieved at slightly lower catalyst loading at 40% and 50% loading (Table 2, entries 4 and 5). Every experiment directly compared to between the wet and dry conditions favored the wet conditions in terms of conversion and the convenience of accessing the pyridyl alcohol product **2.82**, which would decrease the overall synthesis by one step, eliminating a desilylation step after isolating silyl-pyridine **2.81**. Unfortunately, both the dry and wet systems suffered from severe purification and degradation issues. Although the conversion values were high in both dry and wet conditions, the best isolated yield for each was only 27% and 35% respectively. This suggests that we are losing a lot of material during the work-up and purification manipulations and/or there is a significant degradation pathway diminishing the yields. While we were investigating improved methods of workups and

purification, we also briefly explored desilylation conditions in the event that we decided to proceed through silyl-pyridyl **2.81** as an isolated intermediate (Scheme 2.14).

Initially, we sought to use TBAF, a very common desilyating agent, however we found it to be too harsh, leading to decomposition. We found that dilute HCl (2.5%) in MeOH at 40 °C resulted in complete desilylation overnight (Scheme 2.15). The reaction does not proceed at all at room temperature.

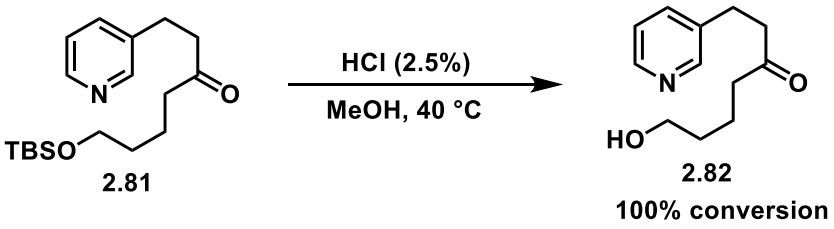

Scheme 2.15 Desilylation of silyl-pyridyl **2.81**

Refocusing on the Heck reaction, we explored the use of variously modified allylic alcohols for the Heck reaction (Scheme 2.16). Specifically, if we could perform the Heck reaction with a tosyl or mesyl activating group instead of the TBS group, this could also eliminate an activating step in the synthesis before the macrocyclization step. We were also interested in performing the Heck reaction with simply the unprotected alcohol with our improved reaction conditions. We attempted to synthesize the tosylate, mesylate, and free OH through somewhat similar routes to the silylated substrate (Scheme 2.16). Beginning from bromobutanol **2.80**, silylation by treatment with TBSCl and imidazole gave bromobutoxy silane **2.76** in 90% yield, which is transformed into silylated allylic alcohol **2.75** in 85% yield by lithium-halogen exchange and addition into acrolein. To synthesize the tosylated derivative, we begin the tosylation of bromobutanol **2.80** by

treatment with TsCl and TEA to give bromobutyltosylate **2.86** in 63% yield. Next, we

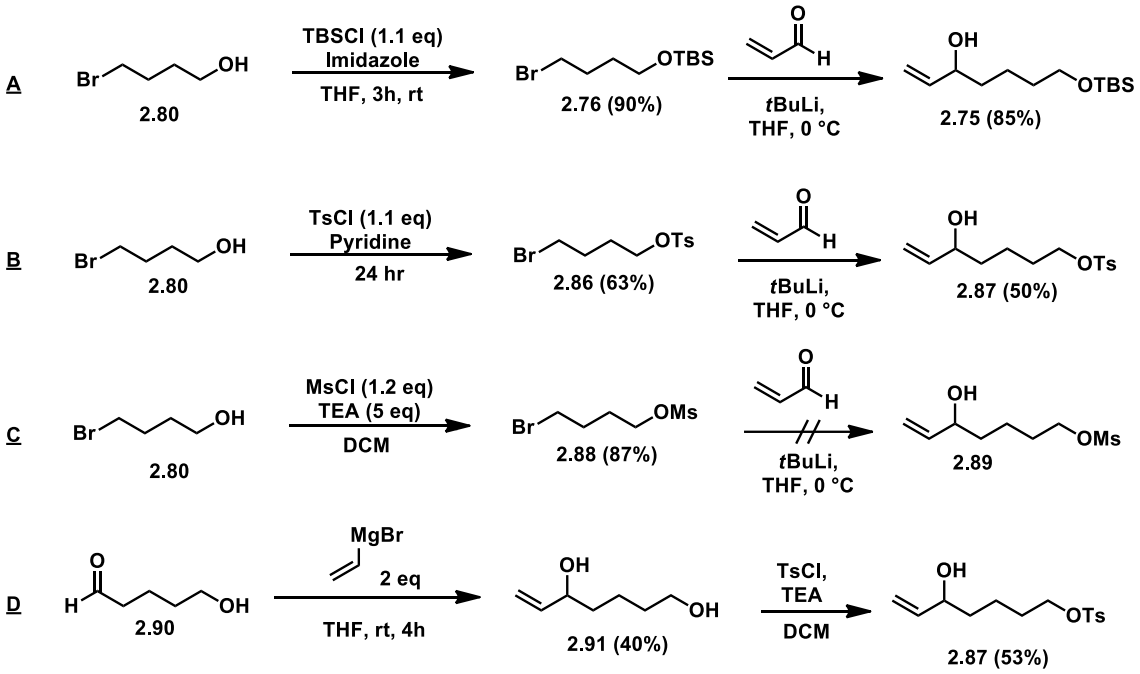

Scheme 2.16 Synthesis of substrates for optimization of Heck reaction

performed a lithium-halogen exchange and addition in acrolein to generate the desired tosylated allylic alcohol **2.87** in approximately 50% yield, but with impurities that could not be fully removed. Attempted synthesis of the mesylated substrate (**2.89**) was attempted beginning from bromobutanol **2.80** as well: mesylation by treatment with MsCl and TEA gave bromobutylmesylate **2.88** in 87% yield. Although tosyl alcohol **2.87** was synthesized successfully, purification was a concern so we synthesized the same compound instead by reacting vinylmagnesium bromide with aldehyde **2.90**, yielding diol **2.91** in 40% yield. Finally, diol **2.91** was mono-tosylated by treatment with TsCl and TEA to give the desired tosyl allylic alcohol **2.92** in 53% yield. Unfortunately, the subsequent lithium-halogen exchange and addition into acrolein did not proceed well, resulting in possibly elimination

of the mesylate. To synthesize the desired allylic alcohol mesylate **2.89**, we may have to proceed through a route similar to that used for tosylate **2.87** (reaction D), however we are concerned with the stability of the mesylate during the subsequent Heck reaction.

When we implemented the variously modified allylic alcohol substrates in the Heck reaction, we observed unsatisfactory yields for the corresponding pyridine product (Scheme 2.17). By comparison, the dry and wet versions of our previously optimized Heck reaction both outperformed the free alcohol and the tosyl activated derivative. The free alcohol substrate (**2.91**) resulted in very little product formation, which we at the time, speculated could be due to the side-reactivity of the free alcohol. We were cautiously optimistic that we would see exciting results with the tosylated allylic alcohol **2.92** since the alcohol was masked. We had hoped that with the tosylate, the Heck reaction would at least proceed as well as the sillyated allylic alcohol **2.75**, if not better, and then set us up to explore the macrocyclization step. Unfortunately, the Heck reaction with the tosylated allylic alcohol **2.92** resulted in only a trace amount of product formation by LCMS analysis under our optimized conditions. The Heck reaction with the tosylated substrate under dry conditions resulted in complete decomposition and no detectable product formation by NMR analysis. This was a disappointing result, but which motivated us to find an alternative path to arrive at the desired pyridyl tosylate (**2.83**), as we were eager to test the proposed key steps en-route to annotinolides A and B.

To overcome this challenge, we found inspiration in the literature from Heck coupling chemistry performed by Dr. Zenichi Yoshida in 1978, where they generated 3-alkylpyridines through a palladium catalyzed Heck reactions between allylic alcohols and

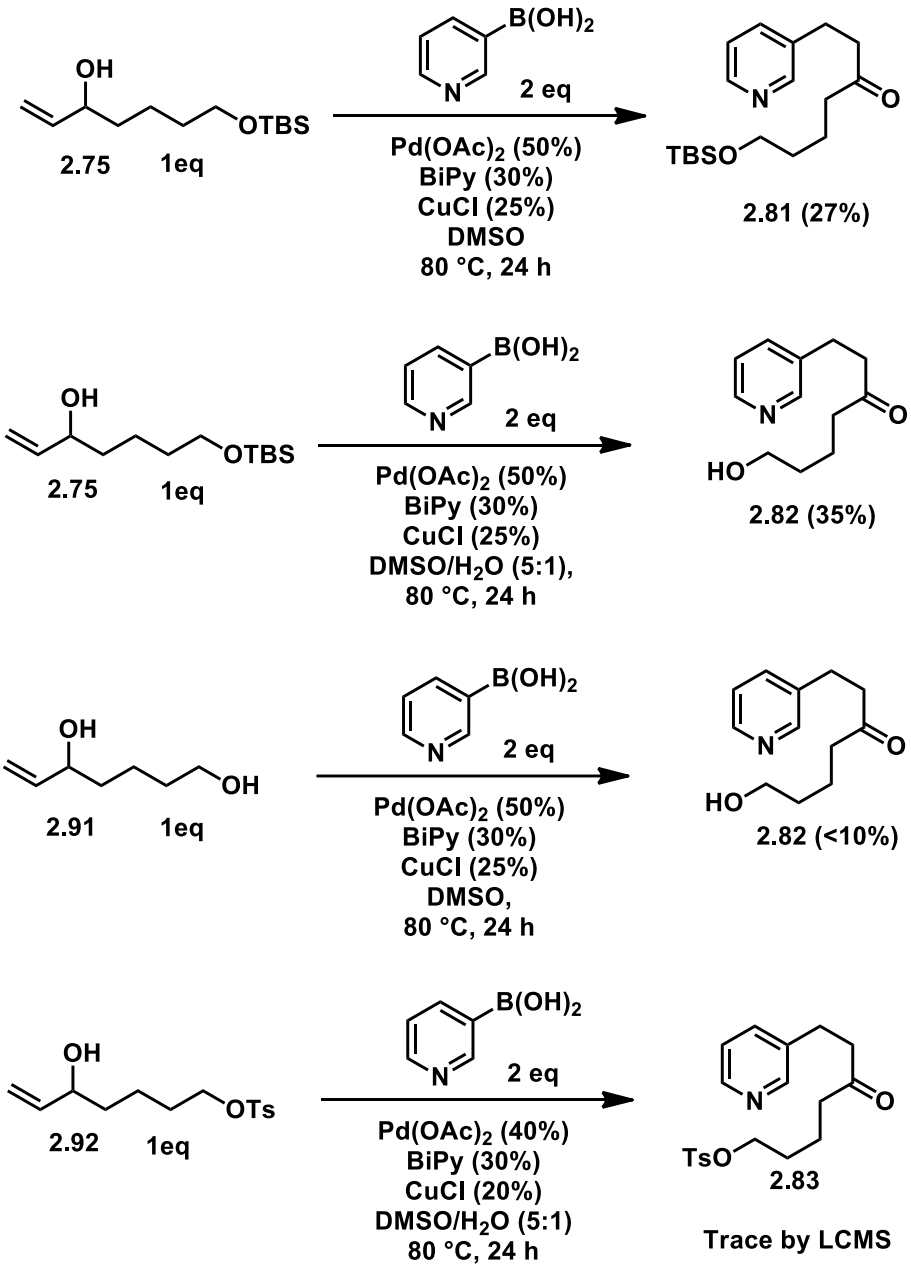

3-iodopyridines.[47] Yoshida's modified conditions of the Heck reaction were attractive because they were high yielding and proceeded without the need of a ligand in some examples. This was important because we experienced significant difficulties separating BiPy from our desired products. Additionally, these reactions could be run in DMF or HMPA as a solvent, both of which are easier to remove than DMSO. Beginning with

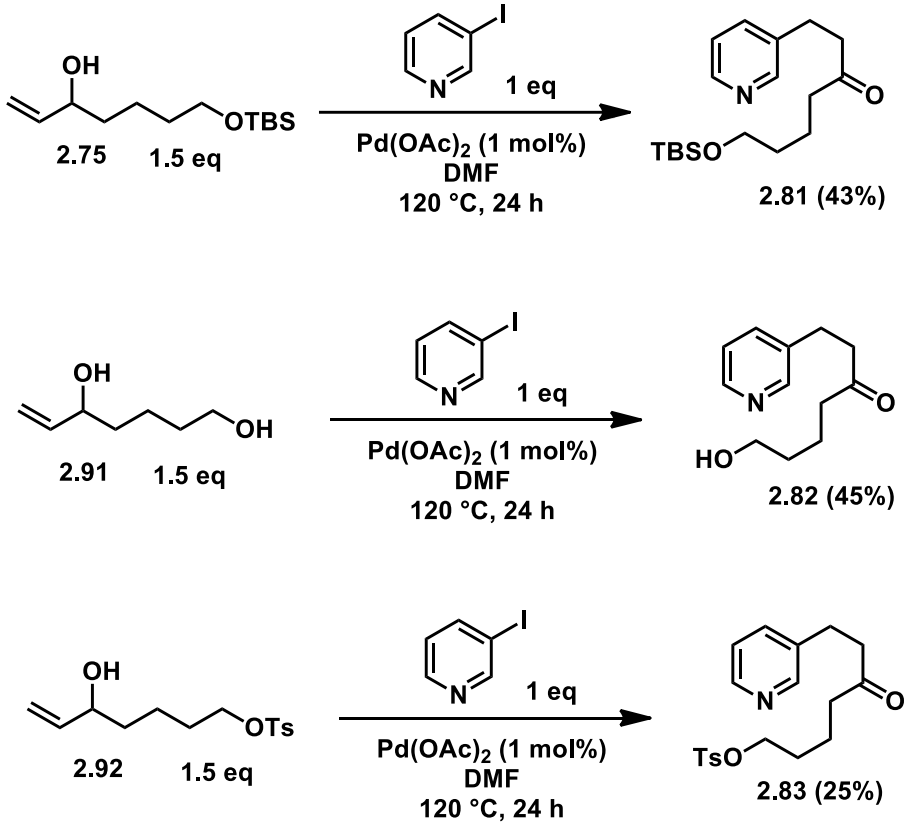

Scheme 2.18 Modified ligand free Heck conditions with tosylate, free alcohol, and silylated allylic alcohol

Yoshida's Heck conditions, we re-investigated the Heck reaction with our variously modified allylic alcohol substrates, and pleasingly found encouraging initial results (Scheme 2.18). The silyl allylic alcohol proceeded in 43% yield. The allylic diol proceeded with a slightly better yield at 45%. The tosylated allylic alcohol seemed to suffer from some decomposition. These reactions proceed much more cleanly than our

previously used conditions and are much easier to purify without the use BiPy as a ligand. DMF must be removed as much as possible to further improve the purification, especially when the reaction is scaled up. Although the yields and purification are a significant improvement from our previous conditions, there is still much room for improvement. Optimization of these reactions will need to be performed, including variation of Iodopyridine to the bromo- or chloro- derivative and switching solvent to perhaps HMPA. However, HMPA is a documented carcinogen, so unless the yield for these reactions with HMPA improve dramatically, it may be better from a safety perspective to use DMF instead, especially when considering large scale reactions.

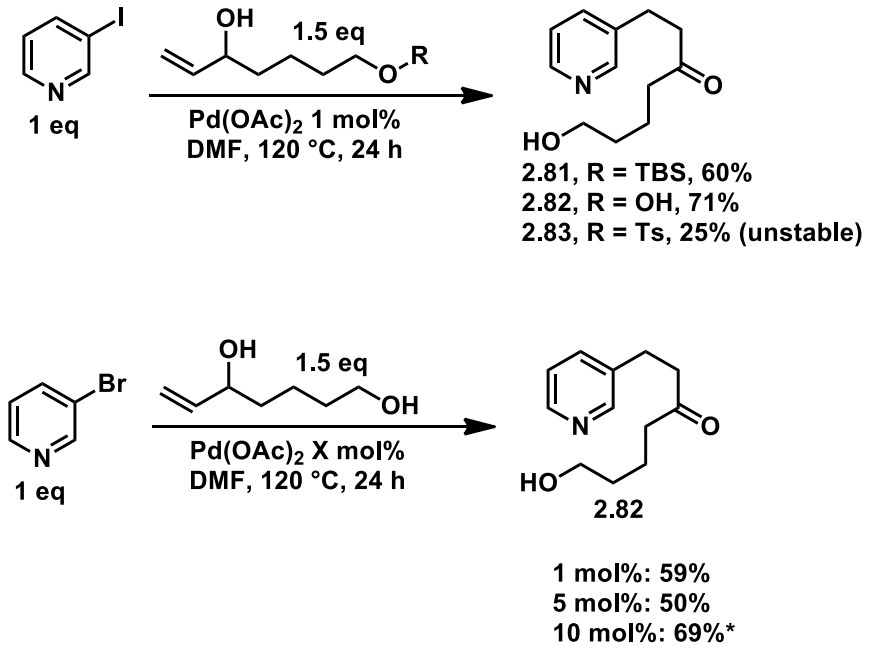

Scheme 2.19 Improved yields of Heck reaction with iodopyridine and use of bromopyridine for comparison

Significant improvement in the yield of the Heck reaction with 3-iodopyridine were observed by simply modifying the extraction procedure (Scheme 2.19). Yoshida's original extraction procedure used diethyl ether as the extracting solvent, which work well for their

substrates as they often obtained very high yields with many examples above 90%. However, for our substrates, Et_2O was observed to have significant solubility issues. Upon this observation, the extraction solvent was changed to EtOAc and the number of extractions was increased. This simple observation and adjustment led to a significant increase in yield from 45% to 62% for pyridyl-alcohol **2.82.** When the catalyst loading was increased to 3% for pyridyl-alchol **2.82**, the yield increased to 71% but there was more undesired side-reactivtiy. The tosyl pyridine was not revaluated due to stability concerns.

After improving the extraction procedure, we evaluated 3-bromopyrdine as the Heck coupling substrate (Scheme 2.19). We found that with 1 mol % $Pd(OAc)_2$ catalyst loading, the yield of the Heck reaction to produce pyridyl alcohol **2.82** fell by about 10% from 71% down to 59%. The same reaction as also performed with 5 mol% and 10 mol% $Pd(OAc)_2$ catalyst loading. Interestingly, the 5 mol% $Pd(OAc)_2$ loading led to a 50% yield on a gram scale, and the 10 mol% $Pd(OAc)_2$ led to a 69% yield. These results are somewhat inconsistent. The increase from 1 mol% to 5 mol% of $Pd(OAc)_2$ led to a lower yield which could suggest that increasing the catalyst loading is actually detrimental to the efficiency of the reaction and could lead to side reactions. When the catalyst loading is increased to 10 mol% of $Pd(OAc)_2$, the yield is 69% which is significantly higher, but there appears to be side reactions that are difficult to remove from the desired product. It was generally observed that an increase in catalyst loading led to less efficient reactions with more side reactivity and unreacted 3-bromopyridine. By comparison to the 3-iodopyridine, the 3-bromopyridine Heck reaction was generally less efficient and less clean of a reaction. Given these interesting results, it is clear that much more rigorous and exhaustive

optimization efforts are necessary to improve the reaction conditions. One significant improvement would be investigate if it is possible to lower the equivalents of the allylic diol **2.91** from 1.5 equivalents to perhaps 1.1 or 1.2 equivalents and what loading of $Pd(OAc)_2$ would be required to obtain satisfactory yields. However, the reliability and reproducibility of the Heck reaction adapted from Yoshida's conditions have allowed us to produce pyridyl alcohol **2.82** in sufficient amounts of material to begin developing the next reaction in this total synthesis, which is the synthesis of the pyridinium macrocycle *in situ* to access the tricyclic key intermediate **2.72**.

Pyridinium Cyclization Reactions and Characterization by LCMS

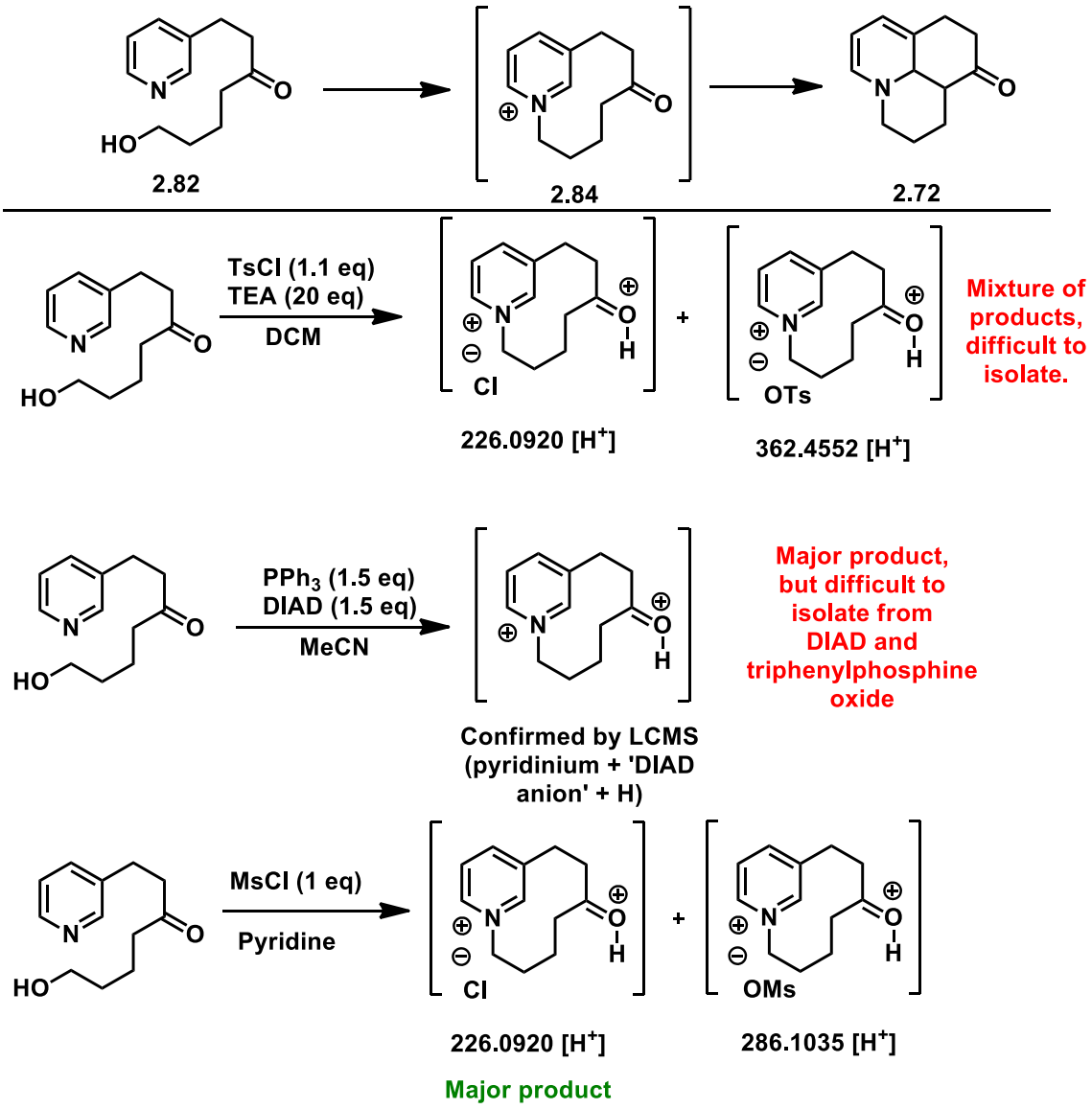

Scheme 2.20 Pyridinium cyclization reactions and characterization by LCMS

Our general strategy for the synthesis of the pyridinium macrocycle is to activate the alcohol to become a better leaving group so that the nucleophilic pyridine moiety could displace the activated alcohol and generate a pyridinium macrocycle that would be set up for a subsequent Mannich-type reaction to generate tricycle **2.72** (Scheme 2.20). Our first

conditions used TsCl and TEA to tosylate the alcohol. Initially, we attempted to isolate and purify the tosylated product but it was very difficult to purify by silica gel chromatography, suggesting that perhaps the tosylated product was forming *in situ* and then immediately displaced by the pyridine under very mild conditions to form the pyridinium macrocycle **2.84**. Given this fortuitous discovery, we began looking for the pyridinium macrocycle as an intermediate product, however obtaining full conversion and full characterization have been problematic. Treatment of pyridyl alcohol **2.82** with TsCl and TEA led to a mixture of pyridinium salts with the counterion as a chloride or the tosylate as detected by LCMS. Unfortunately, there also appeared to be significant amounts of unreacted pyridyl alcohol **2.82** and TsCl, making isolation and characterization difficult and thus we were not able to push this material forward successfully to access tricycle **2.72**. The next conditions explored was an intramolecular Mitsunobu-type reaction to access pyridinium **2.84**. When pyridyl alcohol **2.82** was treated with triphenylphosphine and diisopropyl azodicarboxylate (DIAD), by LCMS we observed the desired pyridinium product with counterion being the anion of DIAD. Although we observed good conversion by LCMS, we critical issue in purifying this salt was the triphenylphosphine oxide by product of the Mitsunobu reaction. Despite several recrystallization procedures, we were not able to separate the desired pyridinium from the triphenylphosphine oxide. Both species had similar solubility properties, but it was also difficult because the DIAD was extremely viscous and seemed to solubilize both species readily. Since purification was not possible yet and we observed the product mass primarily by LCMS in the crude mixture, we attempted to use the crude mixture to proceed through the next reaction to the

tricycle (Table 2.3). Various bases were evaluated, such as KHMDS, NaH, Na_2CO_3, LDA, and *t*BuOK. Unfortunately, none of the reaction conditions led to product formation with only starting material recovered. The only reactivity observed was decomposition with *t*BuOK in DME at 50 °C (Table 2.3, entry 7).

We were concerned that the crude pyridinium formed from the Mitsunobu-type conditions were simply not clean enough and that perhaps the byproducts of that reaction could be hindering the next cyclization to the tricycle. To address this concern, we revisited the conditions used to form pyridinium **2.84**. The next conditions explored utilized activation of the alcohol by mesylation (Scheme 2.19). When pyridyl alcohol **2.82** was treated with MsCl (1 equiv) in pyridine solvent, we observed conversion to the pyridinium macrocycle (**2.84**) with the major product being the pyridinium with the chloride

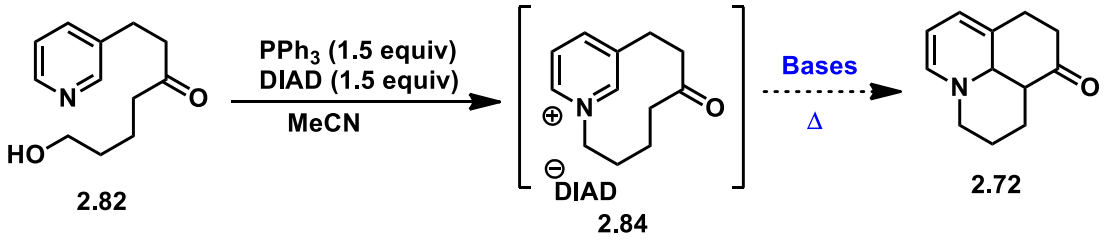

2.82 **2.84** **2.72**

Entry	Conditions	Temp	Result
1	KHMDS (1.1 equiv), THF	rt	No reaction
2	NaH (1.1 equiv), THF	rt	No reaction
3	NaH (3 equiv), THF	rt	No reaction
4	Na_2CO_3 (2 equiv), MeCN	rt	No reaction
5	LDA (2 equiv), THF	rt	No reaction
6	LDA (2 equiv), THF	40 °C	No reaction
7	*t*BuOK (1.2 equiv), DME	50 °C	Decomp

counterion when compared to the mesylate counterion. A practical advantage of this procedure was that the pyridine base/solvent could be simply removed by rotary evaporation. In addition to the LCMS data, additional support for the pyridinium species comes from analysis of the NMR data, which shows a shift in alkyl protons adjacent to the newly formed nitrogen–carbon bond (1.71ppm). By crude NMR analysis, this reaction is much cleaner than the Mitsunobu-type conditions and the tosylation procedure.

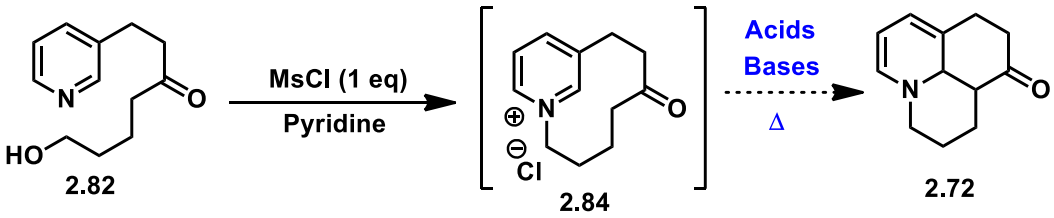

Entry	Conditions	Temp	Result
1	*t*BuOk (1.1eq), THF	rt	No reaction
2	*t*BuOk (1.1eq), DMF	rt	No reaction
3	*t*BuOk (1.1eq), DCM	rt	No reaction
4	*t*BuOk (1.1eq), DMF	100 °C	No reaction
5	Na_2CO_3 (1.1eq), DMF	100 °C	No reaction
6	LDA (1.1eq), DMF	100 °C	No reaction
7	pyridine	150 °C (MW)	Decomp
8	$HClO_4$	105 °C	Decomp
9	$HClO_4$ (2.1eq), Dioxane	105 °C	Decomp
10	HCl (10 mol%), MeOH	rt	Decomp
11	HCl (10 mol%), THF	50 °C	Decomp
12	DMF	120 °C	No reaction
13	HCl (10 mol%), DMF	120 °C	No reaction
14	$HClO_4$ (10 mol%), DMF	120 °C	Decomp

Table 2.4 Pyridinium cyclization reactions from pyridinium-Cl salt

With a more promising and reliable method of synthesizing pyridinium **2.84**, we again began exploring the use of acids and bases to access tricycle **2.72** (Table 2.4). We evaluated *t*BuOK in various such as THF, DMF, and DCM at room temperature and at elevated temperatures (entries 1–4) but observed no reactivity. We also tried elevated temperatures with LDA and Na_2CO_3 as the base but again saw a lack of reactivity (entries 5–6). To examine more harsh conditions, we used pyridine as the base/solvent at 150 °C in a microwave reaction but now only observed decomposition (entry 7). After unsuccessful attempts with bases, we began treating with acids in the hopes of facilitating tautomerization of the ketone to the enol which could then reaction with the pyridinium still through a Mannich-type mechanism. The acids we evaluated were $HClO_4$ and HCl in various solvents such as dioxane, MeOH, and THF at room temperature and at elevated temperatures (entries 8–14). Unfortunately, acidic conditions most often led to decomposition or unknown side reactivity.

2.3 Conclusions and Future Directions

In conclusion, we have made significant progress towards the divergent synthesis of annotinolides A and B. With the recent development of methods to form the pyridinium macrocycle **2.84**, we are actively working to perform the Mannich-type tricyclization to access key intermediate **6** where we can then begin to explore divergent routes to annotinolides A and B. Although we feel confident in pyridinium formation based on

LCMS, HRMS, and NMR analysis, we still need to fully characterize the pyridinium salt to better under and design the subsequent Mannich-type reaction.

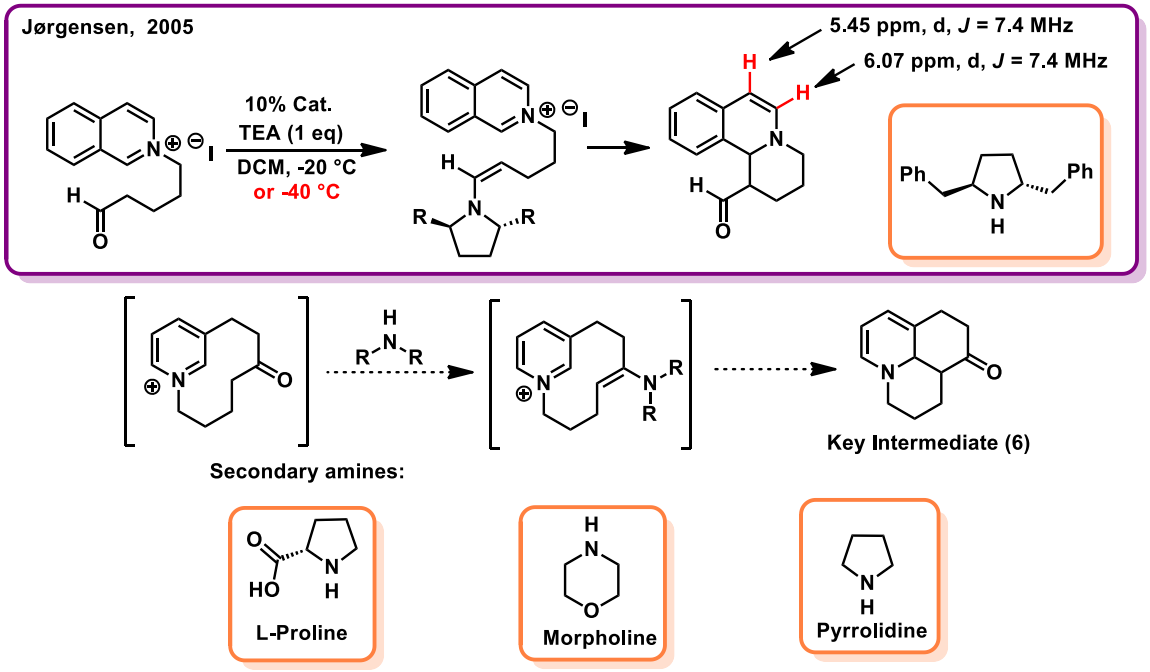

Scheme 2.21 Enamine Mannich-type reaction approach.

Thus far neither acidic nor basic conditions, at any temperature, have been productive for the Mannich-type reaction of pyridinium **2.84** in affording the key intermediate tricycle **6**. However, we are very optimistic about an enamine facilitated Mannich-type reaction that we are currently exploring (Scheme 2.21). Using this approach, we propose that treatment of the pyridinium macrocycle with a secondary amine will under a condensation to the corresponding enamine. From the enamine, we propose that under the right conditions, the enamine should be a competent nucleophile for the desired Mannich-type reaction to access the tricyclic key intermediate (**6**). We are currently exploring a broad range of reaction conditions to successfully form the enamine and perform the Mannich-type cyclization.

Future work for this project is focused upon developing this Mannich-type reaction to access key intermediate **6** and then proceeding through the divergent routes to annotinlides A and B (Scheme 2.22). To synthesize annotinolide A from key intermediate **6**, we are proposing a biomimetic cyclopropanation by treatment with base and an oxidant. The resulting tertiary radical **2.71** can then be trapped through a Michael addition to methacryloyl chloride to yield α,β-unsaturated acyl chloride **2.70**. To synthesize annotinlide B from key intermidate **6**, we propose beginning with a hydride reduction of the ketone to the secondary alcohol which can then be acylated with methacryloyl chloride to afford α,β-unsaturated ester **2.73.** This sets the stage for the ultimate photochemical [2+2] cycloaddition to synthesize annotinolide B.

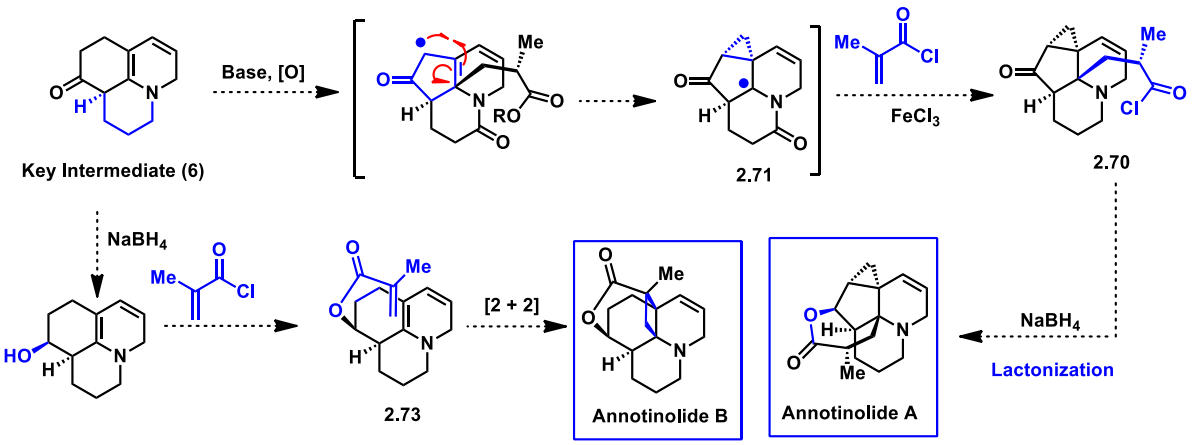

Scheme 2.22 Synthesis of annotinlides A and B

2.4 Experimental Section

General Considerations

i) Solvents and reagents

Unless noted below, commercial reagents were purchased from MilliporeSigma, Acros Organics, Chem-Impex, Combi-blocks, TCI, and/or Alfa Aesar, and used without additional purification. Solvents were purchased from Fisher Scientific, Acros Organics, Alfa Aesar, and Sigma Aldrich. Tetrahydrofuran (THF), diethyl ether (Et_2O), acetonitrile (CH_3CN), benzene, methanol (MeOH), and triethylamine (Et_3N) were sparged with argon and dried by passing through alumina columns using argon in a Glass Contour solvent purification system. Dichloromethane (CH_2Cl_2) was freshly distilled over calcium hydride under a N_2 atmosphere prior to each use. DMSO and toluene (PhMe) were distilled over calcium hydride under a N_2 atmosphere, degassed via freeze-pump-thaw (3 cycles), and stored over 4 Å molecular sieves in a Schlenk flask under N_2. Dimethoxyethane (DME), *p*-xylene, dimethylformamide (DMF), MeLi solution, *n*-BuLi solution, LiHMDS solution, Red-Al solution, and pyridine were purchased in Sure/Seal, AcroSeal, or ChemSeal bottling, and used directly. 1,4-Dioxane was purchased in AcroSeal bottling (99.5%, anhydrous, stabilized, over 4 Å molecular sieves) and additionally sparged with N_2 prior to use.

ii) Reaction setup, progress monitoring, and product purification

Unless otherwise noted in the experimental procedures, reactions were carried out in flame or oven dried glassware under a positive pressure of N_2 in anhydrous solvents using standard Schlenk techniques. Reaction progresses were monitored using thin-layer chromatography (TLC) on EMD Silica Gel 60 F254 or Macherey–Nagel SIL HD (60 Å mean pore size, 0.75 mL/g specific pore volume, 5–17 μm particle size, with fluorescent indicator)silica gel plates. Visualization of the developed plates was performed under UV light (254 nm). Purification and isolation of products were performed via silica gel chromatography (both column and preparative thin-layer chromatography). Commercial reagents were purchased from Sigma Aldrich, Acros Organics, Chem-Impex, TCI, Oakwood, and Alfa Aesar, and used without additional purification. Solvents were purchased from Fisher Scientific, Acros Organics, Alfa Aesar, and Sigma Aldrich. Tetrahydrofuran (THF), diethyl ether (Et_2O), acetonitrile (MeCN), dichloromethane (CH_2Cl_2), benzene, 1,4-dioxane, and triethylamine (Et_3N) were sparged with argon and dried by passing through alumina columns using argon in a Glass Contour (Pure Process Technology) solvent purification system. Dimethylformamide (DMF), dimethyl sulfoxide (DMSO), and dichloroethane (DCE) were purchased in Sure/Seal or AcroSeal bottling and additionally sparged with N_2 prior to use.

iii) Analytical instrumentation

NMR spectral data were obtained using deuterated solvents obtained from Cambridge Isotope Laboratories, Inc. ^{1}H NMR and ^{13}C NMR data were recorded on Bruker Avance

NEO400 or Bruker Avance 600 MHz spectrometers using $CDCl_3$, typically at 20–23 °C.. Chemical shifts (δ) are reported in ppm relative to the residual solvent signal (δ 7.26 for ^1H NMR, δ 77.16 for ^{13}C NMR in $CDCl_3$). Data for ^1H NMR spectroscopy are reported as follows; chemical shift (δ ppm), multiplicity (s = singlet, d = doublet, t = triplet, q = quartet, m = multiplet, br = broad, dd = doublet of doublets, dt = doublet of triplets), coupling constant (Hz), integration. Data for ^{13}C and ^{19}F NMR spectroscopy are reported in terms of chemical shift (δ ppm). IR spectroscopic data were recorded on a NICOLET 6700 FT-IR spectrophotometer using a diamond attenuated total reflectance (ATR) accessory. Samples are loaded onto the diamond surface either neat or as a solution in organic solvent and the data acquired after the solvent had evaporated. High resolution accurate mass spectral data were obtained from the Analytical Chemistry Instrumentation Facility at the University of California, Riverside, on an Agilent 6545 Q-TOF LC/MS instrument (supported by NSF grant CHE-0541848)

2.5 Experimental Procedures and Characterization Data

Preparation of 4-(tert-Butyldimethylsilyloxy)butan-1-ol (2.78)

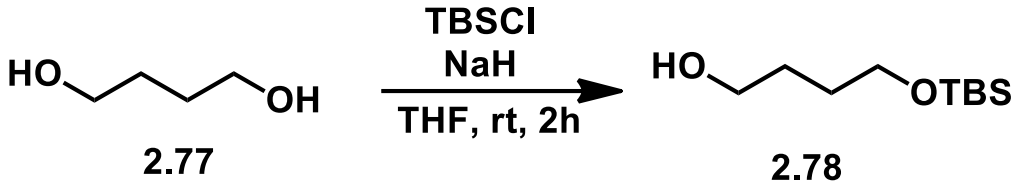

2.77 2.78

4-(*tert*-Butyldimethylsilyloxy)butan-1-ol (2.78). To a 250 mL round-bottomed flask with THF (66 mL) was added sodium hydride (812 mg, 33.8 mmol, 1 equiv), followed by 1,4-butanediol (3.0 mL, 33.9 mmol, 1 equiv). The mixture was allowed to stir at rt for 60 min. After 60 min, *tert*-butyldimethylsilyl chloride (5.31 g, 33.8 g, 1 equiv) was added in portions over 5 minutes. The reaction was stirred vigorously for 60 min, after which time the reaction mixture was poured into Et_2O, washed with 10% K_2CO_3, and brine. The organic layer was dried over Na_2SO_4, filtered, and then concentrated under reduced pressure to provide a transparent dark yellow oil of crude product. The crude product was purified by silica gel flash column chromatography eluting with 40% EtOAc in hexanes to provide **2.78** as a clear oil (6.71 g, 32.8 mmol, 97%).

^{1}H NMR (400 MHz, $CDCl_3$) δ 3.66 (m, 4H), 1.65 (m, 4H), 1.56 (br s, 1H), 0.91 (s, 9H), 0.08 (s, 6H); ^{13}C NMR (101 MHz, $CDCl_3$) δ 63.5, 63.0, 30.4, 30.1, 25.8, 18.3, -5.3 ppm. HRMS (ESI+) *m/z* calc'd for $C_{10}H_{25}O_2Si$ $[M+H]^+$: 205.1546, found 205.1617 $[H^+]$ and 227.1438 $[Na^+]$. Spectral data matches literature references.[45,48] Procedure adapted from literature references.[45]

Preparation of (4-bromobutoxy)(tert-butyl)dimethylsilane (2.76)

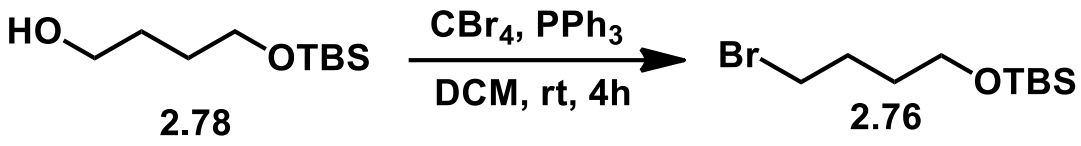

4-bromobutoxy)(tert-butyl)dimethylsilane (2.76). To a 25 mL round-bottomed flask with DCM (2 mL) was added 4-(*tert*-butyldimethylsilyloxy)butan-1-ol **2.78** (500 mg, 2.45 mmol, 1 equiv) and carbon tetrabromide (892 mg, 2.68 mmol, 1.1 equiv). The round-bottomed flask was cooled to 0 ˚C in an ice bath. After cooling triphenylphosphine (706 mg, 2.69 mmol, 1.1 equiv) was added in small portions with vigorous stirring. The reaction was allowed to warm to rt and stirred for 4 h. After 4 h, the reaction mixture was concentrated in *vacuo* to a brown oil, which then was added hexanes (10 mL). The resulting suspension was stirred for 15 min, then the supernatant was decanted off and then filtered through a pad of celite and then concentrated under reduced pressure. The crude mixture was purified by gradient flash silica gel column chromatography eluting with 0–100% EtOAc in hexanes to provide **2.76** as a clear oil (577 mg, 2.16 mmol, 88%).

^{1}H NMR (400 MHz, $CDCl_3$) δ 3.64 (t, *J* = 6.2 Hz, 2H), 3.45 (t, *J* = 6.8 Hz, 2H), 1.94 (qui, *J* = 7.1 Hz, 2H), 1.66 (m, 2H), 0.90 (s, 9H), 0.06 (s, 6H); ^{13}C NMR (100 MHz, CDCl3) δ 62.3, 34.1, 31.4, 29.6, 26.1, 18.5, –3.4, –5.2. Spectral data matches literature references.[44]

Preparation of 4-Bromo-1-butanol (2.80)

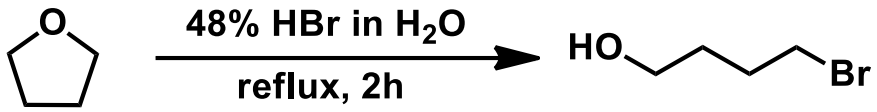

2.79 **2.80**

4-Bromo-1-butanol (2.80). To a 1000 mL round-bottomed flask with refluxing THF (100 mL, 1.24 mol) was added HBr (72 mL, 618 mmol, 47% in water, 1 equiv) dropwise over 60 min. The reaction was refluxed for 2 h, after which time the reaction mixture was cooled to rt and then diluted with H_2O (100 mL) and Et_2O (150 mL). Then, the mixture was neutralized with $NaHCO_3$ (45 g) and the organic layer was separated. The aqueous layer was extracted with Et_2O (75 mL x 2) and brine (50 mL x 2) sequentially. The organic layer was dried over Na_2SO_4 and concentrated under reduced pressure to provide 4-bromo-1-butanol (**2.80**) (29.79 g, 194.8 mmol, 32%) as a colourless liquid which was used without further purification.

^{1}H NMR (400 MHz, $CDCl_3$) δ 3.72 (t, *J* = 6.4 Hz, 2H), 3.47 (t, *J* = 6.8 Hz, 2H), 2.25 (br, 1H), 1.97 (qui, *J* = 6.9 Hz, 2H), 1.74 (qui, *J* = 6.8 Hz, 2H); ^{13}C NMR (100 MHz, $CDCl_3$) δ 62.0, 33.6, 31.0, 29.2. Spectral data matches literature references.[44] Procedure adapted from literature references.[6]

Preparation of (4-bromobutoxy)(tert-butyl)dimethylsilane (2.76)

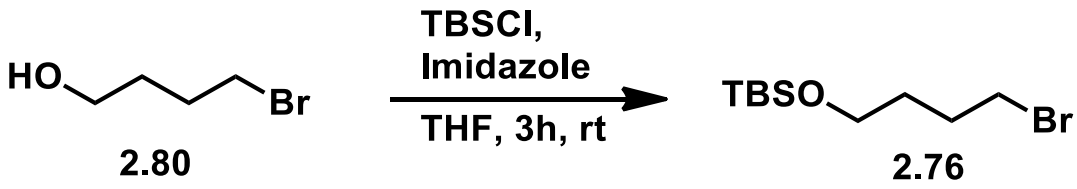

(4-bromobutoxy)(tert-butyl)dimethylsilane (2.76). To a 1000 mL round-bottomed flask was added THF (400 mL), 4-bromo-1-butanol **2.80** (25.0 g, 163 mmol, 1 equiv), and imidazole (16.7 g, 245 mmol, 1.5 equiv). The reaction was stirred at rt for 15 min, *tert*-butyldimethylsilyl chloride (27.1 g, 180 mmol, 1.1 equiv) was added portion wise and then stirred for 3 h at rt. After 3 h, the THF was evaporated on the rotary evaporator and diluted with Et_2O (300 mL) and washed with 10% $NaHCO_3$ (30 mL) and brine (50 mL x 2) sequentially. The combined organic layer was dried over Na_2SO_4, filtered, and then concentrated under reduced pressure. The crude mixture was purified by silica gel flash chromatography eluting with 5% EtOAc/hexanes to provide (4-bromobutoxy)(*tert*-butyl)dimethylsilane **2.76** (39.3 g, 147 mmol, 90%) as a viscous colorless oil.

^{1}H NMR (400 MHz, $CDCl_3$) δ 3.64 (t, *J* = 6.2 Hz, 2H), 3.45 (t, *J* = 6.8 Hz, 2H), 1.94 (quintet, *J* = 7.1 Hz, 2H), 1.66 (m, 2H), 0.90 (s, 9H), 0.06 (s, 6H); ^{13}C NMR (100 MHz, CDCl3) δ 62.3, 34.1, 31.4, 29.6, 26.1, 18.5, –3.4, –5.2. Spectral data matches literature references.[44] Procedure adapted from literature references.[44]

Preparation of 7-((tert-Butyldimethylsilyl)oxy)hept-1-en-3-ol (2.75)

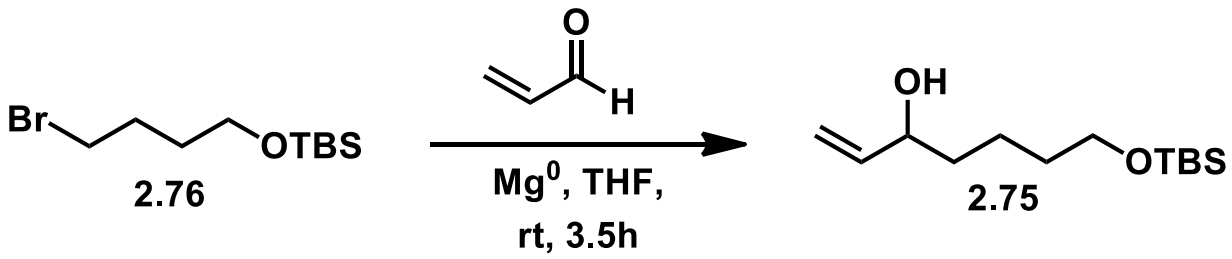

7-((tert-Butyldimethylsilyl)oxy)hept-1-en-3-ol (2.75). A 10 mL two-neck round-bottomed flask equipped with a stir bar and magnesium (32.8 mg, 1.35 mmol, 1.5 equiv) was flame dried and then Et_2O (2.0 mL) was added. (4-Bromobutoxy)(*tert*-butyl)dimethylsilane **2.76** (200 mg, 0.90 mmol, 1 equiv) was subsequently added as a solution in 1.0 mL of Et_2O dropwise, followed by a single crystal of iodine. The magnesium-halide mixture was allowed to stir at rt for 60 min. In a separate two-neck round-bottomed flask, $CeCl_3$ (331.8 mg, 1.35 mmol, 1.5 equiv) was flamed dried, then acrolein (90.2 μL, 1.35 mmol, 1.5 equiv) was added as a solution in 2.0 mL of Et_2O dropwise. The acrolein solution was allowed to stir at rt for 60 min. After both round bottoms had stirred for an hour, the Grignard solution was transferred to the acrolein solution via cannula. The reaction was allowed to stir at rt for 3.5 h. The reaction mixture was quenched with water (5 mL) and extracted with Et_2O (3 x 5 mL). The organic layer was washed with brine and dried over Na_2SO_4 and then filtered and concentrated under reduced pressure. The crude mixture was purified by silica gel flash chromatography eluting with 50% EtOAc in hexanes to provide 7-((*tert*-butyldimethylsilyl)oxy)hept-1-en-3-ol **2.75** (90 mg, 41%) as a yellow oil.

^{1}H NMR (400 MHz, $CDCl_3$) δ 5.87 (ddd, *J* = 17.1, 10.4, 6.2 Hz, 1H), 5.22 (dt, *J* = 17.2, 1.4 Hz, 1H), 5.10 (ddd, *J* = 10.4, 1.4, 1.3 Hz, 1H), 4.10 (q, *J* = 6.3 Hz, 1H), 3.61 (t, *J* = 6.5 Hz, 2H), 1.73 (m, 1H), 1.59 – 1.38 (m, 6H), 0.89 (s, 9H), 0.04 (s, 6H); ^{13}C NMR (101 MHz, $CDCl_3$) δ 141.2, 114.6, 73.2, 63.1, 36.7, 32.6, 26.0, 21.7, 18.4, –5.3. Spectral data matches literature references.[49]

Preparation of 7-((tert-butyldimethylsilyl)oxy)hept-1-en-3-ol (2.75)

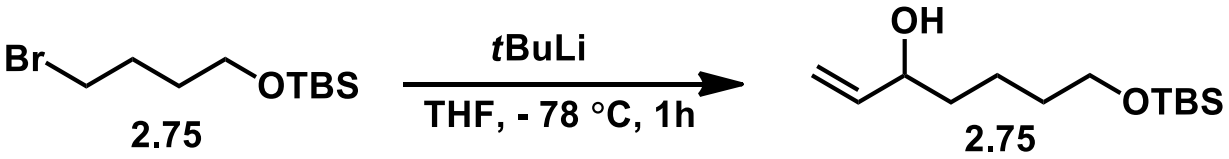

7-((tert-Butyldimethylsilyl)oxy)hept-1-en-3-ol (2.75). A 100 mL two-neck round-bottomed flask equipped with a stir bar was added (4-bromobutoxy)(tert-butyl)dimethylsilane (2.0 g, 9.0 mmol, 1 equiv) and 50 mL of THF. The round-bottomed flask was then cooled to -78 ℃ with an acetone and dryice bath. Once the reaction was cooled to –78 ℃, *t*-Buli (11.1 mL, 18.9 mmol, 2.1 equiv) was added to the reaction drop-wise. The reaction mixture was then allowed to stir for 60 min at –78 ℃. After 60 min, acrolein (900 μl, 13.5 mmol, 1.5 equiv) was added as a solution in 3 mL of THF dropwise. The reaction was allowed to stir at –78 ℃ for 60 min. After 60 min, the reaction was quenched with $NaHCO_3$ (10 mL) and water (10 mL). The quenched reaction mixture was extracted with Et_2O (3 x 15 mL). The organic layer was washed with brine and dried over Na_2SO_4 and then filtered and concentrated under reduced pressure. The crude mixture was purified by silica gel flash chromatography eluting with 50% EtOAc in hexanes to provide 7-((*tert*-butyldimethylsilyl)oxy)hept-1-en-3-ol **2.75** (1.85 g, 85%) as a yellow oil.

^{1}H NMR (400 MHz, $CDCl_3$) δ 5.86 (ddd, *J* = 17.1, 10.4, 6.2 Hz, 1H), 5.22 (dt, *J* = 17.2, 1.4 Hz, 1H), 5.10 (ddd, *J* = 10.4, 1.4, 1.3 Hz, 1H), 4.10 (q, *J* = 6.3 Hz, 1H), 3.61 (t, *J* = 6.5 Hz, 2H), 1.73 (m, 1H), 1.59 – 1.38 (m, 6H), 0.89 (s, 9H), 0.04 (s, 6H); ^{13}C NMR (101 MHz, $CDCl_3$) δ 141.2, 114.6, 73.2, 63.1, 36.7, 32.6, 26.0, 21.7, 18.4, –5.3. Spectral data matches literature references.[49]

Preparation of hept-6-ene-1,5-diol (2.91)

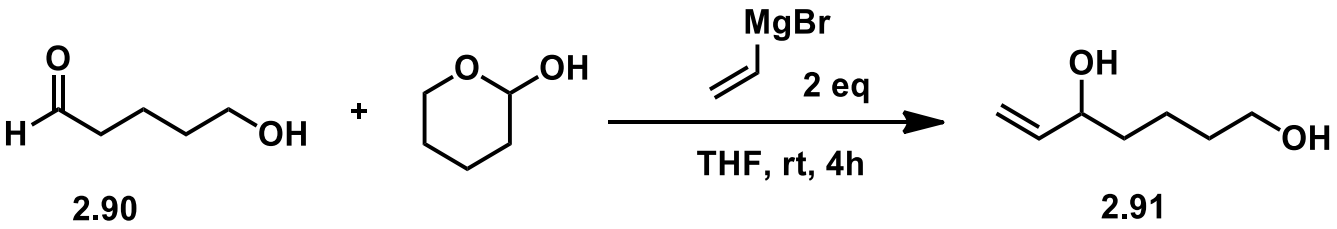

Hept-6-ene-1,5-diol (2.91). To a 50 mL round-bottomed flask was added a crude mixture of aldehyde **2.90** and its corresponding hemiacetal (1.0 g, 7.64 mmol, 1 equiv) and 6.3 mL of THF. The reaction mixture was cooled to 0 ℃, then vinyl magnesium bromide (19.2 mL, 19.1 mmol, 2.5 equiv) was added dropwise. The reaction was stirred at rt for 15 min, *tert*-butyldimethylsilyl chloride (27.1 g, 180 mmol, 1.1 equiv) was added portion wise and then allowed to warm up to rt. After 4 h, the reaction was quenched with NH_4Cl (10 mL). The quenched reaction was then extracted with DCM (3 x 10 ml) and washed with brine (3 x *10* mL). The combined organic layer was dried over Na_2SO_4, filtered, and then concentrated in under reduced pressure. The crude mixture was purified by silica gel flash chromatography eluting with 1:1 hexanes/EtOAc to provide hept-6-ene-1,5-diol **2.91** (395.10 mg, 40%) as a viscous yellow oil.

1H NMR (400 MHz, $CDCl_3$) δ 5.88 (ddd, J = 16.7, 10.4, 6.2 Hz, 1H), 5.24 (dt, J = 17.2, 1.4 Hz, 1 H), 5.12 (dt, J = 10.4, 1.3 Hz, 1H), 4.13 (dd, J = 12.1, 6.2 Hz, 1H), 3.67 (t, J = 6.3 Hz, 2H), 1.67–1.32 (m, 6H). ^{13}C NMR (151 MHz, $CDCl_3$) δ 141.2, 114.8, 73.2, 62.8, 36.6, 32.5, 21.5. Spectral data matches literature references.[50]

Preparation of 7-((tert-butyldimethylsilyl)oxy)-1-(pyridine-3-yl)heptan-3-one (2.81)

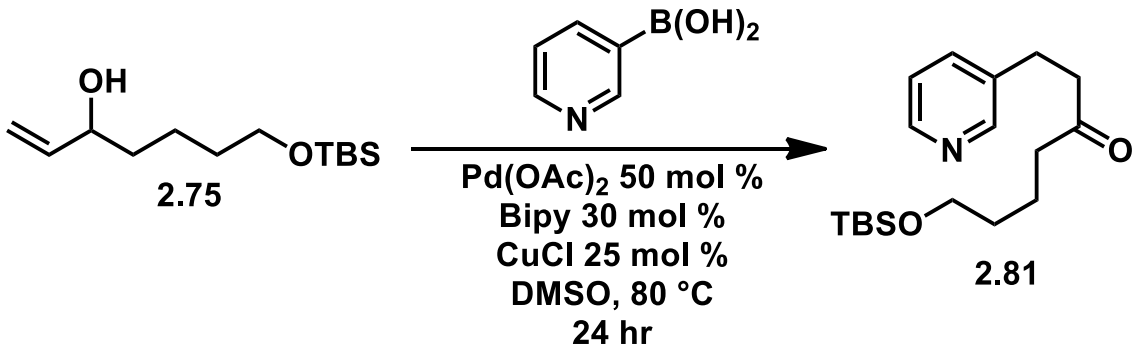

7-((*tert*-Butyldimethylsilyl)oxy)-1-(pyridin-3-yl)heptan-3-one (2.81). To a 4 mL vial equipped with a stir bar was added 7-((*tert*-butyldimethylsilyl)oxy)hept-1-en-3-ol **2.75** (0.20 mmol, 50 mg), 3-pyridyl boronic acid (0.41 mmol, 50.3 mg), BiPy (0.06 mmol, 9.6 mg), CuCl (0.51 mmol, 4.6 mg), $Pd(OAc)_2$ (0.10 mmol, 22.9 mg) and 0.6 mL of DMSO/H_2O (5:1). The reaction was stirred open to air at 80 °C for 24 h. After 24 h, the reaction was allowed to cool to rt. The reaction mixture was diluted with water (3 mL) and DCM (3 mL) and then filtered through celite. The resulting mixture was extracted with DCM (3 x 5 mL). The organic phase was washed brine (3 x 5 mL). The combined organic layer was dried over Na_2SO_4, filtered, and then concentrated under reduced pressure to

provide 7-((*tert*-butyldimethylsilyl)oxy)-1-(pyridin-3-yl)heptan-3-one **2.81** (17 mg, 27%) as a viscous yellow oil.

^{1}H NMR (600 MHz, $CDCl_3$) δ 8.51 – 8.40 (m, 2H), 7.57 (d, *J* = 7.5 Hz, 1H), 7.25 (dd, *J* = 7.7, 4.8 Hz, 1H), 3.60 (t, *J* = 6.3 Hz, 2H), 2.92 (t, *J* = 7.3 Hz, 2H), 2.76 (t, *J* = 7.4 Hz, 2H), 2.43 (t, *J* = 7.4 Hz, 2H), 1.63 (dt, *J* = 15.2, 7.5 Hz, 2H), 1.49 (dt, *J* = 13.3, 6.2 Hz, 2H), 0.89 (s, 9H), 0.04 (s, 6H). ^{13}C NMR (151 MHz, $CDCl_3$) δ 209.4, 149.9, 147.7, 136.7, 136.1, 123.5, 77.2, 62.9, 43.7, 42.9, 32.3, 26.9, 26.1, 20.4, 18.5. HRMS (ESI+) *m/z* calc'd for $C_{18}H_{32}NO_2Si$ $[M+H]^+$: 322.2124, found 322.2199 $[H^+]$ and 344.2004 $[Na^+]$. IR (ATR): 2953, 2929, 2857, 1715, 1255, 1099, 913, 836, 776, 745 cm^{-1}

Preparation of 7-hydroxy-1-(pyridin-3-yl)heptan-3-one (2.82)

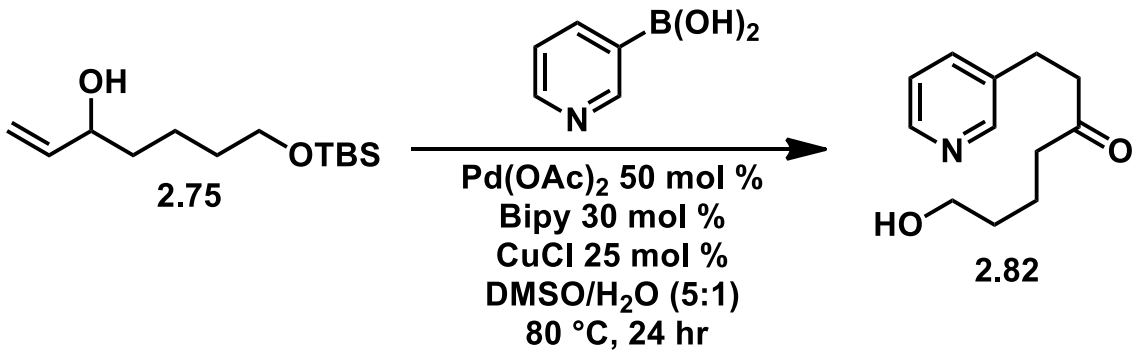

7-Hydroxy-1-(pyridin-3-yl)heptan-3-one (2.82). To a 4 mL vial was added 7-((*tert*-butyldimethylsilyl)oxy)hept-1-en-3-ol **2.75** (0.20 mmol, 50 mg), 3-pyridyl boronic acid (0.41 mmol, 50.3 mg), BiPy (0.06 mmol, 9.6 mg), CuCl (0.51 mmol, 4.6 mg), $Pd(OAc)_2$ (0.10 mmol, 22.9 mg) and 0.6 mL of DMSO/H_2O (5:1). The reaction was stirred open to air at 80 °C for 24 hr. After 24 h, the reaction was allowed to cool to rt. The reaction mixture was diluted with water (3 mL) and DCM (3 mL) and then filtered through celite.

The resulting mixture was extracted with DCM (3 x 5 ml). The organic phase was washed brine (3 x 5 mL). The combined organic layer was dried over Na_2SO_4, filtered, and then concentrated under reduced pressure to provide 7-hydroxy-1-(pyridin-3-yl)heptan-3-one **2.82** (15 mg, 35%) as a viscous yellow oil.

^{1}H NMR (600 MHz, $CDCl_3$) δ 8.46 (d, *J* = 10.3 Hz, 2H), 7.54 (d, *J* = 7.8 Hz, 1H), 7.23 (dd, *J* = 7.8, 4.7 Hz, 1H), 3.62 (t, *J* = 6.3 Hz, 2H), 2.92 (t, *J* = 7.4 Hz, 2H), 2.77 (t, *J* = 7.4 Hz, 2H), 2.46 (t, *J* = 7.2 Hz, 2H), 1.67 (p, *J* = 7.2 Hz, 3H), 1.57 – 1.50 (m, 3H). ^{13}C NMR (151 MHz, $CDCl_3$) δ 209.5, 149.7, 147.6, 136.7, 136.4, 123.6, 77.2, 62.4, 43.7, 42.7, 32.2, 26.9, 19.9. HRMS (ESI+) *m/z* calc'd for $C_{12}H_{18}NO_2$ $[M+H]^+$: 208.1261, found 208.1328 $[H^+]$ and 230.1139 [M+Na]. IR(ATR): 3400, 2936, 2869, 1709, 1578, 1480, 1425, 1375, 1046, 1030, 913, 801, 744, 714, 637, 616, 553, 540 cm^{-1}

Preparation of 4-bromobutyl 4-methylbenzenesulfonate (2.86)

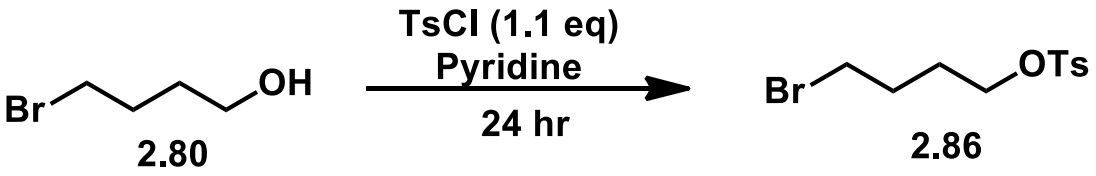

4-Bromobutyl 4-methylbenzenesulfonate (2.86). To a solution of 4-bromobutanol (1.0 g, 6.6 mmol) in pyridine (10 ml) cooled to 0° C, tosyl chloride (1.38 g, 7.24 mmol) was added. The resulting solution was kept under stirring for 20 min and then stored overnight at –18° C. The reaction mixture was poured in a water/ice mixture (about 50 mL) and extracted with ethyl ether (3 x 10 ml). The organic phase was washed with 3 M HCl (15 ml). The combined organic layer was dried over Na_2SO_4, filtered, and then concentrated

under reduced pressure to provide 4-bromobutyl 4-methylbenzenesulfonate **2.86** (1.27 g, 63%) as a viscous orange oil.

^{1}H NMR (300 MHz, $CDCl_3$) d 7.79 (d, 2H, J = 8.1 Hz), 7.36 (d, 2H, J = 8.1 Hz), 4.06 (t, 2H, J = 6.0 Hz), 3.37 (t, 2H, J = 6.0 Hz), 2.46 (s, 3H), 1.91 (m, 2H), 1.81 (m, 2H). ^{13}C NMR (151 MHz, $CDCl_3$) δ 145.0, 133.1, 130.1, 128.0, 77.2, 69.5, 32.8, 28.6, 27.6, 21.8. Spectral data matches literature references.[51]

Preparation of 4-bromobutyl methanesulfonate (2.88)

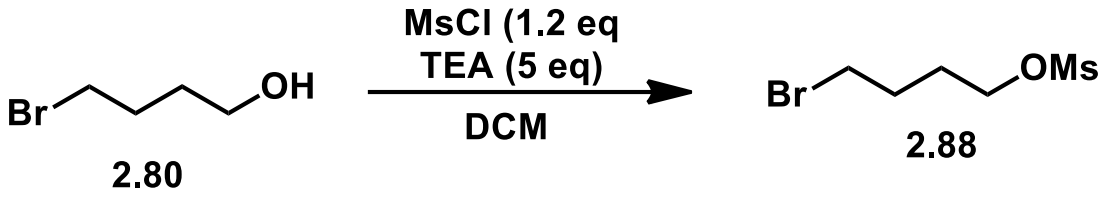

4-Bromobutyl methanesulfonate (2.88). To a stirred solution of 4-bromobutanol **2.80** (6.58 mmol, 1.0 g) and MsCl (7.90 mmol, 612 μL) in DCM (33 mL) at 0 °C, Et_3N (32.9 mmol, 4.6 mL) was added dropwise. After 1 h the reaction mixture was diluted with H_2O (10 mL) and extracted with DCM (3 × 5 mL). The combined organic layers were washed with H_2O (2 × 5 mL) and brine (2 × 5 mL). The combined organic layer was dried over Na_2SO_4, filtered, and then concentrated under reduced pressure to provide 4-bromobutyl methanesulfonate **2.88** (1.31g, 87%) as a viscous yellow oil.

^{1}H NMR (600 MHz, Chloroform-*d*) δ 4.29 (t, *J* = 6.1 Hz, 2H), 3.46 (t, *J* = 6.3 Hz, 2H), 2.06 – 1.98 (m, 2H), 1.97 – 1.92 (m, 2H). ^{13}C NMR (151 MHz, $CDCl_3$) δ 68.9, 37.6, 32.8, 28.7, 27.9. HRMS (ESI+) *m/z* calc'd for $C_5H_{12}BrO_3S$ $[M+H]^+$: 230.9606, found 247.9945

[H^+] and 247.9945 [M + NH_4]. (ESI+) *m/z* calc'd for $C_{12}H_{18}NO_2$ [M+H]$^+$: 208.1261, found 208.1328 [H^+] and 230.1139 [M+Na]. IR(ATR): 1346, 1249, 1168, 971, 924, 835, 795, 765, 720, 746 cm^{-1}.

Preparation of 5-hydroxyhept-6-en-1-yl 4-methylbenzenesulfonate (2.97)

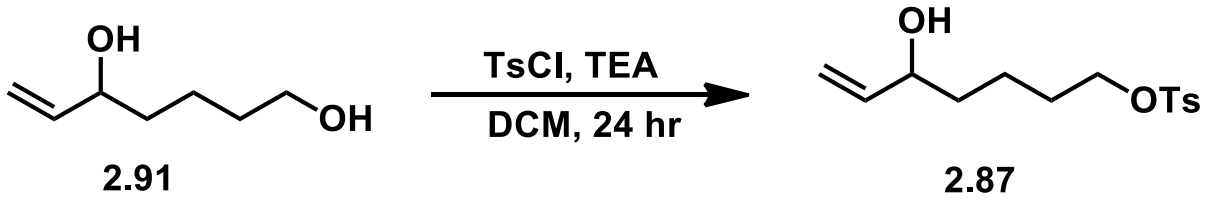

2.91 2.87

5-Hydroxyhept-6-en-1-yl 4-methylbenzenesulfonate (2.87). To a solution of hept-6-ene-1,5-diol **2.91**(3.8 mmol, 500 mg) in DCM (35 mL) at 0 ºC was added Et_3N (7.7 mmol, 1.1 mL) and TsCl (3.84 mmol, 732 mg). The solution was slowly warmed to rt and allowed to stir overnight (16 h). The reaction was quenched with saturated $NaHCO_3$ (10 mL) and extracted with DCM (3 x 10 mL). The combined organic layer was dried over Na_2SO_4, filtered, and then concentrated under reduced pressure. Purification by flash chromatography (1:1 hexanes/EtOAc) provided 5-hydroxyhept-6-en-1-yl 4-methylbenzenesulfonate **2.87** (585 mg, 53%) as a viscous orange oil.

^{1}H NMR (600 MHz, $CDCl_3$) δ 7.80 (d, *J* = 8.3 Hz, 2H), 7.35 (d, *J* = 8.1 Hz, 2H), 5.82 (ddd, *J* = 16.9, 10.4, 6.3 Hz, 1H), 5.21 (d, *J* = 17.2 Hz, 1H), 5.11 (d, *J* = 10.4 Hz, 1H), 4.04 (dt, *J* = 12.9, 6.2 Hz, 3H), 2.46 (s, 3H), 1.69 (p, *J* = 8.3 Hz, 2H), 1.52 – 1.32 (m, 4H). ^{13}C NMR (151 MHz, $CDCl_3$) δ 144.9, 141.0, 133.3, 130.0, 128.0, 115.1, 77.2, 73.0, 70.5, 36.2, 28.9, 21.8, 21.4. Spectral data matches literature references.[50]

Preparation of 5-hydroxyhept-6-en-1-yl 4-methylbenzenesulfonate (2.87).

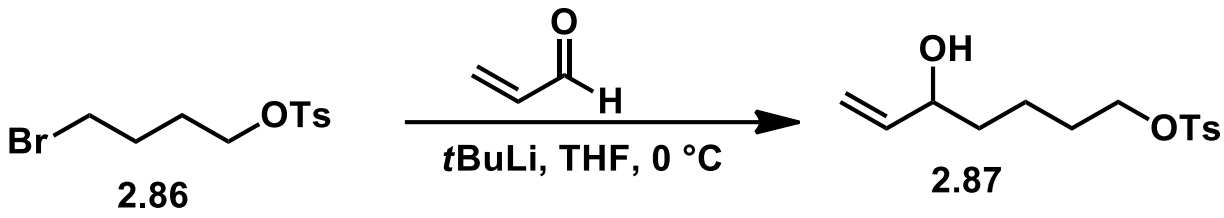

5-Hydroxyhept-6-en-1-yl 4-methylbenzenesulfonate (2.87). To a flame dried two-neck round-bottomed flask equipped with a stir bar was added 4-bromobutyl 4-methylbenzenesulfonate **2.86** (1.63 mmol, 500 mg) and 10.5 mL of THF. The round-bottomed flask was then cooled to –78 ℃ with an acetone and dry-ice bath. Once the reaction was cooled to –78 ℃, *t*-Buli (1.7 M in hexanes, 1.6 mL, 3.4 mmol) was added to the reaction drop-wise. The reaction mixture was then allowed to stir for 15 min at –78 ℃. After 15 min, acrolein (131 μl, 1.96 mmol) was added as a solution in 1 mL of THF dropwise. The reaction was allowed to stir at –78 ℃ for 60 min. After 60 min, the reaction mixture was quenched with saturated $NaHCO_3$ solution (10 mL) and water (10 mL). The quenched reaction mixture was extracted with Et_2O (3 x 15 mL). The organic layer was washed with brine (3 x 5 mL) and dried over Na_2SO_4 and then filtered and then concentrated under reduced pressure. The crude mixture was purified by silica gel flash chromatography eluting with 4:1 hexanes /EtOAc to provide 7-((*tert*-5-hydroxyhept-6-en-1-yl 4-methylbenzenesulfonate **2.87** (232 mg, 50%) as an orange oil.

^{1}H NMR (600 MHz, $CDCl_3$) δ 7.80 (d, *J* = 8.3 Hz, 2H), 7.35 (d, *J* = 8.1 Hz, 2H), 5.82 (ddd, *J* = 16.9, 10.4, 6.3 Hz, 1H), 5.21 (d, *J* = 17.2 Hz, 1H), 5.11 (d, *J* = 10.4 Hz, 1H), 4.04 (dt, *J* = 12.9, 6.2 Hz, 3H), 2.46 (s, 3H), 1.69 (p, *J* = 8.3 Hz, 2H), 1.52 – 1.32 (m, 4H). ^{13}C NMR

(151 MHz, $CDCl_3$) δ 144.9, 141.0, 133.3, 130.0, 128.0, 115.1, 77.2, 73.0, 70.5, 36.2, 28.9, 21.8, 21.4. Spectral data matches literature references.[50]

Preparation of 5-oxo-7-(pyridin-3-yl)heptyl 4-methylbenzenesulfonate (2.83)

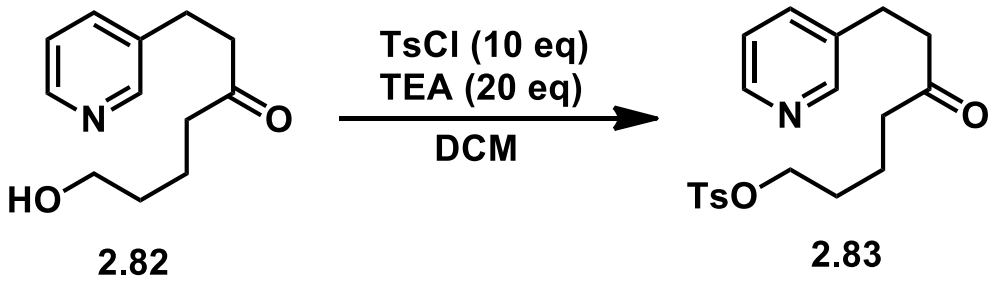

2.82 2.83

5-Oxo-7-(pyridin-3-yl)heptyl 4-methylbenzenesulfonate (2.83). To a solution of 7-hydroxy-1-(pyridin-3-yl)heptan-3-one **2.82** (0.16 mmol, 33 mg) in DCM (3 mL) at 0 ºC was added Et_3N (6.37 mmol, 888 μL) and TsCl (3.18 mmol, 607 mg). The solution was slowly warmed to rt and allowed to stir overnight (16 h). The reaction was quenched with saturated $NaHCO_3$ solution (10 mL) and extracted with DCM (3 x 10 mL). The combined organic layer was dried over Na_2SO_4, filtered, and then concentrated under reduced pressure. Purification by preparative TLC in 1:1 hexanes/acetone provided 5-oxo-7-(pyridin-3-yl)heptyl 4-methylbenzenesulfonate **2.83** (272 mg, 50%)

^{1}H NMR (600 MHz, $CDCl_3$) δ 8.48 (s, 2H), 7.79 (t, *J* = 8.1 Hz, 2H), 7.58 (d, *J* = 7.8 Hz, 2H), 7.35 (t, *J* = 8.0 Hz, 3H), 7.26 (m, 1H) 4.01 (t, *J* = 5.7 Hz, 2H), 2.91 (t, *J* = 7.4 Hz, 2H), 2.74 (t, *J* = 7.4 Hz, 2H), 2.46 (s, 2H), 2.40 (t, *J* = 6.6 Hz, 3H), 1.65 – 1.60 (m, 2H), 0.89 (t, *J* = 6.9 Hz, 4H). HRMS (ESI+) *m/z* calc'd $C_{19}H_{24}NO_4S$ $[M+H]^+$: 362.1335, found

362.1409 [H^+]. ^{13}C NMR (151 MHz, $CDCl_3$) δ 208.4, 130.0, 128.0, 77.2, 70.2, 43.6, 29.8, 26.8, 21.8, 19.7, 14.3. HRMS (ESI+) m/z calc'd for C19H24NO4S $[M + H]^+$: 362.1348, found 362.1409 [H+]. IR (ATR): 2924, 2853, 1713, 1357, 1188, 1176, 1098, 913, 815, 742, 665, 555, 536 cm^{-1}

Preparation of 7-((*tert*-butyldimethylsilyl)oxy)-1-(pyridine-3-yl)heptan-3-one (2.81)

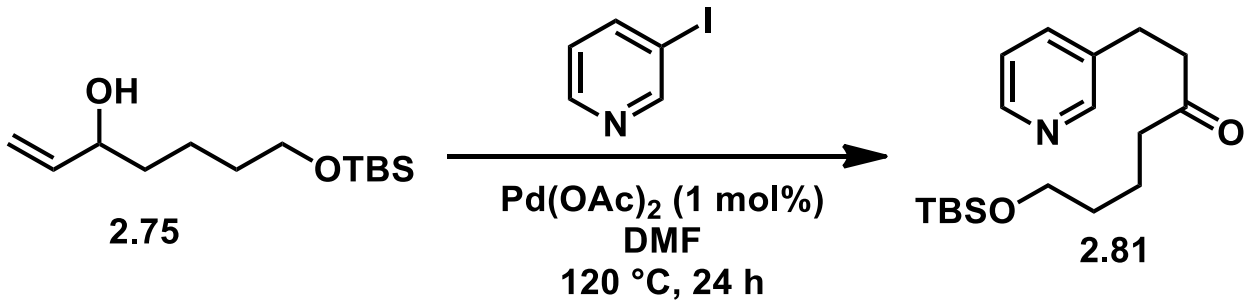

7-((*tert*-Butyldimethylsilyl)oxy)-1-(pyridine-3-yl)heptan-3-one (2.81). To a 4 mL vial equipped with a stir bar was added 3-iodopyridine (0.49 mmol, 100mg), 7-((*tert*-butyldimethylsilyl)oxy)hept-1-en-3-ol **2.75** (0.73 mmol, 179 mg), $Pd(OAc)_2$ (0.01 mmol, 1.1 mg), $NaHCO_3$ (0.88 mmol, 73.8 mg), and 1 mL of DMF. The reaction mixture was stirred at 120 °C for 24 h under nitrogen. After 24 h, the reaction mixture was allowed to cool to rt. The reaction mixture was poured into water (3 mL) and extracted with Et_2O (3 x 8 mL) and the organic phase was washed with brine (3 x 5 mL). The combined organic layer was dried over Na_2SO_4, filtered, and then concentrated under reduced pressure. The crude mixture was purified by silica gel flash chromatography eluting with 1:1 hexanes/acetone to provide to provide 7-((*tert*-butyldimethylsilyl)oxy)-1-(pyridine-3-yl)heptan-3-one **2.81** (68 mg, 43%) as a viscous yellow oil.

^{1}H NMR (600 MHz, $CDCl_3$) δ 8.51 – 8.40 (m, 2H), 7.57 (d, *J* = 7.5 Hz, 1H), 7.25 (dd, *J* = 7.7, 4.8 Hz, 1H), 3.60 (t, *J* = 6.3 Hz, 2H), 2.92 (t, *J* = 7.3 Hz, 2H), 2.76 (t, *J* = 7.4 Hz, 2H), 2.43 (t, *J* = 7.4 Hz, 2H), 1.63 (dt, *J* = 15.2, 7.5 Hz, 2H), 1.49 (dt, *J* = 13.3, 6.2 Hz, 2H), 0.89 (s, 9H), 0.04 (s, 6H). ^{13}C NMR (151 MHz, $CDCl_3$) δ 209.4, 149.9, 147.7, 136.7, 136.1, 123.5, 77.2, 62.9, 43.7, 42.9, 32.3, 26.9, 26.1, 20.4, 18.5. HRMS (ESI+) *m/z* calc'd for $C_{18}H_{32}NO_2Si$ $[M+H]^+$: 322.2124, found 322.2199 $[H^+]$ and 344.2004 $[Na^+]$. IR (ATR): 2953, 2929, 2857, 1715, 1255, 1099, 913, 836, 776, 745 cm^{-1}

Preparation of 7-hydroxy-1-(pyridin-3-yl)heptan-3-one (2.82)

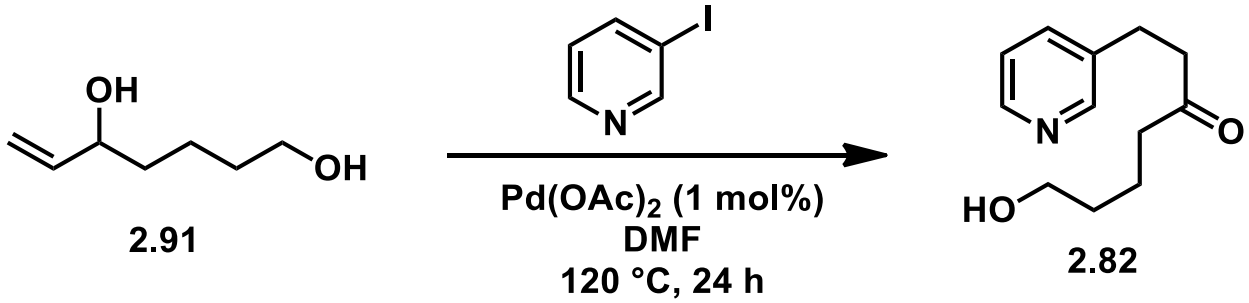

7-Hydroxy-1-(pyridin-3-yl)heptan-3-one (2.82). To a 4 mL vial equipped with a stir bar was added 3-iodopyridine (0.98 mmol, 200 mg), hept-6-ene-1,5-diol **2.91** (1.46 mmol, 191 mg), $Pd(OAc)_2$ (0.01 mmol, 2.2 mg), $NaHCO_3$ (1.76 mmol, 148 mg), and 1 mL of DMF. The reaction mixture was stirred at 120 °C for 24 h under nitrogen. After 24 h, the reaction was allowed to cool to rt. The reaction mixture was poured into water (3 mL) and extracted with Et_2O (3 x 8 mL) and the organic phase was washed with brine (3 x 5 mL). The combined organic layer was dried over Na_2SO_4, filtered, and then concentrated under reduced pressure. The crude mixture was purified by silica gel flash chromatography

eluting with 1:1 hexanes/acetone to provide 7-hydroxy-1-(pyridin-3-yl)heptan-3-one **2.82** (91 mg, 45%) as a viscous yellow oil.

^{1}H NMR (600 MHz, $CDCl_3$) δ 8.46 (d, *J* = 10.3 Hz, 2H), 7.54 (d, *J* = 7.8 Hz, 1H), 7.23 (dd, *J* = 7.8, 4.7 Hz, 1H), 3.62 (t, *J* = 6.3 Hz, 2H), 2.92 (t, *J* = 7.4 Hz, 2H), 2.77 (t, *J* = 7.4 Hz, 2H), 2.46 (t, *J* = 7.2 Hz, 2H), 1.67 (p, *J* = 7.2 Hz, 3H), 1.57 – 1.50 (m, 3H). ^{13}C NMR (151 MHz, $CDCl_3$) δ 209.5, 149.7, 147.6, 136.7, 136.4, 123.6, 77.2, 62.4, 43.7, 42.7, 32.2, 26.9, 19.9. HRMS (ESI+) *m/z* calc'd for $C_{12}H_{18}NO_2$ $[M+H]^+$: 208.1261, found 208.1334 $[H^+]$ and 230.1139 [M+Na]. IR(ATR): 3400, 2936, 2869, 1709, 1578, 1480, 1425, 1375, 1046, 1030, 913, 801, 744, 714, 637, 616, 553, 540 cm^{-1}.

Preparation of 7-hydroxy-1-(pyridin-3-yl)heptan-3-one (2.82)

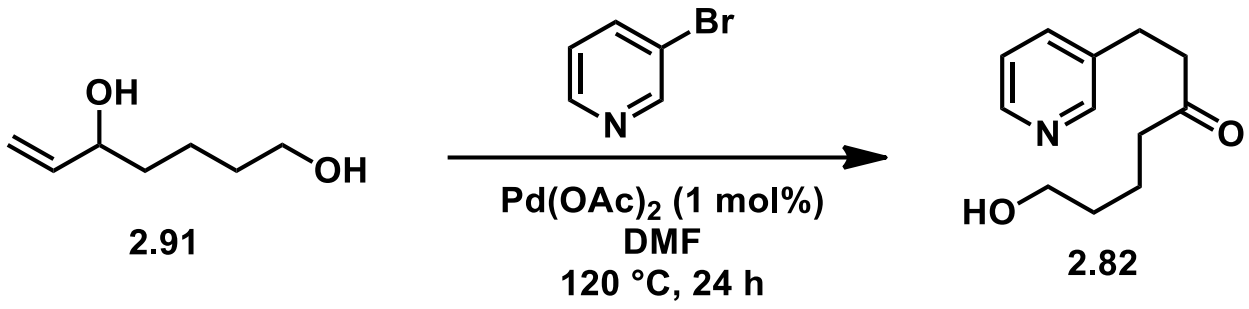

7-Hydroxy-1-(pyridin-3-yl)heptan-3-one (2.82). To a 4 mL vial equipped with a stir bar was added 3-iodopyridine (0.98 mmol, 200 mg), hept-6-ene-1,5-diol **2.91** (2.18 mmol, 284.3 mg), $Pd(OAc)_2$ (0.01 mmol, 3.3 mg), $NaHCO_3$ (1.75 mmol, 146.8 mg), and 1 mL of DMF. The reaction mixture was stirred at 120 °C for 24 h under nitrogen. After 24 h, the reaction mixture was allowed to cool to rt. The reaction mixture was poured into water (3

mL) and extracted with Et_2O (3 x 8 mL) and the organic phase was washed with brine (3 x 5 mL). The combined organic layer was dried over Na_2SO_4, filtered, and then concentrated under reduced pressure. The crude mixture was purified by silica gel flash chromatography eluting with 1:1 hexanes/acetone to provide 7-hydroxy-1-(pyridin-3-yl)heptan-3-one **2.82** (177 mg, 59%) as a viscous yellow oil.

^{1}H NMR (600 MHz, $CDCl_3$) δ 8.46 (d, *J* = 10.3 Hz, 2H), 7.54 (d, *J* = 7.8 Hz, 1H), 7.23 (dd, *J* = 7.8, 4.7 Hz, 1H), 3.62 (t, *J* = 6.3 Hz, 2H), 2.92 (t, *J* = 7.4 Hz, 2H), 2.77 (t, *J* = 7.4 Hz, 2H), 2.46 (t, *J* = 7.2 Hz, 2H), 1.67 (p, *J* = 7.2 Hz, 3H), 1.57 – 1.50 (m, 3H). ^{13}C NMR (151 MHz, $CDCl_3$) δ 209.5, 149.7, 147.6, 136.7, 136.4, 123.6, 77.2, 62.4, 43.7, 42.7, 32.2, 26.9, 19.9. HRMS (ESI+) *m/z* calc'd for $C_{12}H_{18}NO_2$ $[M+H]^+$: 208.1261, found 208.1334 $[H^+]$ and 230.1139 [M+Na]. IR (film): 3400, 2936, 2869, 1709, 1578, 1480, 1425, 1375, 1046, 1030, 913, 801, 744, 714, 637, 616, 553, 540 cm^{-1}.

2.6 NMR Spectra

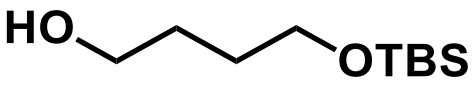

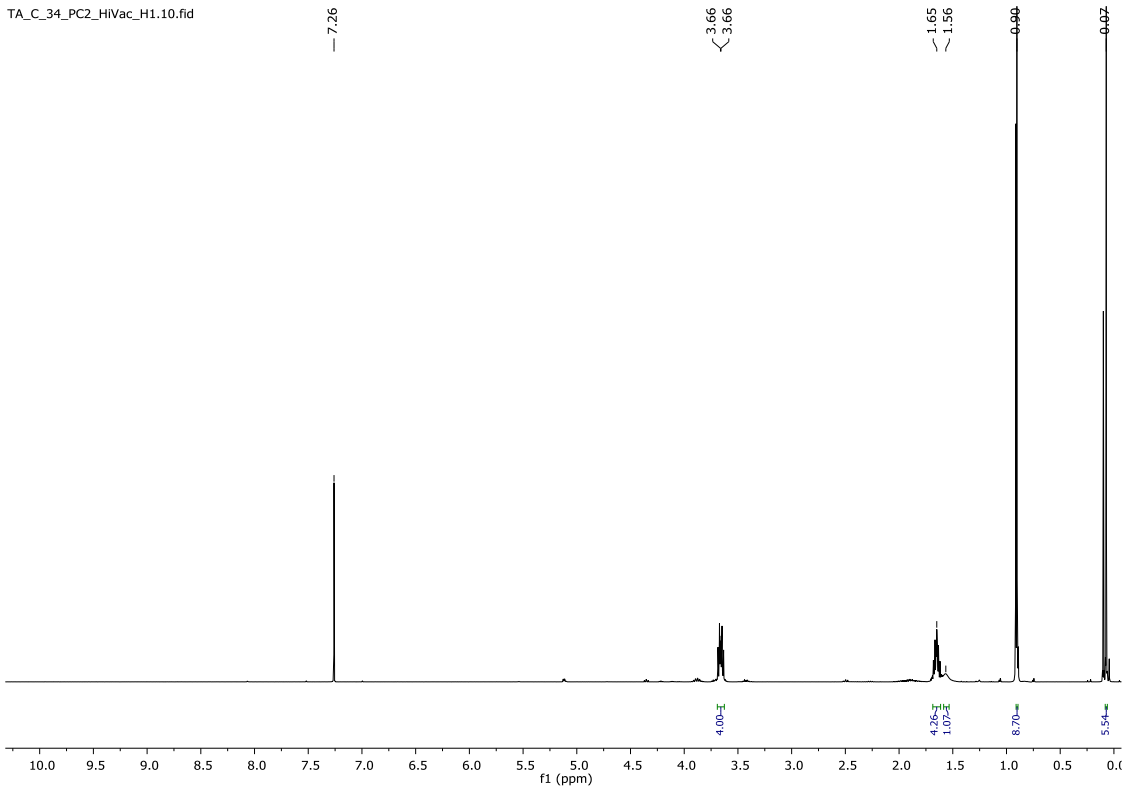

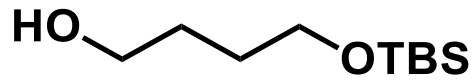
HO
OTBS

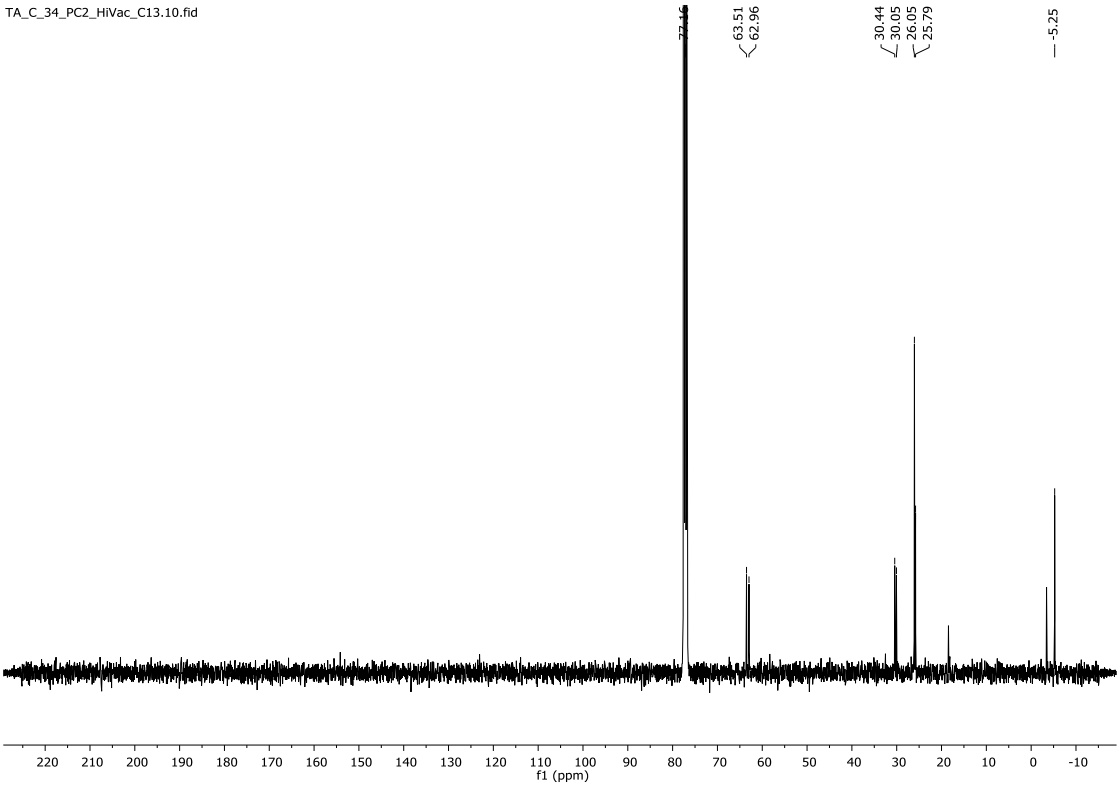
TA_C_34_PC2_HiVac_C13.10.fid
63.51
62.96
30.44
30.05
26.05
25.79
-5.25
220 210 200 190 180 170 160 150 140 130 120 110 100 90 80 70 60 50 40 30 20 10 0 -10
f1 (ppm)

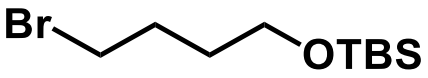
Br
OTBS

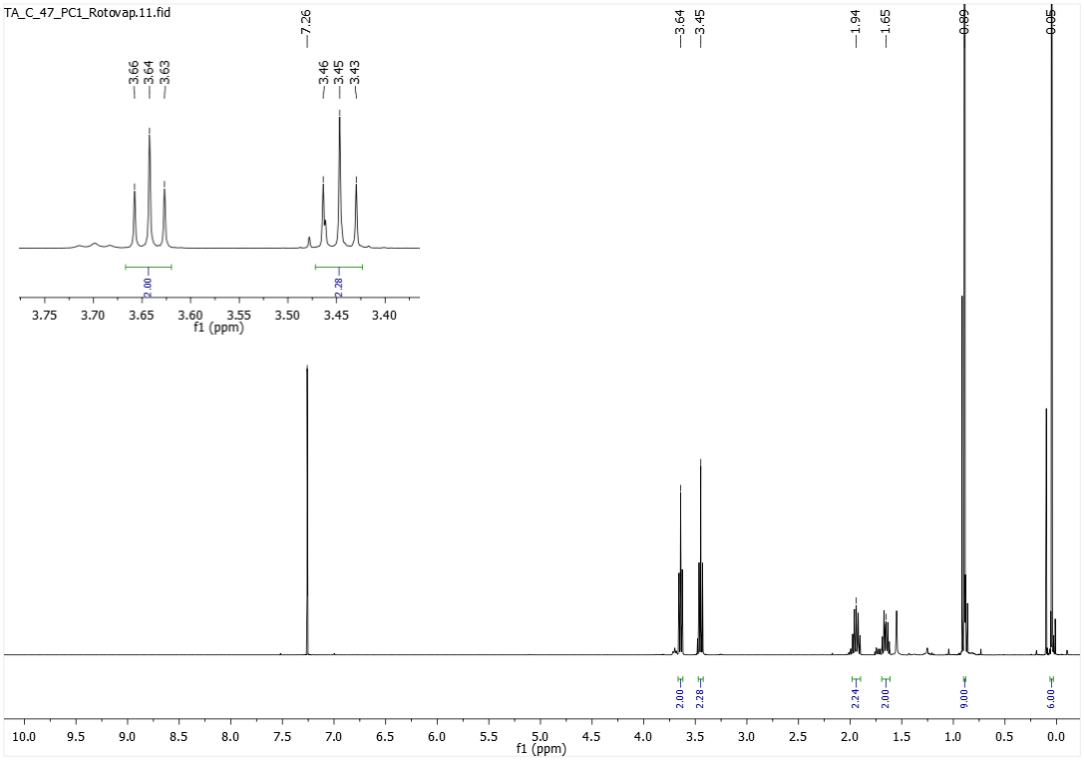
TA_C_47_PC1_Rotovap.11.fid
7.26
3.66
3.64
3.63
3.46
3.45
3.43
3.64
3.45
1.94
1.65
0.89
0.05
2.00
2.28
3.75 3.70 3.65 3.60 3.55 3.50 3.45 3.40
f1 (ppm)
2.00
2.28
2.24
2.00
9.00
6.00
10.0 9.5 9.0 8.5 8.0 7.5 7.0 6.5 6.0 5.5 5.0 4.5 4.0 3.5 3.0 2.5 2.0 1.5 1.0 0.5 0.0
f1 (ppm)

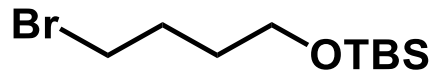
Br
OTBS

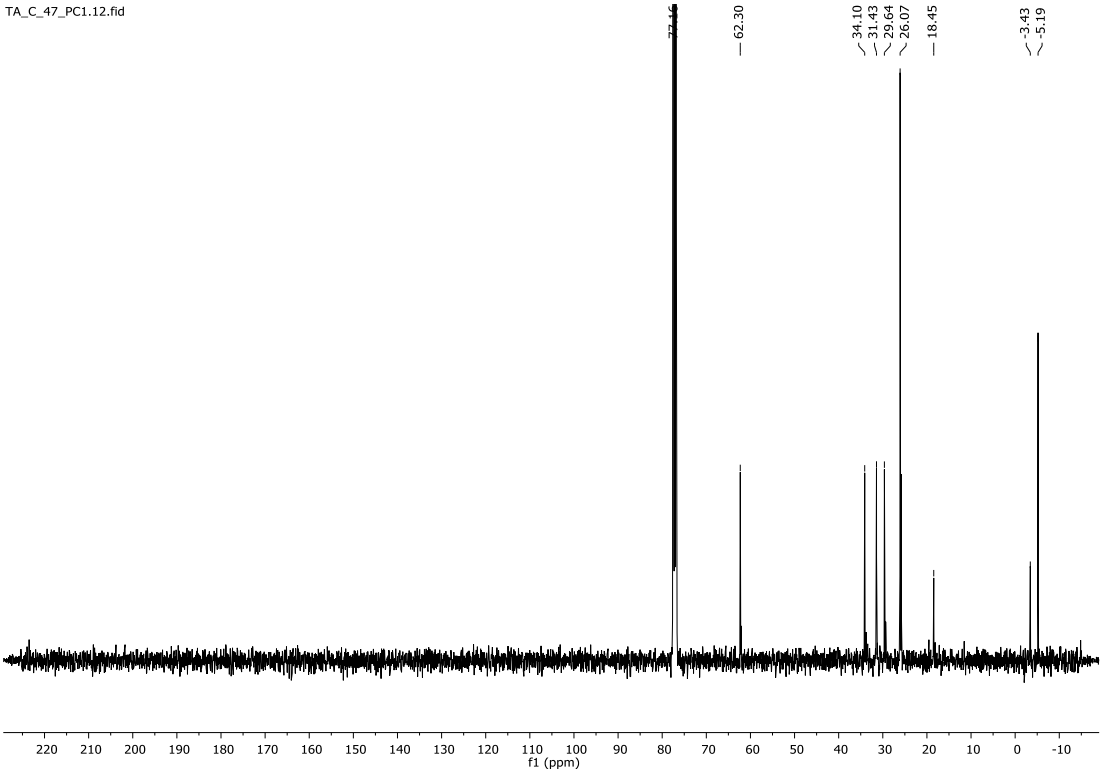
TA_C_47_PC1.12.fid
62.30
34.10
31.43
29.64
26.07
18.45
-3.43
-5.19
220 210 200 190 180 170 160 150 140 130 120 110 100 90 80 70 60 50 40 30 20 10 0 -10
f1 (ppm)

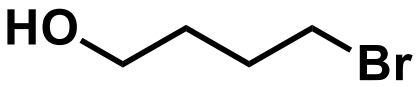
HO
Br

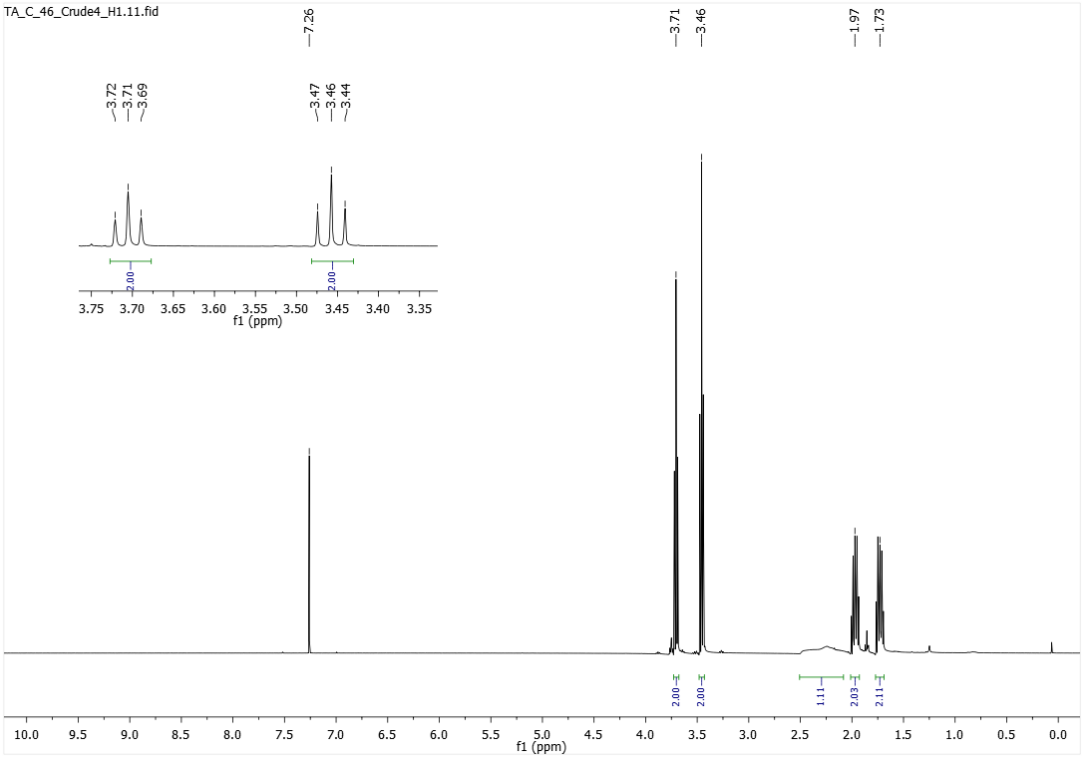
TA_C_46_Crude4_H1.11.fid
7.26
3.71
3.46
1.97
1.73
3.72
3.71
3.69
3.47
3.46
3.44
2.00
2.00
3.75 3.70 3.65 3.60 3.55 3.50 3.45 3.40 3.35
f1 (ppm)
2.00
2.00
1.11
2.03
2.11
10.0 9.5 9.0 8.5 8.0 7.5 7.0 6.5 6.0 5.5 5.0 4.5 4.0 3.5 3.0 2.5 2.0 1.5 1.0 0.5 0.0
f1 (ppm)

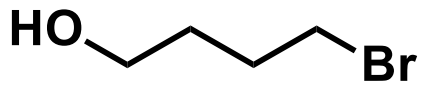
HO
Br

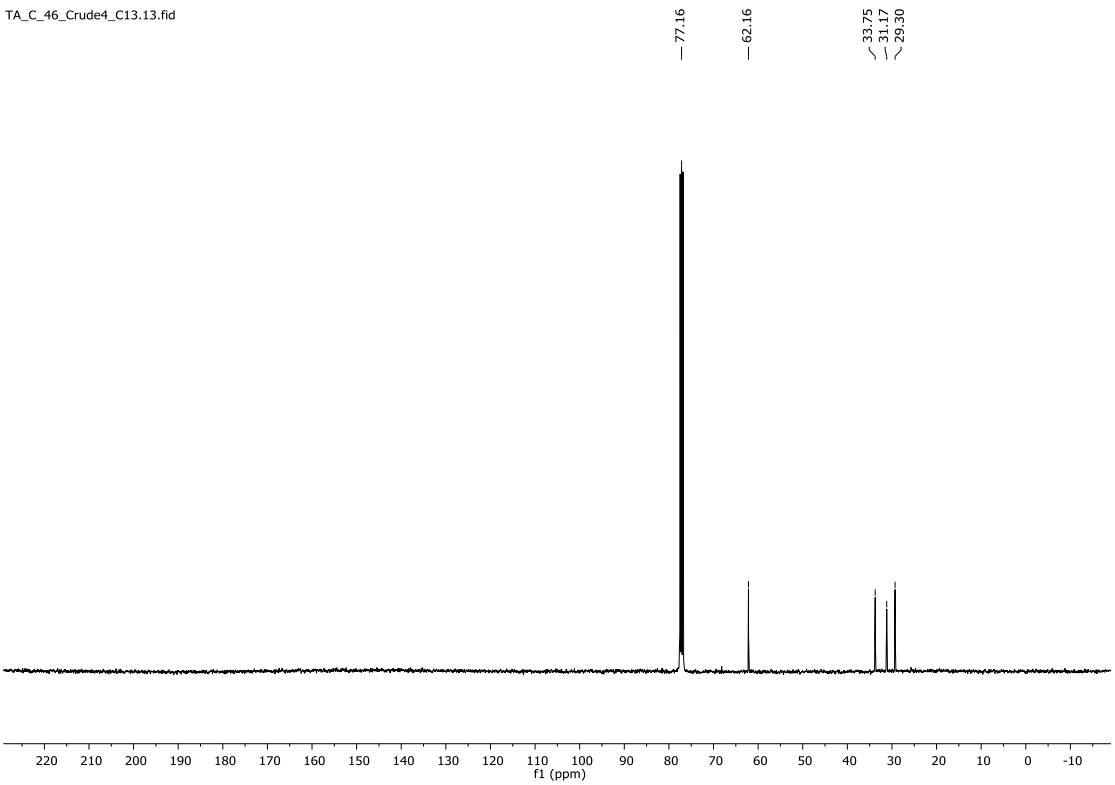
TA_C_46_Crude4_C13.13.fid
77.16
62.16
33.75
31.17
29.30
220 210 200 190 180 170 160 150 140 130 120 110 100 90 80 70 60 50 40 30 20 10 0 -10
f1 (ppm)

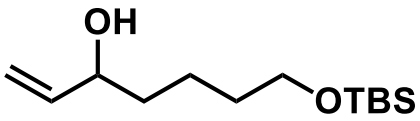
OH
OTBS

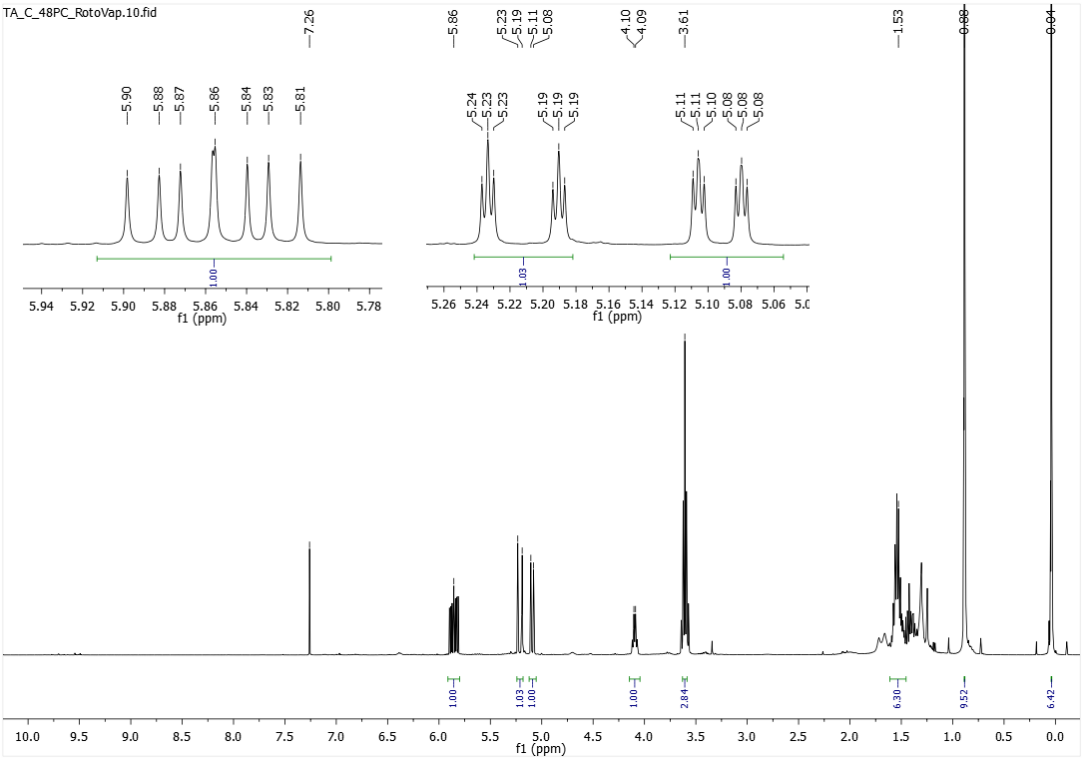
TA_C_48PC_RotoVap.10.fid
f1 (ppm)

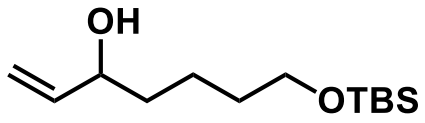
OH
OTBS

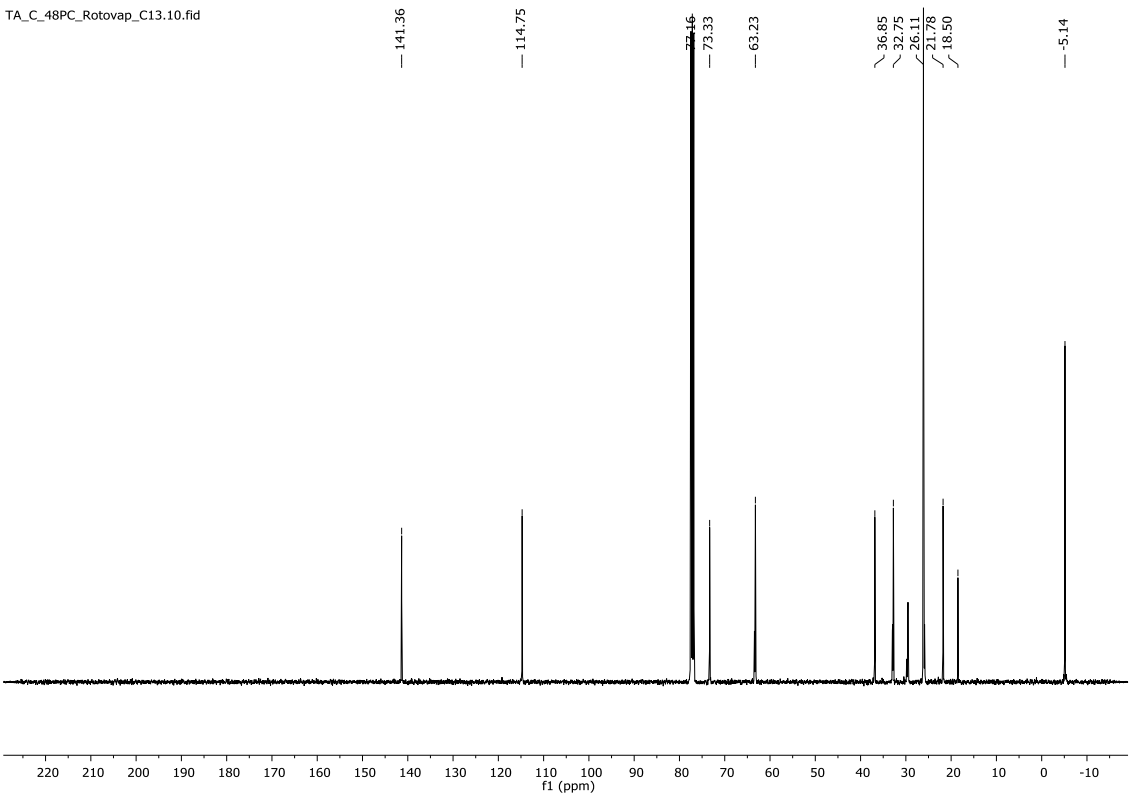
TA_C_48PC_Rotovap_C13.10.fid
141.36
114.75
77.16
73.33
63.23
36.85
32.75
26.11
21.78
18.50
-5.14
220 210 200 190 180 170 160 150 140 130 120 110 100 90 80 70 60 50 40 30 20 10 0 -10
f1 (ppm)

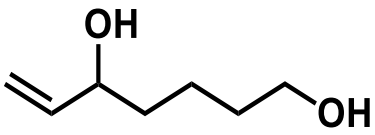
OH
OH

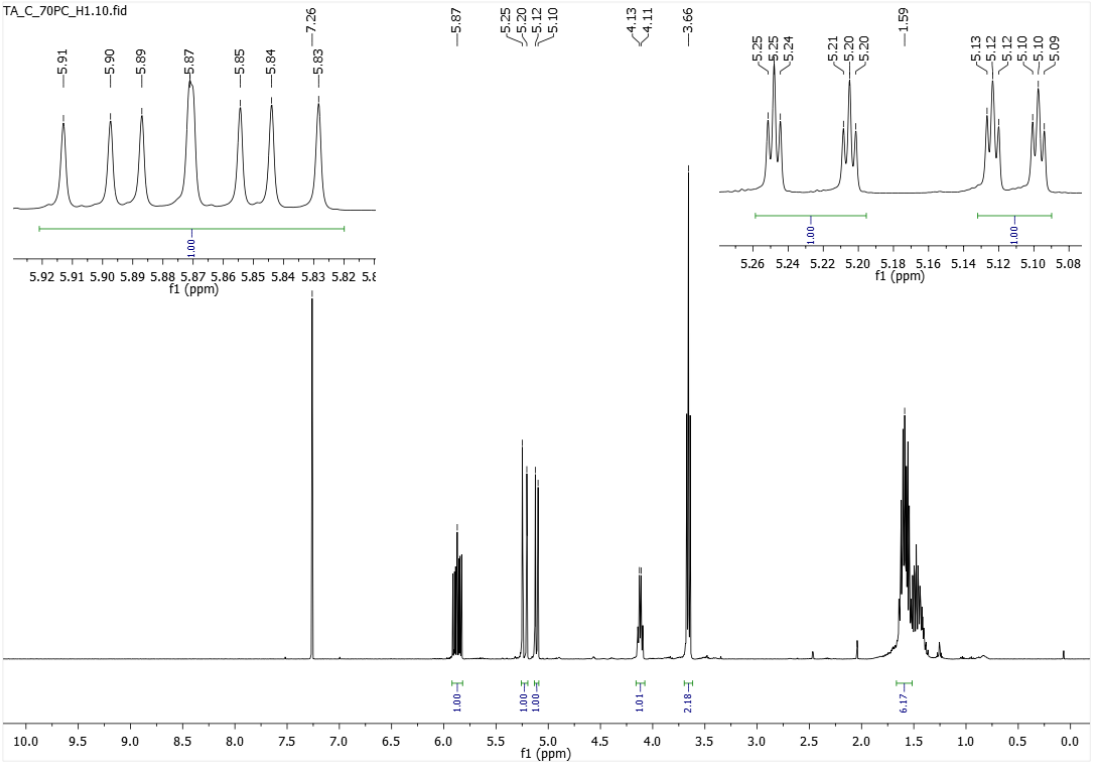
TA_C_70PC_H1.10.fid
f1 (ppm)

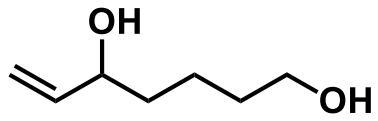
OH
OH

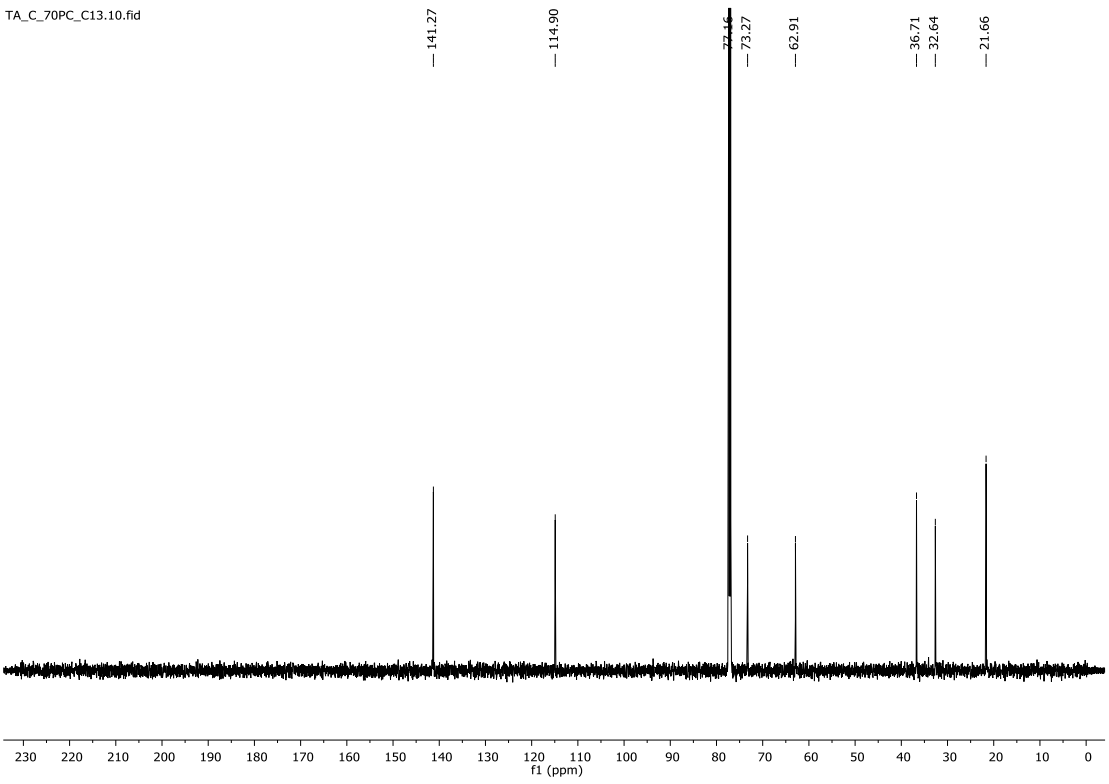
TA_C_70PC_C13.10.fid
141.27
114.90
77.16
73.27
62.91
36.71
32.64
21.66
230 220 210 200 190 180 170 160 150 140 130 120 110 100 90 80 70 60 50 40 30 20 10 0
f1 (ppm)

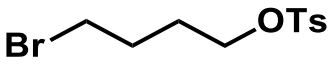
Br
OTs

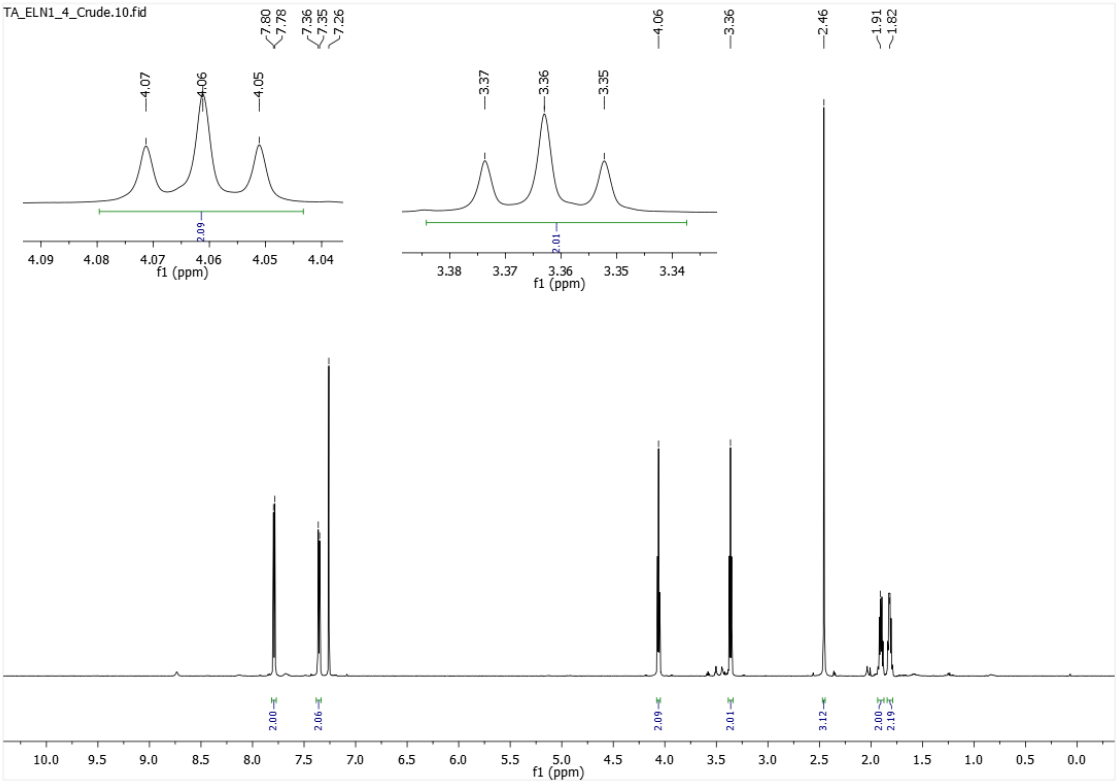
TA_ELN1_4_Crude.10.fid
7.80
7.78
7.36
7.35
7.26
4.06
3.36
2.46
1.91
1.82
4.07
4.06
4.05
3.37
3.36
3.35
2.09
2.01
f1 (ppm)
2.00
2.06
2.09
2.01
3.12
2.00
2.19

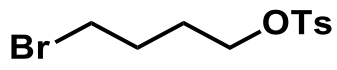
Br
OTs

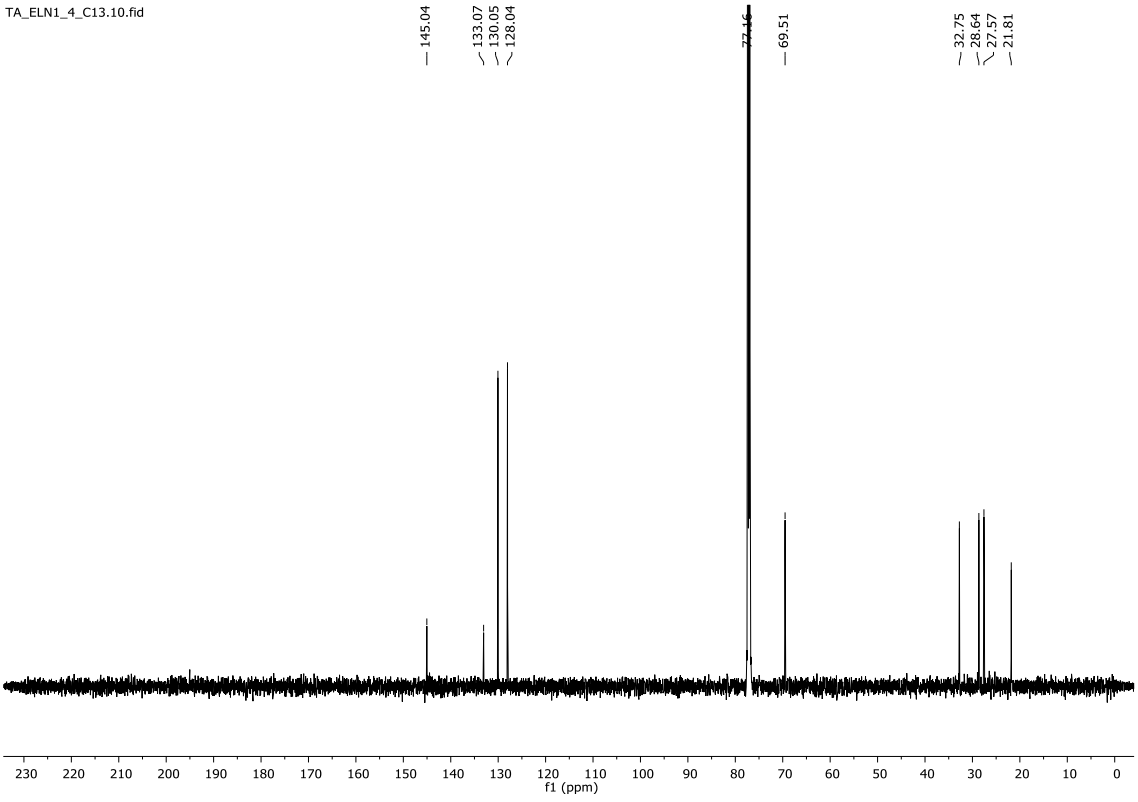
TA_ELN1_4_C13.10.fid
145.04
133.07
130.05
128.04
77.16
69.51
32.75
28.64
27.57
21.81
230 220 210 200 190 180 170 160 150 140 130 120 110 100 90 80 70 60 50 40 30 20 10 0
f1 (ppm)

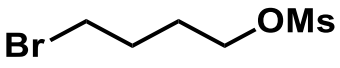
Br
OMs

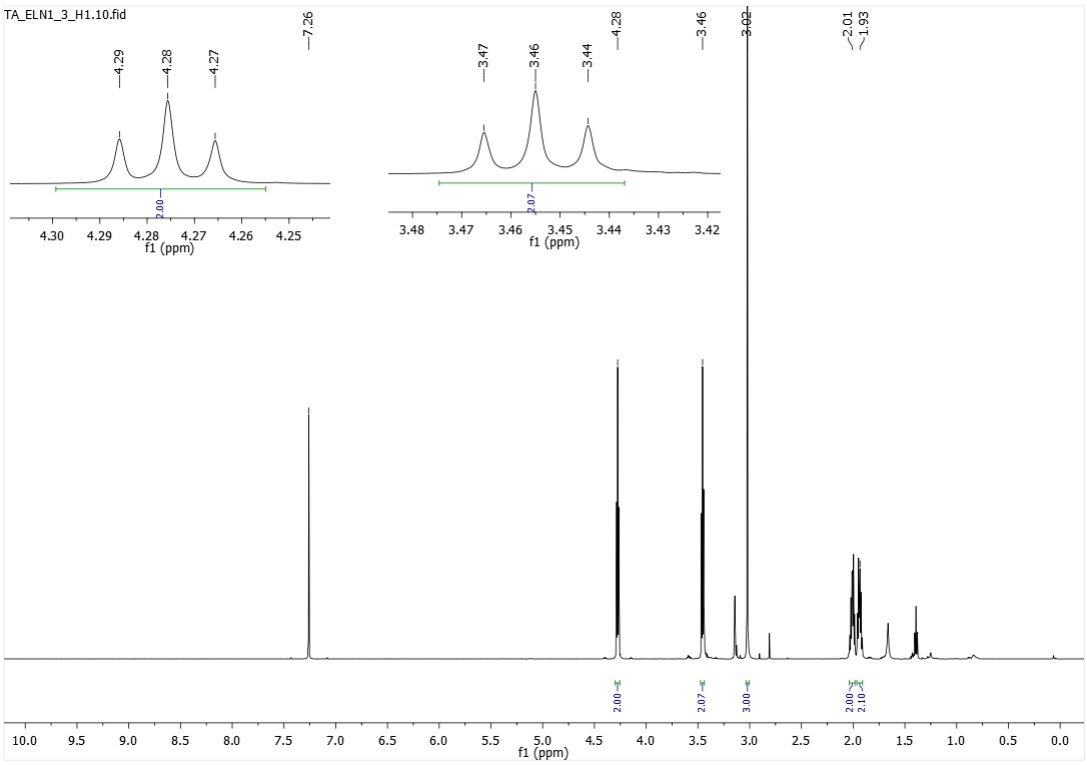
TA_ELN1_3_H1.10.fid
7.26
4.29
4.28
4.27
3.47
3.46
3.44
4.28
3.46
3.02
2.01
1.93
2.00
2.07
f1 (ppm)
2.00
2.07
3.00
2.00
2.10
f1 (ppm)

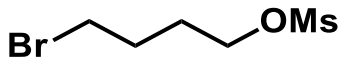
Br
OMs

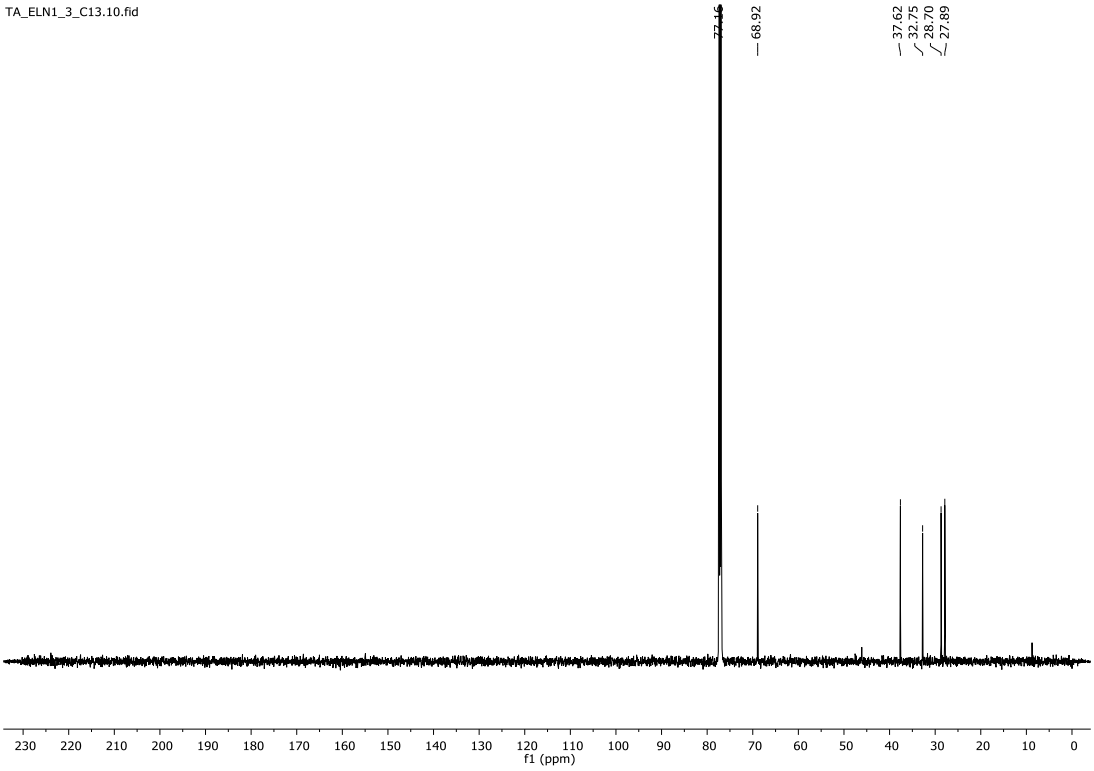
TA_ELN1_3_C13.10.fid
77.46
68.92
37.62
32.75
28.70
27.89
230 220 210 200 190 180 170 160 150 140 130 120 110 100 90 80 70 60 50 40 30 20 10 0
f1 (ppm)

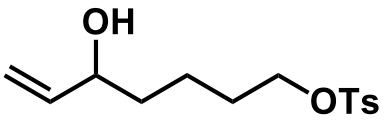
OH
OTs

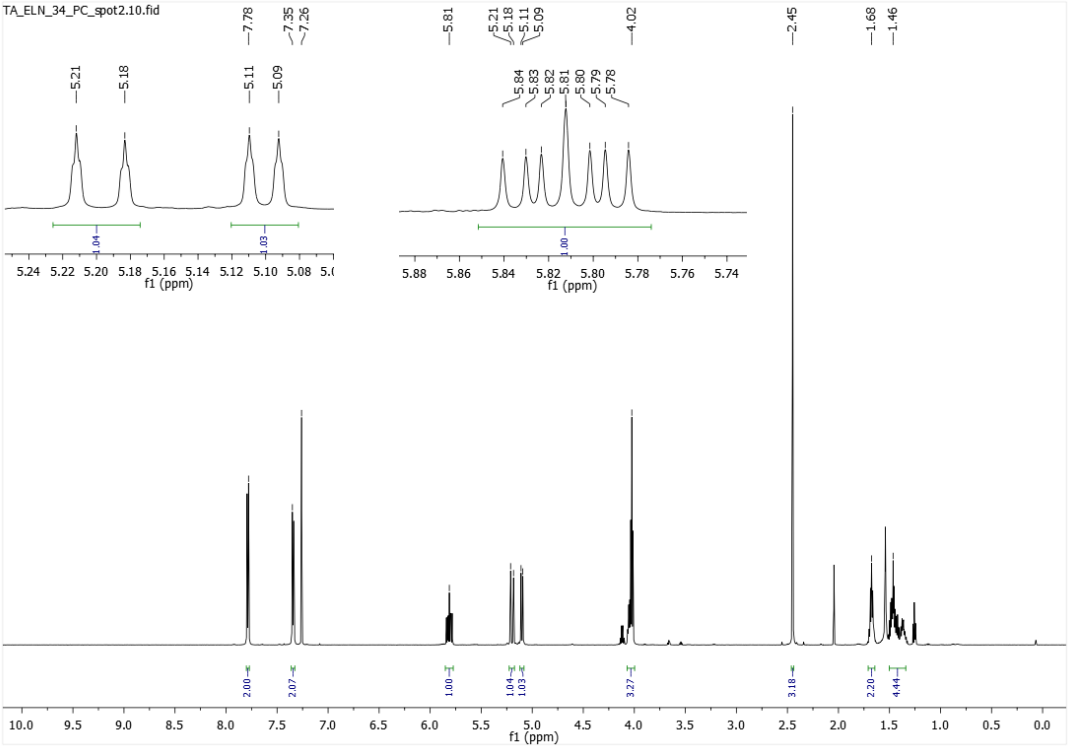
TA_ELN_34_PC_spot2.10.fid
7.78
7.35
7.26
5.81
5.21
5.18
5.11
5.09
4.02
2.45
1.68
1.46
5.84
5.83
5.82
5.81
5.80
5.79
5.78
f1 (ppm)
f1 (ppm)
f1 (ppm)

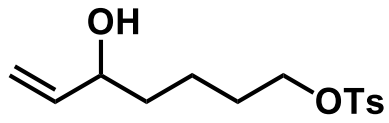
OH
OTs

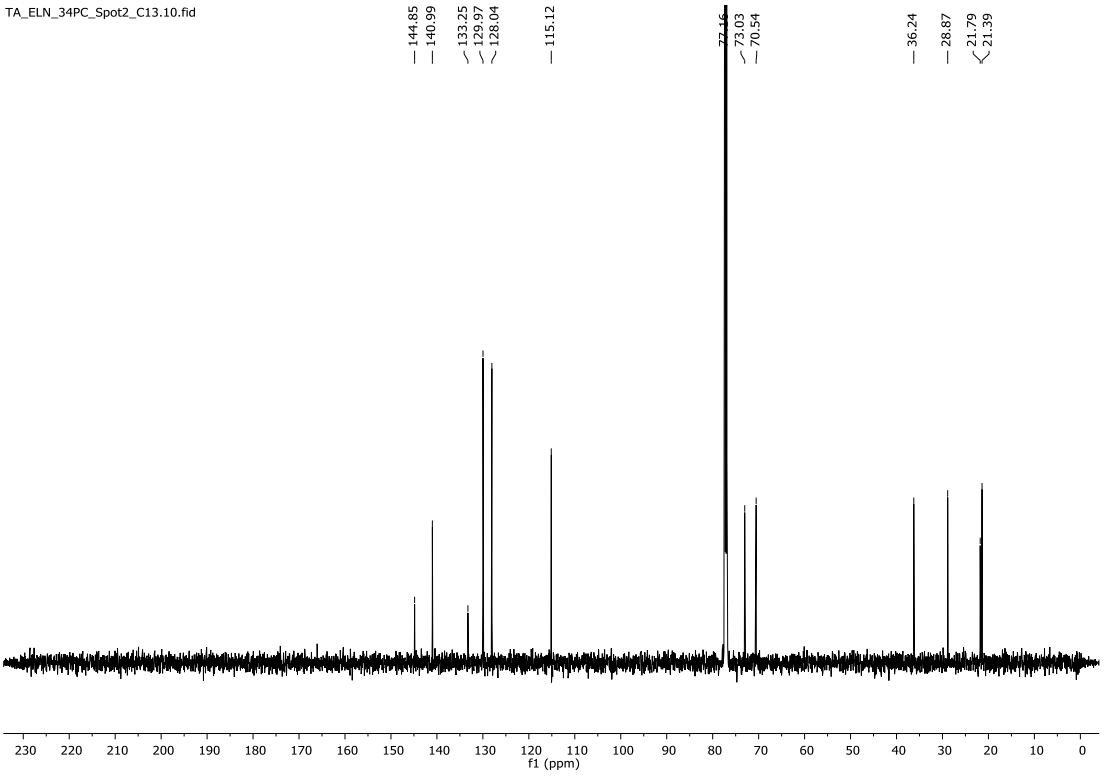
TA_ELN_34PC_Spot2_C13.10.fid
144.85
140.99
133.25
129.97
128.04
115.12
77.16
73.03
70.54
36.24
28.87
21.79
21.39
230 220 210 200 190 180 170 160 150 140 130 120 110 100 90 80 70 60 50 40 30 20 10 0
f1 (ppm)

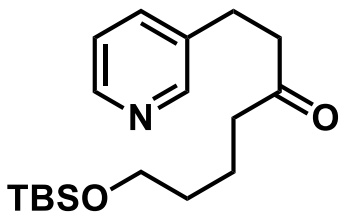
N
O
TBSO

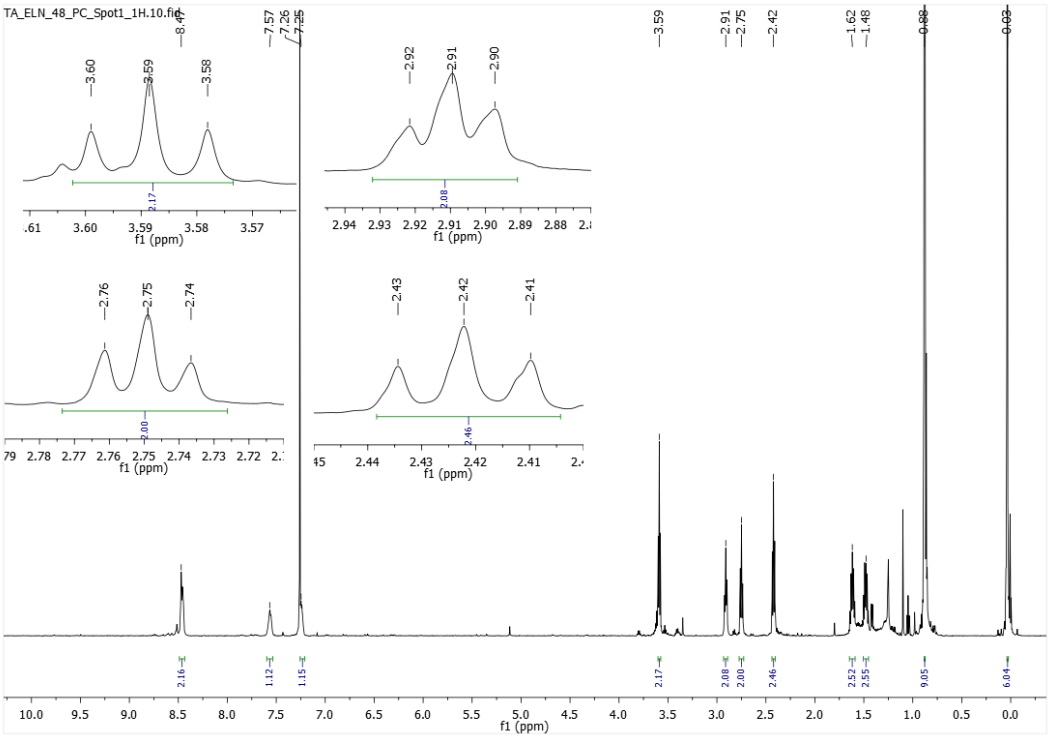
TA_ELN_48_PC_Spot1_1H.10.fid
f1 (ppm)

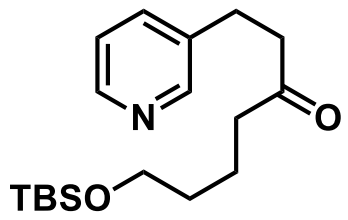
N
O
TBSO

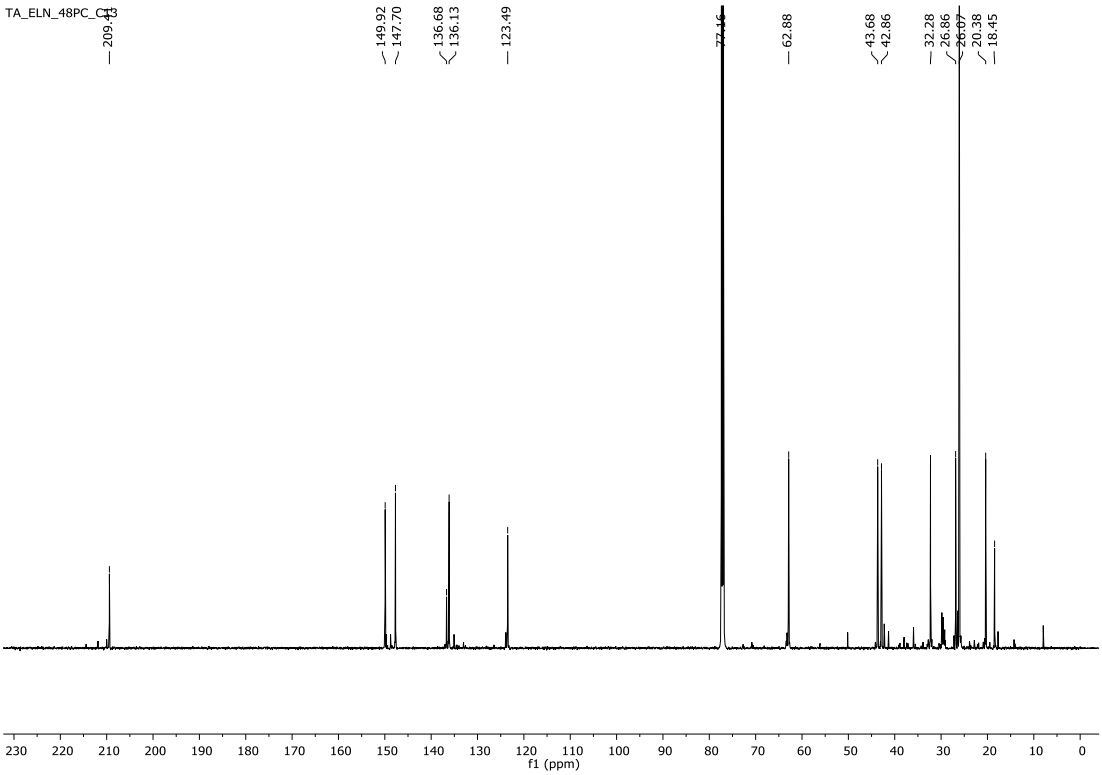
TA_ELN_48PC_C13
209.43
149.92
147.70
136.68
136.13
123.49
77.16
62.88
43.68
42.86
32.28
26.86
26.07
20.38
18.45
230 220 210 200 190 180 170 160 150 140 130 120 110 100 90 80 70 60 50 40 30 20 10 0
f1 (ppm)

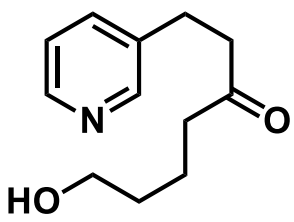
N
O
HO

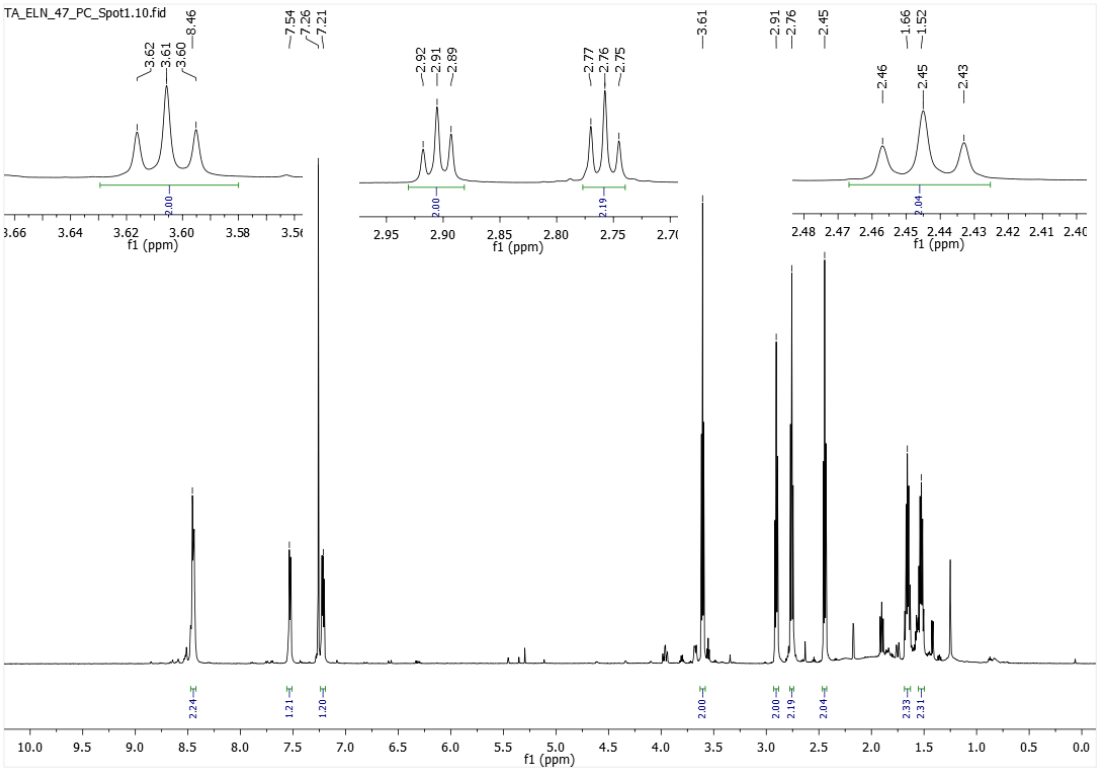
TA_ELN_47_PC_Spot1.10.fid
f1 (ppm)

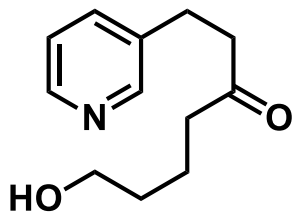
N
O
HO

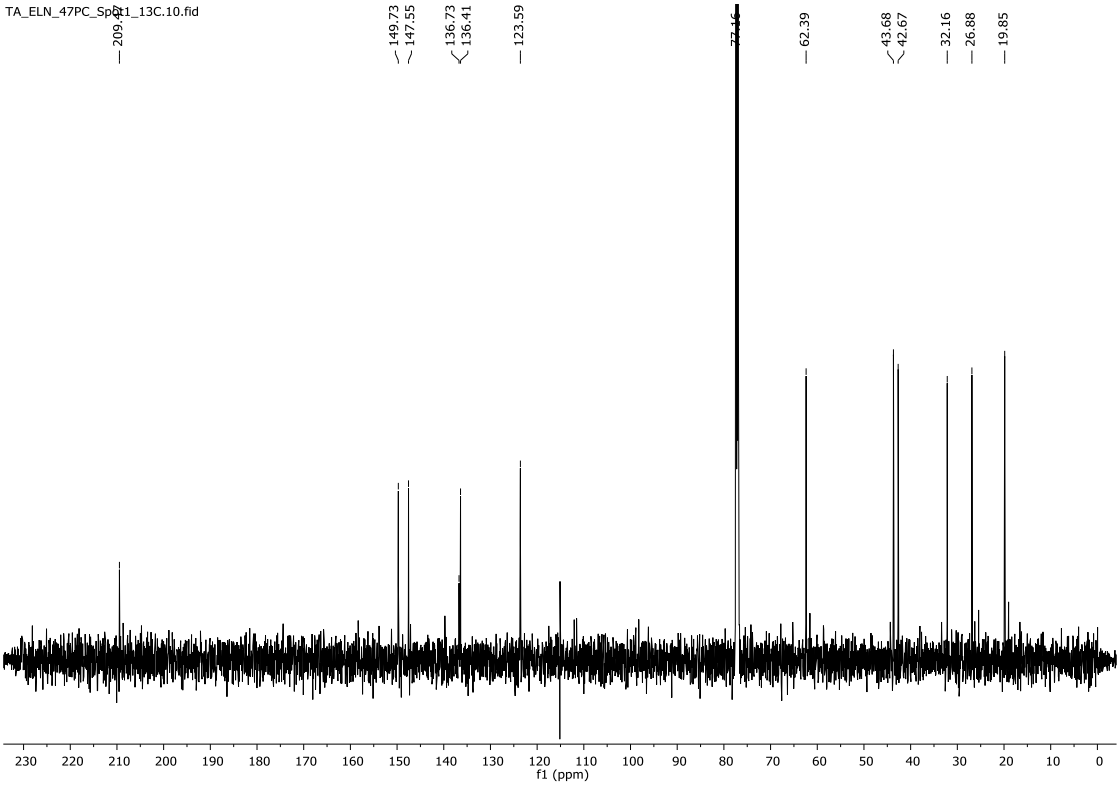
TA_ELN_47PC_Spot1_13C.10.fid
209.41
149.73
147.55
136.73
136.41
123.59
77.16
62.39
43.68
42.67
32.16
26.88
19.85
230 220 210 200 190 180 170 160 150 140 130 120 110 100 90 80 70 60 50 40 30 20 10 0
f1 (ppm)

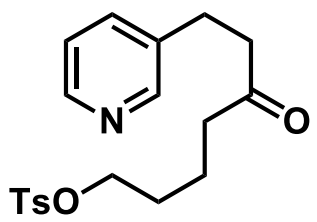
N
O
TsO

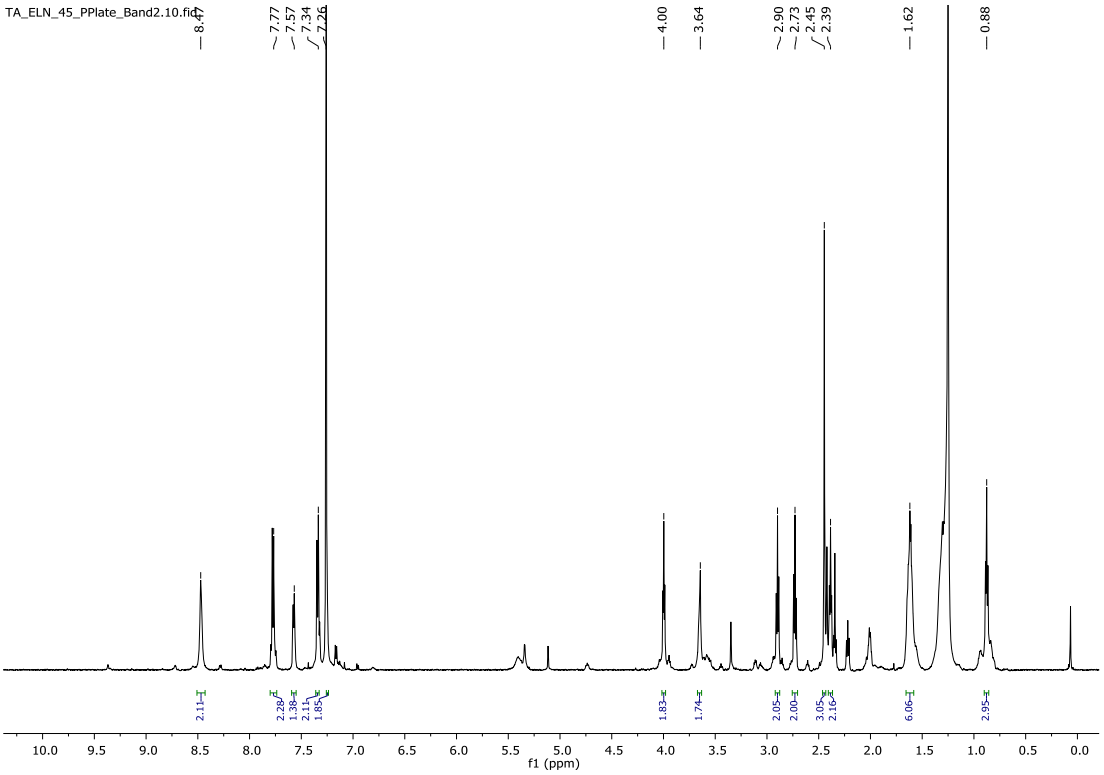
TA_ELN_45_PPlate_Band2.10.fid
8.47
7.77
7.57
7.34
7.26
4.00
3.64
2.90
2.73
2.45
2.39
1.62
0.88
2.11
2.28
1.38
2.11
1.85
1.83
1.74
2.05
2.00
3.05
2.16
6.06
2.95
f1 (ppm)

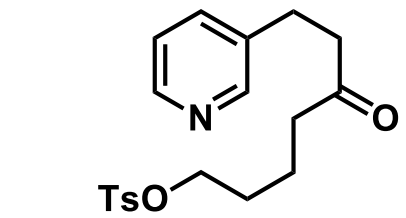
N
O
TsO

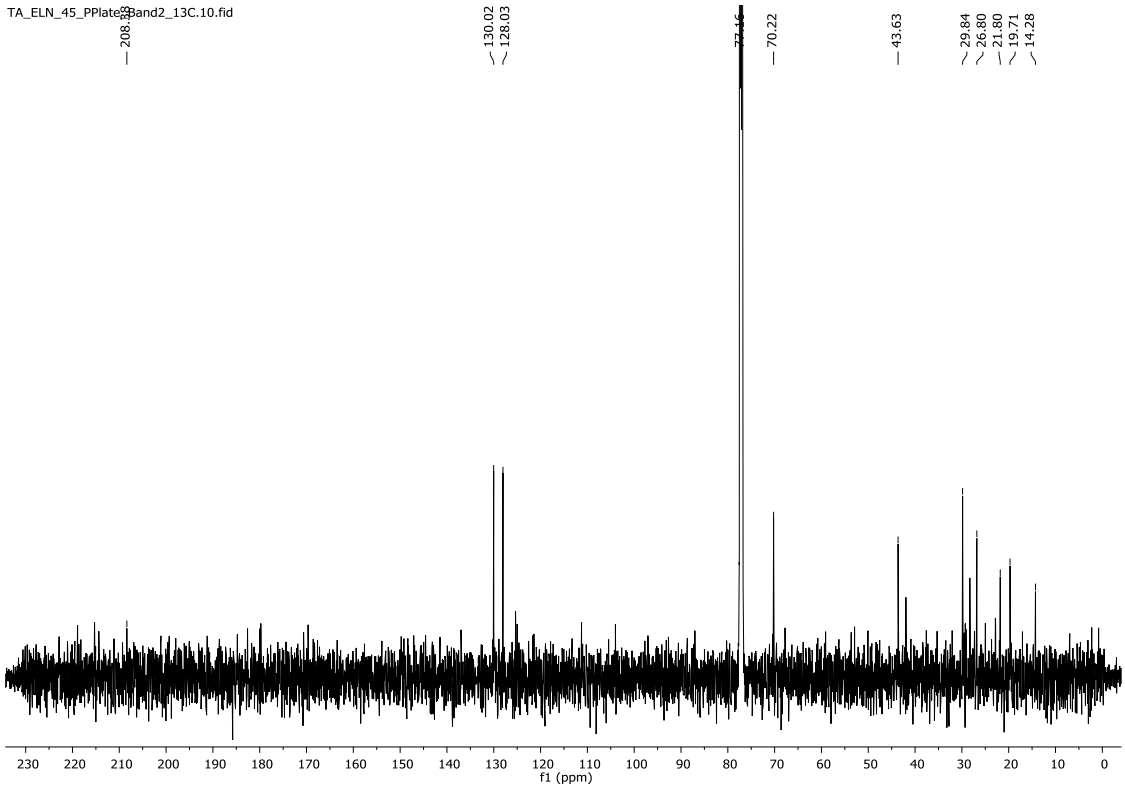
TA_ELN_45_PPlate2Band2_13C.10.fid
208.81
130.02
128.03
77.16
70.22
43.63
29.84
26.80
21.80
19.71
14.28
230 220 210 200 190 180 170 160 150 140 130 120 110 100 90 80 70 60 50 40 30 20 10 0
f1 (ppm)

2.7 References

(1) Ma, X.; Gang, D. R. The Lycopodium Alkaloids. *Nat. Prod. Rep.* **2004**, *21* (6), 752–772. https://doi.org/10.1039/B409720N.

(2) Siengalewicz, P.; Mulzer, J.; Rinner, U. Lycopodium Alkaloids--Synthetic Highlights and Recent Developments. *Alkaloids Chem Biol* **2013**, *72*, 1–151. https://doi.org/10.1016/b978-0-12-407774-4.00001-7.

(3) Bödeker, K. Lycopodin, Das Erste Alkaloïd Der Gefässkryptogamen. *Justus Liebigs Annalen der Chemie* **1881**, *208* (3), 363–367. https://doi.org/10.1002/jlac.18812080308.

(4) García-Ayllón, M.-S.; Small, D. H.; Avila, J.; Sáez-Valero, J. Revisiting the Role of Acetylcholinesterase in Alzheimer's Disease: Cross-Talk with P-Tau and β-Amyloid. *Front Mol Neurosci* **2011**, *4*. https://doi.org/10.3389/fnmol.2011.00022.

(5) Naqvi, E. Alzheimer's Disease Statistics. *Alzheimer's News Today*, 2017.

(6) Talesa, V. N. Acetylcholinesterase in Alzheimer's Disease. *Mechanisms of Ageing and Development* **2001**, *122* (16), 1961–1969. https://doi.org/10.1016/S0047-6374(01)00309-8.

(7) Taylor, P.; Radic, Z. The Cholinesterases: From Genes to Proteins. *Annu. Rev. Pharmacol. Toxicol.* **1994**, *34* (1), 281–320. https://doi.org/10.1146/annurev.pa.34.040194.001433.

(8) Tang, X. C.; Han, Y. F.; Chen, X. P.; Zhu, X. D. [Effects of huperzine A on learning and the retrieval process of discrimination performance in rats]. *Zhongguo Yao Li Xue Bao* **1986**, *7* (6), 507–511.

(9) Tang, X. C.; De Sarno, P.; Sugaya, K.; Giacobini, E. Effect of Huperzine A, a New Cholinesterase Inhibitor, on the Central Cholinergic System of the Rat. *J. Neurosci. Res.* **1989**, *24* (2), 276–285. https://doi.org/10.1002/jnr.490240220.

(10) Wang, R.; Tang, X. C. Neuroprotective Effects of Huperzine A. *NSG* **2005**, *14* (1–2), 71–82. https://doi.org/10.1159/000085387.

(11) Liu, J.-S.; Zhu, Y.-L.; Yu, C.-M.; Zhou, Y.-Z.; Han, Y.-Y.; Wu, F.-W.; Qi, B.-F. The Structures of Huperzine A and B, Two New Alkaloids Exhibiting Marked Anticholinesterase Activity. *Can. J. Chem.* **1986**, *64* (4), 837–839. https://doi.org/10.1139/v86-137.

(12) Liu, J. S.; Yu, C. M.; Zhou, Y. Z. Study on the Chemistry of Huperzine-A and Huperzine-B. **1986**.

(13) Xi-Can, T.; Kindel, G. H.; Kozikowski, A. P.; Hanin, I. Comparison of the Effects of Natural and Synthetic Huperzine-A on Rat Brain Cholinergic Function in Vitro and in Vivo. *Journal of Ethnopharmacology* **1994**, *44* (3), 147–155. https://doi.org/10.1016/0378-8741(94)01182-6.

(14) McKinney, M.; Miller, J. H.; Yamada, F.; Tuckmantel, W.; Kozikowski, A. P. Potencies and Stereoselectivities of Enantiomers of Huperzine A for Inhibition of Rat Cortical Acetylcholinesterase. *European Journal of Pharmacology* **1991**, *203* (2), 303–305. https://doi.org/10.1016/0014-2999(91)90730-E.

(15) Raves, M. L.; Harel, M.; Pang, Y.-P.; Silman, I.; Kozikowski, A. P.; Sussman, J. L. Structure of Acetylcholinesterase Complexed with the Nootropic Alkaloid, (–)-Huperzine A. *Nature Structural Biology* **1997**, *4* (1), 57–63. https://doi.org/10.1038/nsb0197-57.

(16) Xu, Y.; Shen, J.; Luo, X.; Silman, I.; Sussman, J. L.; Chen, K.; Jiang, H. How Does Huperzine A Enter and Leave the Binding Gorge of Acetylcholinesterase? Steered Molecular Dynamics Simulations. *J. Am. Chem. Soc.* **2003**, *125* (37), 11340–11349. https://doi.org/10.1021/ja029775t.

(17) Tang, Y.; Xiong, J.; Zhang, J.-J.; Wang, W.; Zhang, H.-Y.; Hu, J.-F. Annotinolides A–C, Three Lycopodane-Derived 8,5-Lactones with Polycyclic Skeletons from Lycopodium Annotinum. *Org. Lett.* **2016**, *18* (17), 4376–4379. https://doi.org/10.1021/acs.orglett.6b02132.

(18) Ayer, W. A.; Masaki, N.; Nkunika, D. S. Luciduline: A Unique Type of Lycopodium Alkaloid. *Can. J. Chem.* **1968**, *46* (23), 3631–3642. https://doi.org/10.1139/v68-602.

(19) Heathcock, C. H.; Smith, K. M.; Blumenkopf, T. A. Total Synthesis of (.+-.)-Fawcettimine (Burnell's Base A). *J. Am. Chem. Soc.* **1986**, *108* (16), 5022–5024. https://doi.org/10.1021/ja00276a062.

(20) Castillo, M.; Gupta, R. N.; Ho, Y. K.; MacLean, D. B.; Spenser, I. D. Biosynthesis of Lycopodine. Incorporation of Δ1-Piperideine and of Pelletierine. *Can. J. Chem.* **1970**, *48* (18), 2911–2918. https://doi.org/10.1139/v70-489.

(21) Castillo, M.; Gupta, R. Nath.; Ho, Y. K.; MacLean, D. B.; Spenser, I. D. Biosynthesis of Lycopodine. Incorporation of Pelletierine. *J. Am. Chem. Soc.* **1970**, *92* (4), 1074–1075. https://doi.org/10.1021/ja00707a061.

(22) Marshall, W. D.; Nguyen, T. T.; MacLean, D. B.; Spenser, I. D. Biosynthesis of Lycopodine. The Question of the Intermediacy of Piperidine-2-Acetic Acid. *Can. J. Chem.* **1975**, *53* (1), 41–50. https://doi.org/10.1139/v75-005.

(23) Castillo, M.; Gupta, R. N.; MacLean, D. B.; Spenser, I. D. Biosynthesis of Lycopodine from Lysine and Acetate. The Pelletierine Hypothesis. *Can. J. Chem.* **1970**, *48* (12), 1893–1903. https://doi.org/10.1139/v70-312.

(24) Hemscheidt, T.; Spenser, I. D. Biosynthesis of Lycopodine: Incorporation of Acetate via an Intermediate with C2v Symmetry. *J. Am. Chem. Soc.* **1993**, *115* (7), 3020–3021. https://doi.org/10.1021/ja00060a078.

(25) Hemscheidt, T.; Spenser, I. D. A Classical Paradigm of Alkaloid Biogenesis Revisited: Acetonedicarboxylic Acid as a Biosynthetic Precursor of Lycopodine. *J. Am. Chem. Soc.* **1996**, *118* (7), 1799–1800. https://doi.org/10.1021/ja953735q.

(26) Richards, J. C.; Spenser, I. D. The Stereochemistry of the Enzymic Decarboxylation of L-Arginine and of L-Ornithine. *Can. J. Chem.* **1982**, *60* (22), 2810–2820. https://doi.org/10.1139/v82-404.

(27) Burtea, A.; DeForest, J.; Li, X.; Rychnovsky, S. D. Total Synthesis of (−)-Himeradine A. *Angewandte Chemie International Edition* **2019**, *58* (45), 16193–16197. https://doi.org/10.1002/anie.201910129.

(28) Williams, B. M.; Trauner, D. Expedient Synthesis of (+)-Lycopalhine A. *Angewandte Chemie International Edition* **2016**, *55* (6), 2191–2194. https://doi.org/10.1002/anie.201509602.

(29) Bisai, A.; West, S. P.; Sarpong, R. Unified Strategy for the Synthesis of the "Miscellaneous" Lycopodium Alkaloids: Total Synthesis of (±)-Lyconadin A. *J. Am. Chem. Soc.* **2008**, *130* (23), 7222–7223. https://doi.org/10.1021/ja8028069.

(30) Bisai, V.; Sarpong, R. Methoxypyridines in the Synthesis of Lycopodium Alkaloids: Total Synthesis of (±)-Lycoposerramine R. *Org. Lett.* **2010**, *12* (11), 2551–2553. https://doi.org/10.1021/ol100823t.

(31) Murphy, R. A.; Sarpong, R. Heathcock-Inspired Strategies for the Synthesis of Fawcettimine-Type Lycopodium Alkaloids. *Chemistry – A European Journal* **2014**, *20* (1), 42–56. https://doi.org/10.1002/chem.201303975.

(32) Nakayama, A.; Kogure, N.; Kitajima, M.; Takayama, H. Asymmetric Total Synthesis of a Pentacyclic Lycopodium Alkaloid: Huperzine-Q. *Angewandte Chemie International Edition* **2011**, *50* (35), 8025–8028. https://doi.org/10.1002/anie.201103550.

(33) Yen, C.-F.; Liao, C.-C. Concise and Efficient Total Synthesis of Lycopodium Alkaloid Magellanine. *Angewandte Chemie International Edition* **2002**, *41* (21), 4090–4093. https://doi.org/10.1002/1521-3773(20021104)41:21<4090::AID-ANIE4090>3.0.CO;2-#.

(34) Zhang, J.; Wu, J.; Hong, B.; Ai, W.; Wang, X.; Li, H.; Lei, X. Diversity-Oriented Synthesis of Lycopodium Alkaloids Inspired by the Hidden Functional Group Pairing Pattern. *Nature Communications* **2014**, *5* (1), 1–9. https://doi.org/10.1038/ncomms5614.

(35) Leger, P. R.; Murphy, R. A.; Pushkarskaya, E.; Sarpong, R. Synthetic Efforts toward the Lycopodium Alkaloids Inspires a Hydrogen Iodide Mediated Method for the Hydroamination and Hydroetherification of Olefins. *Chemistry – A European Journal* **2015**, *21* (11), 4377–4383. https://doi.org/10.1002/chem.201406242.

(36) Murphy, R. A.; Sarpong, R. Direct Methoxypyridine Functionalization Approach to Magellanine-Type Lycopodium Alkaloids. *Org. Lett.* **2012**, *14* (2), 632–635. https://doi.org/10.1021/ol203269f.

(37) Heathcock, C. H.; Blumenkopf, T. A.; Smith, K. M. Total Synthesis of (.+-.)-Fawcettimine. *J. Org. Chem.* **1989**, *54* (7), 1548–1562. https://doi.org/10.1021/jo00268a015.

(38) Harayama, T.; Takatani, M.; Inubushi, Y. Stereoselective Syntheses of Lycopodium Alkaloids, (±)-Fawcettimine and (±)-8-Deoxyserratinine. *Tetrahedron Letters* **1979**, *20* (44), 4307–4310. https://doi.org/10.1016/S0040-4039(01)86574-6.

(39) Zaimoku, H.; Nishide, H.; Nishibata, A.; Goto, N.; Taniguchi, T.; Ishibashi, H. Syntheses of (±)-Serratine, (±)-Lycoposerramine T, and (±)-Lycopoclavamine B. *Org. Lett.* **2013**, *15* (9), 2140–2143. https://doi.org/10.1021/ol400628h.

(40) DeForest, J. C.; Samame, R. A.; Suryn, G.; Burtea, A.; Rychnovsky, S. D. Second-Generation Synthesis of (+)-Fastigiatine Inspired by Conformational Studies. *J. Org. Chem.* **2018**, *83* (16), 8914–8925. https://doi.org/10.1021/acs.joc.8b01144.

(41) Jakubczyk, D.; Caputi, L.; Hatsch, A.; Nielsen, C. A. F.; Diefenbacher, M.; Klein, J.; Molt, A.; Schröder, H.; Cheng, J. Z.; Naesby, M.; O'Connor, S. E. Discovery and Reconstitution of the Cycloclavine Biosynthetic Pathway—Enzymatic Formation of a Cyclopropyl Group. *Angewandte Chemie International Edition* **2015**, *54* (17), 5117–5121. https://doi.org/10.1002/anie.201410002.

(42) Li, Q.; Zhao, K.; Peuronen, A.; Rissanen, K.; Enders, D.; Tang, Y. Enantioselective Total Syntheses of (+)-Hippolachnin A, (+)-Gracilioether A, (−)-Gracilioether E, and (−)-Gracilioether F. *J. Am. Chem. Soc.* **2018**, *140* (5), 1937–1944. https://doi.org/10.1021/jacs.7b12903.

(43) Zhu, M.; Du, H.; Li, J.; Zou, D.; Wu, Y.; Wu, Y. Synthesis of β-Heteroaryl Carbonyl Compounds via Direct Cross-Coupling of Allyl Alcohols with Heteroaryl Boronic Acids under Cooperative Bimetallic Catalysis. *Tetrahedron Letters* **2018**, *59* (14), 1352–1355. https://doi.org/10.1016/j.tetlet.2018.02.021.

(44) Jana, S.; Sarpe, V. A.; Kulkarni, S. S. Total Synthesis of Emmyguyacins A and B, Potential Fusion Inhibitors of Influenza Virus. *Org. Lett.* **2018**, *20* (21), 6938–6942. https://doi.org/10.1021/acs.orglett.8b03073.

(45) McDougal, P. G.; Rico, J. G.; Oh, Y. I.; Condon, B. D. A Convenient Procedure for the Monosilylation of Symmetric 1,n-Diols. *J. Org. Chem.* **1986**, *51* (17), 3388–3390. https://doi.org/10.1021/jo00367a033.

(46) Mei, T.-S.; Werner, E. W.; Burckle, A. J.; Sigman, M. S. Enantioselective Redox-Relay Oxidative Heck Arylations of Acyclic Alkenyl Alcohols Using Boronic Acids. *J. Am. Chem. Soc.* **2013**, *135* (18), 6830–6833. https://doi.org/10.1021/ja402916z.

(47) Tamaru, Y.; Yamada, Y.; Yoshida, Z. Palladium-Catalyzed Reaction of 3-Bromopyridine with Allylic Alcohols: A Convenient Synthesis of 3-Alkylpyridines. *J. Org. Chem.* **1978**, *43* (17), 3396–3398. https://doi.org/10.1021/jo00411a032.

(48) Ren, R.-G.; Li, M.; Si, C.-M.; Mao, Z.-Y.; Wei, B.-G. Studies toward Asymmetric Synthesis of Leiodelide A. *Tetrahedron Letters* **2014**, *55* (50), 6903–6906. https://doi.org/10.1016/j.tetlet.2014.10.102.

(49) Monjas, L.; Fodran, P.; Kollback, J.; Cassani, C.; Olsson, T.; Genheden, M.; Larsson, D. G. J.; Wallentin, C.-J. Synthesis and Biological Evaluation of Truncated Derivatives of Abyssomicin C as Antibacterial Agents. *Beilstein J. Org. Chem.* **2019**, *15* (1), 1468–1474. https://doi.org/10.3762/bjoc.15.147.

(50) Chen, Y.-G.; Shuai, B.; Ma, C.; Zhang, X.-J.; Fang, P.; Mei, T.-S. Regioselective Ni-Catalyzed Carboxylation of Allylic and Propargylic Alcohols with Carbon Dioxide. *Org. Lett.* **2017**, *19* (11), 2969–2972. https://doi.org/10.1021/acs.orglett.7b01208.

(51) Stehouwer, J. S.; Birnbaum, M. S.; Voll, R. J.; Owens, M. J.; Plott, S. J.; Bourke, C. H.; Wassef, M. A.; Kilts, C. D.; Goodman, M. M. Synthesis, F-18 Radiolabeling, and MicroPET Evaluation of 3-(2,4-Dichlorophenyl)-N-Alkyl-N-Fluoroalkyl-2,5-Dimethylpyrazolo[1,5-a]Pyrimidin-7-Amines as Ligands of the Corticotropin-Releasing Factor Type-1 (CRF1) Receptor. *Bioorganic & Medicinal Chemistry* **2015**, *23* (15), 4286–4302. https://doi.org/10.1016/j.bmc.2015.06.036.

Chapter 3—Morita—Baylis—Hillman Coupling Methodology

3.1 Introduction and Background

The Morita-Baylis-Hillman (MBH) reaction was first described simultaneously by Morita in 1968 and by Baylis and Hillman in 1972 (Scheme 3.1).[1] The MBH reaction can

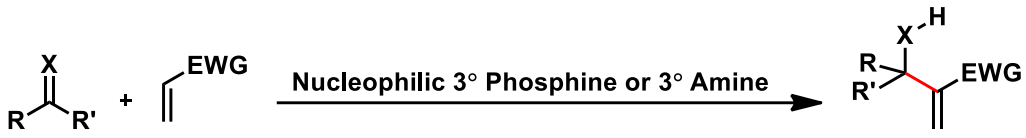

R = aryl, alkyl, heteroaryl, R' = H, CO_2R'', alkyl, etc.
X = O, NCO_2R'', NSO_2Ar
EWG = COR'', CHO, CN, CO_2R'', $PO(OEt)_2$, SO_2Ph, SO_3Ph, SOPh

Scheme 3.1 General Morita-Baylis-Hillman reaction

be utilized to perform α-carbonyl functionalization via carbon–carbon bond formation between an electron-poor α,β-unsaturated ketone and a suitable carbonyl electrophile. This reaction allows for the convenient synthesis of densely functionalized products that can be further derivatized. Additionally, this reaction is catalytic with respect to the tertiary phosphine or a tertiary amine. In seminal reports of the MBH reaction, Morita reported the reaction being catalyzed by a tertiary phosphine, while Baylis and Hillman reported catalysis by a tertiary amine. Nonetheless, the reactivity and bond formations were identical. Notable synthetic advantages of the MBH reaction are that it is atom economical, the starting materials are generally commercially available, the reaction proceeds under mild conditions and under catalytic conditions.[2]

Since the first description of the Morita–Baylis-Hillman reaction, extensive research and development (Scheme 3.2) has been pursued, leading to interesting derivatives and variations upon the classic MBH transformation.[2,3] For example, in 1984 Perlmutter reported an aza-MBH reaction, reacting ethyl acrylate and *N*-(*para*-

toluenesulphony)benzaldimine in the presence of catalytic 1,4-diazabicyclo[2.2.2]octane

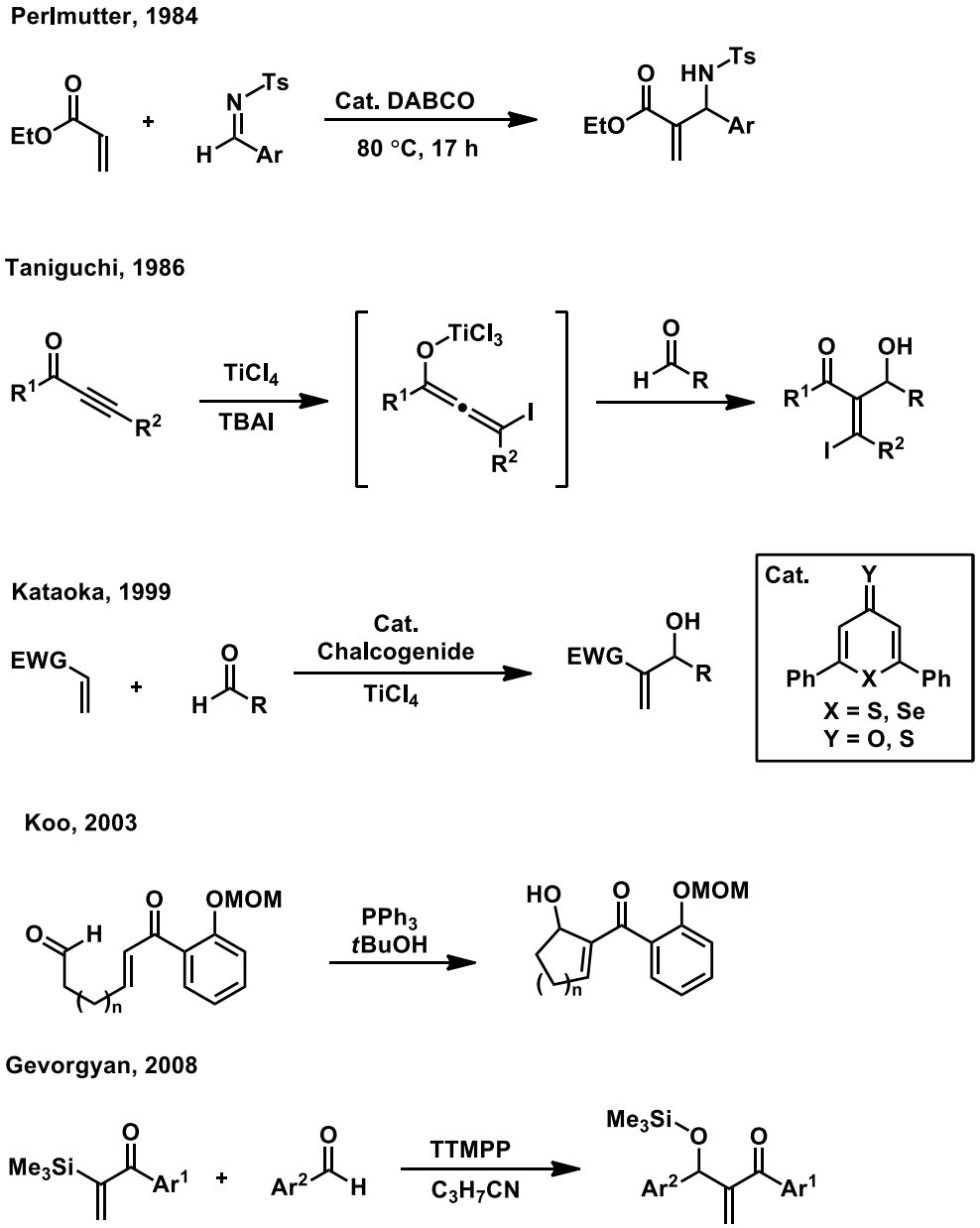

Scheme 3.2 Variations and derivatives of the classical Morita-Baylis-Hillman reaction

(DABCO).[4] A couple years later in 1986, Taniguchi reported a $TiCl_4$/TBAI mediated MBH transformation between electron-deficient alkynes and aldehydes, generating an iodinated allenolate intermediate that nucleophilically attacks the aldehyde, to produce an iodinated

MBH aldol product with high stereoselectivity for the Z-isomer.[5] In 1999, Kataoka reported a chalcogeno-Baylis–Hillman reaction, which utilized a chalcogenide and Lewis acid $TiCl_4$, both as catalysts. Kataoka also developed an asymmetric version of the chalcogeno—Baylis-Hillman.[6] Additionally, in 2003, Koo reported an intramolecular example of the MBH reaction.[7] Another interesting derivative of the MBH reaction is the sila-MBH reaction developed by Gevorgyan in 2008.[8] In addition to these developments, there have also been examples of asymmetric variants and 'double'-MBH reactions via dimerization; however, there have been no reported examples of coupling an electron-deficient α,β-unsaturated carbonyl to an aryl halide through a transition-metal-catalyzed

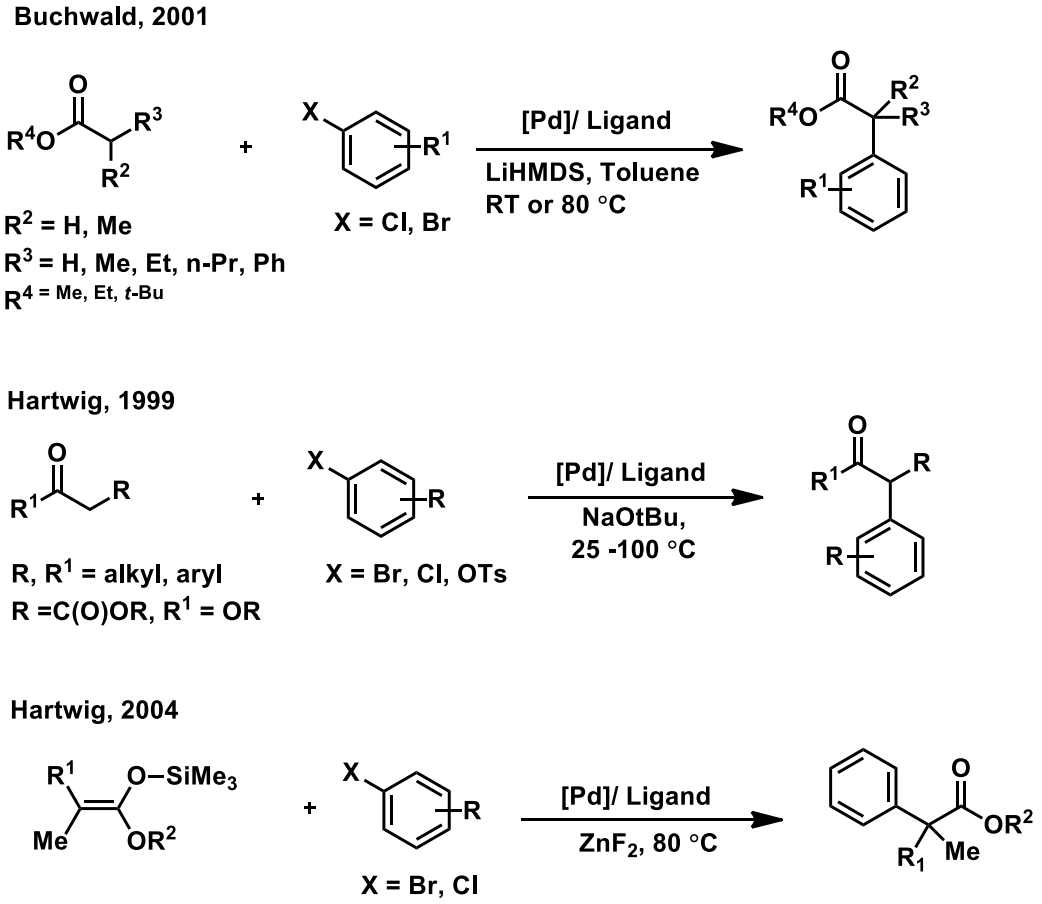

Scheme 3.3 Alpha-arylation methodology utilizing an enolate intermediate

pathway.[9–13] The absence of literature precedent for a MBH-type arylation reaction, despite the extensive literature precedent for MBH chemistry and α-carbonyl arylation chemistry, presents an opportunity to explore a new coupling reaction. If the enolate intermediate of a classical MBH reaction could bind to a transition metal, such as nickel or palladium, then we hypothesize that it should be able to mimic α – carbonyl arylation chemistry from that point to access MBH products with aryl or alkyl groups at the sp^2- α-position, from a wide variety of aryl- and alkyl-halides. A myriad of α–carbonyl arylation chemistry (Scheme 3.3) has been developed by Hartwig and Buchwald, where they are able to couple the α-position to an aryl group via an enolate intermediate that binds to a transition metal.[14–16,16–20] Encouragingly, there is one related example by Huang where an MBH 'coupling' is carried out between an α,β-unsaturated ketone and an allylic acetate using a palladium catalyst, a tertiary phosphine nucleophile, and an acid additive.[21]

Our group has previously demonstrated a strong interest in the development of novel arylation methodologies. Recently in 2020, our group published the first example of

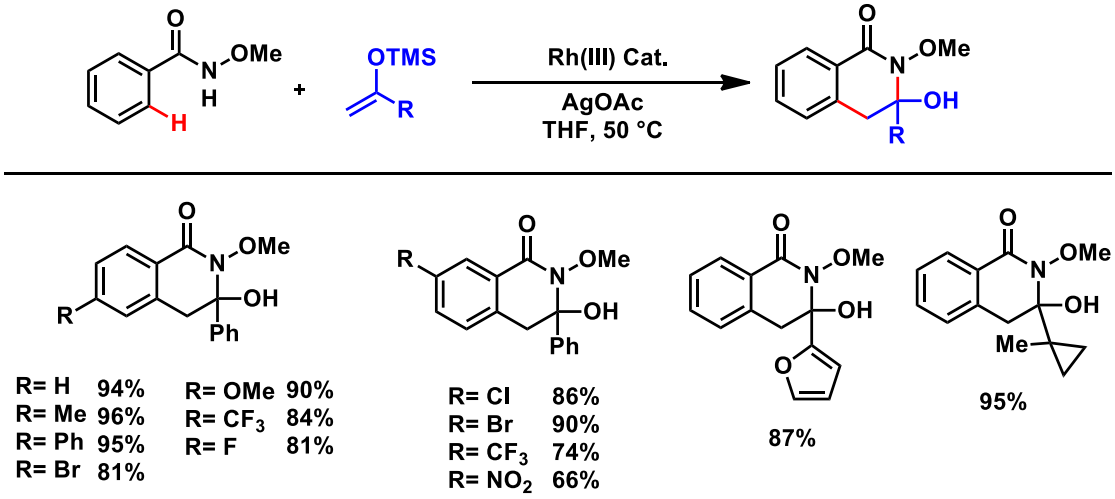

Scheme 3.4 Select examples of rhodium catalyzed C-H functionalization/alpha-arylation developed by the Kou lab

a C–H functionalization/α-arylation methodology utilizing silyl enol ethers and benzamides as well as a rhodium (III) catalyst (scheme 3.4).[22] In this work, we have developed a highly synthetically broad and useful α-arylation/C-H functionalization reaction to access a wide variety of dihydroisoquinolones in moderate to high yields.

As an extension of our interest in advancing novel arylation methodologies, we have focused upon the challenge of developing a methodology for the α-functionalization of α,β-unsaturated ketones, which would achieve an inversion of regioselectivity compared to the regioselectivity of a traditional Heck arylation. Our initial approach for the α-

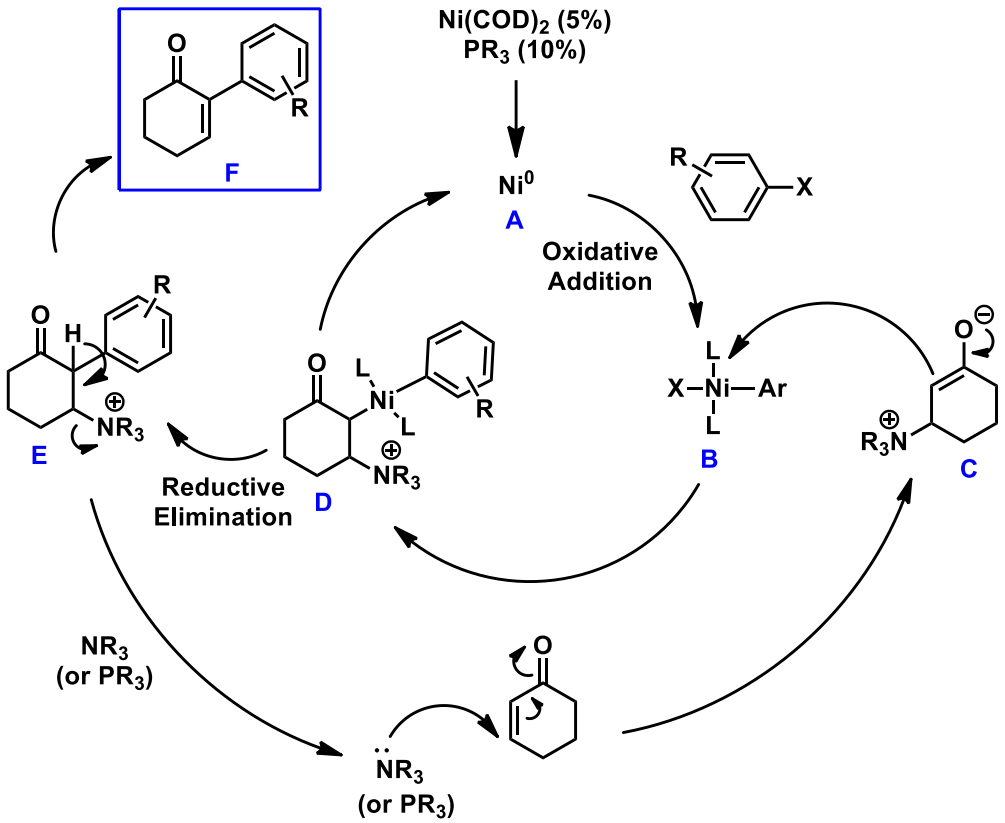

arylation of α,β-unsaturated was adapted from MBH chemistry and enolate derived α-arylation methodologies (Scheme 2, 3, 5).

3.2 Results and Discussion

Research Proposal

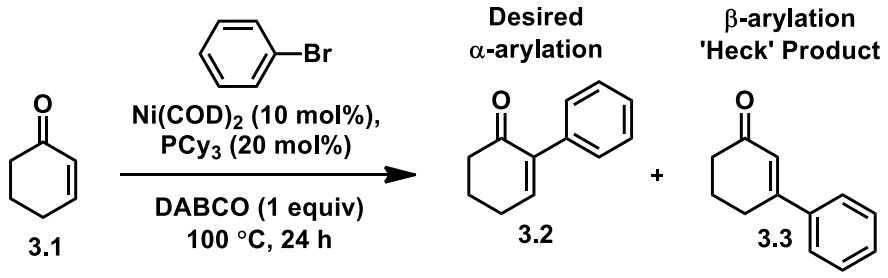

Entry	Metal (10 mol%)	Ligand (20 mol%)	Phosphine /Amine	Solvent	3.2 (%)	3.3 (%)
1	-	-	DABCO	1,4-dioxane	NP	NP
2	$Ni(COD)_2$	PCy_3	-	1,4-dioxane	NP	NP
3	$Ni(COD)_2$	PCy_3	DABCO	1,4-dioxane	NP	NP
4	$Ni(COD)_2$	PCy_3	DABCO	DCM	NP	NP
5	$Ni(COD)_2$	PCy_3	DABCO	THF	NP	NP
6	$Ni(COD)_2$	PCy_3	DABCO	PhMe	NP	NP
7	$Ni(COD)_2$	PCy_3	DABCO	MeCN	NP	NP
8	$Ni(COD)_2$	PCy_3	DABCO	DCE	NP	NP

Table 3.3 Solvent screen using a nickel catalyst system

We envisioned capitalizing upon a reaction mechanism (Figure 1) that was a unification of the respective mechanisms of the classical MBH and traditional α-carbonyl arylation chemistries described previously (Schemes 3.2, 3.3, 3.5). Beginning from a palladium (0) or nickel (0) **A**, we proposed an oxidative addition into a carbon–halide bond of an aryl- or

alkyl halide. The resulting organometallic intermediate (**B**) would then be attacked by enolate **C** that is generated in situ to form intermediate **D**. The enolate (**C**) would be generated in situ following the classical MBH mechanism, where the α,β-unsaturated ketone is attacked at the β-position by a tertiary amine or phosphine. After the enolate adds onto the metal catalyst (**B**)**,** substituting the halide, we hypothesized that reductive

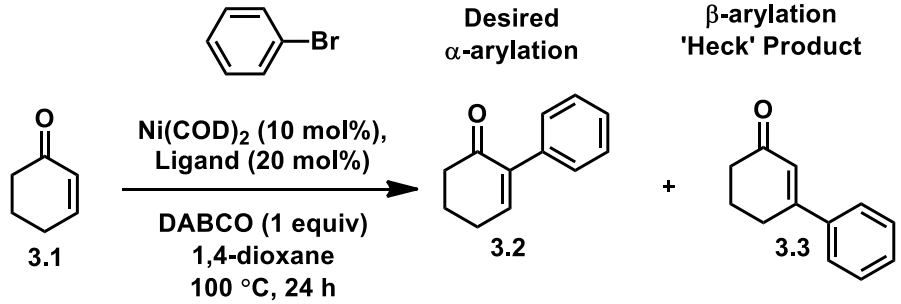

Entry	Ligand	3.2 (%)	3.3 (%)
1	Dppp	NP	NP
2	Dppb	NP	NP
3	Dppe	NP	NP
4	Dppf	NP	NP
5	Dppm	NP	NP
6	Dpp5	NP	NP
7	Dppe	NP	NP
8	Dpe-O	NP	NP
9	Dpe-Phos	NP	NP
10	PCP-Pincer	NP	NP
11	DuMePyr	NP	NP
12	S-BINAP	NP	NP

Table 3.2 Ligand evaluation using a nickel catalyst system

elimination from intermediate **D** would occur, forming the new carbon–carbon double bond in intermediate **E** and regenerating the active catalyst, Ni(0) or Pd(0). Finally, deprotonation of the α-proton would yield our desired product (**F**) by reforming the α,β-unsaturation and regenerate the tertiary phosphine or amine catalyst. We were motivated to develop this chemistry using nickel instead of palladium for sustainability and cost reasons. Being able to develop new organometallic reactions, as well as perform previously developed palladium catalyzed reactions with nickel instead could not only lead to the development of new transformations, but also ensure the sustainability of already developed palladium catalyzed reactions by not having to rely on a diminishing supply of palladium sources.

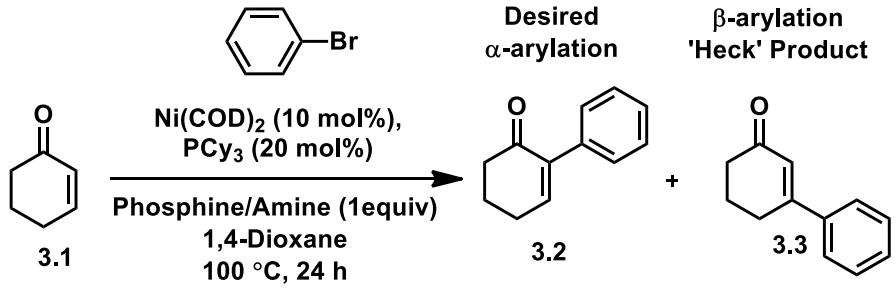

Entry	Phosphine /Amine	3.2 (%)	3.3 (%)
1	PCy_3	NP	NP
2	Imidazole	NP	NP
3	$NMe_3(EtOH)$	NP	NP
4	TEA	NP	NP
5	DMAP	NP	NP
6	Pyrrolidine	NP	NP

Table 3.3 Nucleophile screening using a nickel catalyst system

Despite extensive literature precedent (discussed above) for both the MBH and α–carbonyl arylation chemistry via an enolate intermediate, we have thus far been unsuccessful in our goal of developing a method for the α-functionalization of α,β-unsaturated ketones demonstrating reversed selectivity to the traditional Heck reaction. We have explored myriad reaction conditions to effect this transformation, beginning with a solvent screen shown in Table 3.1. Our starting reaction conditions, which were adapted from MBH literature precedent[1,21], included cyclohexanone (1 equiv), bromobenzene (1.2 equiv), DABCO (1.2 equiv), $Ni(COD)_2$ (10 mol%), and PCy3 (20 mol%) with a reaction temperature of 100 ˚C and a reaction time of 24 h. Our goal with this methodology is to reverse the selectivity of the traditional Heck reaction. However, the traditional β-functionalized Heck product could be formed through a competing side-reaction and in fact we do in some experiments observe the β-functionalized product as the predominant reaction pathway. We examined different solvents that have demonstrated success in related MBH reactions, including dioxane, DCM, THF, toluene, MeCN and DCE (Table 3.1, entries 4—8); however, none led to product formation and only starting material was recovered. Next, we performed a sizeable ligand screen (Table 3.2). We focused on bidentate phosphine ligands such as dppp, dppb, dppe, dppf, BINAP, and many others due

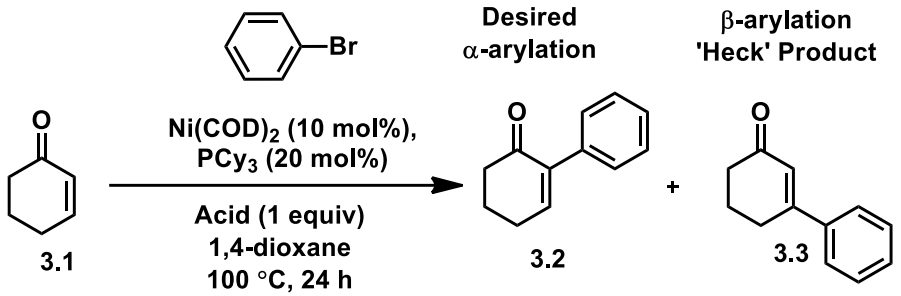

Entry	Acid	3.2 (%)	3.3(%)
1	BzOH	NP	NP
2	pTSA-H_2O	NP	NP
3	AcOH	NP	NP
4	PPTs	NP	NP

Table 3.4 Acid additive screening using a nickel catalyst system

to previous examples in the literature that we hoped would provide reactivity in this reaction; however, only starting materials were recovered. We moved on to evaluate different nucleophiles (Table 3.3), aiming to identify one that would be suitable to engage the β-position of cyclohexenone to generate the enolate in situ, which could then undergo α-metalation and proceed through our proposed mechanism. We evaluated PCy_3 (1.2 equiv, Table 3.3, entry 1), as both the ligand for nickel to reduce Ni(II)$(COD)_2$ to Ni(0) as well as the nucleophile since MBH reactions can be catalyzed by a tertiary amine or phosphine, but this again resulted in no reaction. We also tried other nitrogen-containing nucleophiles such as imidazole, trimethylamine, triethylamine, dimethyl amino pyridine, and pyrrolidine, all of which returned starting material (Table 3.3, entries 1–6). The next reaction parameter we visited was acid additives (Table 3.4). We hoped that the appropriate acid would be able to activate the β-position of cyclohexnone by protonating

the carbonyl, and the resulting conjugate base could act as a nucleophile by attacking the β-position of cyclohexenone and proceeding through our desired mechanism. However, each acid evaluated returned starting materials or decomposition products.

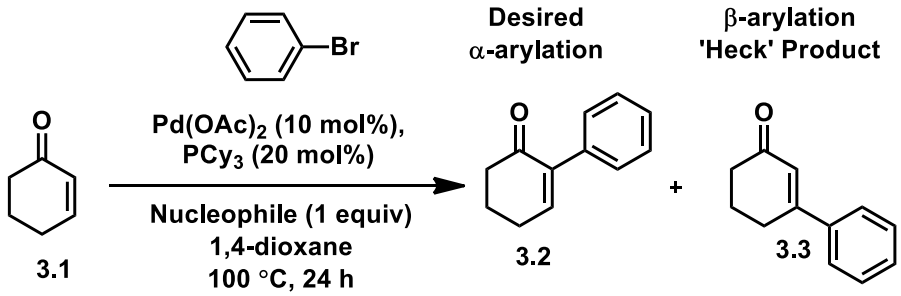

Entry	Acid	Nucleophile	3.2 (%)	3.3 (%)
1	$Pd(OAc)_2$	PCy_3	NP	NP
2	$Pd(OAc)_2$	DABCO	NP	30%
3	$Pd(OAc)_2$	Imidazole	NP	NP
4	$Pd(OAc)_2$	$NMe_3(EtOH)$	NP	27%
5	$PdCl_2$ + $AgBF_4$ (5%)	DABCO	NP	NP
6	$PdCl_2$ + $AgSbPF_6$(5%)	DABCO	NP	NP

Table 3.5 Nucleophile screening using palladium catalyst system

Given the lack of reactivity, we decided to switch from a catalyst system of nickel to that of palladium. Although there are examples of nickel catalyzed arylations, all of the α-arylation chemistry utilizing an aryl halide (Scheme 3.3) by Hartwig and Buchwald used palladium catalysts. Upon switching to palladium, we revisited nucleophiles and explored cationic palladium complexes (Table 3.5).[23,24] Specifically, we evaluated PCy_3 (1.2 equiv) acting as both the nucleophile as well as the ligand to reduce palladium(II) to palladium(0),

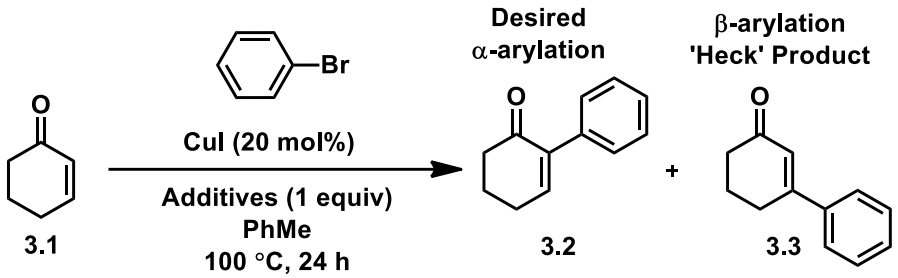

Entry	Additives	3.2 (%)	3.3 (%)
1	-	NP	NP
2	NaI	NP	NP
3	TBAI	NP	NP
4	NaI, K_3PO_4	NP	NP
5	TBAi, K_3PO_4	NP	NP

Table 3.6 Iodide source screening with a copper catalyst system

but only observed starting material. We also evaluated DABCO, imidazole, and NMe_3. With DABCO and NMe_3 we observed and isolated the undesired regioisomer where the phenyl group was coupled to the β-position instead of the desired α- position, in about 30% yields. We propose that the β-arylated product **3.3** arises from a traditional Heck reaction, although in lower yields than a traditional Heck reaction.[25] This result seems to suggest that the Heck pathway is more reactive than the desired α-arylation pathway. We also evaluated cationic palladium complexes by using $PdCl_2$ and $AgBF_4$ (5 mol%) or $AgSbPF_6$ (5 mol %) but neither system resulted in product formation. Inspired by the Gilman coupling literature, we decided to explore copper (Table 3.6).[26] We evaluated different iodide sources, such as sodium iodide (NaI) and *tert*-butyl ammonium iodide (TBAI), as well as potassium phosphate (K_3PO_4) as a base additive. We chose to evaluate

copper/iodide sources in the hopes that an iodide source would act as a suitable nucleophile to attack the β-position of cyclohexenone and proceed through a copper catalyzed coupling pathway. Unfortunately, various permutations of conditions using copper with NaI or TBAI additives individually or simultaneously with K_3PO_4 were unsuccessful, only returning starting materials.

The lack of reactivity in this system leading to the generation of the desired α-arylation product or the β-arylation Heck product led us to speculate that perhaps the enone and bromobenzene were incompatible coupling partners for either pathway. To briefly investigate this hypothesis, we evaluated more common Heck coupling conditions using a

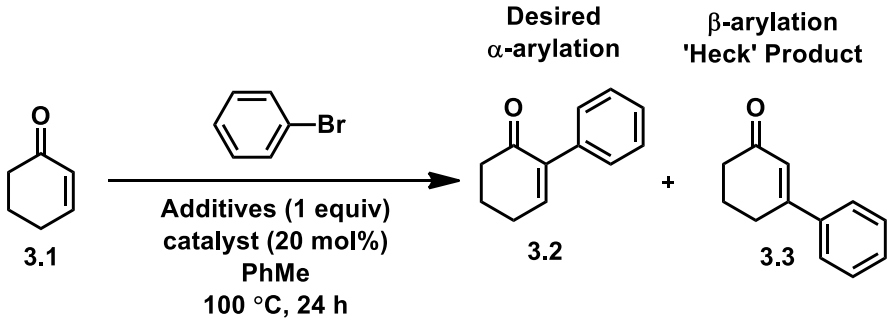

Entry	Catalyst	Base	Solvent	Result
1	$Ni(COD)_2$, dppf	DIPEA	1,4-dioxane	NP
2	$Pd_2(dba)_3$	K_3PO_4	Toluene	NP

Table 3.7 Coupling reactions under Heck conditions

catalyst ligand system of $Ni(COD)_2$ (10 mol%), dppf (10 mol%), and DIPEA (2 equiv) in 1,4-dioxane (Table 3.7, entry 1) and a palladium(0) source in $Pd_2(dba)_3$ (10 mol%) and K_3PO_4 (2 equiv) in toluene (Table 3.7, entry 2), both stirred at 100 ˚C for 24 h. Surprisingly, neither set of conditions generated the expected β-arylated Heck product

(**3.3**). This suggests that perhaps the electronic withdrawing effects of the carbonyl maybe deactivating the alkene to the extent that it is not coordinating very well to the metal, and therefore cannot efficiently proceed through a Heck pathway. Based on these results and the previous formation of the β-arylation product (**3.3**), although relatively low yielding, it would appear that the Heck pathway is more favorable than the desired α-arylation pathway, which appears to be very much unfavorable, at least with cyclohexenone and bromobenzene as coupling partners.

To follow up on the hypothesis that cyclohexenone and bromobenzene may be incompatible coupling partners, we evaluated different halide electrophiles (Table 3.8). We first tested iodobenzene and chlorobenzene to eliminate the possibility that this chemistry is only incompatible with aryl bromides, but such was not the case as starting

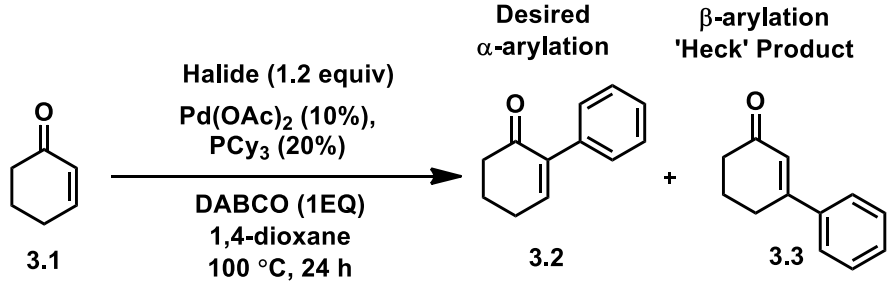

Entry	Halide	Results
1	ClPh	NP
2	IPhMe	NP
3	4-Iodoacetophenone	NP
4	4-Bromoacetophenone	NP
5	4-Nitroacetophenone	NP

Table 3.8 Halide screening with a palladium or nickel catalyst system

materials were recovered in all cases. We also experimented with electron poor aryl halides because oxidative addition into these tends to be faster than their more electron-rich counterparts. We experimented with 4-iodoacetophenone, 4-bromoacetophenone, and 4-nitroacetophenone. Lastly, we tried Suzuki-type conditions using phenylboronic acid with $NiCl_2$ and DIPEA.[27] Dissatisfying, none of these electrophiles provided the desired α-arylated product (**3.2**) or the undesired β-arylated regioisomer (**3.2**).

Due to the lack of desired reactivity between cyclohexenone and bromobenzene, or any other evaluated aryl halide, we decided to change model substrates to methyl acrylate

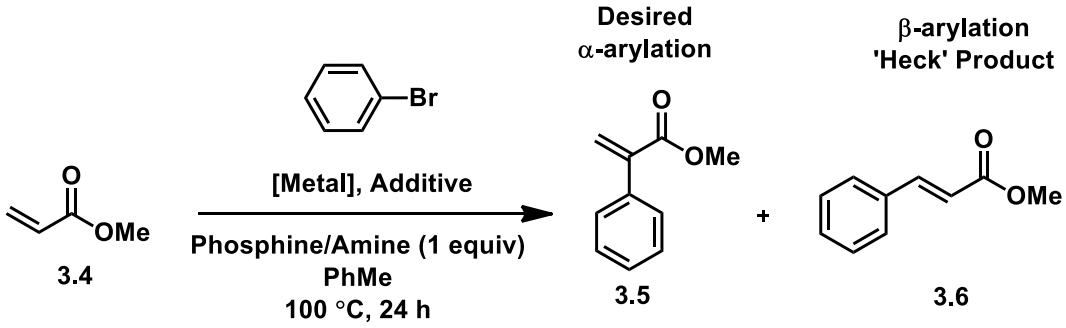

Entry	Metal (10%)	Nuc/ Additive 20 mol%	Result
1	$Pd(OAc)_2$	PCy_3	NP
2	$Pd(OAc)_2$	DABCO	Heck Product - 35%
3	$Pd(OAc)_2$	DMAP	NP
4	$Pd(OAc)_2$	PhOH, K_3PO_4	NP
5	$Pd(OAc)_2$	DABCO	Heck Product - 35%
6	$Ni(COD)_2$	DABCO	Heck Product

Table 3.9 Nucleophile screening with methyl acrylate and a palladium or nickel catalyst system

(Table 3.9). We hypothesized that methyl acrylate could be a better electrophile to initiate the conjugate addition part of proposed MBH mechanism because it was less sterically hindered at the β-position (as a mono-substituted α,β-unsaturated ketone) with terminal hydrogens compared to the di-substituted double bond in cyclohexenone. However, despite significant efforts by varying the reaction conditions and setup, such as pre-mixing the ligand and catalyst, pre-mixing methyl acrylate and nucleophile to generate the enolate, and varying temperatures, the Heck pathway was more favorable. No desired product was observed through these experiments. Nucleophiles screened included PCy_3 (1.2 equiv), DABCO, DMAP, and PhOH/K_3PO_4. We also briefly re-evaluated a nickel catalyst system using $Ni(COD)_2$ but again only observed the β-arylated methyl acrylate product (**3.6**).

3.3 Morita—Baylis—Hillman Umpolung Inspired Strategy

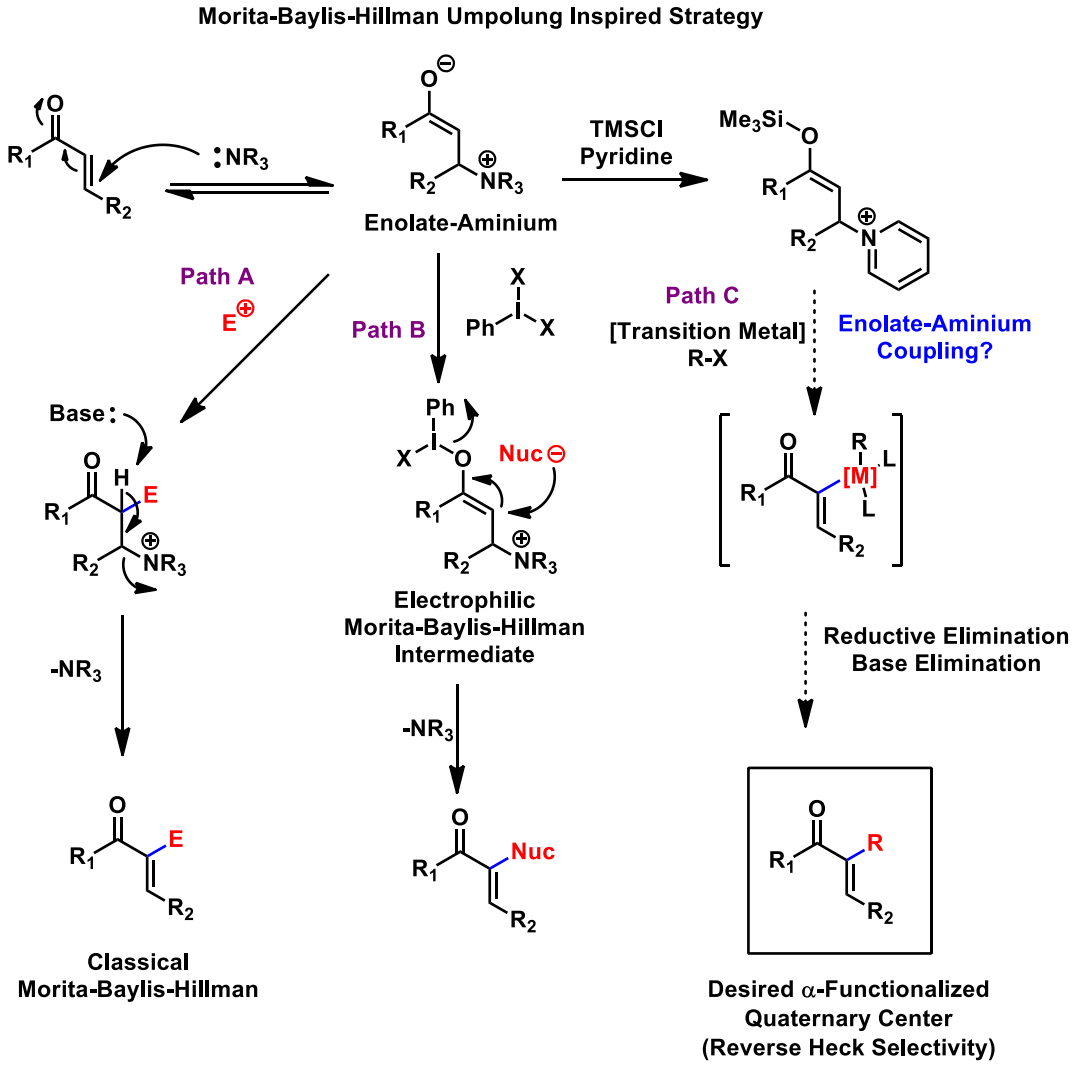

Scheme 3.6 Summary Morita-Baylis-Hillman reaction pathways

We are inspired by recent advances in MBH chemistry performed by Dr. Alex Szpilman and co-workers, who published an umpolung variation of the MBH reaction to accomplish α-functionalization of enone C-H bonds.[28] As shown in Scheme 3.5, the traditional MBH pathway involves the nucleophilic attack of a sterically hindered base, or phosphine, to the β-position of the enone forming a reactive enolate-aminium species in-situ. From this enolate-aminium species, the reaction pathway diverges. Traditionally, the enolate-

aminium would react with an electrophile, such as an aldehyde, through enolate reactivity, followed by elimination of the base to produce α-functionalized enones. In the recent study, Szpilman's group treats the enolate-aminium species with a hypervalent iodine species, which generates an electrophilic intermediate which can now participate in umpolung chemistry. Specifically, Szpilman utilizes chloride and tosyl nucleophiles at the α-position of the final enone product. Subsequently, Szpilman demonstrated that the tosylated products could be used to perform Negishi coupling reactions. Using a two-step

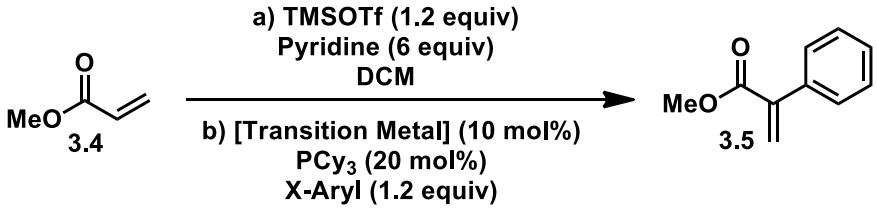

Entry	[TM]	Aryl Electrophile	Result
1	$NiCl_2$	$PhB(OH)_2$	No Rxn
2	$NiCl_2$	IPhMe	No Rxn
3	$NiCl_2$	ClPh	No Rxn
4	$Pd(OAc)_2$	$PhB(OH)_2$	No Rxn
5	$Pd(OAc)_2$	IPhMe	No Rxn
6	$Pd(OAc)_2$	ClPh	No Rxn
7	$CoBr_2$	$PhB(OH)_2$	No Rxn
8	$CoBr_2$	IPhMe	No Rxn
9	$CoBr_2$	ClPh	No Rxn

Table 3.10 Lewis-acid catalyzed reactions with nickel, palladium, and cobalt catalyst systems

method of functionalization by activating the α-position by chlorination or tosylation and then performing a coupling reaction affords the desired α-functionalized enones; however, we hypothesized that by advancing Szpilzman's approach, it could be possible to access the same types of products directly from the unfunctionalized enones.

We began the exploration of our hypothesis by performing reactions with TMSOTf as an activating Lewis- acid and pyridine as the nucleophile as reported in Szpilman's work (Table 3.10). However, we sought new reactivity by incorporating transition metal catalysts such as nickel, palladium, and cobalt and aryl coupling partners such as phenyl boronic acid, iodotoluene, and chlorobenzene. Unfortunately, these preliminary reactions did not lead to any reactivity and only starting materials were recovered. We were

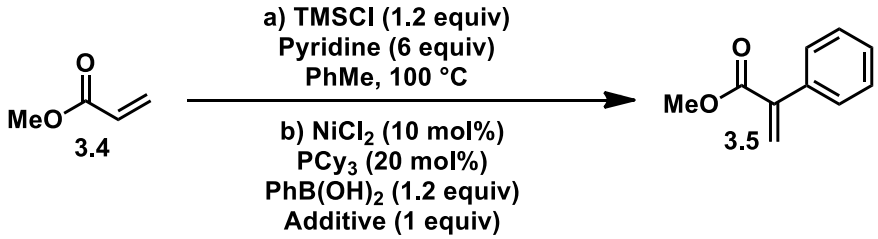

Entry	Additive	Result
1	NaOAc	No Rxn
2	AgOAc	No Rxn
3	LiOAc	No Rxn
4	ZnF_2	β-Arylation observed
5	TBAF	No Rxn
6	AgF	No Rxn

Table 3.11 Additives evaluation for desilylation

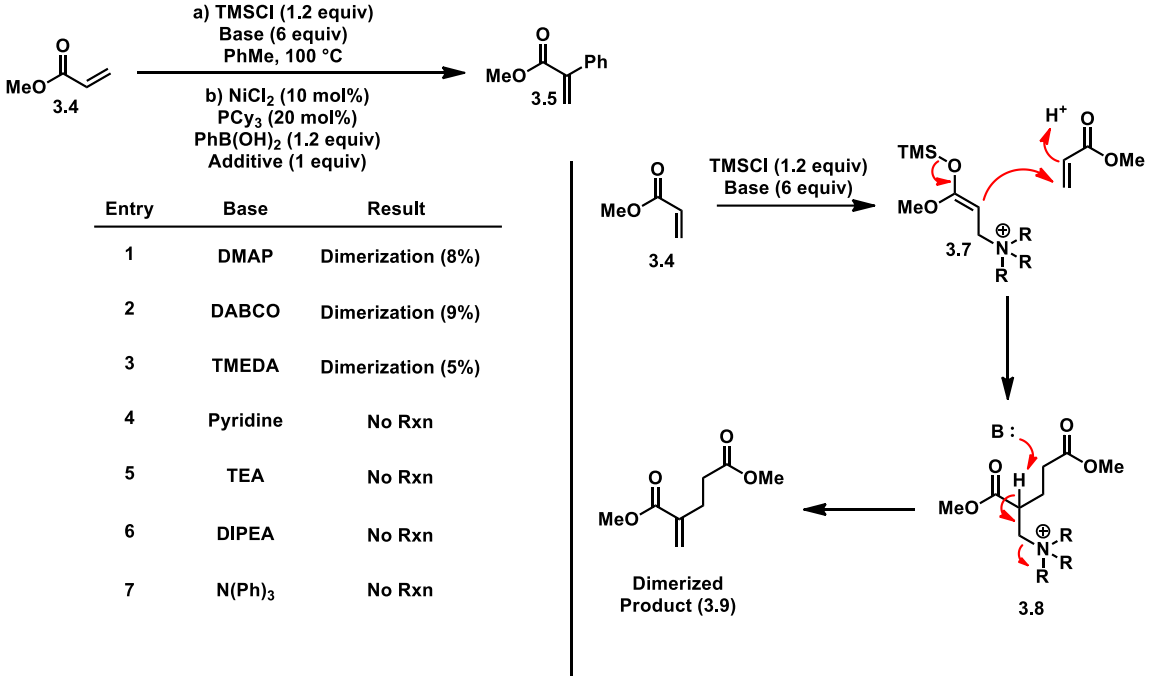

Table 3.12 Evaluation of tertiary amine nucleophillic bases

reasonably confident that the desired enolate-aminium species was being generated in-situ, so we speculated that perhaps a lack of nucleophilicity was preventing interaction with the metal catalyst. To explore this possibility, we next evaluated additives to facilitate desilylation to generate a naked enolate instead of a silylenol ether nucleophile (Table 3.11). The additives screened were NaOAc, AgOAc, LiOAc, ZnF_2, TBAF, and AgF in stoichiometric amounts. Again, we saw no product formation; however, we did observe the β-arylated product of the traditional Heck reaction, which we have previously isolated and confirmed. Since there was literature precedent for pyridine engaging the β-position as a nucleophile to form the desired enolate-aminium species, we investigated various tertiary amine bases for this reaction (Table 3.12).[28] The bases evaluated were DMAP, DABCO, TMEDA, TEA, DIPEA, and $N(Ph)_3$. Interestingly, we observed reactivity from the use of DMAP, DABCO, and TMEDA. Unfortunately, we did not observe the desired

α-arylated product. Instead, we isolated and confirmed the production of a dimerized product (**3.9**). DMAP, DABCO, and TMEDA led to an 8%, 9%, and 5% yield, respectively, of the dimerized product (Table 3.12, entries 1,2 and 3). This was encouraging because the only way to generate the dimerized product was through the desired silyl enol ether aminium intermediate and confirms that the species is somewhat nucleophilic. However, even though we were generating the desired silyl enol ether aminium in situ, it was evidently not reacting with the metal catalyst as desired. To improve the reactivity, we sought to vary the catalytic metal species by changing aryl halide and switching to $Pd_2(dba)_3$, a commonly used palladium(0) source (Table 3.13).

The aryl halides investigated were bromobenzene (**3.10**), iodoacetophenone (**3.11**), and methyl 4-bromobenzoate (**3.12**). Iodoacetophenone (**3.11)** and methyl 4-bromobenzoate (**3.12**) were possibly better suited for this chemistry because they are electron-deficient, thus rendering oxidative addition by palladium(0) easier, which can also lead to a more electrophilic aryl-palladium intermediate to react with the silyl enol ether aminium species. We chose to continue using DMAP, DABCO, and TMEDA as the

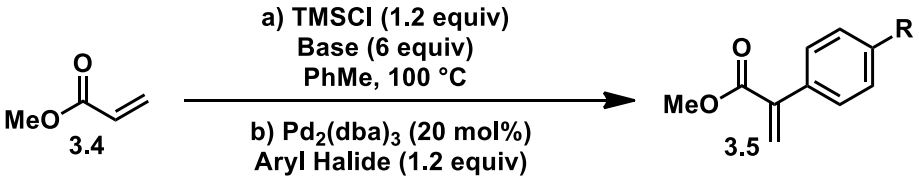

Entry	Base	Aryl Halide	Result
1	DMAP	3.10	No rxn
2	DMAP	3.11	β-Arylation
3	DMAP	3.12	No rxn
4	DABCO	3.10	No rxn
5	DABCO	3.11	β-Arylation
6	DABCO	3.12	No rxn
7	TMEDA	3.10	No rxn
8	TMEDA	3.11	No rxn
9	TMEDA	3.12	No rxn

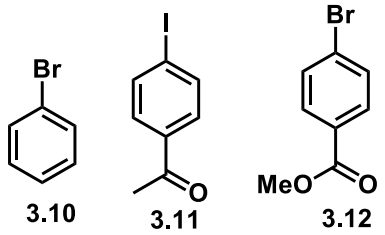

Table 3.13 Evaluation of electron withdrawn aryl halides with most reactive nucleophilic bases using $Pd_2(dba)_3$ catalyst

base because these bases had given rise to dimerized product (**3.9**, Table 3.12). However, we only observed formation of the undesired β-arylated product when iodoacetophenone was used with DMAP and DABCO (Table 3.13, entries 2 and 5). All other reaction conditions with these substrates resulted in no reactivity.

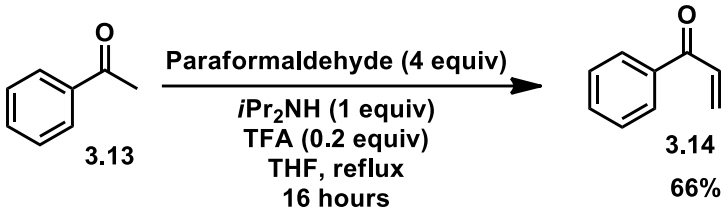

Scheme 3.7 Synthesis of acrylophenone substrate

At this point, we were unsure if perhaps the starting enone was simply not compatible for the proposed reaction, so we synthesized the acrylophenone (**3.14**) that was

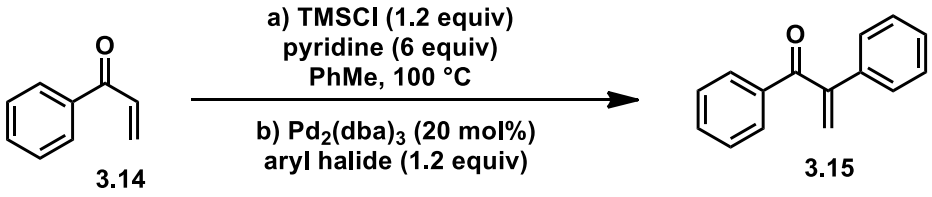

Entry	Aryl Halide	Result
1	3.10	No rxn
2	3.11	No rxn
3	3.12	No rxn

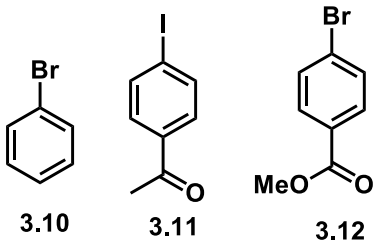

Table 3.14 Evaluation of electron withdrawn aryl halides with most reactive nucleophilic amine bases using $Pd_2(dba)_3$

used by Szpilman's group to develop the umpolung MBH methodology and then revisited these reaction conditions (Scheme 3.7).

Acrylophenone **3.14** was synthesized through an aldol condensation between acetephenone **3.13** and paraformaldehyde catalyzed by diisopropylamine and trifluoroacetic acid (Scheme 3.7). With acrylophenone **3.14** in hand, we attempted using an α-arylation using electron-deficient aryl halides but unfortunately still did not observe any reactivity (Table 3.14). Without any encouraging or promising results from these Lewis cid catalyzed strategy to guide future work, we decided to explore frustrated Lewis air conditions, which have not been previously explored in the context of α-arylations.

3.4 Frustrated Lewis Pair Exploration

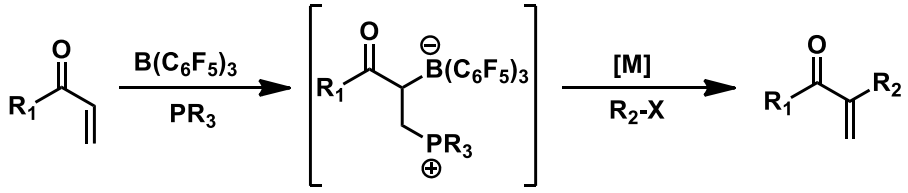

Scheme 3.8 Potential reaction pathway using frustrated ligand pairs to access α-functionalization of α,β-unsaturated ketones

Another intriguing possibility for future work is to incorporate frustrated Lewis pairs to facilitate and capture new and unexpected reactivity. In its application to organic chemistry, a frustrated Lewis pair can be described as a compound containing a Lewis acid and a Lewis base that cannot come together to form a classical adduct due to steric hinderance.[29–31] The inherent energy from the 'frustration' of the Lewis pairs not being able to combine could lead to new and unexpected reactivity. Although an interesting proposal, there has been relatively little exploration for the application of frustrated Lewis

pairs to organic chemistry and what type of reactivity may be observed. To that effect, we would still like to find a way to perform an α-functionalization of an α,β-unsaturated ketone (Scheme 3.8); however, we are open to the possibility of uncovering new unexpected reactivity and products that may lead us in a new direction away from our originally intended path. Although frustrated Lewis pairs have not been explored extensively in organic chemistry, there has been some investigations into catalysis and the activation of small molecules.[31] Specifically, frustrated Lewis pairs have been explored with hydrogenations, activating alkynes, and reactions with carbon dioxide (Scheme 3.9).

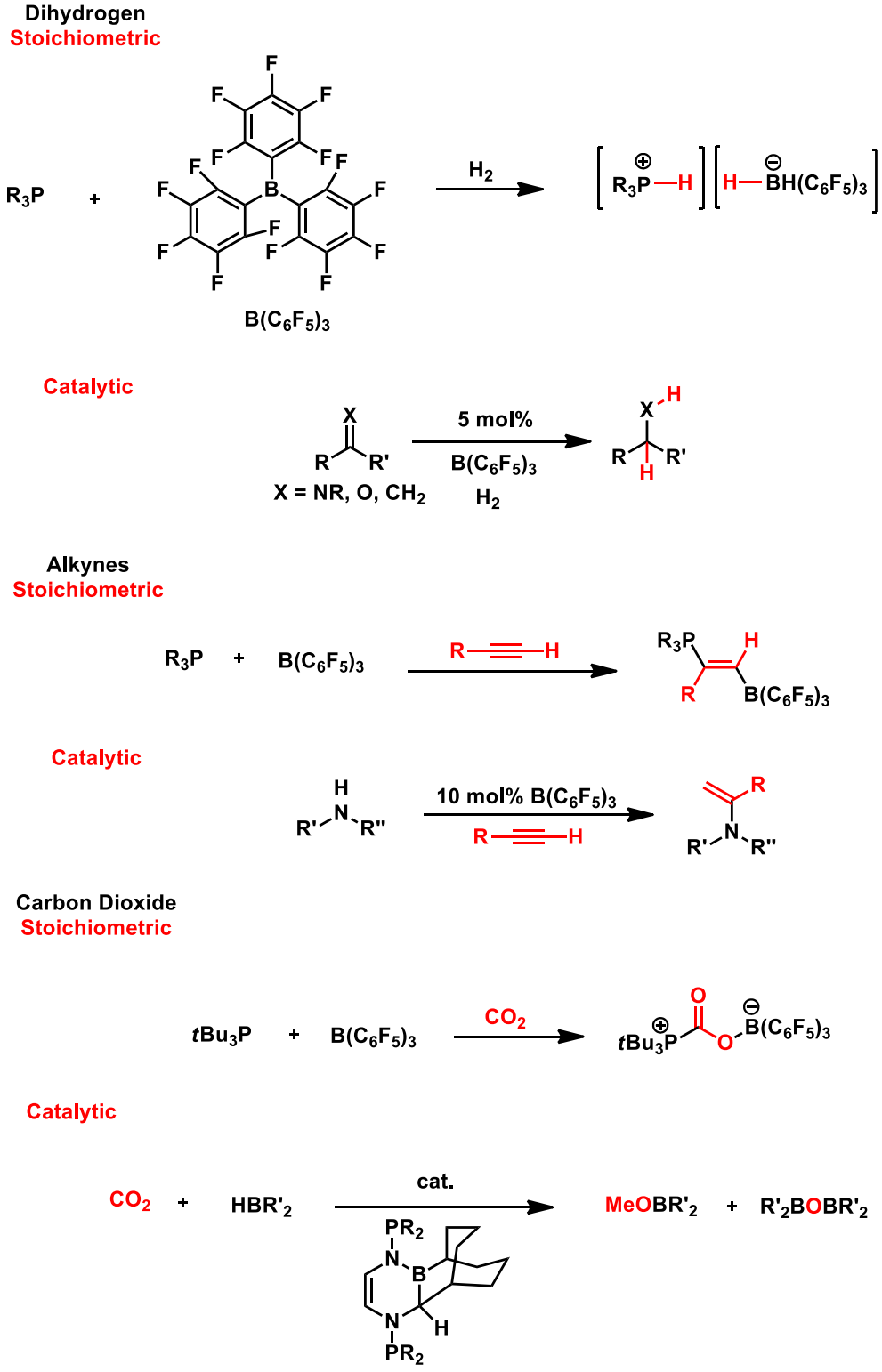

Scheme 3.9 Frustrated Lewis pair reactions with dihydrogen, alkynes, and carbon dioxide

To explore the frustrated Lewis pair concept, we selected to begin with cyclohexenone (**3.1**), tris(pentafluorophenyl)borane, and various bulky phosphines (Table 3.15). The phosphine ligands evaluated were PCy_3, $P(tBu)_3$, PCP Pincer, and PCP Pincer Pyridine. These ligands were chosen because of their varying degrees of steric bulk. Generally, we hypothesized that a very bulky phosphine ligand would be ideal because of

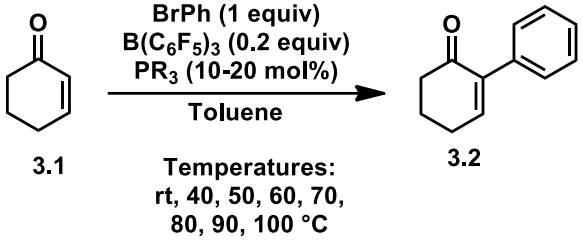

3.1 3.2

Entry	Ligand	Result
1	$P(Cy)_3$	No Rxn
2	$P(tBu)_3$	No Rxn
3	PCP Pincer	No Rxn
4	PCP Pincer Pyridine	No Rxn

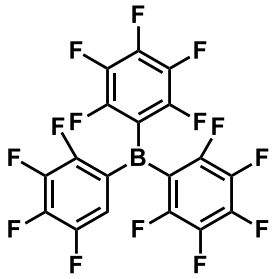

Tris(pentafluorophenyl)borane (3.16)

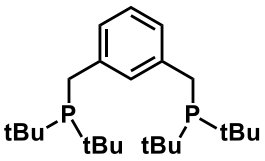

PCP Pincer (3.17)

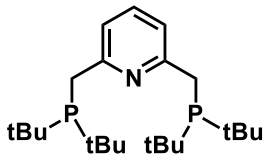

PCP Pyridine (3.18)

Table 3.15 Exploration of frustrated Lewis pair strategy

the increased "frustration" associated with the bulk of the phosphine and borane, which could possibly effect new reactivity. We also added bromobenzene as an aryl source and began with temperature experiments to search for initial reactivity. So far, we have experimented with increasing temperature up to 100 °C in toluene as the solvent, but unfortunately no reaction was observed and only starting materials were recovered.

Our next strategy was to explore the use of transition metal catalysts with the 'frustrated Lewis pair' strategy in the presence of 2-aminoethyl diphenylborinate as a phenylating

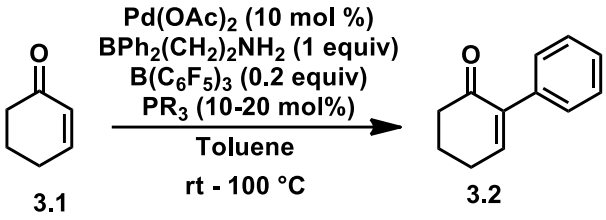

Entry	Ligand	Result
1	$P(Cy)_3$	No Rxn
2	$P(tBu)_3$	No Rxn
3	PCP Pincer	No Rxn
4	PCP Pincer Pyridine	No Rxn

Table 3.16 Exploration of frustrated Lewis pair strategy with palladium

agent (Table 3.16 and 3.17). We hypothesized that perhaps a transition metal could catalyze a coupling reaction between an enolate-type intermediate of enone **3.1** and the diphenylborinate in order to access the desired α-functionalized enone product **3.2**. First,

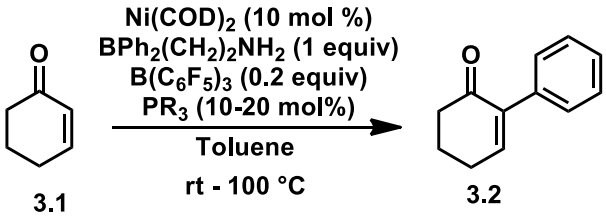

Entry	Ligand	Result
1	$P(Cy)_3$	No Rxn
2	$P(tBu)_3$	No Rxn
3	PCP Pincer	No Rxn
4	PCP Pincer Pyridine	No Rxn

Table 3.17 Exploration of frustrated Lewis pair strategy with nickel

we evaluated palladium acetate (II) as the catalyst with various phosphine ligands, all of which remained bulky in order to maintain the 'frustrated Lewis pair' strategy (scheme 3.16). Unfortunately, at room temperature and elevated temperatures of 100 °C, no reaction was observed and only starting material was recovered. We similarly employed bis(1,5-cyclooctadiene)nickel (0) as the catalyst, but again at room temperature and elevated temperatures, no reaction occurred and only starting materials were recovered (Scheme 3.17).

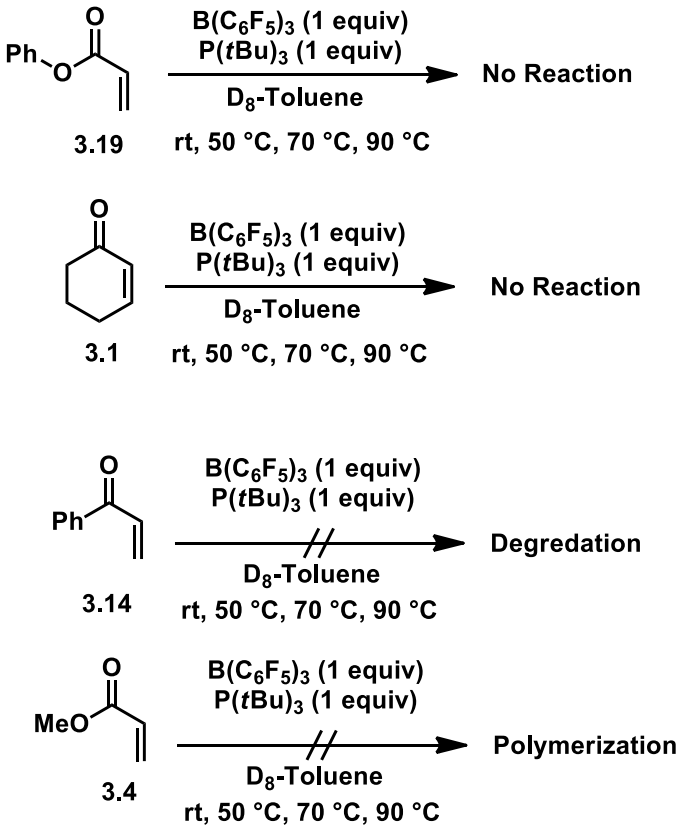

Scheme 3.10 VT NMR experiments of enones under frustrated Lewis pair conditions

Since we have been experiencing difficulties observing any reactivity under the frustrated Lewis pair conditions, we performed variable temperature (VT) NMR

experiments on four different enones that had the highest potential of success for this type of chemistry: phenyl acrylate (**3.19**), cyclohexenone (**3.1**), acrylophenone (**3.19**), and methyl acrylate (**3.4**) (Scheme 3.10). The goal of these experiments was to subject each enone to equimolar amounts of the highly bulky tris(pentafluorophenyl)borane (**3.16**) and P(*t*Bu)$_3$ and use VT-NMR experiments to observe the reactivity. We hypothesized that if the enone reacted with the borane and phosphine, we would at least see a shift in the NMR signals corresponding to the alkene protons if there was a simple ketone-borane coordination. We also hypothesized that if the borane coordinated to the ketone and activated the β-position for the phosphine attack, then we would observe the disappearance of the alkene protons and the emergence of new signals corresponding to the enolate intermediate. For the VT-NMR experiments, we prepared the reaction mixtures in a nitrogen-filled glovebox using deuterated toluene, and then upon removal from the glovebox, the VT-NMR experiments were immediately started. Proton NMR spectra were collected at room temperature, 50 °C, 70 °C, and 90 °C. Unfortunately, by comparison to reference spectra of each enone, we observed no reactivity or degradation at any of these temperatures for phenyl acrylate (**3.19**) or cyclohexenone (**3.1**). Surprisingly, acrylophenone (**3.14**) rapidly degraded by the first experiment at room temperature. It is unclear whether the acrylophenone was completely degraded before the borane and phosphine was added or if they contributed to the decomposition, so this experiment will have to repeated. When methyl acrylate (**3.4**) was subjected to the frustrated Lewis pair conditions, it immediately polymerized but this is likely due to the heat of the reaction catalyzing the polymerization. Given the susceptibility of methyl acrylate to readily

polymerize, it suggests that methyl acrylate is not the ideal enone to develop this chemistry because the polymerization reaction will likely be a competitive side-reaction that will be difficult to overcome.

3.5 Secondary Amine Additives

Although we did not explore many transition metals, we were interested to see if any interesting reactivity could be achieved by the addition of a secondary amine and a nucleophilic amine or phosphine. We hypothesized that the secondary amine could

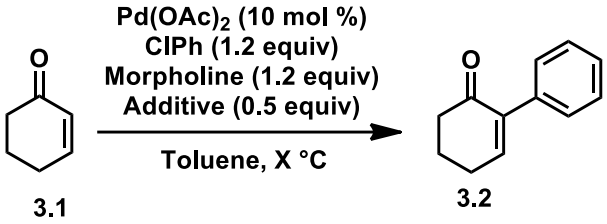

Entry	Additive	Temp.	Result
1	DMAP	rt	No Rxn
2	DMAP	50 °C	No Rxn
3	DMAP	100 °C	No Rxn
4	PCy_3	rt	No Rxn
5	PCy_3	50 °C	No Rxn
6	PCy_3	100 °C	No Rxn

Table 3.18 Evaluation of morpholine addition with DMAP and PCy_3

condense onto ketone **3.1** forming the corresponding iminium which may then be more reactive to the nucleophilic attack of the amine-base or phosphine. For these experiments we chose to use a morpholine as the secondary amine and PCy_3 or DMAP as the nucleophilic additive (Table 3.18). Additionally, we also switched the phenylating agent to chlorobenzene. We screened each set of conditions at room temperature, 50 °C, and 100

°C (Table 3.18, entries 1–6). However, the varied conditions and temperatures resulted in no reaction. Concurrently, we also explored similar conditions but instead with piperidine as the secondary amine (Table 3.19). However, these reactions with piperidine also resulted in no reaction, with only starting materials recovered. In each of these sets of

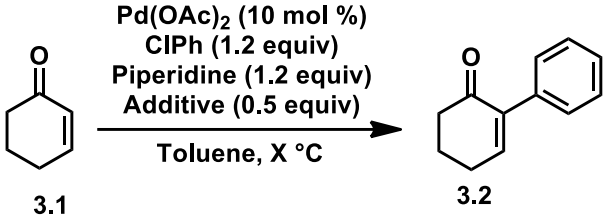

3.1 3.2

Entry	Additive	Temp.	Result
1	DMAP	rt	No Rxn
2	DMAP	50 °C	No Rxn
3	DMAP	100 °C	No Rxn
4	PCy_3	rt	No Rxn
5	PCy_3	50 °C	No Rxn
6	PCy_3	100 °C	No Rxn

Table 3.19 Evaluation of piperidine addition with DMAP and PCy_3

experiments, at 100 °C the palladium catalyst crashed out of solution eventually, perhaps suggesting that these conditions were too harsh or simply unstable for the palladium catalyst. To follow up on these experiments, it would be very interesting to study this reaction by NMR to perhaps be able to observe the condensation reaction followed by addition of the nucleophile in order to better understand the reaction sequence and determine the unsuccessful step in the sequence.

3.6 Conclusions and Future Directions

Despite exploring and evaluating many different reaction conditions in attempt to develop an MBH inspired cross coupling reaction with reverse selectivity to the traditional Heck reaction, which would generate valuable α-arylated products, we unfortunately only observed low degrees of reactivity towards traditional Heck coupling and dimerization products. We found it especially surprising that we did not observe any α-arylation reactivity given the abundance of literature precedent for α-functionalization utilizing an enolate intermediate, such as the work by Buchwald, Hartwig, and others.[14–20] However, despite the discouraging results, the value and utility of a MBH coupling reaction motivates us to continue to propose and evaluate hypotheses to develop this reaction. Future work for the development of this Morita–Baylis–Hillman reaction includes investigating different conditions to access an activated highly reactive intermediate *in situ* that is primed to react with electrophiles at the α-position. Our work until this point has been focused on arylation reactions utilizing the feedstock of aryl halides that are readily available as well as 2-aminoethyl diphenylborinate. However, there are still a wide variety of possible coupling partners to be examined. Interesting coupling partners include triflates, boronic acids, acyl fluorides, and other less commonly used moieties. Additionally, another relatively simple variation to explore is alkyl and vinylic halides as coupling partners. There are also many unexplored possibilities for finding new and unpredictable reactivity using the frustrated Lewis-pair strategy, which makes this route more motivating.

3.7 Experimental Section

General Considerations

i) Solvents and reagents

Unless noted below, commercial reagents were purchased from MilliporeSigma, Acros Organics, Chem-Impex, Combi-blocks, TCI, and/or Alfa Aesar, and used without additional purification. Solvents were purchased from Fisher Scientific, Acros Organics, Alfa Aesar, and Sigma Aldrich. Tetrahydrofuran (THF), diethyl ether (Et_2O), acetonitrile (CH_3CN), benzene, methanol (MeOH), and triethylamine (Et_3N) were sparged with argon and dried by passing through alumina columns using argon in a Glass Contour solvent purification system. Dichloromethane (CH_2Cl_2) was freshly distilled over calcium hydride under a N_2 atmosphere prior to each use. DMSO and toluene (PhMe) were distilled over calcium hydride under a N_2 atmosphere, degassed via freeze-pump-thaw (3 cycles), and stored over 4 Å molecular sieves in a Schlenk flask under N_2. Dimethoxyethane (DME), *p*-xylene, dimethylformamide (DMF), MeLi solution, *n*-BuLi solution, LiHMDS solution, Red-Al solution, and pyridine were purchased in Sure/Seal, AcroSeal, or ChemSeal bottling, and used directly. 1,4-Dioxane was purchased in AcroSeal bottling (99.5%, anhydrous, stabilized, over 4 Å molecular sieves) and additionally sparged with N_2 prior to use.

ii) Reaction setup, progress monitoring, and product purification

Unless otherwise noted in the experimental procedures, reactions were carried out in flame or oven dried glassware under a positive pressure of N_2 in anhydrous solvents using standard Schlenk techniques. Reaction progresses were monitored using thin-layer chromatography (TLC) on EMD Silica Gel 60 F254 or Macherey–Nagel SIL HD (60 Å mean pore size, 0.75 mL/g specific pore volume, 5–17 μm particle size, with fluorescent indicator)silica gel plates. Visualization of the developed plates was performed under UV light (254 nm). Purification and isolation of products were performed via silica gel chromatography (both column and preparative thin-layer chromatography). Commercial reagents were purchased from MilliporeSigma, Acros Organics, Chem-Impex, TCI, Oakwood, and Alfa Aesar, and used without additional purification. Solvents were purchased from Fisher Scientific, Acros Organics, Alfa Aesar, and Sigma Aldrich. Tetrahydrofuran (THF), diethyl ether (Et_2O), acetonitrile (MeCN), dichloromethane (CH_2Cl_2), benzene, 1,4-dioxane, and triethylamine (Et_3N) were sparged with argon and dried by passing through alumina columns using argon in a Glass Contour (Pure Process Technology) solvent purification system. Dimethylformamide (DMF), dimethyl sulfoxide (DMSO), and dichloroethane (DCE) were purchased in Sure/Seal or AcroSeal bottling and additionally sparged with N_2 prior to use.

iii) Analytical instrumentation

NMR spectral data were obtained using deuterated solvents obtained from Cambridge Isotope Laboratories, Inc. ^{1}H NMR and ^{13}C NMR data were recorded on Bruker Avance

NEO400 or Bruker Avance 600 MHz spectrometers using $CDCl_3$, typically at 20–23 °C. Chemical shifts (δ) are reported in ppm relative to the residual solvent signal (δ 7.26 for ^1H NMR, δ 77.16 for ^{13}C NMR in $CDCl_3$). Data for ^1H NMR spectroscopy are reported as follows; chemical shift (δ ppm), multiplicity (s = singlet, d = doublet, t = triplet, q = quartet, m = multiplet, br = broad, dd = doublet of doublets, dt = doublet of triplets), coupling constant (Hz), integration. Data for ^{13}C and ^{19}F NMR spectroscopy are reported in terms of chemical shift (δ ppm). IR spectroscopic data were recorded on a NICOLET 6700 FT-IR spectrophotometer using a diamond attenuated total reflectance (ATR) accessory. Samples are loaded onto the diamond surface either neat or as a solution in organic solvent and the data acquired after the solvent had evaporated. High resolution accurate mass spectral data were obtained from the Analytical Chemistry Instrumentation Facility at the University of California, Riverside, on an Agilent 6545 Q-TOF LC/MS instrument (supported by NSF grant CHE-0541848)

3.8 Experimental Procedures and Characterization Data

Preparation of 3-Phenylcyclohex-2-enone (3.3)

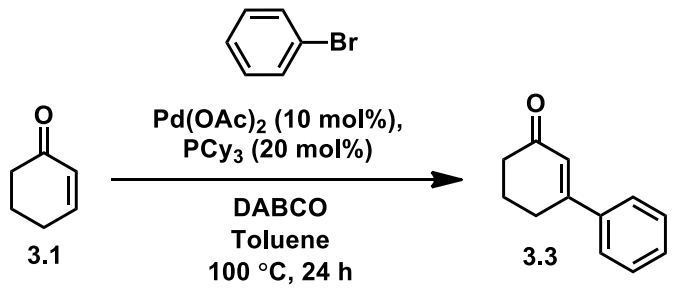

3-Phenylcyclohex-2-enone (3.3). Procedure 1: In a nitrogen-filled glovebox, to a 4 mL vial was added 2-cyclohexenone (51.6 μL, 0.52 mmol, 1 equiv), bromobenzene (67.1 μL, 0.62 mmol, 1.2 equiv), and 1,4-diazabicyclo[2.2.2]octane (58.4 mg, 0.52 mmol, 1 equiv) followed by 1 mL of toluene. In a separate 4 mL vial was added palladium acetate (11.2 mg, 0.050 mmol, 0.1 equiv), tricyclohexylphosphine (16.3 mg, 0.058 mmol, 0.2 equiv), and 1.0 mL of toluene. Each solution was allowed to pre-mix at rt for 10 min, after which the catalyst solution was transferred to the organic reagents solution. The reaction vial was then removed from the glovebox and allowed to stir at 100 ˚C for 24 h. The reaction mixture was allowed to cool to rt, and then filtered through a pad of silica gel (eluting with diethyl ether) and concentrated in *vacuo*. The crude reaction mixture was then purified by silica gel flash column chromatography eluting with hexanes/EtOAc (4:1) to provide **3.3** as a clear oil (26.9 mg, 0.156 mmol, 30%).

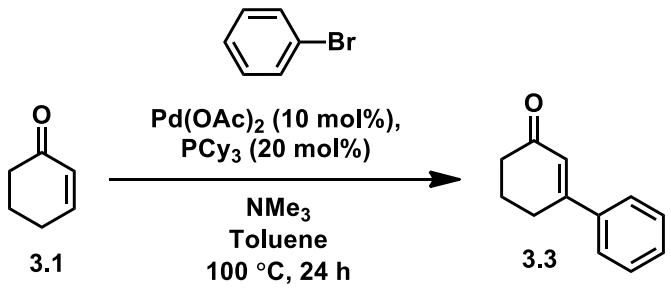

Procedure 2: In a nitrogen-filled glovebox, to a 4 mL vial was added 2-cyclohexenone (51.6 μL, 0.52 mmol, 1 equiv), bromobenzene (67.1 μL, 0.62 mmol, 1.2 equiv), and trimethylamine (200 μL, 0.52 mmol, 1 equiv) followed by 1.0 mL of toluene. In a separate

4 mL vial was added palladium acetate (11.2 mg, 0.050 mmol, 0.1 equiv), tricyclohexylphosphine (16.3 mg, 0.10 mmol, 0.2 equiv), and 1 mL of toluene. Each solution was allowed to pre-mix at rt for 10 min, after which the catalyst solution was transferred to the organic reagents solution. The reaction vial was then removed from the glovebox and allowed to stir at 100 ˚C for 24 h. The reaction mixture was allowed to cool to rt, then filtered through a pad of silica gel (eluting with diethyl ether) and concentrated under reduced pressure.. The crude reaction mixture was then purified by silica gel flash column chromatography eluting with hexanes/EtOAc (4:1) to provide 3.**3** as a clear oil (24.2 mg, 0.140 mmol, 27%).

^{1}H NMR (400 MHz, $CDCl_3$) δ 7.55–7.48 (m, 2H), 7.43–7.36 (m, 3H), 6.44 (m, 1H), 2.79–2.72 (m, 2H), 2.50–2.43 (m, 2H), 2.19–2.13 (m, 2H); ^{13}C NMR (101 MHz, $CDCl_3$) δ 199.9 159.8, 138.8, 130.0, 128.7, 126.1, 125.5, 37.3, 28.1, 22.8 ppm. HRMS (ESI+) *m/z* calc'd for $C_{12}H_{13}O$ $[M+H]^+$: 173.0888, found 173.0957 $[H^+]$ and 195.0777 $[Na^+]$. Spectral data matches literature references[32]

Preparation of E-Methyl cinnamate (3.6)

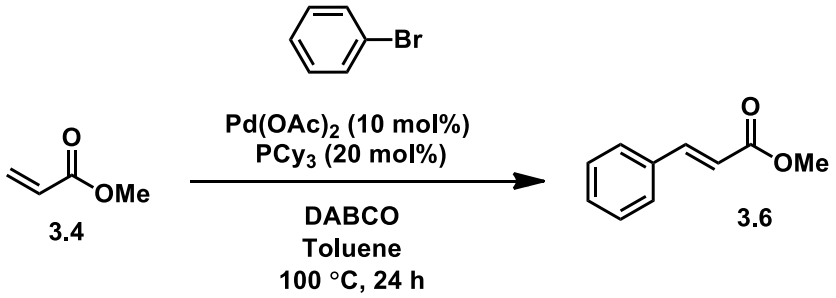

Procedure 1: In a nitrogen-filled glovebox, to a 4 mL vial was added methyl acrylate (53.1 μL, 0.58 mmol, 1 equiv), bromobenzene (75.4 μL, 0.70 mmol, 1.2 equiv), and 1,4-diazabicyclo[2.2.2]octane (65.2 mg, 0.58 mmol, 1 equiv) followed by 1 mL of toluene. In a separate 4 mL vial was added palladium acetate (13.0 mg, 0.06 mmol, 0.1 equiv), tricyclohexylphosphine (32.6 mg, 0.12 mmol, 0.2 equiv), and 1 mL of toluene. Each solution was allowed to pre-mix at rt for 10 min, after which the catalyst solution was transferred to the solution containing reagents. The reaction vial was then removed from the glovebox and allowed to stir at 100 ˚C for 24 h. The reaction was allowed to cool to rt then filtered through a pad of silica gel (eluting with Et_2O) and concentrated in under reduced pressure. The crude reaction mixture was then purified by silica gel flash column chromatography eluting with hexanes/EtOAc (4:1) to provide **3.6** as a clear oil (26.6 mg, 0.164 mmol, 35%).

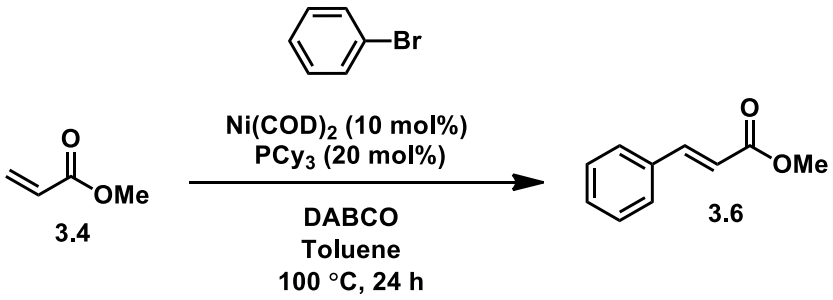

Procedure 2: In a nitrogen-filled glovebox, to a 4 mL vial was added methyl acrylate (53.1 μL, 0.58 mmol, 1 equiv), bromobenzene (75.4 μL, 0.70 mmol, 1.2 equiv), and 1,4-

diazabicyclo[2.2.2]octane (65.2 mg, 0.58 mmol, 1 equiv) followed by 1 mL of toluene. In a separate 4 mL vial was added Bis(1,5-cyclooctadiene)nickel(0) (16.2 mg, 0.059 mmol, 0.1 equiv), tricyclohexylphosphine (32.6 mg, 0.116 mmol, 0.2 equiv), and 1 mL of toluene. Each solution was allowed to pre-mix at rt for 10 min, after which the catalyst solution was transferred to the solution containing reagents. The reaction vial was then removed from the glovebox and allowed to stir at 100 ˚C for 24 h. The reaction mixture was allowed to cool to rt, and then filtered through a pad of silica gel, eluting with Et_2O and concentrated *under reduced pressure*. The crude reaction mixture was then purified by silica gel flash column chromatography eluting with hexanes/EtOAc (4:1) to provide **3.6** as a clear oil.

^{1}H NMR (400 MHz, $CDCl_3$) δ 7.70 (d, *J*= 16.0 Hz, 1H), 7.56 –7.46 (m, 2H), 7.43 –7.31 (m, 3H), 6.44 (d, *J*= 16.0 Hz, 1H), 3.80 (s, 3H). ^{13}C NMR (101 MHz, $CDCl_3$) δ 167.5, 144.9, 134.4, 130.4, 128.9, 128.1, 117.8, 51.8. Spectral data matches literature reference.[33]

Preparation of acrylophenone (3.14)

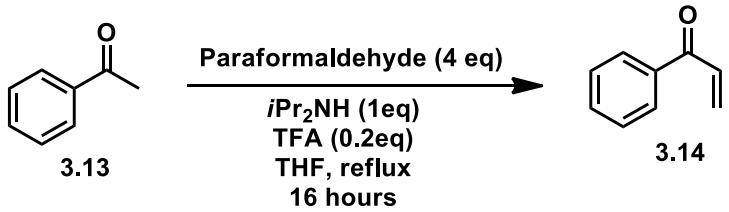

Arylophenone 3.14. According to a modified procedure[34], to a solution of acetophenone (25.0 mmol, 2.91 mL) and paraformaldehyde (49.9 mmol, 1.50 g) in dry THF (25 mL) was

added diisopropylamine (25 mmol, 3.5 mL) and trifluoroacetic acid (5.0 mmol, 0.38 mL). The reaction mixture was stirred at reflux for 2 h, then cooled to rt and a second batch of paraformaldehyde (50 mmol, 1.50 g) was added. Next, the reaction mixture was stirred at reflux overnight (16 h). Upon completion, the reaction was cooled and the solvent was removed under reduced pressure. The resulting residue was suspended in Et_2O and washed with 1N HCl, 1N NaOH, and brine. The resulting solution was dried over Na_2SO_4 and concentrated under reduced pressure. The crude product was purified by silica gel flash column chromatography eluting with hexanes/EtOAc (20:1) to give **3.14** as a light orange oil (2.91 g, 16.6 mmol, 66%)

^{1}H NMR ($CDCl_3$, 400 MHz) δ 7.93 (2H, d, *J* = 9.2 Hz), 7.53-7.55 (1H, m), 7.43-7.47 (2H, m), 7.15 (1H, dd, *J* = 17.2, 10.8 Hz), 6.42 (1H, d, *J* = 17.2 Hz), 5.90 (1H, d, *J* = 10.8 Hz); ^{13}C NMR ($CDCl_3$, 100 MHz) δ 190.8, 137.1, 132.8, 132.1, 130.0, 128.5, 128.4. Spectral data matches literature reference.[34]

3.9. ^{1}H and ^{13}C NMR Spectra

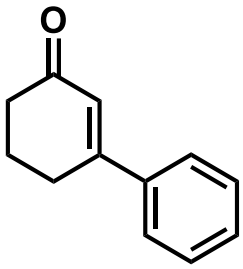

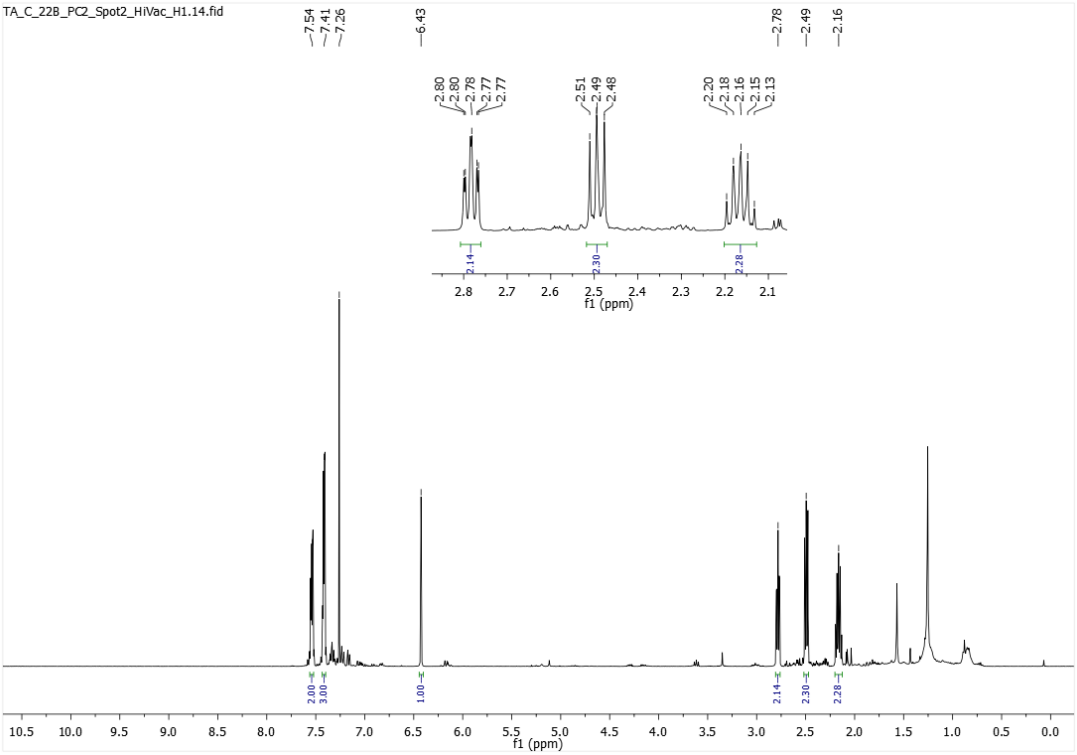

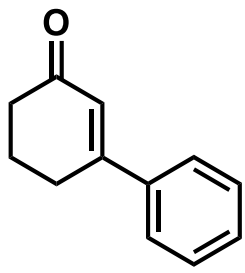

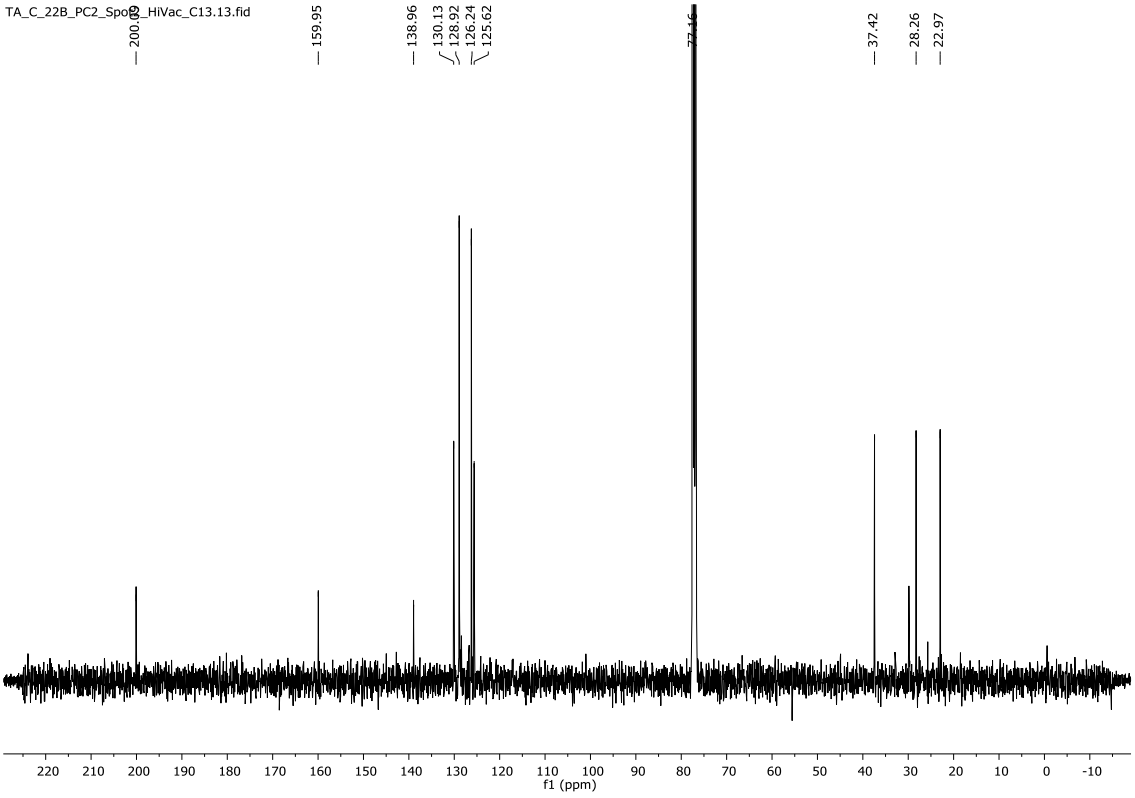
TA_C_22B_PC2_Spot3_HiVac_C13.13.fid
200.03
159.95
138.96
130.13
128.92
126.24
125.62
77.16
37.42
28.26
22.97
220 210 200 190 180 170 160 150 140 130 120 110 100 90 80 70 60 50 40 30 20 10 0 -10
f1 (ppm)

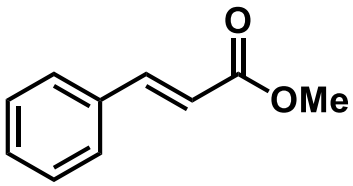
O
OMe

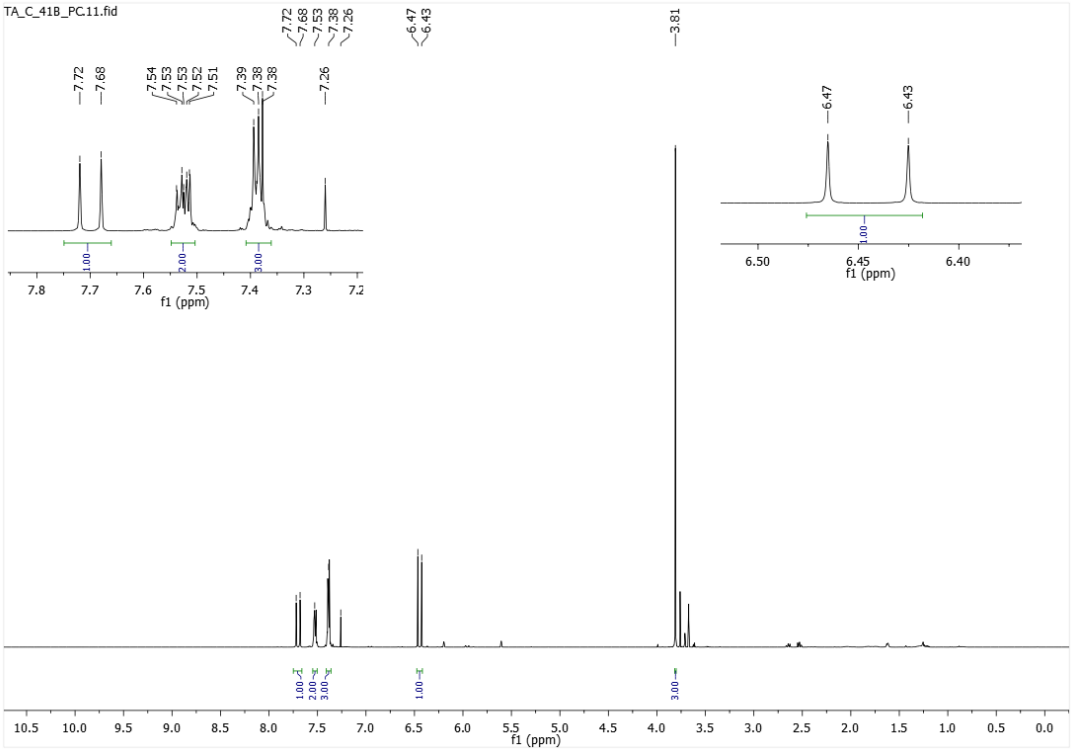
TA_C_418_PC.11.fid
f1 (ppm)

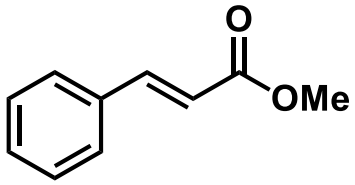
O
OMe

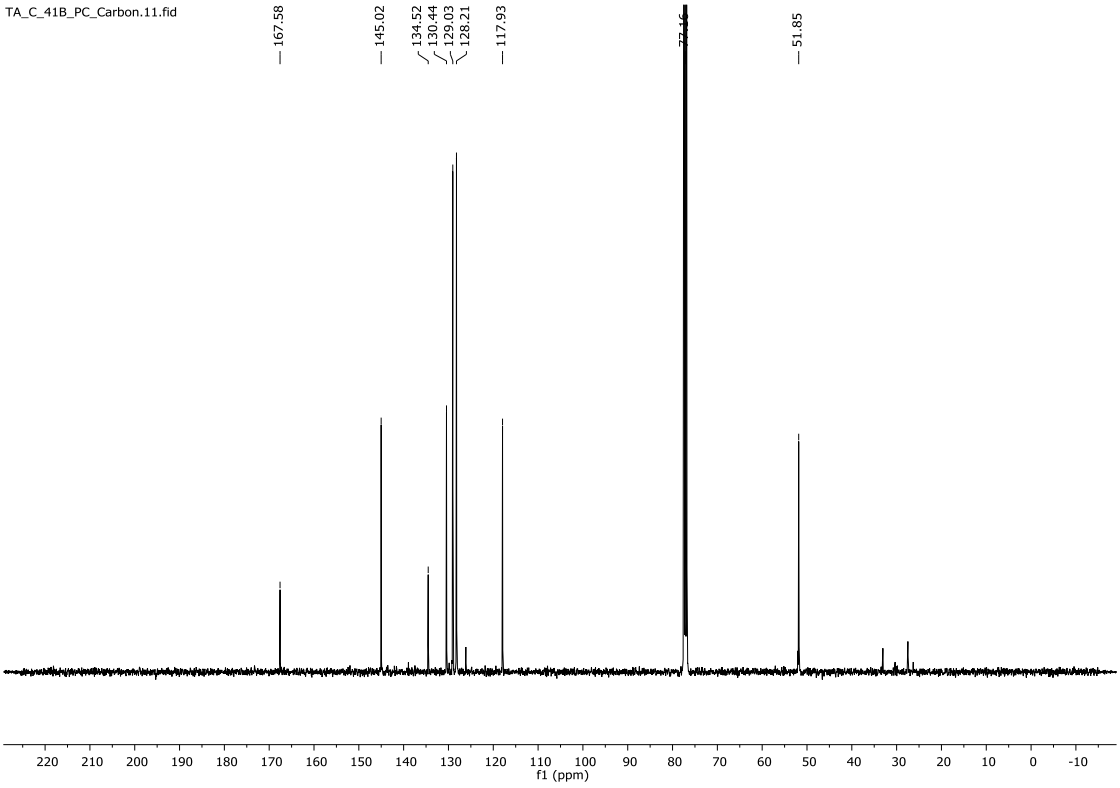
TA_C_41B_PC_Carbon.11.fid
167.58
145.02
134.52
130.44
129.03
128.21
117.93
77.16
51.85
220 210 200 190 180 170 160 150 140 130 120 110 100 90 80 70 60 50 40 30 20 10 0 -10
f1 (ppm)

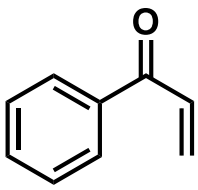

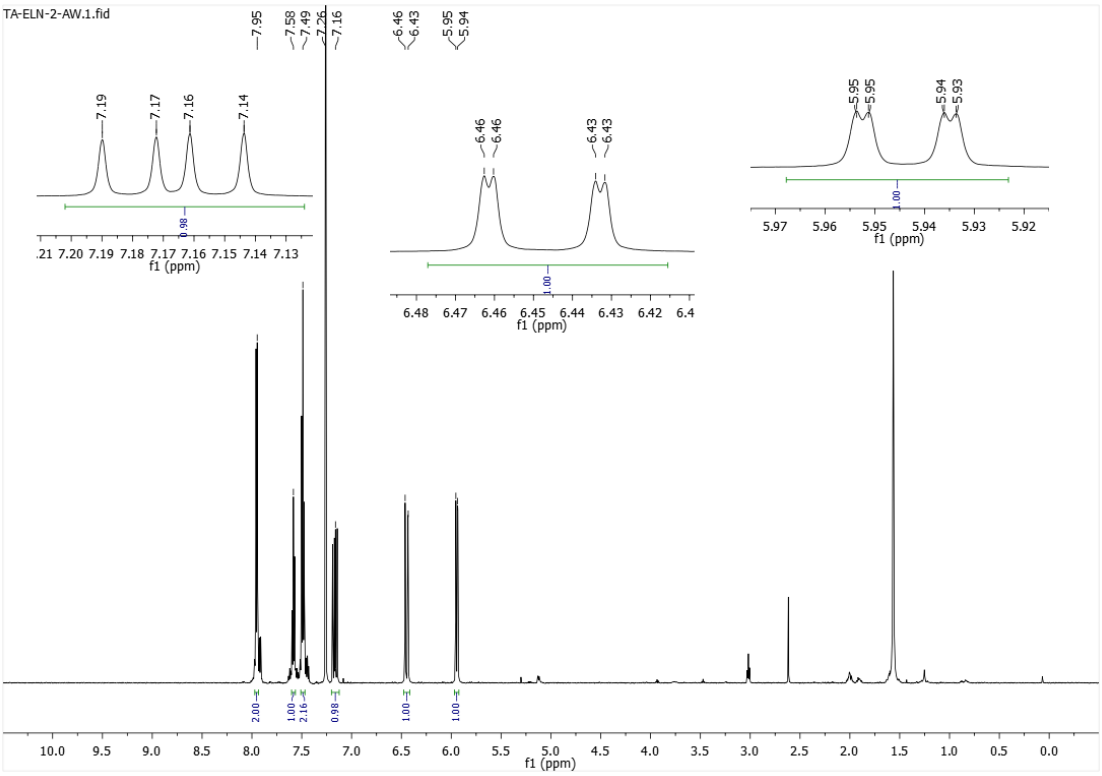
TA-ELN-2-AW.1.fid
7.95
7.58
7.49
7.26
7.16
6.46
6.43
5.95
5.94
7.19
7.17
7.16
7.14
6.46
6.46
6.43
6.43
5.95
5.95
5.94
5.93
f1 (ppm)
2.00
1.00
2.16
0.98
1.00
1.00

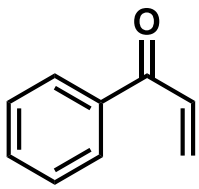

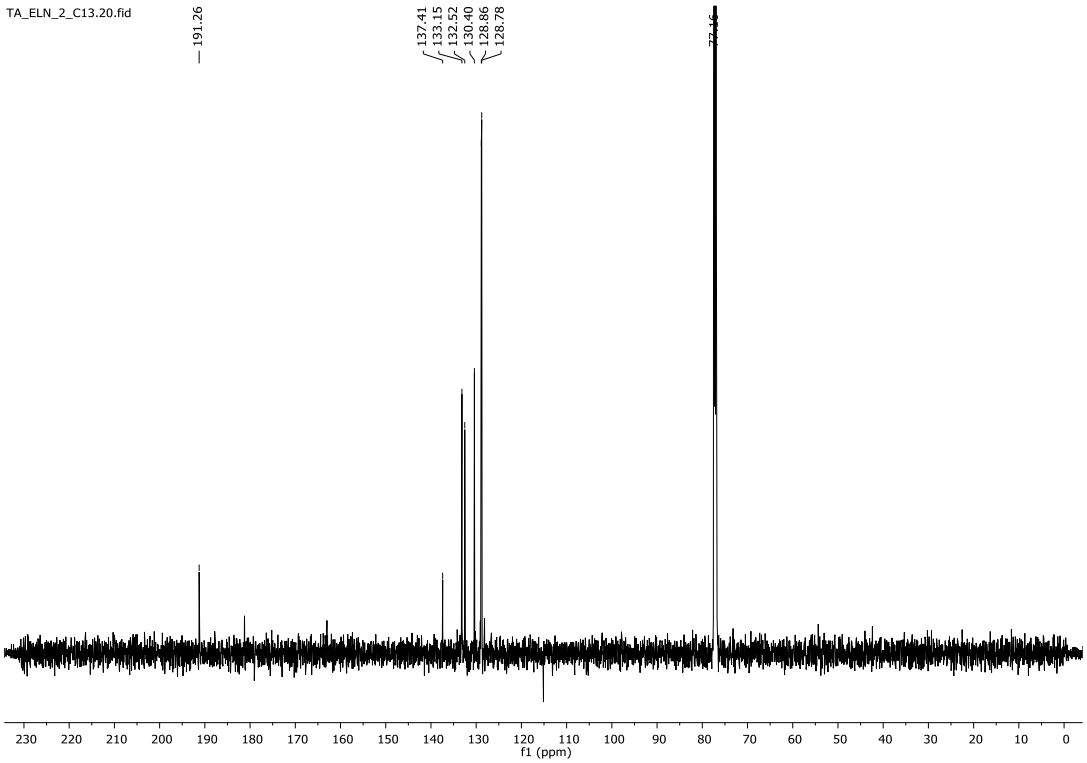
TA_ELN_2_C13.20.fid
191.26
137.41
133.15
132.52
130.40
128.86
128.78
77.16
230 220 210 200 190 180 170 160 150 140 130 120 110 100 90 80 70 60 50 40 30 20 10 0
f1 (ppm)

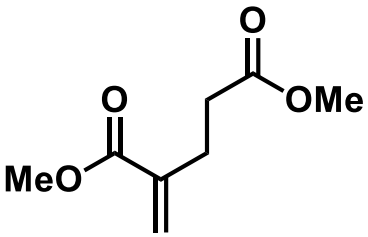
O
O
OMe
MeO

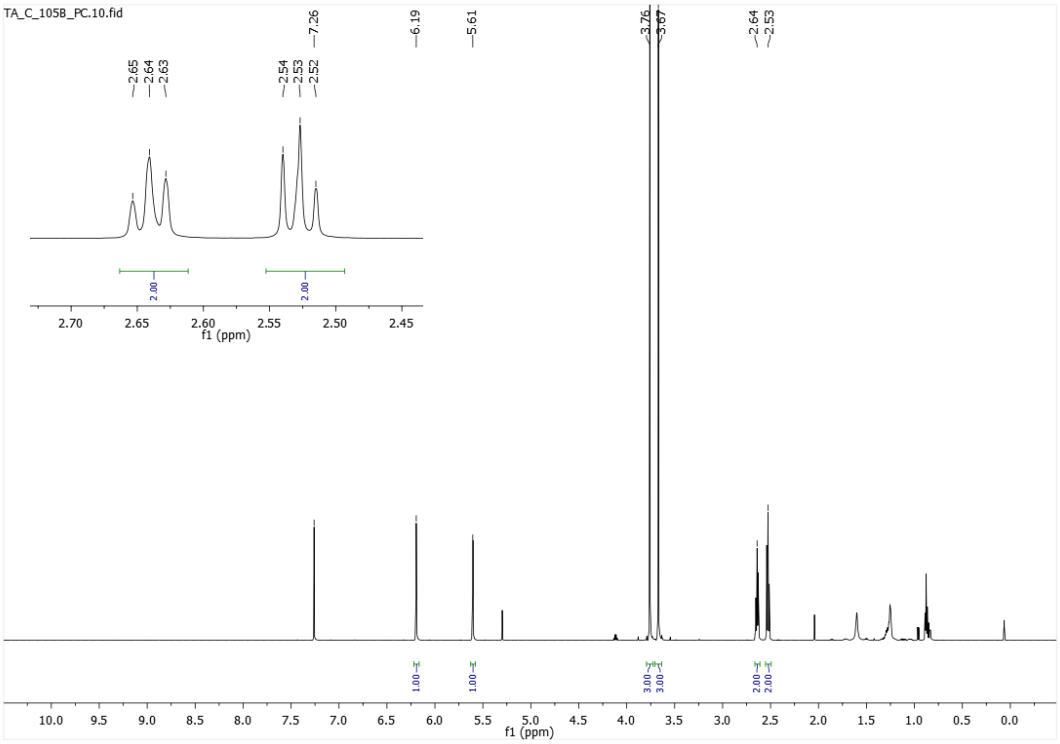
TA_C_105B_PC.10.fid
7.26
6.19
5.61
3.76
3.67
2.64
2.53
2.65
2.64
2.63
2.54
2.53
2.52
2.00
2.00
2.70
2.65
2.60
2.55
2.50
2.45
f1 (ppm)
1.00
1.00
3.00
3.00
2.00
2.00
10.0
9.5
9.0
8.5
8.0
7.5
7.0
6.5
6.0
5.5
5.0
4.5
4.0
3.5
3.0
2.5
2.0
1.5
1.0
0.5
0.0
f1 (ppm)

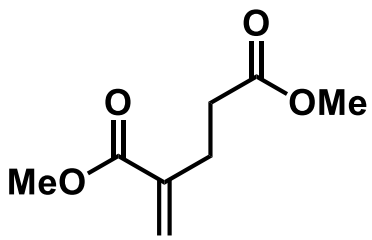
O
O
OMe
MeO

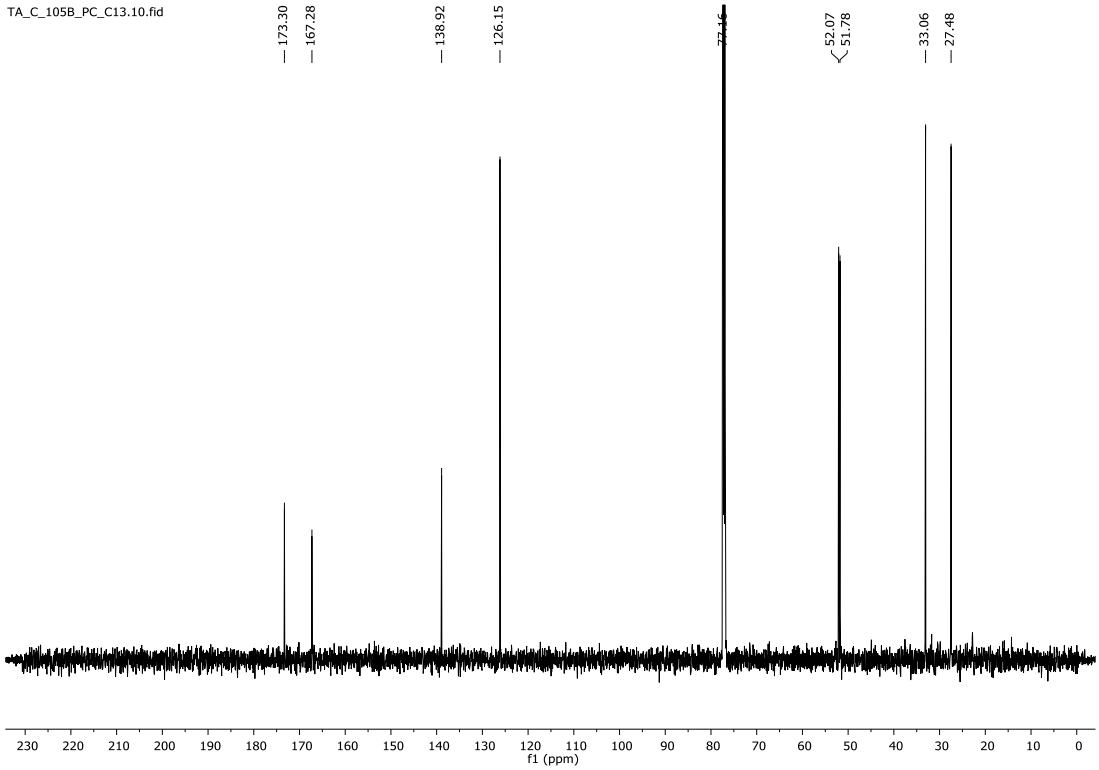
TA_C_105B_PC_C13.10.fid
173.30
167.28
138.92
126.15
77.46
52.07
51.78
33.06
27.48
230 220 210 200 190 180 170 160 150 140 130 120 110 100 90 80 70 60 50 40 30 20 10 0
f1 (ppm)

3.10 References

(1) Morita, K.; Suzuki, Z.; Hirose, H. A Tertiary Phosphine-Catalyzed Reaction of Acrylic Compounds with Aldehydes. *BCSJ* **1968**, *41* (11), 2815–2815. https://doi.org/10.1246/bcsj.41.2815.

(2) Zhong, N.-J.; Wang, Y.-Z.; Cheng, L.; Wang, D.; Liu, L. Recent Advances in the Annulation of Morita–Baylis–Hillman Adducts. *Org. Biomol. Chem.* **2018**, *16* (29), 5214–5227. https://doi.org/10.1039/C8OB00929E.

(3) Ma, G.-N.; Jiang, J.-J.; Shi, M.; Wei, Y. Recent Extensions of the Morita–Baylis–Hillman Reaction. *Chem. Commun.* **2009**, No. 37, 5496–5514. https://doi.org/10.1039/B909405A.

(4) Perlmutter, P.; Chin Teo, C. A Simple Synthesis of 2-Methylidene-3-Aminopropanoates. *Tetrahedron Letters* **1984**, *25* (51), 5951–5952. https://doi.org/10.1016/S0040-4039(01)81730-5.

(5) Taniguchi, M.; Hino, T.; Kishi, Y. Aldol Reaction of Allenolates Generated via 1,4-Addition of Iodide Anion or Its Equivalent to α,β-Acetylenic Ketones. *Tetrahedron Letters* **1986**, *27* (39), 4767–4770. https://doi.org/10.1016/S0040-4039(00)85060-1.

(6) Iwama, T.; Kinoshita, H.; Kataoka, T. 2,6-Diphenyl-4H-Chalcogenopyran-4-Ones and 2,6-Diphenyl-4H-Chalcogenopyran-4-Thiones: A New Catalyst for the Baylis-Hillman Reaction. *Tetrahedron Letters* **1999**, *40* (19), 3741–3744. https://doi.org/10.1016/S0040-4039(99)00585-7.

(7) Yeo, J. E.; Yang, X.; Kim, H. J.; Koo, S. The Intramolecular Baylis–Hillman Reaction: Easy Preparation of Versatile Substrates, Facile Reactions, and Synthetic Applications. *Chem. Commun.* **2004**, No. 2, 236–237. https://doi.org/10.1039/B311951C.

(8) Trofimov, A.; Gevorgyan, V. Sila-Morita−Baylis−Hillman Reaction of Arylvinyl Ketones: Overcoming the Dimerization Problem. *Org. Lett.* **2009**, *11* (1), 253–255. https://doi.org/10.1021/ol8026522.

(9) Brzezinski, L. J.; Rafel, S.; Leahy, J. W. The Asymmetric Baylis−Hillman Reaction. *J. Am. Chem. Soc.* **1997**, *119* (18), 4317–4318. https://doi.org/10.1021/ja970079g.

(10) Aggarwal, V. K.; Castro, A. M. M.; Mereu, A.; Adams, H. The Use of Enantiomerically Pure N-Sulfinimines in Asymmetric Baylis–Hillman Reactions. *Tetrahedron Letters* **2002**, *43* (8), 1577–1581. https://doi.org/10.1016/S0040-4039(02)00021-7.

(11) Shi, M.; Xu, Y.-M. Diastereoselective Baylis–Hillman Type Reactions of Chiral Non-Racemic N-Sulfinimines with Cyclopent-2-En-1-One. *Tetrahedron: Asymmetry* **2002**, *13* (11), 1195–1200. https://doi.org/10.1016/S0957-4166(02)00269-0.

(12) Shi, M.; Li, C.-Q.; Jiang, J.-K. New Discovery in the Traditional Baylis-Hillman Reaction of Arylaldehydes with Methyl Vinyl Ketone. *Chemical Communications* **2001**, *0* (9), 833–834. https://doi.org/10.1039/B101019K.

(13) Shi, M.; Li, C.-Q.; Jiang, J.-K. Reexamination of the Traditional Baylis–Hillman Reaction. *Tetrahedron* **2003**, *59* (8), 1181–1189. https://doi.org/10.1016/S0040-4020(03)00041-3.

(14) Beare, N. A.; Hartwig, J. F. Palladium-Catalyzed Arylation of Malonates and Cyanoesters Using Sterically Hindered Trialkyl- and Ferrocenyldialkylphosphine Ligands. *J. Org. Chem.* **2002**, *67* (2), 541–555. https://doi.org/10.1021/jo016226h.

(15) Culkin, D. A.; Hartwig, J. F. Palladium-Catalyzed α-Arylation of Carbonyl Compounds and Nitriles. *Acc. Chem. Res.* **2003**, *36* (4), 234–245. https://doi.org/10.1021/ar0201106.

(16) Kawatsura, M.; Hartwig, J. F. Simple, Highly Active Palladium Catalysts for Ketone and Malonate Arylation: Dissecting the Importance of Chelation and Steric Hindrance. *J. Am. Chem. Soc.* **1999**, *121* (7), 1473–1478. https://doi.org/10.1021/ja983378u.

(17) Su, W.; Raders, S.; Verkade, J. G.; Liao, X.; Hartwig, J. F. Pd-Catalyzed Alpha-Arylation of Trimethylsilyl Enol Ethers with Aryl Bromides and Chlorides: A Synergistic Effect of Two Metal Fluorides as Additives. *Angew. Chem. Int. Ed. Engl.* **2006**, *45* (35), 5852–5855. https://doi.org/10.1002/anie.200601887.

(18) Moradi, W. A.; Buchwald, S. L. Palladium-Catalyzed α-Arylation of Esters. *J. Am. Chem. Soc.* **2001**, *123* (33), 7996–8002. https://doi.org/10.1021/ja010797+.

(19) Liu, X.; Hartwig, J. F. Palladium-Catalyzed Arylation of Trimethylsilyl Enolates of Esters and Imides. High Functional Group Tolerance and Stereoselective Synthesis of α-Aryl Carboxylic Acid Derivatives. *J. Am. Chem. Soc.* **2004**, *126* (16), 5182–5191. https://doi.org/10.1021/ja031544e.

(20) Hama, T.; Liu, X.; Culkin, D. A.; Hartwig, J. F. Palladium-Catalyzed α-Arylation of Esters and Amides under More Neutral Conditions. *J. Am. Chem. Soc.* **2003**, *125* (37), 11176–11177. https://doi.org/10.1021/ja036792p.

(21) Li, Y.-Q.; Wang, H.-J.; Huang, Z.-Z. Morita–Baylis–Hillman Reaction of α,β-Unsaturated Ketones with Allylic Acetates by the Combination of Transition-Metal Catalysis and Organomediation. *J. Org. Chem.* **2016**, *81* (11), 4429–4433. https://doi.org/10.1021/acs.joc.6b00684.

(22) Kou, X.; Kou, K. G. M. α-Arylation of Silyl Enol Ethers via Rhodium(III)-Catalyzed C–H Functionalization. *ACS Catal.* **2020**, *10* (5), 3103–3109. https://doi.org/10.1021/acscatal.9b05622.

(23) Nishikata, T.; Abela, A. R.; Huang, S.; Lipshutz, B. H. Cationic Pd(II)-Catalyzed C–H Activation/Cross-Coupling Reactions at Room Temperature: Synthetic and Mechanistic Studies. *Beilstein J. Org. Chem.* **2016**, *12* (1), 1040–1064. https://doi.org/10.3762/bjoc.12.99.

(24) Nishikata, T.; Abela, A. R.; Huang, S.; Lipshutz, B. H. Cationic Palladium(II) Catalysis: C−H Activation/Suzuki−Miyaura Couplings at Room Temperature. *J. Am. Chem. Soc.* **2010**, *132* (14), 4978–4979. https://doi.org/10.1021/ja910973a.

(25) Beletskaya, I. P.; Cheprakov, A. V. The Heck Reaction as a Sharpening Stone of Palladium Catalysis. *Chem. Rev.* **2000**, *100* (8), 3009–3066. https://doi.org/10.1021/cr9903048.

(26) Bertz, S. H.; Cope, S.; Dorton, D.; Murphy, M.; Ogle, C. A. Organocuprate Cross-Coupling: The Central Role of the Copper(III) Intermediate and the Importance of the Copper(I) Precursor. *Angewandte Chemie International Edition* **2007**, *46* (37), 7082–7085. https://doi.org/10.1002/anie.200703035.

(27) Guo, L.; Srimontree, W.; Zhu, C.; Maity, B.; Liu, X.; Cavallo, L.; Rueping, M. Nickel-Catalyzed Suzuki–Miyaura Cross-Couplings of Aldehydes. *Nature Communications* **2019**, *10* (1), 1–6. https://doi.org/10.1038/s41467-019-09766-x.

(28) Arava, S.; Santra, S. K.; Pathe, G. K.; Kapanaiah, R.; Szpilman, A. M. Direct Umpolung Morita–Baylis–Hillman like α-Functionalization of Enones via Enolonium Species. *Angewandte Chemie International Edition* **2020**, *59* (35), 15171–15175. https://doi.org/10.1002/anie.202005286.

(29) Stephan, D. W. "Frustrated Lewis Pairs": A Concept for New Reactivity and Catalysis. *Org. Biomol. Chem.* **2008**, *6* (9), 1535–1539. https://doi.org/10.1039/B802575B.

(30) Stephan, D. W.; Erker, G. Frustrated Lewis Pair Chemistry: Development and Perspectives. *Angewandte Chemie International Edition* **2015**, *54* (22), 6400–6441. https://doi.org/10.1002/anie.201409800.

(31) Stephan, D. W. Frustrated Lewis Pairs: From Concept to Catalysis. *Acc. Chem. Res.* **2015**, *48* (2), 306–316. https://doi.org/10.1021/ar500375j.

(32) Brenna, E.; Crotti, M.; De Pieri, M.; Gatti, F. G.; Manenti, G.; Monti, D. Chemo-Enzymatic Oxidative Rearrangement of Tertiary Allylic Alcohols: Synthetic Application and Integration into a Cascade Process. *Advanced Synthesis & Catalysis* **2018**, *360* (19), 3677–3686. https://doi.org/10.1002/adsc.201800299.

(33) Hauptmann, R.; Petrosyan, A.; Fennel, F.; Argüello Cordero, M. A.; Surkus, A.-E.; Pospech, J. Pyrimidopteridine N-Oxide Organic Photoredox Catalysts: Characterization, Application and Non-Covalent Interaction in Solid State. *Chemistry – A European Journal* **2019**, *25* (17), 4325–4329. https://doi.org/10.1002/chem.201900118.

(34) Guo, S.-H.; Xing, S.-Z.; Mao, S.; Gao, Y.-R.; Chen, W.-L.; Wang, Y.-Q. Oxa-Michael Addition Promoted by the Aqueous Sodium Carbonate. *Tetrahedron Letters* **2014**, *55* (49), 6718–6720. https://doi.org/10.1016/j.tetlet.2014.10.019.